联合国
大会

Distr.
GENERAL

A/AC.105/545
1 April 1993
CHINESE
ORIGINAL: ENGLISH

和平利用外层空间委员会

联合国/国际摄影测量和遥感学会关于遥感数据分析方法和应用讲习班的报告和记录

（1992年8月6日至7日，华盛顿特区）

目 录

附 件

93-18831 150493 150493 030593

导 言

A. 背景和目标

1. 本报告载有联合国/国际摄影测量和遥感学会关于遥感数据分析方法和应用讲习班的记录摘要。讲习班是空间应用专家提出的及和平利用外层空间委员会科学和技术小组委员会建议的，1992年联合国空间应用方案的组成部分。该方案后来获得委员会和大会的核可。

2. 讲习班由摄测遥感学会主持并且共同赞助，由联合国(外层空间事务厅)和摄测遥感学会举办。讲习班于1992年8月6日至7日在华盛顿特区举行。

3. 讲习班在摄测遥感学会第十七届大会于1992年8月2日至14日在华盛顿特区举行的期间举办；讲习班的参与者也参加了摄测遥感学会大会。此外，有些讲习班的参与者还参加了1992年8月28日至9月5日在华盛顿特区举行的世界空间大会，国际科学联合会理事会(科学理事会)、空间研究委员会(空间联委会)和国际宇宙航行联合会(宇航联合会)联席会议。

4. 讲习班的目标是为有关数据的压缩和分析及其应用所使用的规则系统、软件开发、软件系统和硬件方面的科学家提供一个论坛。这种论坛有助于在摄影测量和遥感应用的软件包的制造和使用方面具有广泛专门知识的开发者与使用者之间进行交流。

5. 本报告载述了讲习班的背景、目标和安排，以及向讲习班提出的各项文件的全文，本报告是为和平利用外层空间委员会及其科学和技术小组委员会编写的。参与者将向他们自己国家的有关当局提出报告。

B. 讲习班的安排和方案

6. 下列各国参加了讲习班：澳大利亚、巴西、加拿大、中国、芬兰、法国、

德国、日本、荷兰、尼日利亚、瑞士、中国台湾省、大不列颠及北爱尔兰联合王国和坦桑尼亚联合共和国。

7. 联合国和摄测遥感学会为举办讲习班所提供的经费用来支付国际航空旅费、参与者和演讲者在讲习班和摄测遥感学会大会期间的每日津贴以及大会的登记费。

8. 大会由丹麦哥本哈根的哥本哈根大学地理学研究所的拉斯穆森作了主题演讲正式开幕。联合国空间应用专家阿维奥敦博士也致了欢迎词。

9. 联合国与摄测遥感学会合作拟订了讲习班的方案(见本报告附件一)。讲习班举行了三次全体会议。

10. 参与者对联合国和国际摄影测量和遥感学会主办讲习班和提供财政援助表示感谢,并对方案的技术素质表示赞扬。

提交讲习班的文件

11. 向讲习班提出了若干文件。这些文件按照讲习班的会议可以分为三个主要主题:㈠ 数据格式,基本数据处理和影象增强技术;㈡ 计算机辅助数据解释和数字化测图;和㈢ 遥感数据和通用信息系统连接。提交讲习班的文件的全文和/或图表,载于本报告附件二。因为这些文件大多数是技术性文件,因此只用提出文件的语文印发。

Annexes

Annex I

PROGRAMME OF THE WORKSHOP

Thursday, 6 August, 0830-1645 Opening statement	A.A. Abiodun, United Nations Expert on Space Applications
Key lecture: Remote sensing data analysis methods	K. Rasmussen, Institute of Geography, University of Copenhagen

Session I: Data formats, basic processing and image enhancement techniques

(Chairman: D.G. Goodenough, Canada)

Geometric and radiometric models in processing SPOT imagery for object-space surfaces	J. Wu, Center for Space and Remote Sensing Research, National Central University, Taiwan, Republic of China
Image processing: edge and feature extraction, linear feature extraction, general segmentation, image matching and object orientation	J.C. Trinder, School of Surveying, University of New South Wales, Sydney, Australia
Image analysis software	L.W. Hayes, University of Dundee, Dundee, Scotland

Session II: Computer-assisted data interpretation and digital mapping

(Chairman: B. Forster, Australia)

Intelligent information extraction at the Canada Centre for Remote Sensing	D. G. Goodenough, Pacific Forestry Centre, Ottawa, Ontario, Canada
Radiometric corrections for quantitative analysis of multispectral, multitemporal and multisystem satellite data	G. Guyot, INRA Bioclimatologie, Montfavet, France
Multivariate analysis techniques	N.J. Mulder, International Institute for Aerospace Survey and Earth Science (ITC), the Netherlands

/...

Annex I (continued)

Image scanners and interactive workstations for semi-automatic mapping, with emphasis on low-cost solutions	T. T. Sarjakoski, Finnish Geodetic Institute, Helsinki Finland

Friday, 7 August, 0830-1500

Session III: Integration of remote sensing data and GIS

(Chairman: A. MacDonald, United Kingdom)

Extraction of quantitative information from remote sensing data and integration into GIS	E. Baltsavias, Institute of Geodesy and Photogrammetry, Swiss Federal Institute of Technology, Zurich, Switzerland
Integrations of sea surface temperature data sets using MOS-1 satellite data for validation and monitoring	S. Takeuchi, Remote Sensing Technology Center, Tokyo, Japan
Deforestation assessment using satellite imagery and GIS techniques	D. Alves, National Institute for Space Research, Sao Jose dos Campos, Brazil

Session IV: Discussion and Conclusions

(Chairman: A.A. Abiodun, United Nations)

Annex II

PRESENTATIONS TO THE WORKSHOP

CONTENTS

/...

REMOTE SENSING DATA ANALYSIS METHODS

K. Rasmussen

Institute of Geography

University of Copenhagen, Denmark

Methodologies and software for satellite image processing: User needs and development trends

by

Kjeld Rasmussen
Institute of Geography
University of Copenhagen

Keywords: Remote sensing, satellite image processing, natural resources

Abstract:

The application of optical remote sensing in national-level natural resources monitoring and management, in particular in developing countries, implies development of methodologies adapted to users with backgrounds quite different from those of remote sensing scientists and technicians. This paper discusses the nature of the methodologies, data analysis methods and image processing systems required by the people actively engaged in natural resources management. The point of departure will be a brief review of which optical remote sensing methodologies might contribute to natural resources management in developing countries in a cost-efficient way. Subsequently, an attempt will be made to identify development trends with respect to satellite image processing methodologies, software and hardware. Finally, organizational models will be discussed in the light of these trends, and the 'Center for Ecological Monitoring' (CSE), Dakar, Senegal, will be mentioned as an example of how national-level application of remote sensing data in environmental monitoring may be achieved, based on relatively simple and low-cost technology.

1. Introduction

Growing concern for global environmental change, as expressed in the 'agenda 21' document of the UNCED, has implicated that tools such as satellite remote sensing should be used as efficiently as possible on two levels: For assessing and monitoring environmental changes on the global level and for managing natural resources on the local level. Change processes on the planetary scale are mostly being studied by extremely resourceful organizations with ample access to remote sensing equipment and expertise. Local environmental management has to be carried out by institutions on national or sub-national level, and it is a far greater challenge to those involved in development of methodologies and software for environmental remote sensing to produce models for useful applications of remote sensing on that level, taking into consideration the limited resources and expertise available. This is true in highly technologically developed countries, yet even more so in developing countries.

/...

This paper will mainly focus on how remote sensing techniques can come into practical use in management of natural resources, especially in developing countries: What demands do this imply on the scientific, technical and organizational levels.

Initially an attempts will be made to identify more precisely what are the demands of this group of users, then current trends in remote sensing, image processing and computer technology will be briefly discussed, and finally some suggestions, concerning institutional arrangements furthering the utilization of remote sensing methodologies in natural resources management in developing countries, will be made.

2. User needs with regard to development of remote sensing methodologies

2.1 The case for satellite remote sensing

Before discussing specific remote sensing methodologies and image processing algorithms a short discourse may be required, in order to identify user needs in a wider context, i.e. with regard to mapping and monitoring themes, to which remote sensing may contribute in a cost-efficient manner. The scientific literature contains a wealth of studies demonstrating the potential usefulness or (less often) uselessness of remote sensing techniques for a wide spectrum of applications, also with reference to developing countries. Relatively few of these are being used operationally in the management of natural resources. The reasons for this are various:

- Remote sensing techniques do simply not in all cases provide the information required in an operational context, even though the literature may claim it. There is a long way between demonstration of the value of a certain remote sensing technique in a specific experiment and proving its reliability in a practical context. Also, scientists tend to 'oversell' remote sensing methodologies.

- Relevant data provided by remote sensing techniques may be difficult to integrate with other 'conventional' data and procedures in an existing system for management of natural resources.

- Some developing countries (and wealthy, industrialized countries as well) have insufficiently developed organizational frameworks for natural resources management, making them unable to demand, receive and utilize remote sensing data.

- The wealthy, industrialized countries, which possess the major part of the technological capacity within the remote sensing field, have not been particularly successful in finding ways of making these methodologies accessible to most countries in the developing world. Better models for cooperation are required.

/...

2.2 Some development trends of remote sensing methodologies

Methodologies for processing and analyzing satellite remote sensing data are diverse, and it is difficult to make useful generalizations with respect to development trends. The following observations probably hold true, however:

1) Satellite images are to an increasing extent being integrated with other (often spatial) data, sometimes organized in 'geographical information systems' (GIS).

2) The belief that more or less automatic procedures, such as multispectral classification methods, will replace manual/visual interpretation techniques gives space to a more balanced view, where manual/visual and computer-based methods supplement each other.

3) Conversion of raw satellite images into estimates of well-defined physical or biological parameters require still more complex models of the entire measurement situation, incl. satellite/sensor-properties, the atmosphere, radiation-target interaction and effects of spatial heterogeneity.

4) Remote sensing applications in natural resources management rely to an increasing extent on the use of time-series of satellite images and on combination of data from two or more satellite/sensor-systems.

2.3 Image processing hardware

The development of image processing hardware has been substantial during recent decades. In the seventies satellite image processing was generally carried out on mainframe systems often with limited multispectral image display capabilities. Later, minicomputer-based systems became the standard. These were quite costly, which implied that they were used and managed by specialists, and 'common users' and students usually had limited access. In recent years personal computer (PC) and workstation-based image processing systems have largely divided the market between them, and prices on hardware have been decreasing fast. Quite powerful '486 PC'-based systems with full multispectral image display capabilities (32 bitplanes) may now be acquired at prices lower than 10.000 USdollars. Storage media, such as hard-disks, magnetic tape and optical disks, have undergone similar developments, implying that even full scenes of Landsat TM images, taking up almost 300 Mbytes, may be handled on PC-based systems. There is no reason to suggest that this development will slow down in the near future, since new and even more powerful processors will become available soon. Presently full-color image display demands special 'display controllers', yet sometime within the next decade standard display systems of both PCs and workstations will attain the necessary quality (with respect to the number of bitplanes and the way they may be handled) allowing 'professional' multispectral satellite image display. When this happens the category 'image processing system' will loose its meaning, hardware-wise. In most institutions computers are/will become connected in networks, and image processing tasks

/...

requiring substantial computing-power, will be carried out by the computer best suited for it in the network.

These technological and economic development trends have the consequence that image processing systems will (or at least should) be on the desktop of most potential users. This will imply that the number of users will increase considerably, if other bottlenecks do not slow down the development.

2.4 Operational and semi-operational remote sensing methodologies

Attempts have been made in the past to point out which remote sensing methodologies may be considered suitable for practical utilization. For a specific geographical area, the Sahel, Prince, Justice & Los (1990) have produced a useful review of methodologies, and in spite of the fast developments within the field most of their conclusions probably still hold true. The following applications are labeled as ready for transition to operational use:

- Rainfall estimation
- Rangeland production monitoring
- Food security and early warning systems
- Bush-fire monitoring
- Ground water survey
- Land cover mapping

For other areas the set of 'operational' methodologies may be slightly different. e.g. methods relying on optical satellite remote sensing are less suitable in more humid areas.

In the present context it may be just as relevant to point out methodologies which may not yet be ready for operational use but carry great potential. Prince et al (1990) discuss several methodologies requiring further development:

- Crop production monitoring and modelling
- Evapotranspiration estimation
- Hydrological catchment modelling
- Fuelwood estimation
- Erosion modelling and prediction

These lists of applications loosely define a set of requirements with regard to satellite image processing procedures and software.

2.5 Cost considerations

One topic seldom discussed in the scientific literature is the cost of applying the various methodologies suggested. Balancing costs and benefits is probably impossible within the field of environmental remote sensing, since the potential benefits, i.e. improved understanding of our environment, have no easily defined economic value, and the involved costs are highly intransparent. Cost-assessments are therefore limited to comparisons between different remote sensing methods and between remote sensing

methods and alternative means of data acquisition, and even this is often difficult. Major remote sensing applications in wealthy, technologically advanced countries are highly subsidized, and in many developing countries foreign donors finance almost all such activities. This may imply serious non-sustainability of remote sensing activities, once subsidies or outside support disappear. To cope with this situation, a socalled 'demand-driven approach' to the development of remote sensing applications has been promoted (Falloux, 1989)(Prince et al, 1990).

However, certain remote sensing methodologies are basicly inexpensive and no relevant alternatives can compete, and it is suggested that the potential of these methodologies is fully utilized in developing countries, possibly as a first step in the establishment of operational environmental satellite remote sensing activities, provided that the methodologies are suited for the area in question and that a certain information-demand exists. The use of meteorological satellite data, with high repetivity of coverage, large area-coverage and moderate cost, for monitoring of vegetation, crops, bush-fires and agroclimatic parameters is the best example of such a cost-efficient remote sensing methodology. Since it is also among those considered to be partly "operational" in a Sahelian context by Prince et al (1990), there are good reasons to promote it.

Establishment and running of satellite image processing facilities is an important cost-component. In developing countries it is often extremely difficult to assure continuous function of complex computer-equipment, due to lack of a technical back-up system, without costly outside assistance. Thus, there are good reasons for basing the application of remote sensing methods on the technology for which the need for technical back-up is smallest, i.e. PC-technology. It is often stated that more complex technologies, such as workstations, are better suited for image processing and GIS operations, and even though this may be true, the difficulties of service outweigh the advantages. Software-wise, the standard PC operating system, DOS, has considerable shortcomings in an image processing and GIS context, yet the alternative, UNIX, which is technically preferable, is so much more complex and require so much more training, that this again outweighs its advantages. New developments in the area of operating systems, such as OS2 or NT, will probably combine the relative simplicity of DOS and the technical advantages of UNIX.

3. The user community

3.1 The 'typical' user

Precise pictures of 'the typical user' of satellite remote sensing for natural resources management are difficult to produce, because the differences are enormous between and within countries. However, it is a widespread observation that remote sensing methods are slowly becoming tools used decentrally rather than merely objects of research dealt with by few specialized institutions, and this has certain implications for the composition of the 'user community': Users are now more often

than before technicians and professionals, whose main area of expertise is not remote sensing and image processing, but rather fields such as geography, geology, geophysics, biology, forestry or agricultural science. These users spend a minor fraction of their working hours doing satellite image processing, as compared to the 'remote sensing scientists' who used to constitute the majority of the user community. This is, of course, a natural and desireable development, if one wishes to see remote sensing methodologies being utilized efficiently, yet it has a number of consequences for the character of the image processing methods and software to be applied:

- Image processing software is required to become integrated in methodologies and software used in practical natural resources management within a range of disciplines, rather than to remain isolated 'stand-alone systems'. This will require an improved transparency and openness of the software

- Users will typically require 'decision support' when selecting methods and algorithms. This involves discipline specific training materials, user-friendly interfaces, and possibly 'decision support systems'/'expert systems', assisting the user in finding optimal data-sources and processing procedures.

- Operational applications of remote sensing in natural resource management, carried out by non-specialists of satellite image processing, will require that the amount of human labor involved in the more technical image processing steps is minimized. E.g. geometrical correction and co-registration of time-series of satellite images should be possible with little human involvement, yet without compromising the accuracy.

3.2 Towards a hierarchy of users ?

In some regions and for some data-sources it has been suggested to organize users hierarchically. The 'high level users', e.g. regional centers, will be responsible for certain preprocessing steps (incl. radiometric, atmospheric and/or geometrical correction) and production of 'derived data-sets'. This may seem logical, since end-users will then not need to cope with the numerous and tedious processing steps involved, nor to possess precise knowledge on details of complex topics such as atmospheric correction algorithms. Such arrangements may evolve as a natural division of labor, beneficial to all levels in the hierarchy, or be imposed through monopolization of the data-flow. Monopolization may, however, seriously delay the development of practical applications of remote sensing in natural resource management, especially if the 'high-level user' is a supra-national institution, while the management takes place on the national or sub-national level. In addition, monopolization of the flow of remote sensing data is probably unrealistic and undesired for other reasons:

- There are few computational and economic advantages of

centralization within the field of satellite image preprocessing. In other words, any reasonably well-equipped user will be able to carry out his own geometrical and radiometric preprocessing of images, and given the widespread underutilization of computer capacity, it will be economically advantageous for him to do so.

- There are no widely accepted and generally applicable preprocessing procedures which will in the long run satisfy any end-user. Geometrical correction, carried out by institutions handling large data-volumes, tends not to live up to the standards required by some end-users, especially those using time-series of images. Thus, the reasonably advanced end-user will sooner or later wish to have access to the raw data himself.

- In order to fully appreciate the information content, application potential and inherent limitations of remote sensing data, the user must be able to access the raw data, rather than or in addition to derived data-sets.

4. Examples of remote sensing methodologies and software

4.1 Use of high-resolution optical satellite images for land-cover classification

Use of Landsat and SPOT-data for land-cover and land-use mapping and monitoring is becoming a standard methodology in regions where other data-sources are unreliable or absent. Methodologies vary considerably, yet in operational contexts visual interpretation techniques play an important role. In the following the demands on satellite image processing methodologies and software, defined by this type of application, will be discussed.

In fig.1 the outlines of a sequence of image processing steps, typical for Landsat- or SPOT-based land-cover classification, are shown. The radiometric and geometrical correction procedures will not be discussed here, emphasis will be on how visual and computer-based analysis methods may be combined in order to utilize the analyst's a priori knowledge of the area efficiently.

The 'feature selection' and spectral transformation procedures aim at replacing the original image bands by new artificial ones, having desireable properties, such as:

1) Low correlations with other bands/features.
2) High content of 'relevant' information or 'variance'.
3) Simple interpretation, strong relations to interesting physical or biological parameters.

Identification of such features involves use of an intricate mixture of expertise within the field of remote sensing, knowledge about the optical properties of the object, insight into multivariate statistics and common sense. No simple or generally applicable methodology for feature identification can be pointed out, and trial-and-error plays a significant role in

/...

the process.

What demands on the image processing software does this 'feature selection' imply ? A non-exhaustive list will include:

- Efficient and flexible multispectral image display routines, allowing both automatic and manual, interactive contrast manipulation, since feature selection will often involve an element of subjective visual judgement.
- Routines for calculation of a variety of more or less complex indices, linear combinations etc on the basis of the original bands. These include simple ratios, standard vegetation indices and generally applied transformations, such as the 'tasseled cap' transformation.
- A selection of multivariate statistical techniques, incl. principal components analysis, aiming at decorrelation of image bands.
- Methods for measuring the spectral properties and 'separability' of a number of 'classes', specified by the analyst. The success of various spectral transformations may be studied using such measures of separability.

The 'classification' step may involve a mixture of visual interpretation and user-guided automatic classification. Standard classification algorithms, such as the 'minimum distance' and 'maximum likelihood' procedures, involve that the analyst points out training areas, representative for each class, and the rest is left to the computer/algorithm. Results are often not satisfactory, since the analyst's full knowledge, as well as the non-spectral information in the image, are not utilized. Innumerable attempts have been made to refine classification techniques, yet in spite of many improvements, visual interpretation techniques are still preferable in many situations, especially where identification of spatial entities play a significant role. With respect to image classification software, this calls for procedures geared for interactive analysis, allowing efficient utilization of the analyst's expertise, rather than 'once-and-for-all classification algorithms'. Simple, fast and flexible hierarchical procedures, as the one sketched in fig.2, will probably support the analyst better than complex statistically based methods.

The visual interpretation will usually be based upon a spectrally transformed image, as discussed above. In addition, it might be useful to enhance the image by suppressing noise and sharpening boundaries. Again, an interactive set of procedures for image filtering will be required. The interpretation will often result in 'drawing' of boundaries between classes, and an efficient interface between the image processing system, which is raster-oriented, and a vector-oriented GIS is essential in this context.

As mentioned earlier, the non-specialist analyst will require assistance in order to select the most suitable sequence of procedures to solve a given problem. On-line help, good documentation and proper training will, of course, be of great value, yet development of 'decision support' or 'expert systems' might become relevant.

/...

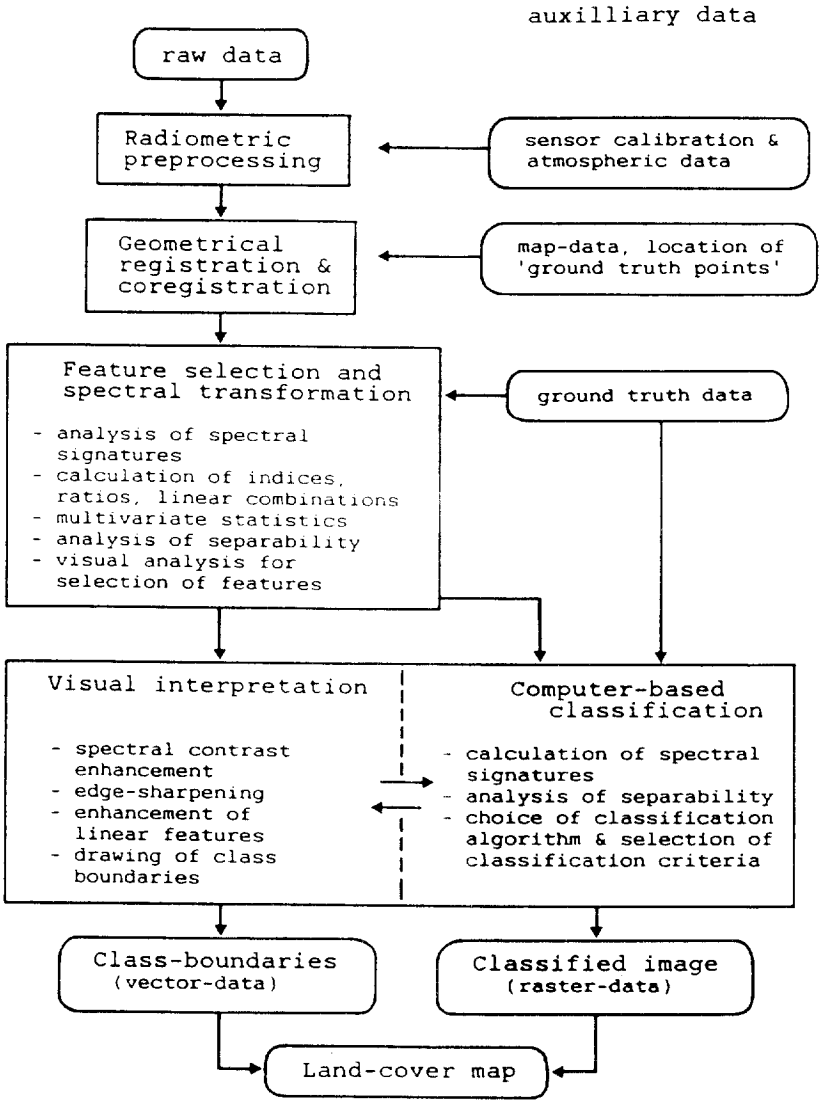

Fig.1 Outline of a typical sequence of image processing and analysis steps involved in application of SPOT or Landsat data for land cover mapping

/...

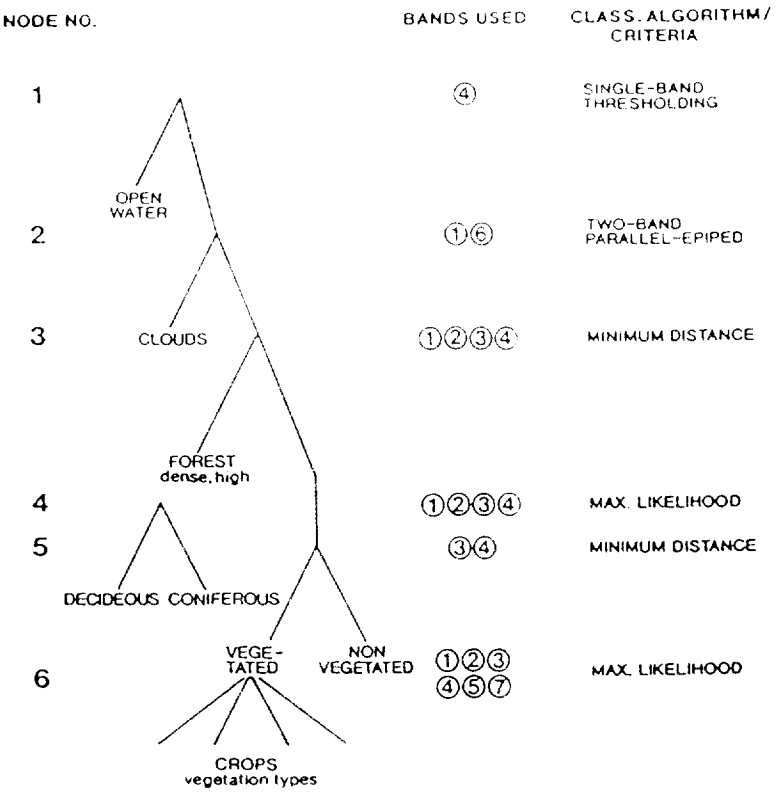

Fig.2 A sketch of a hierarchical classification procedure for land-cover mapping based on a Landsat TM image. Simple classification tasks, e.g. classification of open water, are first carried using simple and fast methods and few bands, and increasingly complex methods and more band are being used in later stages, where fewer pixels have to be dealt with.

/...

4.2 NOAA AVHRR based monitoring of natural vegetation, crops and bush-fires

The theory and methodology of monitoring herbaceous vegetation in the semi-arid tropics have been quite extensively described in the literature, in particular in the work of the GIMMS group documented in special issues of 'International Journal of Remote Sensing' (Justice, 1986)(Prince & Justice, 1991), and no attempt to present it in any detail will be made here. The principle is simply that the photosynthetic activity is closely related to the 'normalized difference vegetation index' (NDVI), calculated from NOAA AVHRR bands 1 and 2, and by monitoring NDVI through the growing season the biomass production may be obtained by integration. Atmospheric effects and effects of off-nadir viewing, which affect the individual NOAA AVHRR bands quite considerably because of the wide scan-angle, are suppressed by using NDVI rather than the original bands and by using 'maximum value composites' (MVC). MVCs are created by assigning to each pixel the highest NDVI-value encountered in the NOAA images from a certain period, usually 10 days, and since all effects of haze, clouds etc tend to decrease the NDVI, the highest value encountered is probably the most correct. Similar methods may be used to monitor crops in semi-arid areas, such as millet, and to estimate yields.

The same NOAA AVHRR data are also well-suited for monitoring the extent of bush-fires by observing fire-scars. No generally applicable and fully automatic method seems to have emerged in this field, yet visual interpretation of NOAA-images appears to be quite efficient.

These applications of NOAA AVHRR data are, as mentioned earlier, among the candidates for operational applications in many dryland areas in the tropics: The parameters monitored are of great economic and environmental interest, the amounts of data involved are not exceedingly large, the cost of data is small, entire countries may be covered, and the required investments in equipment are limited.

The requirements concerning image processing methodologies and software may be summarized as follows:

1) The full 10-bit data should be handled by system, discarding of the last 2 bits to make the data fit into a standard 8-bit data format will have strong negative effects on the quality of the results.

2) Proper software for utilization of the TBUS data, distributed with the NOAA AVHRR images, allowing radiometric calibration and more precise localization of the geographical position of each pixel, must be available.

3) Labor-saving 'production-line' software for geometrical registration and co-registration of time-series of NOAA-images with sub-pixel accuracy is a presumption for operational use of the methodology. The high co-registration accuracy is particularly necessary in crop monitoring, since fields in semi-arid zones most often are small and sometimes scattered, and

/...

degradation of the 'efficient spatial resolution' of a multi-temporal NOAA data-set to several kilometers, due to unprecise co-registration, is therefore detrimental. Furthermore, MVCs tend to overestimate NDVI, if the co-registration is not sufficiently precise.

4) Routines for cloud masking, calculation of MVCs, for integration of NDVI and for spatial and temporal interpolation to 'fill in holes' in NDVI time-series caused by cloud-cover are required.

5) Efficient and flexible routines for multispectral image display, required for visual identification of bush-fire scars, will be necessary.

6) Links to raster- and vector-oriented GISs, containing information of relevance for the interpretation of NDVI, e.g. maps of vegetation types and soil color, are likewise necessary.

These demands are an example of application-specific requirements not usually met by standard general image processing software. Also the precise requirements on methods and software will depend on the management context in which this monitoring activity takes place, and so all systems will have to be modified, requiring openness and modularity beyond what is often seen.

5. Institutional arrangements

5.1 Consequences of changes in the technological basis

Satellite remote sensing has from the outset been considered a high-technological activity, requiring complex and expensive equipment, highly skilled labor and high running costs, and this has resulted in a centralized top-down organizational structure, both in many industrialized countries and in the developing countries. Many developing countries have not been able to utilize satellite remote sensing to its full potential, and the organizational model may be one of the causes of this situation.

As outlined above, the technological development and the results of 20 years of training effort may now have changed the fundamental preconditions to the extent that a more democratic (or anarchistic, if one prefers) bottom-up organizational model has become a realistic alternative: Small, decentral, local-level organizations, be it within the public natural resources management sector, small companies, individual development projects or NGOs, will now be able to utilize certain satellite remote sensing methods efficiently. This opens new perspectives for the effect of remote sensing on natural resources management, since the technology will be on the desk-tops of those directly involved in the management process. Therefore this change in organizational model should be supported, and it is a major challenge for the international remote sensing community and for those financing development activities to find ways of promoting such local-level activities. Also it is important to discuss the future role of supra-national remote sensing centers, to ensure

/...

that the experience accumulated in these centers is utilized to support national and sub-national level organizations.

5.2 The example of 'Centre de Suivi Écologique' (CSE) in Senegal

CSE has roots back to the early eighties, where it was created by FAO and worked on monitoring of grasslands in northern Senegal in collaboration with the GIMMS group at NASA GSFC, see f.i. Tucker et al (1985). Later the financing has been taken over by UNSO, and it has expanded its activities greatly, to encompass a wide spectrum of environmental monitoring tasks, including a number of satellite-based:

1) NOAA-based monitoring of the development of the natural vegetation in the entire Senegal, using the abovementioned NDVI-concept (operational). The data is combined with data from systematic air-based counting of livestock and information on water-provision from boreholes (in a GIS) to produce estimates of grazing pressure and fodder sufficiency.

2) NOAA-based estimation of crop yields, particularly millet and groundnuts (semi-operational/experimental).

3) NOAA-based monitoring of bush-fire scars (operational) and ongoing fires (experimental).

4) Meteosat-based assessment of rainfall, using the 'cold cloud duration' methodology (Dugdale & Milford, 1986) (operational).

5) Estimation of agroclimatic parameters, such as actual evapotranspiration, from NOAA and Meteosat (experimental).

6) Use of high-resolution data for land-use/land-cover mapping (operational).

All these remote sensing and image processing activities are carried out locally, using PC-based image processing equipment, and equipment-costs constitutes only a small part of CSEs budget. CSE is in the process of establishing receiving facilities for NOAA-data, in order to support near-real-time applications, such as monitoring of ongoing bush-fires.

CSE has a semi-independent status within the public sector in Senegal and is attempting to establish close links to local users of information, both within the national and local-level administration, parastatal organizations and development projects, in order to approach the ideal of being 'demand driven'.

Since 1987 CSE has collaborated closely with the Institute of Geography, University of Copenhagen, (IGUC), which has developed all the image processing software used by CSE (the CHIPS system), assisted in establishment of facilities and carried out training of CSE-staff. By now CSE requires very little outside support in its daily activities, and the collaboration with IGUC is therefore aimed towards more long-term objectives, such as development of new methodologies and provision of new software-

/...

modules, supporting CSEs growing field of activities. Presently methodological developments in support of CSE include establishment of long time-series of directly comparable NOAA AVHRR NDVI data for assessment of long-term environmental trends in the Sahel, development of methodologies for estimation of the actual evapotranspiration, which is of great relevance for monitoring vegetation and crops in the drier parts of Senegal, where the 'NDVI-signal' is small, and development of more sophisticated and interactive feature selection and multispectral classification methods.

CSE has had considerable success in proving satellite remote sensing useful in natural resources monitoring, and it may serve as a model for establishment of similar activities in other places. Furthermore, the collaboration between IGUC and CSE, financed by the Danish Agency for International Development Assistance, DANIDA, exemplify how such 'twinning-arrangements' with a long time-perspective may be to the benefit of both sides, and contribute to overcome thresholds in the process of operationalization of satellite remote sensing methodologies.

6. Conclusions and critical issues

The technological development has implied that many satellite remote sensing methodologies have or will become within reach of a large number of potential users involved in natural resources management. The main constraints on the efficient utilization of these methodologies in developing countries are probably related to questionable cost-efficiency (sometimes related to high prices of satellite data), lack of local demand for environmental information and inappropriate organizational structures on both national and international levels.

It is suggested that developers of methodologies and software should now realize and support that the use of remote sensing techniques will to an increasing extent take place on a decentral level and become integrated in practical management activities. This again implies that demands on methodologies and software will change, since the composition of the user-community will shift from dominance of 'remote sensing scientists' to 'thematic professionals', spending a minor fraction of their time on satellite image processing. Emphasis will have to be placed on improvement of facilities for integration of satellite-derived information and other data, on methods allowing efficient combination of visual and computer-based interpretation techniques and on improved user-interfaces and 'decision support systems', making techniques more accessible to the natural resource management professionals.

References

Dugdale, G. & Milford, J.R. (1986): The use of Meteosat data to evaluate rainfall in tropical Africa. Proc. 21th Int. Symp. Rem. Sens. of Environment, Nairobi, Kenya, vol.2 pp 499-506. ERIM, Ann Arbor, Michigan.

/...

Falloux, F. (1989): Land information and remote sensing for renewable resource management in Sub-Saharan Africa. A demand driven approach. World Bank Technical Paper 108, the World Bank, New York.

Justice, C.O. (1986) (ed.): International Journal of Remote Sensing, 7.

Prince, S.D., Justice, C.O. & Los, S.O. (1990): Remote Sensing of the Sahelian Environment. CEC, DG8, JRC-Ispra/CTA-Wageningen. ISBN 92 9081072 6.

Prince, S.D. & Justice, C.O. (1991) (eds.): International Journal of Remote Sensing, 12.1

Tucker, C.J., Vanpraet, C.L., Boerwinkel, E. & Gaston, A. (1983): Satellite remote sensing of total dry matter accumulation in the Senegalese Sahel. Remote Sensing of Environment 13, pp 461-474.

GEOMETRIC AND RADIOMETRIC MODELS IN PROCESSING SPOT IMAGERY FOR OBJECT-SPACE SURFACES

J. Wu

National Central University

Taiwan, Republic of China

/...

GEOMETRIC AND RADIOMETRIC MODELS IN PROCESSING SPOT IMAGERY FOR OBJECT-SPACE SURFACES

J. Wu, M. J. Hsyu, C. H. Liu and D. C. Lin

Center for Space and Remote Sensing Research
National Central University
Chung-Li, Taiwan, ROC, 32054

XVII ISPRS Congress in Washington, D.C.
Comm. III , August 2-14, 1992

Abstract

For digital photogrammetry, an integrated approach to image matching and 3D positioning is proposed for stereoscopic SPOT images. The nonlinear functional models for space resection and the integrated approach are explicitly written down. Specifically, we use both piecewise linear models for time-dependent orientation parameters and a patchwise bilinear model for height parameters at elementary ground resolutions.

Our experiments show that fewer than 10 ground control points are more than enough to obtain in resection sub-pixel accuracies ± 7.2m, ± 4.6m and ± 5.5m in a local horizon coordinate system, respectively. The integrated approach can yield in one case a digital elevation model having ± 5m as a height root mean square error, when good approximations to terrain form and large weight constraints on heights are prerequisites.

Based on our experiences up to now, we review at the end our models and discuss their prospects.

Key Words: Space resection with SPOT imagery. Integrated image matching and 3D positioning.

1. INTRODUCTION

For analogue stereoscopic images, conjugate image points are best determined by an operator, e.g., on comparators. Of course, when the number of image points grows, working loads on the operator become very heavy. Thus, people have endeavoured to take full advantage of electronic computers to facilitate image correspondance processes since wide availability of digital images in early 1980's (e.g. Hannah, 1989). And least squares image matching is a representative algorithmic development (Ackermann, 1984). For digital stereo images, general practices follow a two-step solution by determining conjugate image points first and then by intersecting directional imaging rays to arrive at 3D point coordinates.

It is known that photogrammetric point positioning deals with geometric and radiometric distortions which result from taking optical pictures at different times and camera stations. When an analysis model takes perspective displacements, relief displacements and radiometric degradations all into account, the model becomes integral in nature and is more suitable for photogrammetric processing. Our proposed integrated approach to image matching and 3D positioning has been initially tested for aerial photos (Wu and Chang, 1990). Now the approach is applied to SPOT stereo images with a model extension that allows for time-varying characteristics of sensor's orientation along orbital paths.

While our interests in research on this topic are high, we feel motivated by engineers who desire up-to-date wide-coverage accurate height data for planning major governmental civil constructions.

/...

2. MATHEMATICAL MODELS

2.1 Space Resection

Photogrammetric collinearity conditions used for SPOT panchromatic imagery with linear CCD arrays are:

$$x_i + a0_x + a1_x s_i + a2_x s_i^2 = -c\frac{a_{11_j}(X_i - X_{o_j}) + a_{12_j}(Y_i - Y_{o_j}) + a_{13_j}(Z_i - Z_{o_j})}{a_{31_j}(X_i - X_{o_j}) + a_{32_j}(Y_i - Y_{o_j}) + a_{33_j}(Z_i - Z_{o_j})} \quad (1a)$$

$$y_i + a0_y + a1_y y_i + a2_y y_i^2 = -c\frac{a_{21_j}(X_i - X_{o_j}) + a_{22_j}(Y_i - Y_{o_j}) + a_{23_j}(Z_i - Z_{o_j})}{a_{31_j}(X_i - X_{o_j}) + a_{32_j}(Y_i - Y_{o_j}) + a_{33_j}(Z_i - Z_{o_j})} \quad (1b)$$

where c : camera constant;

x_i, y_i : image coordinates of point i and $x_i = 0$;

s_i : strip coordinate in units of length or time;

$X_{o_j}, Y_{o_j}, Z_{o_j}$: time-dependent position parameters at sensor station j when point i is imaged;

$a_{11_j} \ldots a_{33_j}$: elements of an orthogonal matrix; they are functions of time-dependent attitude parameters $\omega_j, \phi_j, \kappa_j$;

X_i, Y_i, Z_i : object-space coordinates of point i;

$a0_x \ldots a2_y$: additional self-calibrating parameters.

In order to be practical for implementation, the time-dependent parameters of exterior orientation $X_{o_j}, Y_{o_j}, Z_{o_j}, \omega_j, \phi_j, \kappa_j$ are described by piecewise continuous linear models:

$$\begin{aligned} X_{o_j} &= (1 - s/d)X_{o_k} + (s/d)X_{o_{k+1}} \\ Y_{o_j} &= (1 - s/d)Y_{o_k} + (s/d)Y_{o_{k+1}} \\ Z_{o_j} &= (1 - s/d)Z_{o_k} + (s/d)Z_{o_{k+1}} \\ \omega_j &= (1 - s/d)\omega_k + (s/d)\omega_{k+1} \\ \phi_j &= (1 - s/d)\phi_k + (s/d)\phi_{k+1} \\ \kappa_j &= (1 - s/d)\kappa_k + (s/d)\kappa_{k+1} \end{aligned} \quad (2)$$

In Eq.(2) d is the separation between two neighboring sensor stations k and $k+1$; station j lies between k and $k+1$, and j is away from k in s units. For space resection, Eqs.(1,2) serve as our functional model in least squares adjustments. Based on weighted ground control points, we estimate mainly the position and attitude parameters $\ldots X_{o_k}, Y_{o_k}, Z_{o_k}, \omega_k, \phi_k, \kappa_k \ldots$ and the self-calibrating parameters.

2.2 Integrated Approach to Image Matching and 3D Positioning

The method of least squares image matching for stereo images can be written as

$$v''_{g'_i} = g'(x'_i, y'_i) - r_0 - r_1 g''(x''_i, y''_i); p''_{g'_i} \quad (3a)$$

in which g', g'' : gray-value functions evaluated at two corresponding image points x'_i, y'_i and x''_i, y''_i;

r_0, r_1 : radiometric additive and multiplicative parameters;

$v''_{g'_i}, p''_{g'_i}$: gray-value residual and its associated weight.

Logically and in a straitforward manner, the collinearity conditions Eqs.(1 with 2) can be used for pairs of image coordinates in Eq.(3a); and in vector notation, we get

$$v''_{g'_i} = g'(Z_i, \mathbf{p}', \mathbf{a}) - r_0 - r_1 g''(Z_i, \mathbf{p}'', \mathbf{a}); p''_{g'_i} \quad (3b)$$

where $\mathbf{p}', \mathbf{p}''$: vectors for position and attitude parameters along single- and double-prime orbital paths, respectively;

$\mathbf{a}$: vector for self-calibrating parameters.

/...

In order to be feasible, height Z_i at the center of each ground resolution X_i, Y_i is described by patchwise continuous bilinear models:

$$Z_i = \frac{(X_{m+1} - X_i)(Y_{n+1} - Y_i)}{(X_{m+1} - X_m)(Y_{n+1} - Y_n)} Z_{m,n} + \frac{(X_i - X_m)(Y_{n+1} - Y_i)}{(X_{m+1} - X_m)(Y_{n+1} - Y_n)} Z_{m+1,n}$$
$$+ \frac{(X_{m+1} - X_i)(Y_i - Y_n)}{(X_{m+1} - X_m)(Y_{n+1} - Y_n)} Z_{m,n+1} + \frac{(X_i - X_m)(Y_i - Y_n)}{(X_{m+1} - X_m)(Y_{n+1} - Y_n)} Z_{m+1,n+1} \qquad (4)$$

Heights $\ldots Z_{m,n}, Z_{m+1,n}, Z_{m,n+1}, Z_{m+1,n+1} \ldots$ at nodes of a square grid are treated as primary unknown parameters in the combined Eqs.(3b,4).

In fact, $\ldots Z_{m,n} \ldots$ stand for the digital elevation model (DEM) we are interested in. So, we conduct iterative digital image matching by minimizing the weighted sum of squares of gray-value residuals and, simultaneously, arrive at object-space 3D point determination. For theories in a stricter sense that gray-value "truth" with each ground resolution is also asked for, readers can refer to among others Ebner and Heipke(1988) and Wrobel(1991).

3. EXPERIMENTS WITH SPOT IMAGERY

A stereoscopic SPOT image pair is selected for studying our models, see Table 1.

As far as the model for space resection with Eqs. (1,2) is concerned, we summarize accuracy results at 25 independent check points in Table 2. The number for dynamic sensor stations varies from 3 to 5. Ground control coordinates have throughout $\pm 50m$ a priori standard deviations while 6 additional self-calibrating parameters are treated as free parameters. Better accuracies result when 4 sensor stations are chosen, a plot of which is shown in Fig.1. We also see that cross-track accuracy in Y is better than along-track accuracy in X. This confirms the fact that SPOT imagery shows better cross-track geometric quality. When two ground control points lie between two adjacent sensor stations a solution for space resection can converge regularly, i.e. nonlinear Eqs. (1,2) are fulfilled in about 7 iterations to within $1.0 \times 10^{-5}[mm]$.

Space resection for SPOT stereo images yields the orientation parameters $\mathbf{p}', \mathbf{p}''$ and a for use in Eqs.(3b,4). The parameters are held fixed when performing experiments with respect to the model integrating image matching and 3D positioning. Our national $40 \times 40m^2$ digital terrain model (DTM) is derived from conventional aerial photographies using analytical plotters. Use of the DTM is made to interpolate heights for $20 \times 20m^2$ or $50 \times 50m^2$ grids. They represent reference heights adopted in comparison with heights estimated form SPOT sub-images, see upper left quadrants in Fig.2a. Table 3 reveals typical results on generation of digital elevation models. In general, the nonlinear functional relationship Eqs.(3b,4) can be satisfied at 95% to within 0.1 digital counts in 10 iterations. We notice that the integrated approach works for spaceborne images but weight constraints have to be imposed on the estimated height parameters. Extensive cases are still being studied. In particular, it is required to construct more reliable reference DEMs for accuracy analyses.

After geometric relationship between object-space elements and picture elements is reconstructed in a convergent solution, direct by-products out of the integrated approach are orthographic images. Fig.2a illustrates digital orthographic images. Their difference image and its histogram are shown in Fig.2b from which it is evident that the mean of differences in gray values is near zero and the distribution nearly Gaussian.

4. DISCUSSIONS

For SPOT imagery, our mathematical models used in space resection and in the integrated approach to image matching and 3D positioning are documented. In the course of our experiments, piecewise continuous linear modeling for time-dependent position and attitude parameters appears quite realistic when we consider the fact that SPOT stereo images of about 4° field of view have in our case 0.65 as a base-to-height ratio. SPOT scene CCTs contain orbital information, see CNES and SPOT Image(1988), which

/...

Table 1. Brief description of a pair of panchromatic 1A images over central Taiwan from SPOT.

Base to height ratio :	0.65	
Heights above ground	827338 m	827271 m
Sensors on SPOT	HRV2	HRV1
Incidence angles	L10.4°	R24.1°
Data acquired on	15 Jan. 1987	16 Jan. 1987
Overlapping area :	57 km × 40 km	

Table 2. Accuracies in terms of root mean square errors in a local horizon system at 25 stationary check points.

		3 stations			4 stations			5 stations		
		Accuracies [m] at check points in								
		X	Y	Z	X	Y	Z	X	Y	Z
GCPs	25	6.83	4.66	7.20	7.16	4.51	5.17	7.43	4.72	5.64
	20	6.73	5.01	7.28	6.89	4.76	5.31	6.75	4.86	6.15
	15	6.97	5.69	7.48	7.41	5.05	5.59	6.46	5.03	6.63
	10	7.56	5.95	7.37	7.24	4.64	5.52	7.56	4.66	6.26
	6	8.25	5.26	7.81	7.54	5.95	6.32	11.59	67.48	148.10
	3	90.11	580.10	340.00	94.06	575.00	626.60	112.40	659.50	838.10

Table 3. Accuracies in height derived from the integrated model for image matching and 3D positioning (radiometric parameters r_0, r_1 in Eq.(3b) get little weighting; in the $1 \times 1 km^2$ test area maximum height difference $\Delta h_{max} = 81.49m$).

Height approximation using	terrain form given		average plane	
A priori standard deviations for heights	± 30m	± 5m	± 30m	± 5m
Height accuracies [m] by the integrated approach				
50 × 50 m grid (21 × 21 nodes)	16.39	8.61	16.58	11.56
20 × 20 m grid (51 × 51 nodes)	16.14	4.89	17.64	11.11

/...

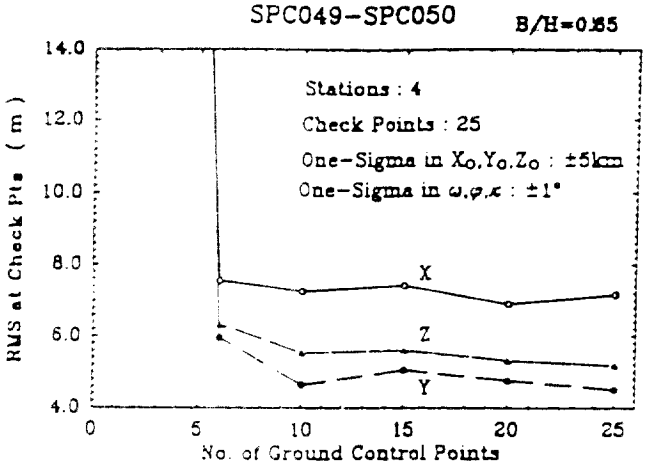

Fig.1. Plot of accuracies in X,Y,Z for 4 sensor stations (refer to Table 2).

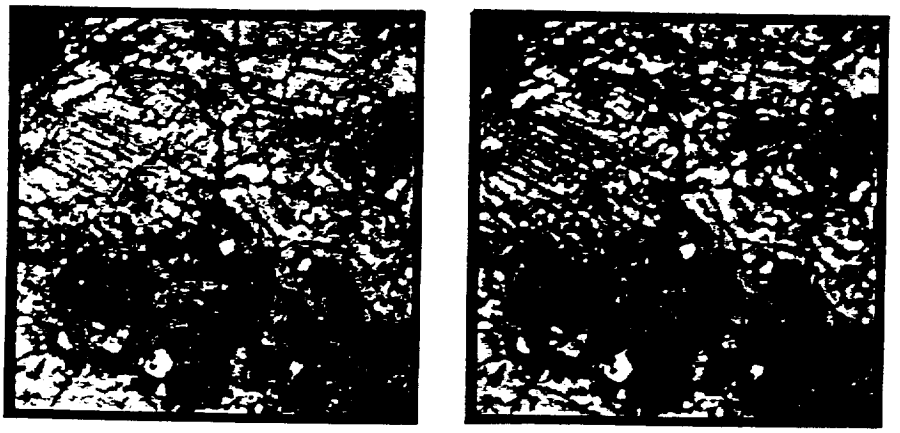

From the left SPOT subimage

From the right SPOT subimage

Fig.2a. Orthographic images ($2 \times 2km^2$ in size; $50 \times 50m^2$ grid meshes; 41×41 grid nodes).

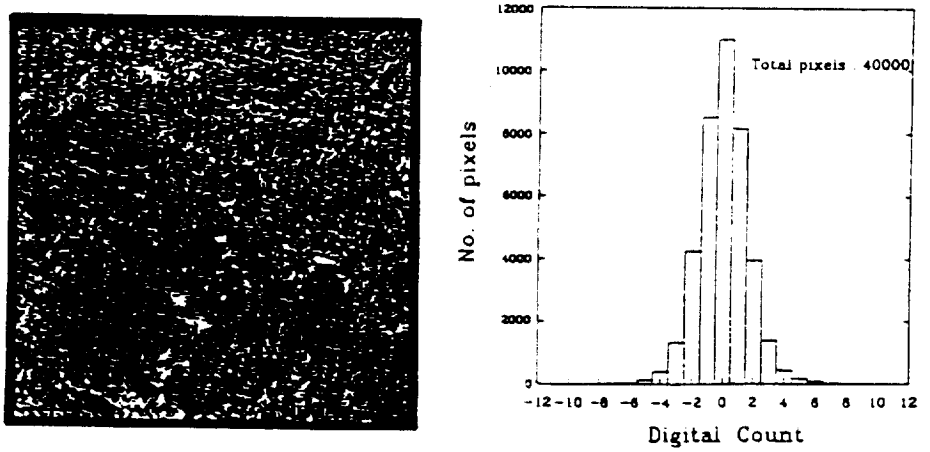

Fig.2b. Difference image (enhanced) between the two ortho-images in Fig.2a; shown to the right its histogram (σ = 1.6078 digital counts at 1 sigma).

/...

is used by us to generate initial approximate orientation parameters along orbital paths. We conclude that fewer than 10 ground control points are quite enough for space resection (Chen and Lee,1990). It is interesting to note that the resection procedure is equally applicable to a single SPOT scene or to multiple scenes in stereoscopy. As far as improvements on additional self-calibrating parameters are concerned more research on our part is necessary.

One of the purposes in studying our integrated model for image matching and 3D positioning is to test its applicability to spaceborne stereo imagery. We know there is an advantage in theoretical analysis on error propagation; it is a worthy trade-off when thinking about rather heavy computational loads. Another advantage inherent in the integrated approach is automatic generation of orthographic (sub-)images along with that of a dense digital elevation model. Currently, we must impose weights in form of a diagonal matrix on unknown height parameters of DEMs. This arises in part from the fact there exists locally no or little image contrast in SPOT sub-images. Therefore, our on-going research efforts are led to

- determine in image preprocessing weighting functions that allow for gray-value contrast, textures or features in (sub-)images;
- design regional radiometric parameters to replace two global parameters r_0, r_1 in Eq.(3b);
- discover methods of interpolation more realistic than those by non-differentiable, continuous piecewise linear or patchwise bilinear modeling;
- as a long-term goal correct radiometrically for atmospheric effects and terrain effects to arrive at normalized reflectance images for photogrammetric multi-point positioning.

At last, we kindly acknowledge the research funds provided by the Sinotech Foundation for Research and Development of Engineering Sciences and Technologies.

5. REFERENCES

Ackermann, F.,1984. High precision digital image correlation. Proc. of the 39th Photogrammetric Week, Stuttgart, pp.231-243.

Chen, L.C. and Lee, L.H., 1990. A systematic approach to digital mapping using SPOT satellite imagery. Journal of the Chinese Institute of Civil and Hydraulic Engineering 2(1), pp.53-62.

CNES and SPOT Image, 1988. SPOT users' handbook. Volumes 1 and 2.

Ebner, H. and Heipke, C., 1988. Integration of digital image matching and object surface reconstruction. Int. Arch. Photogramm. Remote Sensing 27(B11), pp.III-534 to III-545.

Gruen, A.W. and Baltsavias, E.P., 1987. High-precision image matching for digital terrain model generation. Photogrammetria 42, pp.97-112.

Hannah, M.J., 1989. A system for digital stereo image matching. Photogrammetric Engineering and Remote Sensing 55(12), pp.1765-1770.

Heipke, C., 1992. A global approach for least-squares image matching and surface reconstruction in object space. Photogrammetric Engineering and Remote sensing 58(3), pp.317-323.

Rosenholm, D., 1987. Multi-point matching using the least-squares technique for evaluation of three-dimensional models. Photogrammetric Engineering and Remote Sensing 53(6), pp.621-626.

Westin, T., 1990. Precision rectification of SPOT imagery. Photogrammetric Engineering and Remote Sensing 56(2), pp.247-253.

Wrobel, B.P.,1991. Least-squares methods for surface reconstruction from images. ISPRS J. Photogramm. Remote Sensing 46, pp.67-84.

Wu, J. and Chang, J.H., 1990. An algorithm for point positioning on digital images and in object space. Int. Arch. Photogramm. Remote Sensing 28(5/2), pp.1196-1202.

/...

IMAGE PROCESSING: EDGE AND FEATURE EXTRACTION, LINEAR FEATURE EXTRACTION, GENERAL SEGMENTATION, IMAGE MATCHING AND OBJECT ORIENTATION

J.C. Trinder

University of New South Wales

Sydney, Australia

/...

ISPRS CONGRESS WASHINGTON 1992

UNITED NATIONS/ISPRS WORKSHOP ON REMOTE SENSING, DATA ANALYSIS METHODS AND APPLICATIONS

THURSDAY - FRIDAY, 6 - 7 AUGUST 1992

Image Processing:

Edge and feature extraction

Linear feature extraction

General segmentation

Image matching

Object reorientation

by

Professor J.C. Trinder
School of Surveying
University of New South Wales
P.O. Box 1, Kensington, NSW 2033
Sydney, Australia

/...

IMAGE PROCESSING

The goal of image processing is the quantitative description of physical objects on the basis of information extracted from digital images or digital image sequences.

The main procedures involved in the image processing are:

* Filtering and enhancement of the image data

* Geometric corrections of the images

* Feature extraction

* Segmentation and classification

* Image matching

* Object recontruction

/...

IMAGE PROCESSING

FEATURE EXTRACTION

STEPS

* Data preparation --

Preprocessing

* Extraction of Information --

Detection

* Semantic interpretation of extracted information

Recognition

PREPROCESSING

* Radiometric Corrections
* Geometric Correction
* Filtering
* Enhancement

/...

CONVOLUTION

Continuous Function in one dimension

$$y(t) = \int_{-\infty}^{+\infty} x(t-\tau)g(\tau)d\tau$$

where: $x(t)$ = **input signal**

$y(t)$ = **output signal**

$g(\tau)$ = **characteristic filter**

or $y(t) = x(t) * g(\tau)$

Two dimensional formulas also possible

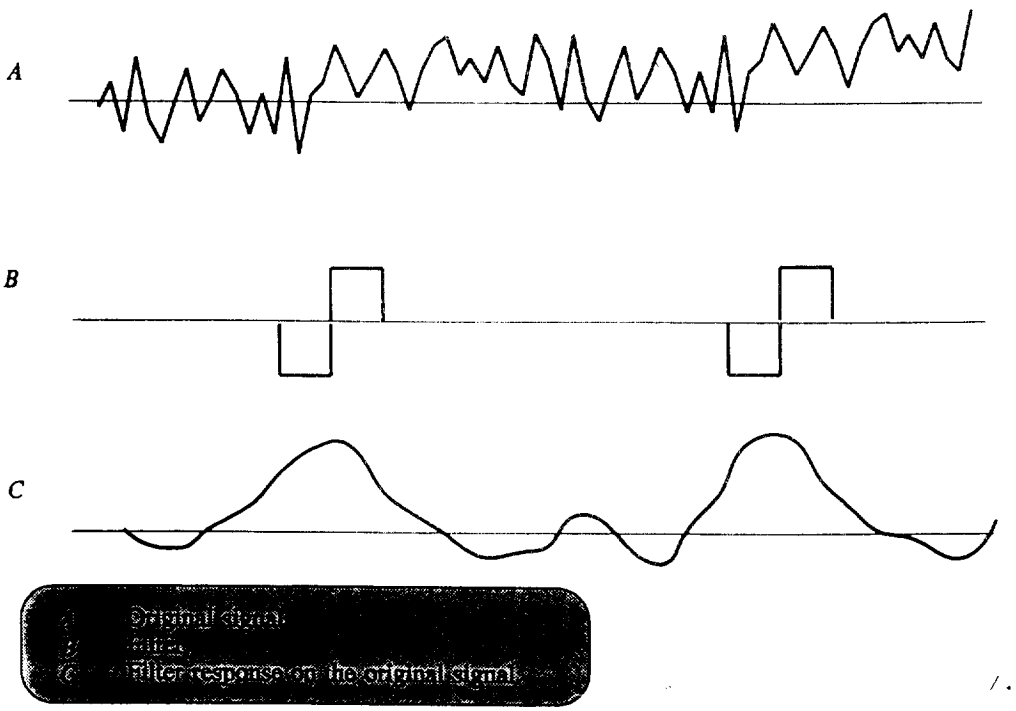

A. Original signal
B. Filter
C. Filter response on the original signal

/...

Discrete Pixels

$$y_i = \sum_{k=-\infty}^{\infty} g_k x_{i-k} \ , \ i = 1,2,..n$$

where n is the number of pixels in window

or

$$y_i = \sum_{k=\frac{-n}{2}}^{\frac{n}{2}} g_k x_{i-k}$$

Convolutions of small windows, which represent the convolution function, and the image can be computed by scanning the window across the image. The convolution window is centred on each pixel on the image and the combination of that window, and the image is computed.

Windows vary in sizes according to the application, but are typically

3x3
2x2
1x3 and 3x1

/...

Example

Steps

1. Overlay windows A and B
2. Multiply the values of the pixels which overlay one another
3. Add up values derived in step 2
4. Assign the value from step 3 to the pixel which corresponds with the centre of the convolution window

10	10	10	10	10
10	10	10	10	10
10	10	20	10	10
10	10	10	10	10
10	10	10	10	10

A
Image window

*

1/9	1/9	1/9
1/9	1/9	1/9
1/9	1/9	1/9

B
Convolution window

=

11	11	11
11	11	11
11	11	11

/...

FILTERING

Image contains information about physical objects plus noise

Prior to image enhancement procedures, it is necessary to reduce the effects of noise by **smoothing or averaging**

Noise is high frequency information, but not useful

Smoothing will reduce the effects of high frequency noise

Smoothing will have disadvantage of also reducing the useful high frequency components in the image

Smoothing introduces loss of image quality in the image

/...

Examples:

1. Simple average of neighbours

10	10	10	10	10
10	10	10	10	10
10	10	20	10	10
10	10	10	10	10
10	10	10	10	10

*

1/9	1/9	1/9
1/9	1/9	1/9
1/9	1/9	1/9

=

11	11	11
11	11	11
11	11	11

The effects of the noisy pixels will be reduced, but the remainder of image will be smoothed with a slight decrease in the quality of the detail.

The size of the neighbourhood used for the averaging, and hence the size of the window, can be varied depending on the degree of noise.

/...

The number of neighbours can be selected according to the sum of the grey levels in the neighbouring pixels. The size of the area used will be determined when this sum reaches a certain criterion. If the grey values are small, the area will consequently be large.

2. Weighted average of neighbours

Select a weighting which does not effect the significant details on the image, such as edges.

Directional averaging

Locate edges and perform smoothing along the edges, not across them.

Use a set of edge detection masks in 4 orientations

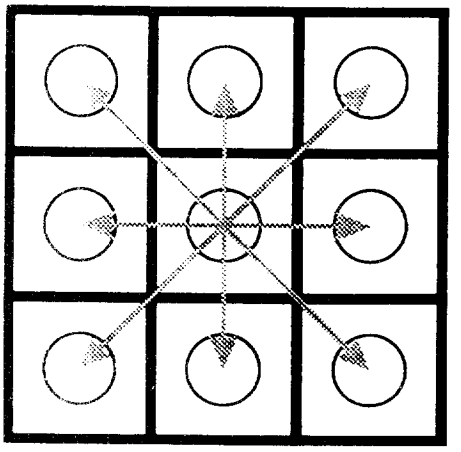

Determine variation in pixel values

/...

If range of values at a given point exceeds a threshold say 't', the point is replace by the average of its neighbours in the direction of minimum edge variation, otherwise the value of the point is replaced by the average of the 8 neighbouring pixels .

The method uses an average of 2 or 8 pixels depending on whether an edge is detected.

Directional Minimum variance

Similar to the previous except it analyses the variance in the various directions

III. Actual computation

III.1. Smoothing : directional min. variance

Set of nine 5x5 masks :

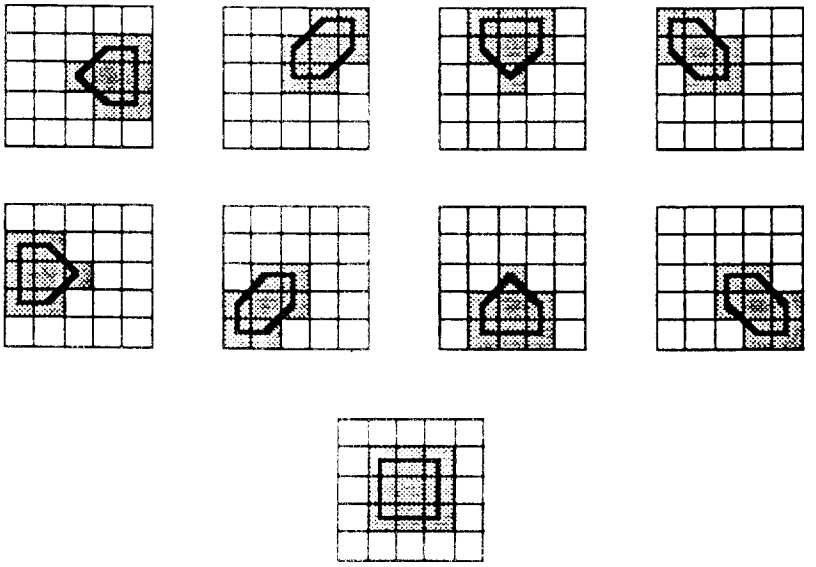

These masks are used for computing the local mean and variance in each direction.
The central value of the window is then replaced by the mean of the corresponding minimum variance direction.

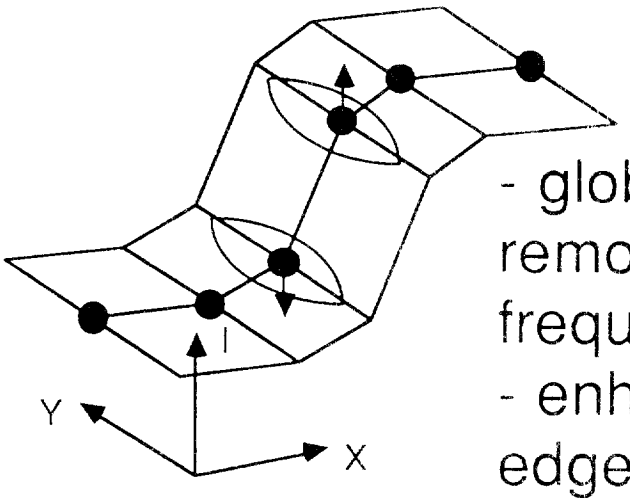

<u>resulting effects :</u>

- global low pass filtering, removing the high spatial frequencies of the noise
- enhancement of the edge definition

/...

3. 5 Neighbours

Select 5 nearest neighbouring pixels with intensity values that are nearest to that of the particular point, and use the average of these pixels.

4. Median filter

Replace the value of a pixel by the median of values in a neighbour.

0 0 0 6 0 0 1 2 1 0 1 2 1 0 2 4 2 0 2 4 2 0 0 1 2 3 4 4 4 4 4

Replace each value by its median

If values are a,b,c and b is between a and c then b is the median.

Result is

0 0 0 0 0 0 1 1 1 1 1 1 1 1 2 2 2 2 2 2 0 0 1 2 3 4 4 4 4 4

The noise is eliminated, but the median filter does not blur edges.

Plot of the example of application of median filter

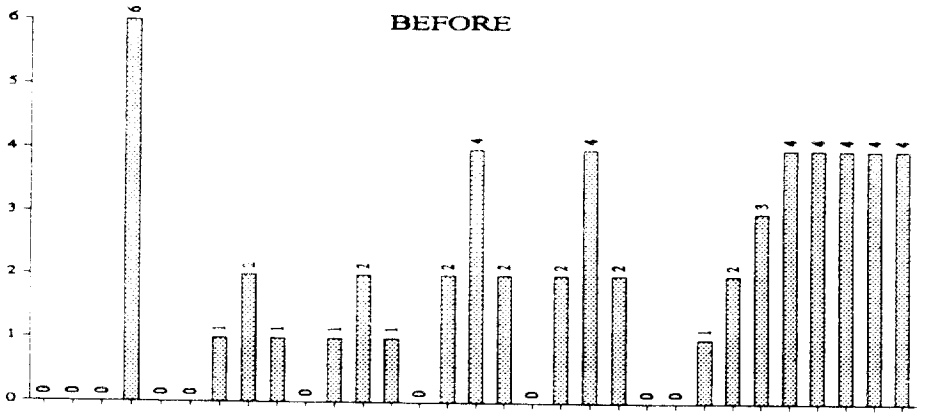

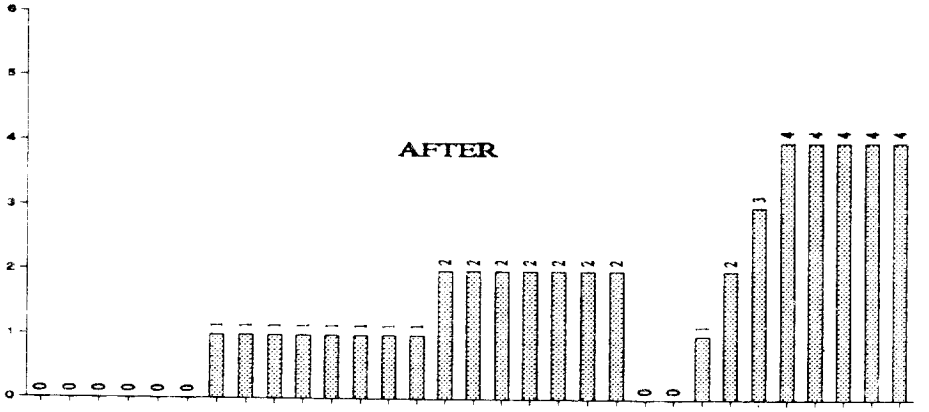

A 2-dimensional median filter can be applied by sorting the values of the neighbouring pixel in terms of size and selecting the middle value for the central pixel. For a 3x3 (9 pixel values) the fifth largest value is taken.

/...

ENHANCEMENT or SHARPENING

Blurring in an image is an averaging or integration process, which weakens the higher spatial frequencies in the image. Enhancing aims to emphasis the spatial higher frequencies.

These operators enhance or sharpen the effects of features in an image but they also enhance noise. It is therefore desirable to apply enhancement where the picture detail are more prominent than the noise. Alternatively, smoothing should be applied first.

The Laplacian is a linear derivative operator, which is based on the slopes in the x and y directions. An example of the application of this filter is as follows:

1	10	1
1	10	1
1	10	1

*

0	-1	0
-1	4	-1
0	-1	0

=

-8	36	-8
-8	36	-8
-8	36	-8

/...

The Laplacian operator is derived from the slopes of the neighbouring pixels in the x and y directions as follows:

$$g'(i,j)=[g(i+1,j)+g(i-1,j)+g(i,j+1)+g(i,j-1)] -4g(i,j)$$

It can also be interpreted as the central pixel minus the average of the 4 neighbouring pixels.

i-1,j-1	i,j-1	i+1,j-1
i-1,j	i,j	i+1,j
i-1,j+1	i,j+1	i+1,j+1

/...

EXTRACTION OF INFORMATION

Detection

EDGE EXTRACTION

STEPS

* Smoothing
* Edge Detection
* Thresholding
* Thinning
* Linking

EDGE DETECTION

Gradient

Gradient in intensity between neighbouring pixels in x and y directions is derived by:

$$\Delta \mathbf{g}_x = (\mathbf{g}_{i+1,j} - \mathbf{g}_{i,j})$$

$$\Delta \mathbf{g}_y = (\mathbf{g}_{i,j+1} - \mathbf{g}_{i,j})$$

where i,j refer to pixel numbers in x- and y-direction respectively

Gradient Orientation

Defined as the direction of the gradient from the combination of the gradients in x and y directions is given by:

$$\tan\theta = \Delta \mathbf{g}_y / \Delta \mathbf{g}_x$$

Operators or also called masks that have been used for edge detection have been grouped under the following heading

/...

DIFFERENCE OPERATORS

Difference operators derive the difference in gradient in the x and y directions and combine them by the formula

$$\Delta g = \sqrt{(\Delta g_x^2 + \Delta g_y^2)}$$

Non-centred gradient operators measure differences asymmetrically with respect to the pixel.

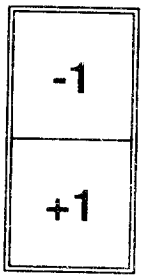

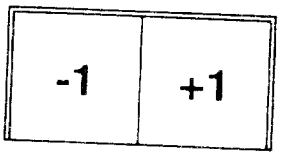

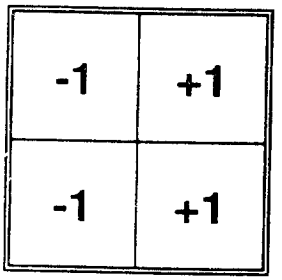

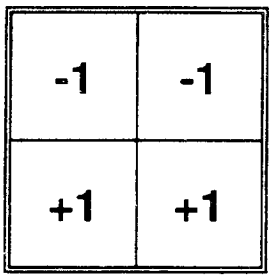

Centred Gradient operators measure 'central differences'

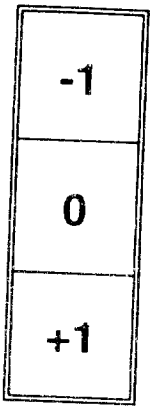

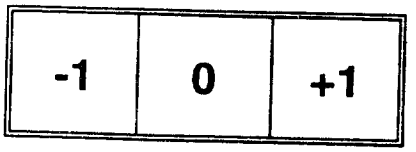

/...

Roberts operator measures 45° and 135° changes.

0	1
-1	0

1	0
0	-1

Differences of Averages. The pixels are weighted by local averaging before differencing. A typical operator in the x- and y-direction is as follows:

1/4

-1	-1	1	1
-1	-1	1	1

1/4

-1 -1
-1 -1
1 1
1 1

/...

The Sobel operator applies weighting to the averaging as follows:

1/4

-1	0	1
-2	0	2
-1	0	1

1/4

1	2	1
0	0	0
-1	-2	-1

Fixed masks are applied by matching patterns with various orientations to the picture for the detection of edges. The orientation which matches best that of the edge of the picture is taken as the edge orientation. The magnitude of the best match is a measure of its strength.

Foerstner operator is primarily designed for the detection of points, but can also be used for extracting edges. It is based on a set of two requirements for the error ellipse which is calculated from the grey values within the window.

A **Hough** transformation has been used sucessfully for edge description on remotely sensed data.

/...

Canny operator

In computing science circles, the operator developed by Canny has greater flexibility detecting edges than most other operators.

Canny sets 3 performance criteria for an effective edge operator:

* low error rate

* selected edge should be close to the 'true' edge

* there should be only response to a single edge

The Canny operator aims to maximise the signal to noise ratio of the image, where the signal represents the feature and the noise and is assumed to be Gaussian.

Selection of an Operator

The selection of edge operators will depend on their suitability for a particular task, since their performance may vary over image. In one test on the application of different operators for the detection of linear features on remotely sensed data, the difference of average operators, such as the Sobel, were found to be superior. However, the Sobel operator tends to produce duplicate edges on each side of the feature.

In another test, the simpler 2x2 masks proved to be suitable. The poor dynamic range of remotely sensed images can lead the non-extraction of essential features in the image that are clearly visible to an observer. In addition, linking of edges becomes difficult in images where there are many edges.

An edge extraction process which involves the selection of edges with like slope orientations as line support regions, has proved successful.

THRESHOLDING

Thresholding involves the conversion of the image comprising the extracted edges into a binary image, where only the edge features are displayed in white and the background in black.

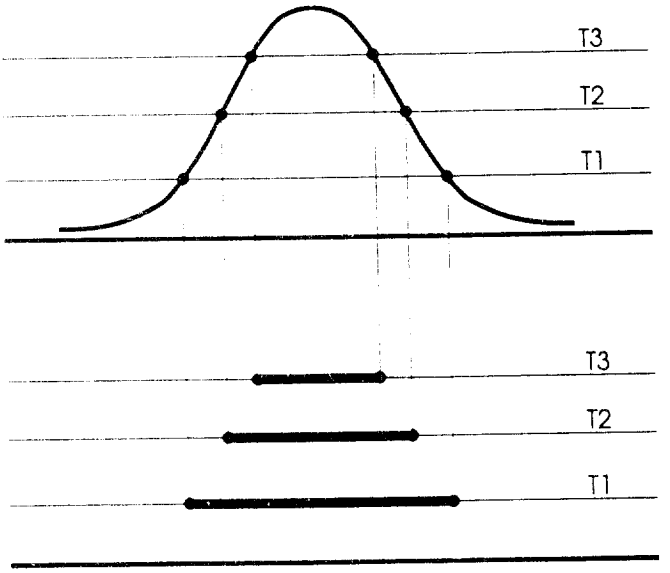

/...

THINNING

The process of thinning is carried out if the edge extracting process produces edges which comprise more than one pixel in width. This process is necessary because the next step of line following or linking, which connects the individual pixels into linear features is difficult when the lines are made up of a number of pixels.

Line thinning can be carried out by a number of different methods. These methods can be grouped into:

* those which analyse the width of the lines represented by the pixels and detect the centre of the line,

* those which study the slope and orientation of each pixel, and determine the most likely position of the actual edge.

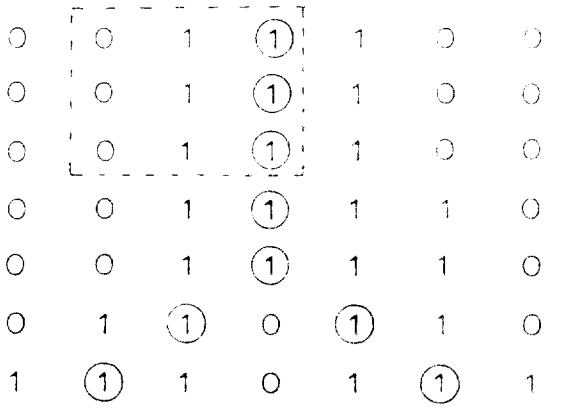

/...

LINKING

Linking connects the pixels, which represent the edges, into linear features. A major problem with this task is to determine whether gaps, which appear between the selected edge pixels, are indeed gaps, or whether they have been caused by the previous processing steps undertaken on the image. Linking converts the image from a raster display of the edges into vectors which can be described by length and direction.

Linking algorithms use several possible **criteria of connectivity** to determine the most likely pixels which form the edge, based on either on simple connection of pixels, to statistical and directional analysis of the neighbouring pixels.

/...

A morphological analysis, based on masks representing possible edge features may also be used.

- morphological analysis

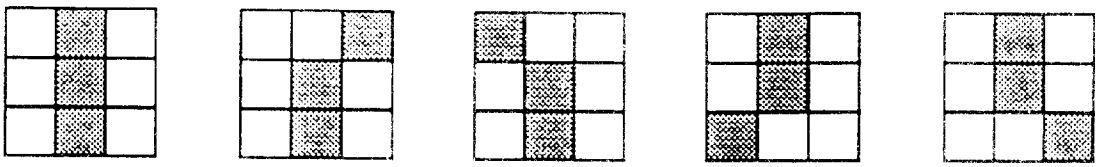

possible pixels configuration for a vertical line

The method based on **gradient orientations** and line support regions, described earlier, will enable the grouping of the pixels which have like orientations and therefore the formation of linked pixels.

Foerstner operator.

The Foerstner operator has been briefly described earlier for the edge operator and has been specially designed for point features. It has proved very successful as an interest operator.

SEGMENTATION

The process of segmentation of an image involves the division of an image into areas that represent certain features or certain common characteristics.

The processes that may be involved are:

* Edge detection can be used to define the identifiable boundaries of regions. The detection and linking of the edge pixels, as described above, will form vectors which can be further linked to form areas.

* Classification of an image into various classes will result in segmentation into regions, which in this case are described by the raster image and not as vectors. Conversion into lines and areas will require the extraction of the divisions between the classes as vectors and their linking.

/...

* Segmentation by thresholding. In this case the thresholding can be set to segment the image into certain intensity ranges. Either global or multi-level thresholding can be used. Thresholding is a simple and rapid method if division of the area by intensity value is adequate.

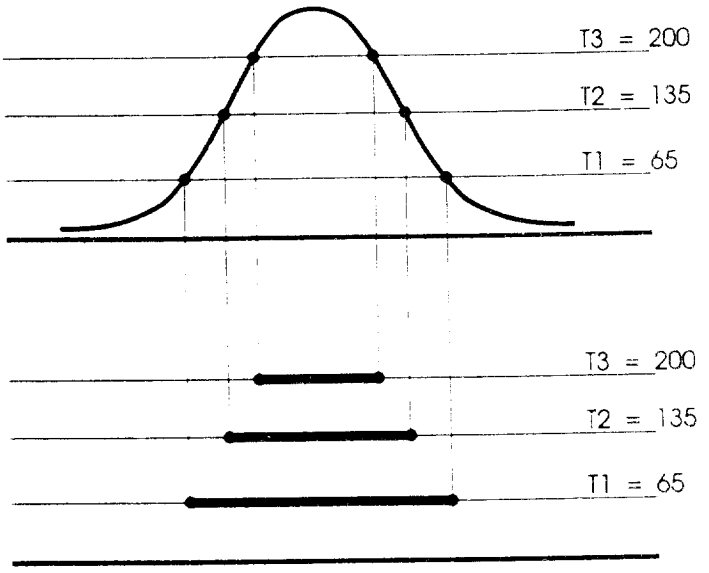

/...

IMAGE MATCHING

AIM: To find areas in two images of the same area which correspond either their features or grey values.

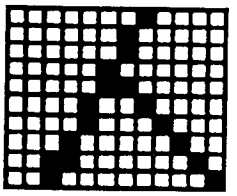

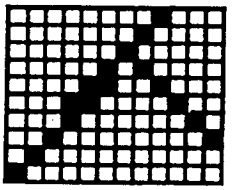

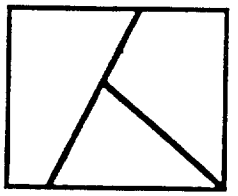

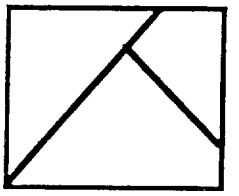

Image matching can be divided into 2 steps:

* Feature extraction and matching

* Area based matching

Feature based matching requires the derivation of features in the two images and determining which ones match. It serves to provide approximate positions for the area base matching.

Point features:

Interest operators determine points which are prominent in the two images. Matching determines which features have similar characteristics with respect to grey values and relative locations.

Linear features:

Require the extraction of linear features by edge detectors and matching by their characteristics eg, length, direction etc

Areal features:

Not well developed, but is based on segmentation.

/...

STAGE I.

EXTRACTION OF THE INTEREST OBJECTS.

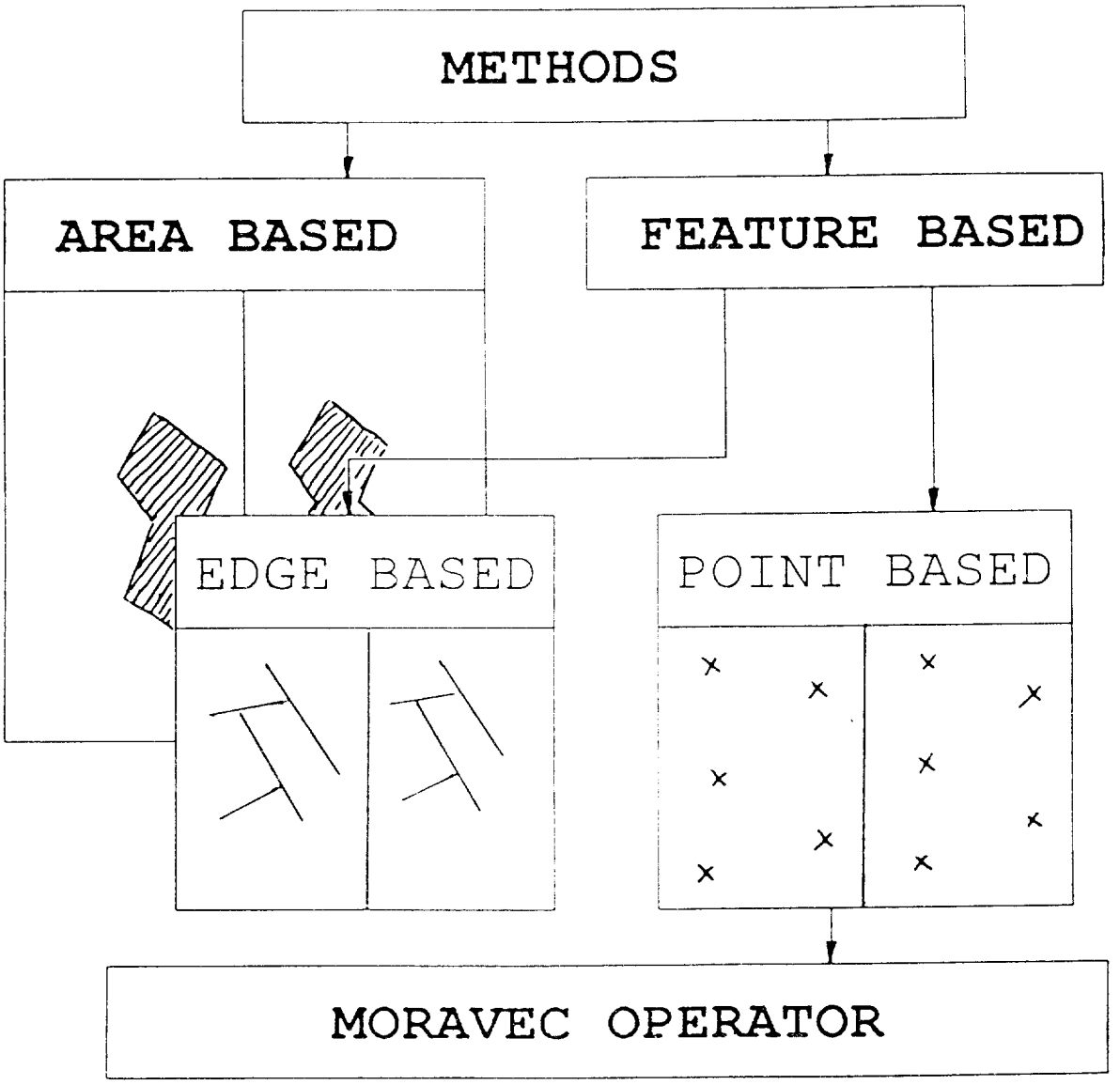

/...

Moravec operator.

THE OPERATOR OF MORAVEC LOOKS FOR THE SMALL, ISOLATED PEAKS AND "BLACK HOLES" IN THE IMAGE.

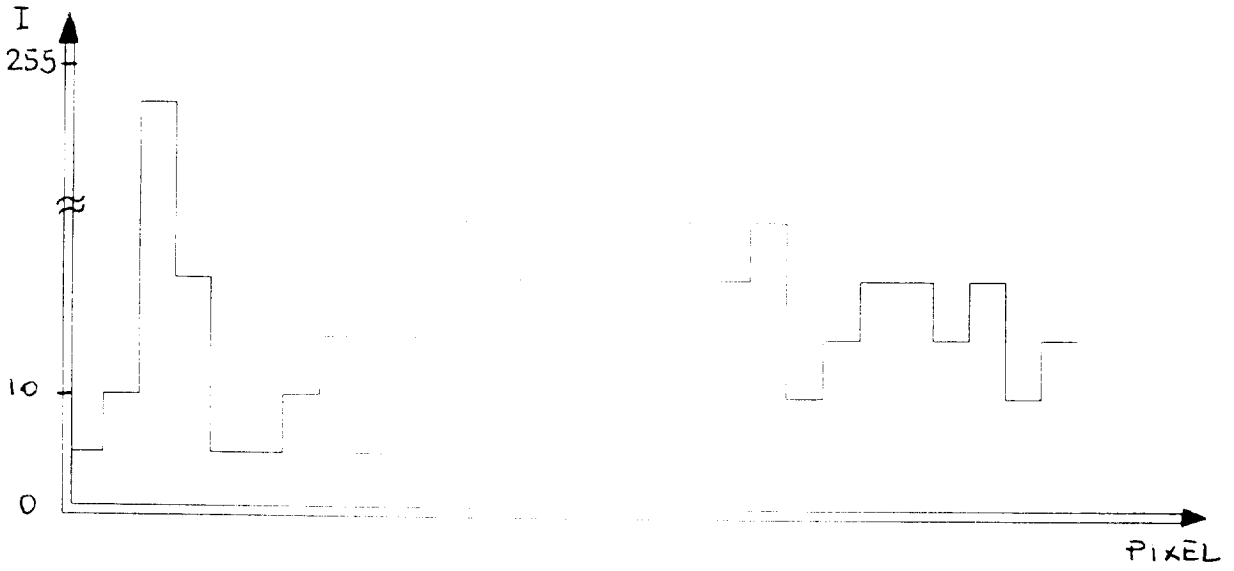

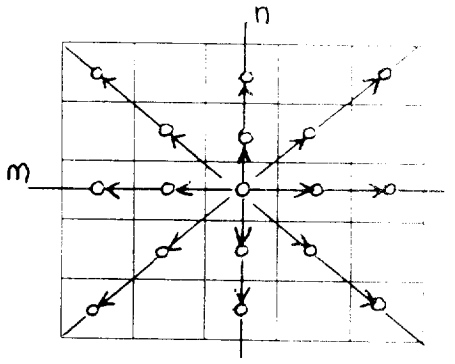

$$M = \min \begin{cases} \sum (G_{i,j} - G_{i,j+1})^2 \\ \sum (G_{i,j} - G_{i-1,j})^2 \\ \sum (G_{i,j} - G_{i+1,j+1})^2 \\ \sum (G_{i,j} - G_{i+1,j+1})^2 \end{cases}$$

$i = n - k, \ldots, n - k;$
$j = m - k, \ldots, m - k;$
k - size of Moravec's window.

M is OK if M > $M_{\_}$ - (THRESHOLD)

/...

THE IMAGE MATCHING

PROBLEM:

How to find corresponding objects in the left and right images without human assistance ??

POETIC APPROACH

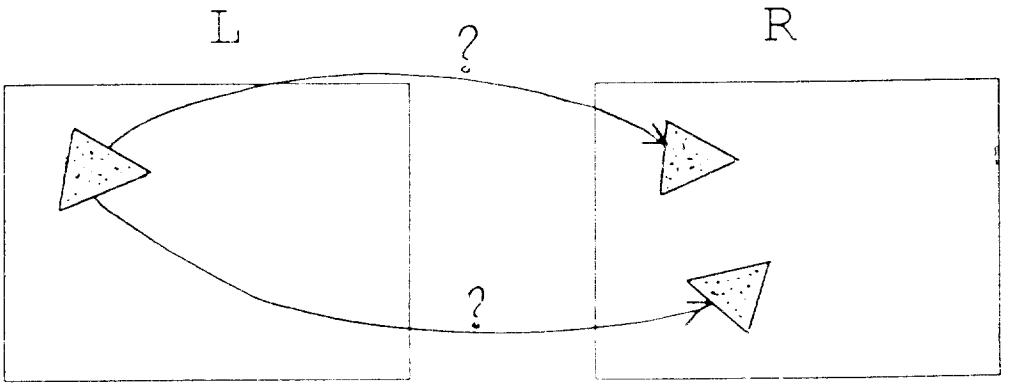

This one, or that one ???
That is the question !!!

/...

Area Based Matching

Methods

* Cross-correlation

This method computes the similarity between two images by the use of the well known cross-correlation formula. This formula in principle is similar to the formula given for the convolution, except in this case one image is scanned over the other.

The formula is a follows:

/...

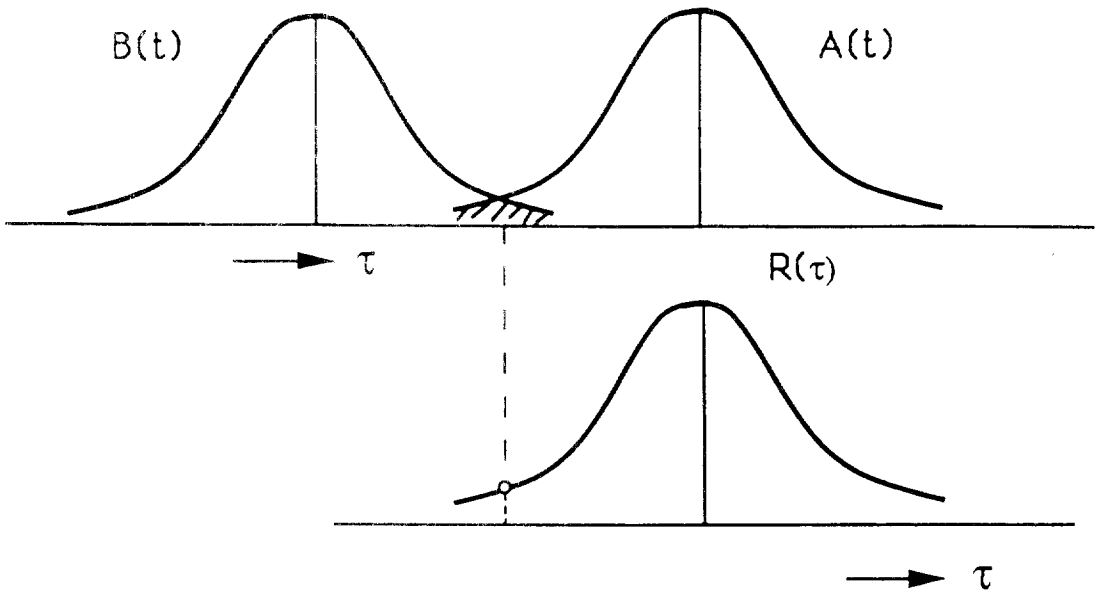

$$R(\tau) = \frac{1}{2T} \int_{-T}^{T} A(t)\, B(t + \tau) \cdot dt$$

Where A (t) is grey level distribution on a reference window.

B (t) is grey level distribution on a search window.

τ is a displacement applied to B (t) to determine the best match.

/...

Application to Pixel Data

For pixel data, a window on one image, let us assume that it is the right or 'search' window, is scanned over a window of the same size on the left or target window. For the areas common to the two windows, the grey values of the overlapping pixels are multiplied and added for the determination of values of the correlation. An evaluation of the location where the correlation is a maximum will determine the location of matching. The resolution of this method is 1 pixel, but sub-pixels resolution can be determined by interpolating a polynomial and deriving the maximum.

The cross-correlation will result in erroneous matches when the images are subject to differences in scale and rotations.

$$\mathbf{R} = \frac{\sum(g_1 - g_1')(g_2 - g_2')}{\sqrt{\sum(g_1 - g_1')^2 \cdot \sum(g_2 - g_2')^2}}$$

where g_1, g_2 are grey values in windows 1, 2

g_1', g_2' are average grey values of windows 1, 2

/...

1	2	2	2	3	3	4	4	5	5
1	**2**	**3**	**2**	3	3	4	4	5	5
3	**3**	**3**	**3**	3	4	4	4	5	5
1	**2**	**3**	**2**	**9**	**3**	3	3	2	3
2	2	2	**9**	**9**	**9**	3	3	3	3
2	2	3	**2**	**9**	**3**	3	3	3	3
4	4	5	5	4	4	5	6	3	2
4	5	5	4	4	6	**6**	**1**	**5**	3
5	4	5	6	4	5	**1**	**1**	**1**	4
1	2	2	2	3	2	**4**	**1**	**4**	5

1	**9**	1
9	**9**	**9**
1	**9**	1

Results: Position (3,3)..... R = 1.00
Position (5,5)..... R = 0.99
Position (9,8)..... R = 0.96

/...

Least Squares Matching.

This method computes the location of matching by minimising the discrepancies between the corresponding pixels. To overcome the effect of differences on geometry, one of the windows, the search window, is resampled, that is its geometry is changed so that it is similar to that of the target window. the parameters of the geometric transformation are determined during the computation.

/...

Area Based matching by Least squares

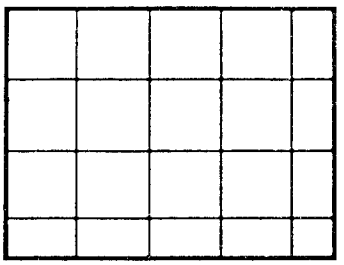
Im

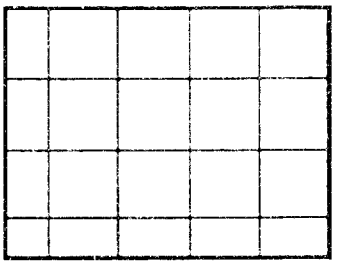
It

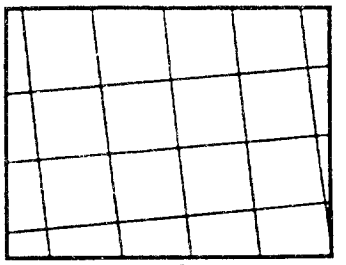
Is

Define windows as follows:

I_m (x_m, y_m) are pixel values in mask window (first image)

I_t (x_t, y_t) are pixel values in a fictitious target image window on the second image, with the same geometry as mask window.

and

I_s (x_s, y_s) are pixel values in a search window in the same position as target window, but with the true geometry of the second image.

/...

Relationship between geometry of I_t and I_s is :

$$x_t = f_1 (x_s , y_s) \quad (3)$$

$$y_t = f_2 (x_s , y_s) \quad (4)$$

$$I_t = f_3 (I_s) \quad (5)$$

Requirement for matching is that for each pixel:

$$I_m (x_m, y_m) + n (x_m, y_m) = I_t (x_t, y_t) \quad (6)$$

where $n(x_m, y_m)$ is arbitrary noise.

Relationship between mask and search window geometries

$$x_t = p_1 + p_3 x_s + p_4 y_s \quad (7)$$

$$y_t = p_2 + p_5 x_s + p_6 y_s \quad (8)$$

/...

Solution : -

- Least squares solution of a linearized form of equations (6), (7) and (8), written for each pixel

$$I'_x \Delta p1 + I'_y \Delta p2 + I'_x x \Delta p3 + I'_y y \Delta p4 + I'_y x \Delta p5 + I'_x y \Delta p6 = \Delta I$$

I'_x, I'_y are intensity slopes in x, y directions

$\Delta p_1 .. \Delta p_6$ are corrections to approximate values of $p_1 .. p_6$

ΔI is the difference in intensities of corresponding pixels in the mask and search windows.

/...

Solution indicates distortion of search image

- Resample search image based on these parameters so that it matches more closely the geometry of the mask window

- Recompute new solution of equations (7) and(8) and continue to iterate least squares and resampling until convergence.

/...

Advantages of least squares solution

- Adaptable to changes in image geometry

- Gives indication of accuracy of matching because it is based on least squares formulation. Standard error propagation methods can be used.

- High precisions possible - 0.3 pixel matching or better.

Disadvantage

Good approximate positions needed.

Hence matching should be based on two steps : -

1. Approximate matching

   e.g. Cross-correlation + epipolar lines or feature based matching

2. Least squares matching

/...

OBJECT RECONTRUCTION

Elements of reconstruction:

* determination of object geometry by coordinates or DEM
  - use geometric model for image formation, either camera of scanner, based on appropriate collinearity equations.

* object description or **Recognition** based on the following characteristics of the image:

  - spectral signatures
  - texture
  - geometry
  - shape
  - size
  - location
  - relationships with other objects
  - topology
  - context

/...

Most of the above characteristics can be derived from the preceeding subject material. However, the recognition of objects is based on elements of artificial intelligence, particularly, expert systems, neural networks and knowledge based systems.

IMAGE ANALYSIS SOFTWARE

L.W. Hayes

University of Dundee

Dundee, Scotland

Image Analysis Software

UN/ISPRS Workshop, 6-7 August 1992

L. Hayes

University of Dundee
Dundee DD1 4HN
Scotland U.K.

Agenda

- Software systems
- Software issues
- Software functionality
- Cost
- Software platform
- The future

Software systems

Data visualisation/manipulation/analysis

Interactive tools

- Point and click
- Menus
- Icons

Computational filters

Subroutine Libraries

Encapsulated environments

Toolsets (image conversion, *etc.*)

Software functionality

Data reduction and subsetting

Multi-dimensionality

Image processing

Pattern recognition

Image analysis

Animation

What if?

Software issues

Optimisation for available hardware

Graphics/Floating point

Portability

Multi-vendor/Multi-platform

Scaleability

Functionality/Sophistication

Flexibility

Extensibility

Rapid prototyping facilities

MTTS/UNIX pipes/Scripting

Developer oriented environment?

Suitable architecture for large images

Cost

Free or commercial software?

- Public domain
- Shareware
- Proprietary

Installation and Maintenance

- Local support personnel

Vendor support

- Bug fixes
- Technical information

Hardware platform

- Future configuration support

Source code/executables

- User hooks

Software Platform

Proprietary platforms

Turn key systems

General purpose workstations

UNIX

MS-DOS

Windows

Graphics accelerators

Turbo this and that

The future

Greater volumes of data

Parallel processing

Improved interactivity

Advanced functionality

INTELLIGENT INFORMATION EXTRACTION AT THE CANADA CENTRE FOR REMOTE SENSING

D.G. Goodenough

Pacific Forestry Centre

Ottawa, Canada

/...

INTELLIGENT INFORMATION EXTRACTION AT CCRS

David G. Goodenough and Ko B. Fung

DGG Mailing address:
Pacific Forestry Centre
506 West Burnside Road
Victoria, B.C. Canada V8Z 1M5

KBF Mailing address:
Canada Centre for Remote Sensing
1547 Merivale Road,
Ottawa, Ontario, Canada K1A 0Y7

CCRS

Outline

- CCRS IMAGE ANALYSIS HISTORY
- LANDSAT DIGITAL IMAGE ANALYSIS SYSTEM
- THE NEED FOR INTELLIGENT SYSTEMS
- SYSTEM OF HIERARCHICAL EXPERTS FOR RESOURCE INVENTORIES (SHERI)
- PHOTO INTERPRETATION KEYS EXPERT SYSTEM (PIKES)
- SYSTEM OF EXPERTS FOR INTELLIGENT DATA MANAGEMENT (SEIDAM)

CCRS

CCRS IMAGE ANALYSIS HISTORY

1973 • Multispectral Analyzer Display System - PDP-10 based system for image enhancement, radiometric and geometric correction, and photo and tape generation for LANDSAT MSS.

1974 • MICA - Modular Interactive Classification Analyzer - PDP-10 based system for pattern recognition, classification and clustering, and spatial filtering of LANDSAT MSS data.

1978 • CCRS Image Analysis System (CIAS) - PDP 11/70 and 11/40 computers with extensively- modified Image 100, home-grown array processor (parallel processing, 100 MIPS), PDS microdensitometer; team developed more than 300,000 lines of code; system used by scientists all over Canada; more than $1 billion worth of resources discovered with the CIAS; monitoring of environmental disasters (floods, air pollution, tornado damage, etc.); technology transferred to industry and universities.

CCRS

LDIAS

1989 • LANDSAT Digital Image Analysis System (LDIAS) - a system created as a result of information extraction research which supports GIS and RS integration and the following sensors: LANDSAT TM, MSS, SPOT, MEIS, AVHRR, airborne SAR, MSS, MEIS, AVIRIS, etc. GISes are Intergraph GIS and PAMAP GIS. Government of Canada Award of Excellence received. Technology transferred to universities and industry.

• LDIAS contains more than 1.5 million lines of FORTRAN code. The software was developed on DEC VAX computers and used Gould Deanza IP 8500 image displays. The software is being ported to UNIX platforms with MOTIF windows. Software was developed using structured design and analysis methodology, code management tools, and an automated documentation system.

CCRS

/...

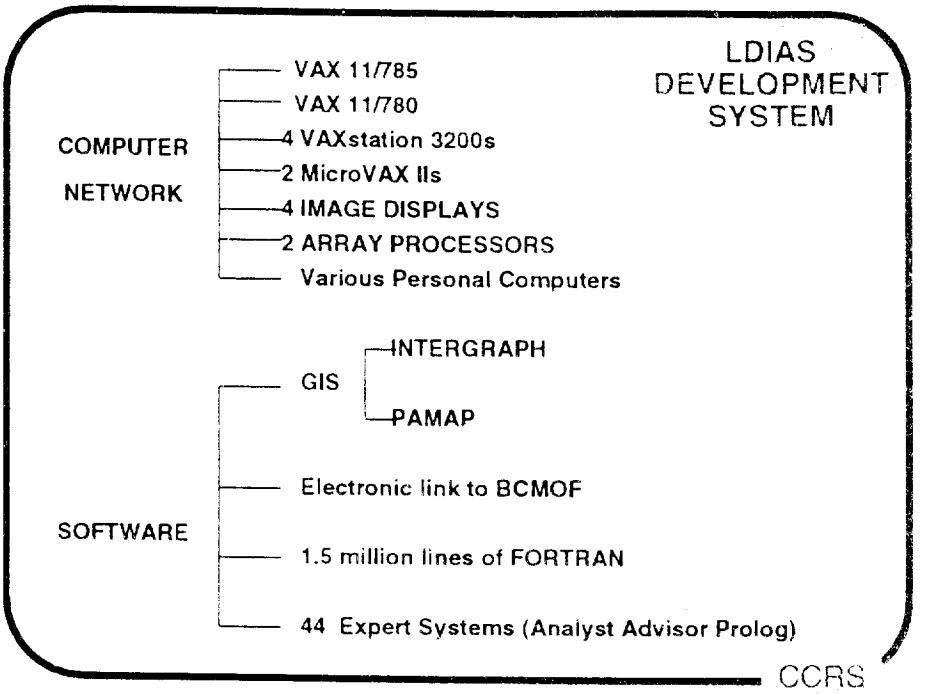

LDIAS FUNCTIONS

- User specification of desired outputs at start establishes most probable analysis procedure.
- Inputs: TM, MSS, AVHRR, SAR, MLA, PLA, MEIS, AVIRIS,CASI, GIS, DTM.
- Corrections: radiometry, geometry, atmosphere, output projections, noise, filtering, image errors, etc.
- Labelling of training and/or test areas: from GIS, from user selection, from both.
- Use of spatial information: texture, morphology, segmentation
- Classification and clustering: parametric and non-parametric; up to 32,000 classes; up to 300 channels;up to 8000 by 8000 images.
- Outputs: enhancements, paper maps, GISes, disks, etc.
- Assessment of accuracy during analysis session.

CCRS

/...

Data Acquisition for Photo Interpretation

1:15 000 Aerial Photo - Stereo B&W

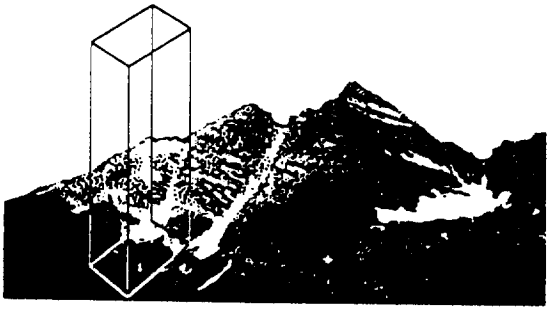

CCRS

Ground Verification

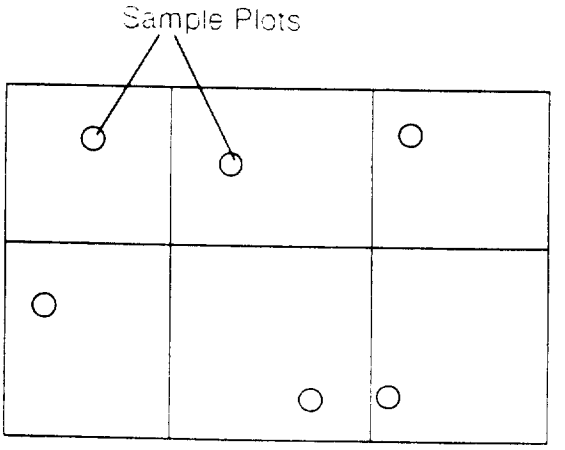

Stratified Random Sampling

CCRS

/...

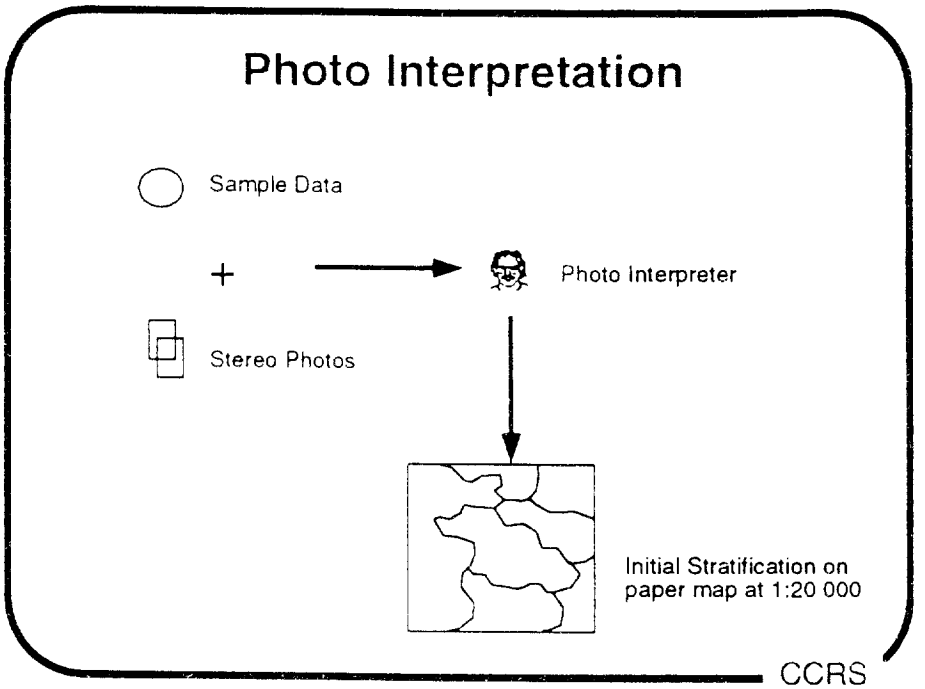
Photo Interpretation
Sample Data
+
Photo Interpreter
Stereo Photos
Initial Stratification on
paper map at 1:20 000
CCRS

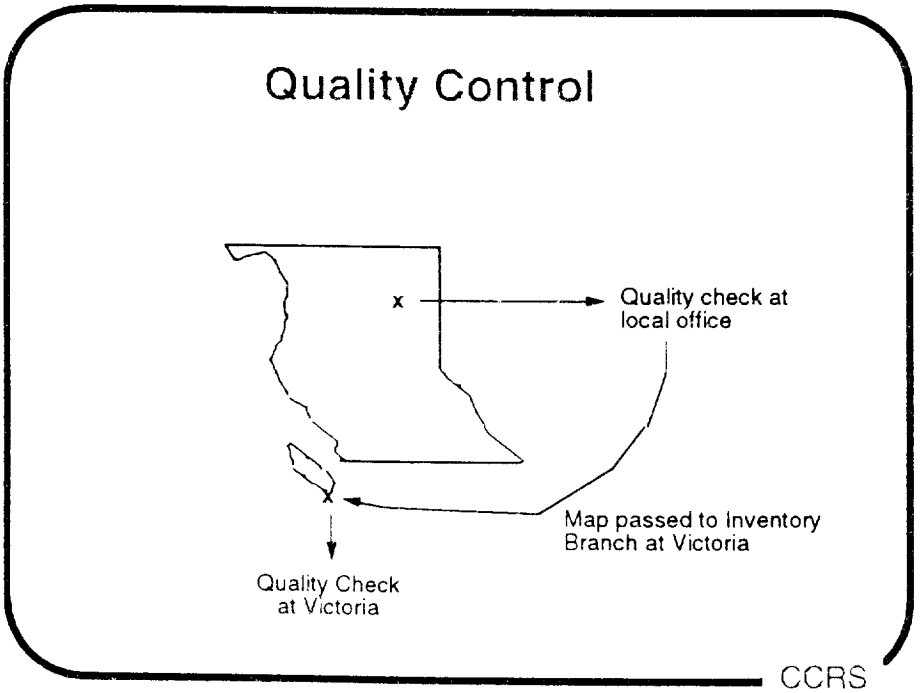
Quality Control
x
Quality check at
local office
x
Map passed to Inventory
Branch at Victoria
Quality Check
at Victoria
CCRS

/...

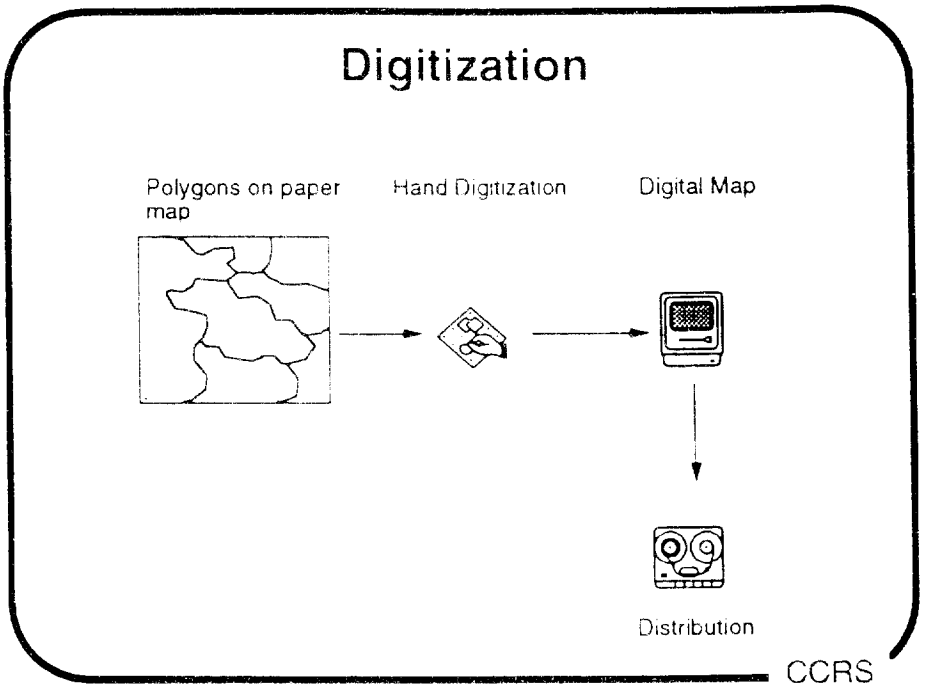
Digitization
Polygons on paper map
Hand Digitization
Digital Map
Distribution
CCRS

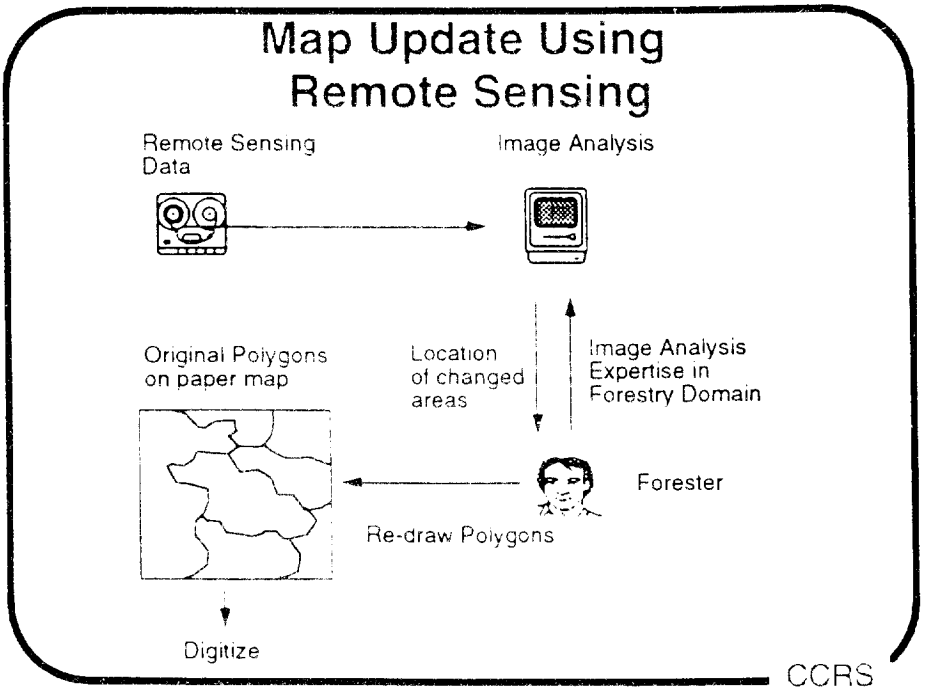
Map Update Using Remote Sensing
Remote Sensing Data
Image Analysis
Original Polygons on paper map
Location of changed areas
Image Analysis Expertise in Forestry Domain
Forester
Re-draw Polygons
Digitize
CCRS

/...

AI Supervision of Map Update

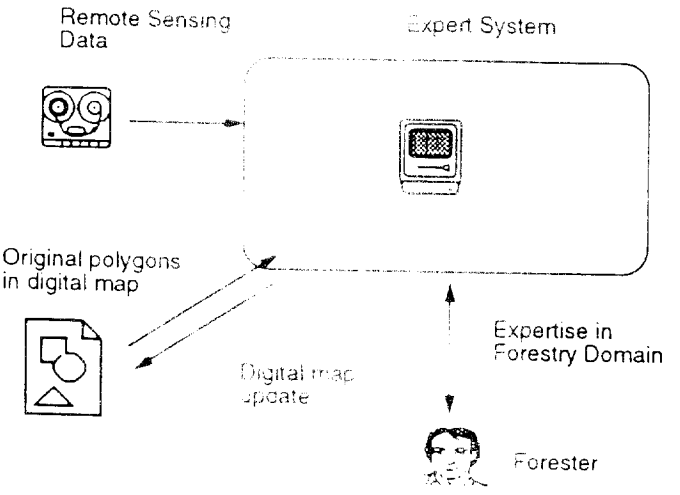

CCRS

ROLE OF ARTIFICIAL INTELLIGENCE IN RESOURCE INVENTORIES

- automation using existing knowledge encapsulated in expert systems
- data integration
- image interpretation
- object representation
- distribution of expertise

CCRS

/...

KNOWLEDGE TO BE ACQUIRED WITH A.I.

- forest inventory and monitoring procedures
- forest photo-interpretation methods
- image analysis methods
- data fusion methods
- environmental methods
- experience updating forest GIS files with remote sensing

CCRS

A.I. DECISIONS AND ADVICE

- advises on appropriate remote sensing imagery for user goals
- integrates GIS and remote sensing imagery and performs appropriate radiometric and geometric corrections
- selects spatial and spectral features for analysis and performs analysis with GIS support.
- reports on success in recognizing forest classes of interest to user specified accuracies.
- if successful, generates updated GIS files and attributes automatically; if unsuccessful, recommends alternative procedures.
- user can add rules and objects to the expert system.

CCRS

/...

Analysis Search Space

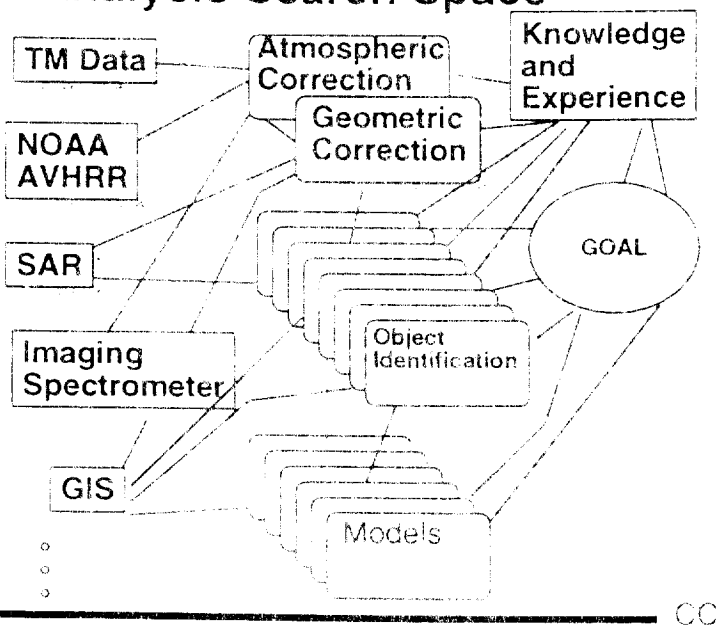

CCRS

INFORMATION VALUE

- There are many analysis methods to extract information from many sources of data.
- From a given data source to a desired goal, there are thus many possible paths. One should select the path yielding the highest information value for the lowest cost.
- The value of information is a function of the desired goals. Because this is difficult to quantify, we are using the cost of transforming from data states through many process states to the final goal. The best path is the one with the lowest costs.

CCRS

/...

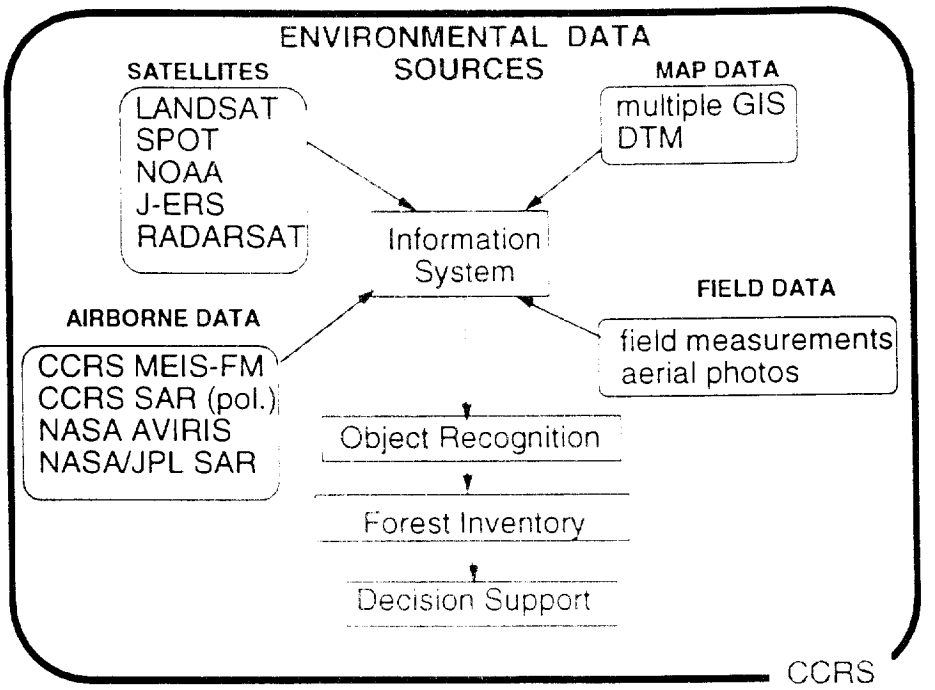

DATA FUSION AND OBJECT RECOGNITION

- Data Fusion -- Combine data from multiple sources and multiple dates

- Object Recognition -- Develop an analysis procedure to identify single objects using all data sources as contributing factors

- represent objects through a logical linkage from the highest level to the lowest:
  - e.g. 1) Where is the forested land?
  - 2) Where are the coniferous trees?
  - 3) How much lodgepole pine is there?
  - 4) Which trees are damaged by insects?

- match objects with model predictions

CCRS

/...

ARTIFICIAL INTELLIGENCE #1

- integration and extraction of useful information require sequences of processes to be executed
- the sequences of processes or programs to be run must be setup and parameter selection made logically based upon the experience of a human expert
- artificial intelligence provides techniques to handle logical inference and the representation of domain-specific knowledge

CCRS

ARTIFICIAL INTELLIGENCE #2

- traditional, algorithmic approaches require the programmer to identify every situation in which a program will be run, and then to hard code the situation of the program. As the number of possible program states grows, the program becomes more complex and difficult to change as new knowledge becomes available
- AI can be viewed as a software methodology which allows programs to be easily changed as new knowledge is acquired or new process sequences are chosen

CCRS

/...

ADVANTAGES OF AI TECHNOLOGY

- permits distribution of knowledge at lower costs
- simplifies operation of complex systems for complex problems
- enhances clarity of issues in multisensor and GIS integration
- increases flexibility of resource management systems as circumstances change

CCRS

DISADVANTAGES OF AI

- expert systems do not include learning
- many unknown aspects of knowledge acquisition, knowledge representation, reasoning with uncertainty, processing architectures, etc.
- steep learning curve for developers and users
- requires long term commitment of users
- there is fear amongst some users that the machine will replace them

CCRS

/...

WHY A HIERARCHICAL EXPERT SYSTEM?

- large variety of expertise and image processing techniques must be applied to the task.
- highly structured, therefore modular approach adopted.
- significant interaction necessary between experts.
- suitable organizational model of the experts is a pyramidal structure consisting of a number of levels of authority.
- highest level sets broad goals for the next level of command.
- lowest level corresponds to GIS and image analysis programs.
- modular approach is most effective by using an expert system shell and instantiating this shell for each module.

CCRS

RESHELL ARCHITECTURE

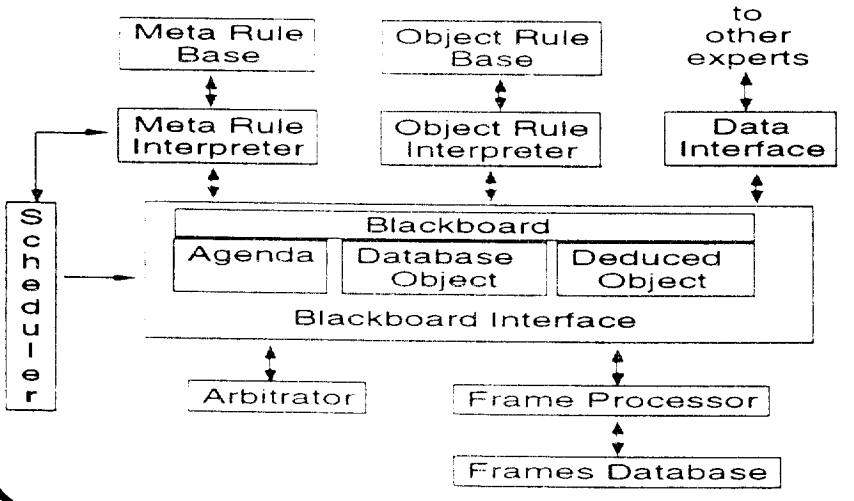

CCRS

/...

SYSTEM OF HIERARCHICAL EXPERTS FOR RESOURCE INVENTORIES - THE SHERI PROJECT

CCRS

SHERI OBJECTIVE

THE OBJECTIVE IS TO CREATE A SYSTEM OF HIERARCHICAL EXPERTS FOR RESOURCE INVENTORIES (SHERI) BY INTEGRATING REMOTE SENSING DATA FROM LANDSAT THEMATIC MAPPER AND SPOT HRV SENSORS, THE INTERGRAPH (MGE) AND PAMAP GEOGRAPHIC INFORMATION SYSTEMS (GIS), AND A RELATIONAL DATA BASE (INGRES) IN ORDER TO:

(1) IMPROVE THE UPDATES OF DEPLETION AND ROAD MAPPING FOR AN EXISTING FOREST INVENTORY;
(2) PERFORM QUALITY CONTROL WITH REMOTE SENSING ON REINVENTORY FOREST LABELS;
(3) DEMONSTRATE SOME BASIC GIS APPLICATIONS WITH REMOTE SENSING;
(4) DEMONSTRATE REMOTE SENSING CONTRIBUTIONS TO GROWTH AND YIELD MODELLING.

CCRS

/...

SYSTEM OF HIERARCHICAL EXPERTS FOR RESOURCE INVENTORIES - THE SHERI PROJECT

CCRS

SHERI OBJECTIVE

THE OBJECTIVE IS TO CREATE A SYSTEM OF HIERARCHICAL EXPERTS FOR RESOURCE INVENTORIES (SHERI) BY INTEGRATING REMOTE SENSING DATA FROM LANDSAT THEMATIC MAPPER AND SPOT HRV SENSORS, THE INTERGRAPH (MGE) AND PAMAP GEOGRAPHIC INFORMATION SYSTEMS (GIS), AND A RELATIONAL DATA BASE (INGRES) IN ORDER TO:

(1) IMPROVE THE UPDATES OF DEPLETION AND ROAD MAPPING FOR AN EXISTING FOREST INVENTORY;
(2) PERFORM QUALITY CONTROL WITH REMOTE SENSING ON REINVENTORY FOREST LABELS;
(3) DEMONSTRATE SOME BASIC GIS APPLICATIONS WITH REMOTE SENSING;
(4) DEMONSTRATE REMOTE SENSING CONTRIBUTIONS TO GROWTH AND YIELD MODELLING.

CCRS

/...

WHICH AGENCIES ARE INVOLVED?

ENERGY, MINES AND RESOURCES CANADA (56%)
- CANADA CENTRE FOR REMOTE SENSING

INDUSTRY, SCIENCE AND TECHNOLOGY CANADA (36%)
- STRATEGIC TECHNOLOGIES BRANCH

BRITISH COLUMBIA MINISTRY OF FORESTS (8%)
- INVENTORY BRANCH

CCRS

WHO IS INVOLVED IN THE R & D?

CCRS

INTERA KENTING

PRICE WATERHOUSE

BCMOF - Dave Gilbert, Raoul Wiart, Cy McConnell (Invermere), John Wakelin

BCMOELP - Gary Sawayama, Roger Balser.

UNIVERSITY OF OTTAWA - Prof. Stan Matwin, Prof. Dan Ionescu

UNIVERSITY OF TORONTO - Prof. Larry Band, Prof. Vince Robinson

UNIVERSITY OF MONTANA - Prof. Steve Running

FERIHILL TECHNOLOGIES - Frank Hegyi

MDA - Bruce Forde

Related efforts: NASA Advanced Information Systems Research Program.

CCRS

/...

AI PROJECTS

- THE PROGRAMMING PARADIGM FOR AN AI PROJECT IS TO CREATE PROGRAMS (EXPERT SYSTEMS) IN WHICH THE PROGRAMS CAN EASILY BE CHANGED AS NEW KNOWLEDGE OR EXPERIENCE IS ACQUIRED OR CAPABILITIES OF SYSTEMS CHANGE.
- SINCE KNOWLEDGE IS THE KEY, THE PROJECT TEAM MUST ADDRESS SUCH ISSUES AS: IS THERE AN EXPERT?, WHO IS IT?, WHAT KNOWLEDGE NEEDS TO BE ACQUIRED?, HOW WILL THIS KNOWLEDGE BE REPRESENTED?, WHAT ARE THE LIMITATIONS OF THIS APPROACH IN COMPARISON WITH THE HUMAN EXPERTS?, WHAT ARE THE GAINS OVER HUMAN EXPERTS?

CCRS

HOW WILL KNOWLEDGE BE ACQUIRED?

- KNOWLEDGE OF FOREST INVENTORIES:
  - BCMOF INVENTORY BRANCH STAFF
  - BCMOF DISTRICT STAFF (INVERMERE FOREST DISTRICT)
  - BCMOF FOREST INVENTORY MANUALS
  - JOINT EXPERIMENTS TO CREATE UPDATED FOREST GIS INVENTORY FILES
  - CONTRACTS WITH EXPERTS IN FOREST INVENTORY PROCEDURES, SAMPLING METHODOLOGIES, ETC.

CCRS

/...

HOW WILL KNOWLEDGE BE ACQUIRED? #2

KNOWLEDGE OF REMOTE SENSING ANALYSIS METHODS AND GIS INTEGRATION WITH REMOTE SENSING

- CCRS STAFF AND CONTRACTORS
- BCMOF INVENTORY BRANCH STAFF
- IMAGE ANALYSIS MANUALS
- JOINT EXPERIMENTS TO CREATE UPDATED FOREST GIS INVENTORY FILES
- CONTRACTS WITH OTHER EXPERTS

KNOWLEDGE IN BUILDING NETWORKS OF EXPERT SYSTEMS

- CCRS STAFF AND CONTRACTORS

CCRS

DTM EXPERT STRUCTURE

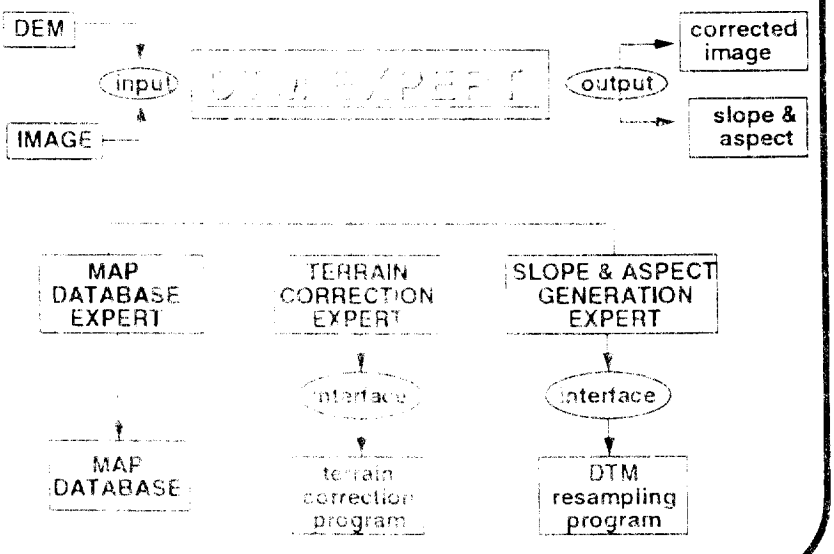

CCRS

/...

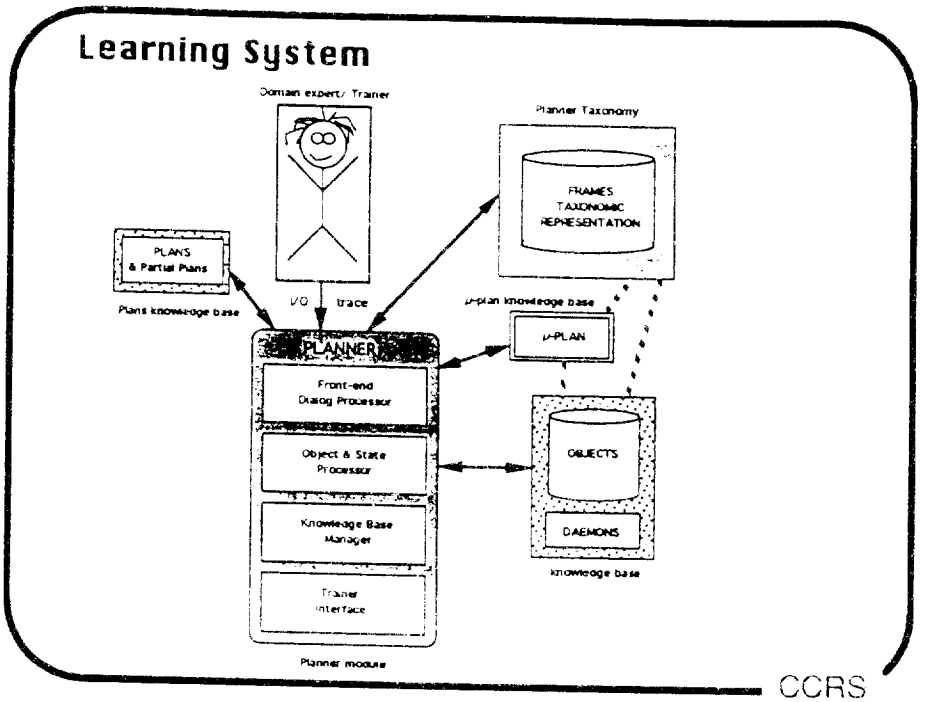
Learning System
Domain expert/ Trainer
Planner Taxonomy
FRAMES
TAXONOMIC
REPRESENTATION
PLANS
& Partial Plans
Plans knowledge base
I/O
trace
μ-plan knowledge base
μ-PLAN
PLANNER
Front-end
Dialog Processor
Object & State
Processor
Knowledge Base
Manager
Trainer
Interface
Planner module
OBJECTS
DAEMONS
knowledge base
CCRS

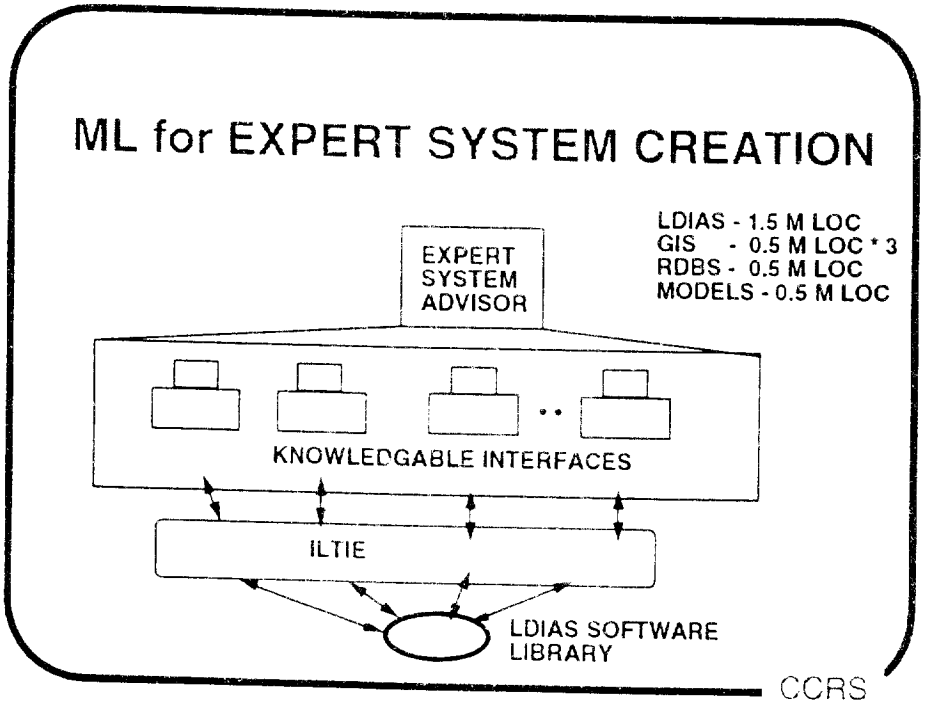
ML for EXPERT SYSTEM CREATION
LDIAS - 1.5 M LOC
GIS - 0.5 M LOC * 3
RDBS - 0.5 M LOC
MODELS - 0.5 M LOC
EXPERT
SYSTEM
ADVISOR
KNOWLEDGABLE INTERFACES
ILTIE
LDIAS SOFTWARE
LIBRARY
CCRS

/...

MICROPLAN PERFORMANCE

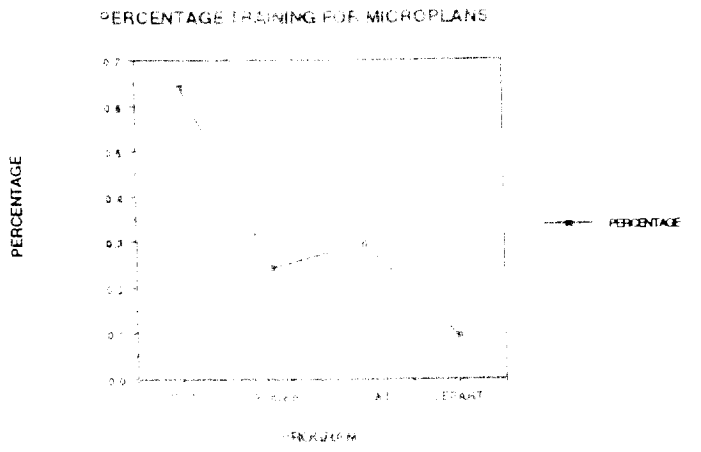

CCRS

ML PRACTICAL ISSUES

- WE HAVE EFFECTIVELY USED ML TO SPEED THE PROCESS OF CREATING NEW EXPERT SYSTEMS AT THE LEVEL OF CONTROLLING AND RUNNING PROCESSES IN A DISTRIBUTED COMPUTER ENVIRONMENT
- WE WANT TO ANALYZE DATA FROM HUNDREDS OF IMAGES AND THOUSANDS OF MAPS (> 7,000). HOW DO WE LEARN FROM EACH ANALYSIS?
- IF WE CREATE NEW KNOWLEDGE, HOW DO WE ENSURE THAT THIS NEW KNOWLEDGE IS CONSISTENT WITH EXISTING KNOWLEDGE IN OUR SYSTEM?
- HOW DO WE ATTACH RATINGS TO THE NEW KNOWLEDGE REFLECTING A LEVEL OF CERTAINTY IN THESE NEW RULES?
- HOW DO YOU IMPRESS A NON-EXPERT, DECISION MAKER WITH THE CAPABILITIES OF MACHINE LEARNING?

CCRS

/...

THE PLANNER

- THE HUMAN EXPERT HAS A GOAL OF CREATING AN EXPERT SYSTEM TO RUN AN EXISTING PROGRAM. HE WISHES TO DO THIS AS SIMPLY AND QUICKLY AS POSSIBLE. HE WILL USE CASES CONSISTING OF IMAGERY, FOREST COVER FILES, AND HIS KNOWLEDGE TO CREATE SUITABLE STATE CONTROLS FOR THE SOFTWARE.
- THE HUMAN EXPERT STARTS THE PLANNER AND TELLS IT WHICH PROGRAM IS TO BE RUN. THROUGH A DIALOG WITH THE EXPERT, AND USING ALREADY ACQUIRED KNOWLEDGE FOR EXPERT SYSTEMS CREATED EARLIER, THE PLANNER BUILDS THE STATE TRANSITIONS FOR THE GIVEN CASE.
- LATER, RULES ARE ADDED TO INCREASE THE EXPERTISE OF THE NEW EXPERT SYSTEM AND TO INTEGRATE THIS NEW SYSTEM INTO THE HIERARCHY OF EXPERT SYSTEMS.

CCRS

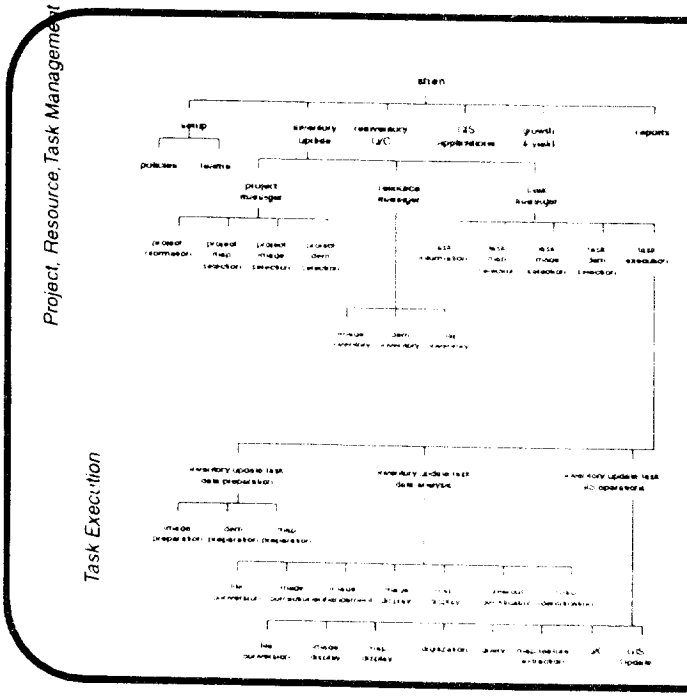

SHERI EXPERT SYSTEM STRUCTURE FOR INVENTORY UPDATE

CCRS

/...

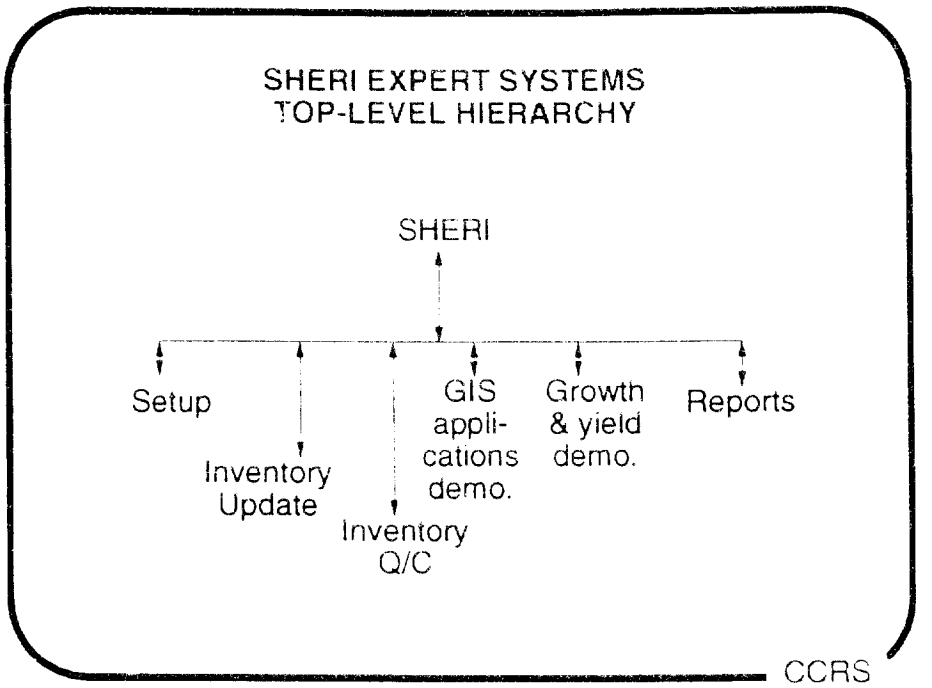
SHERI EXPERT SYSTEMS
TOP-LEVEL HIERARCHY
SHERI
Setup
Inventory Update
Inventory Q/C
GIS appli-cations demo.
Growth & yield demo.
Reports
CCRS

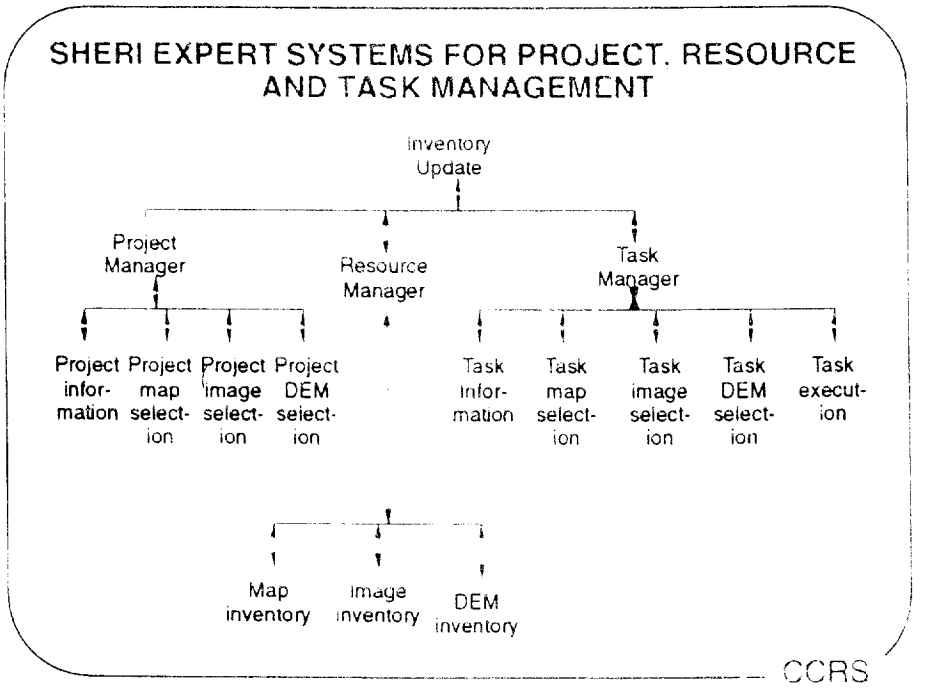
SHERI EXPERT SYSTEMS FOR PROJECT, RESOURCE AND TASK MANAGEMENT
Inventory Update
Project Manager
Resource Manager
Task Manager
Project infor-mation
Project map select-ion
Project image select-ion
Project DEM select-ion
Task infor-mation
Task map select-ion
Task image select-ion
Task DEM select-ion
Task execut-ion
Map inventory
Image inventory
DEM inventory
CCRS

/...

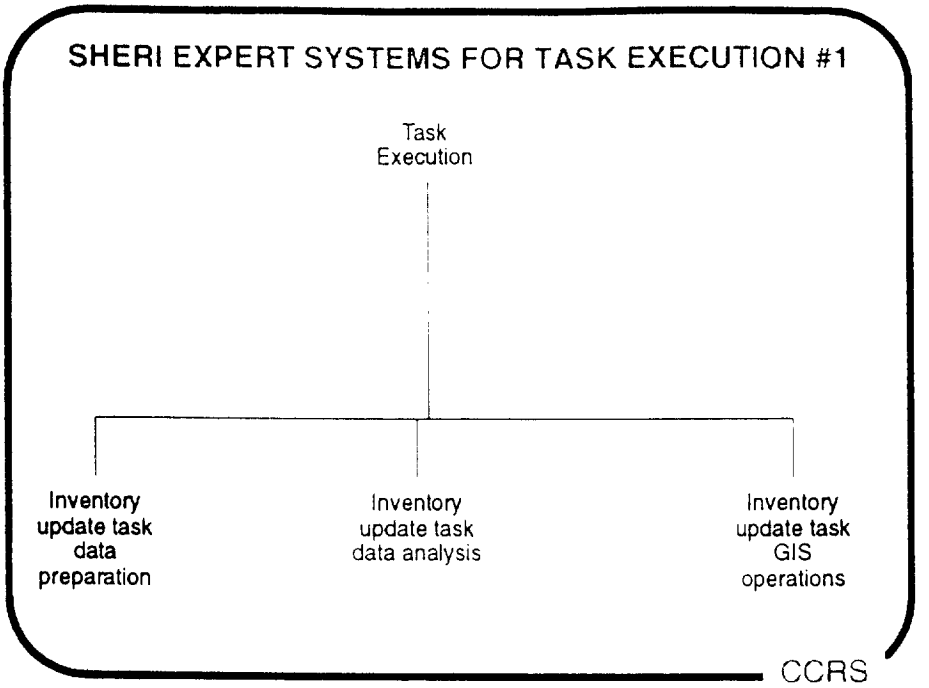
SHERI EXPERT SYSTEMS FOR TASK EXECUTION #1
Task Execution
Inventory update task data preparation
Inventory update task data analysis
Inventory update task GIS operations
CCRS

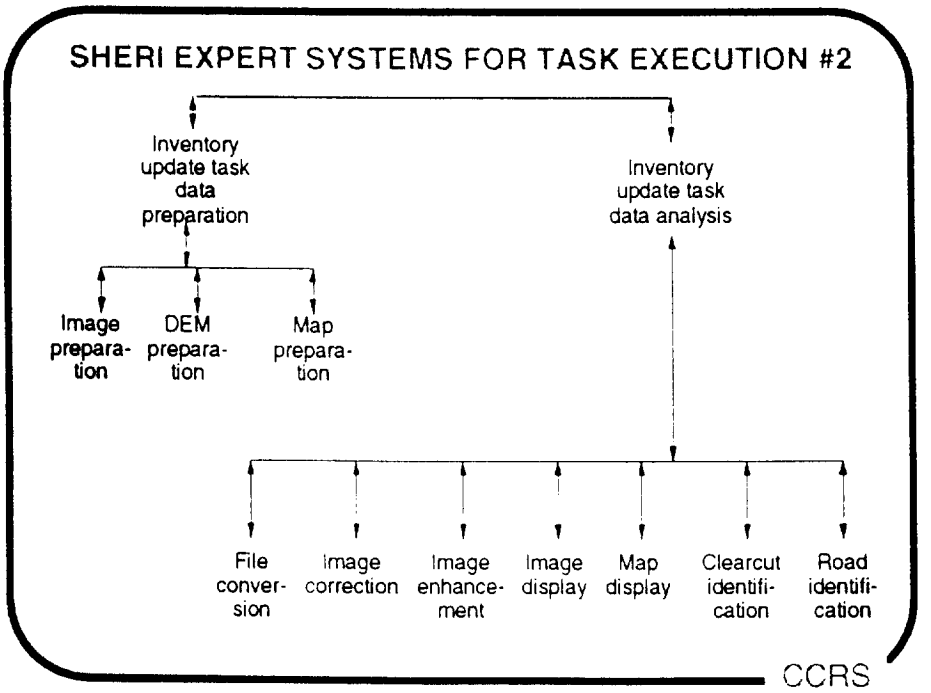
SHERI EXPERT SYSTEMS FOR TASK EXECUTION #2
Inventory update task data preparation
Inventory update task data analysis
Image prepara-tion
DEM prepara-tion
Map prepara-tion
File conver-sion
Image correction
Image enhance-ment
Image display
Map display
Clearcut identifi-cation
Road identifi-cation
CCRS

/...

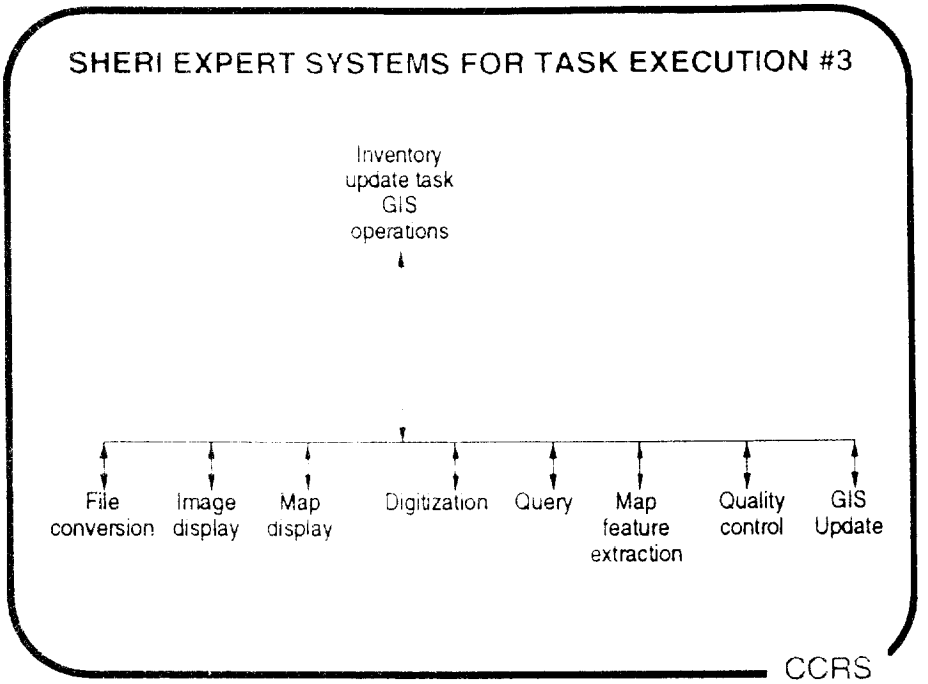

SOFTWARE DEVELOPMENT PLAN

(1) Manual System

⇒ identify and document inventory update tasks
⇒ end-to-end manual operation

(2) Generic System

⇒ design automated task execution
⇒ implement experts to drive task execution

(3) Specialized System

⇒ identify BCMOF requirements
⇒ design project, resource, and task management
⇒ design top-level user interface
⇒ implement experts to drive generic system

CCRS/SHERI

/...

SOFTWARE DESIGN DESCRIPTIONS

(1) Expert Functionality Design

⇒ Identify logical relationships between experts

⇒ verify requirements

(2) Project, Resource, and Task Management

⇒ create and manipulate projects

⇒ inventory and query images, dems, and maps

⇒ create, manipulate, and execute tasks

(3) Task Execution Design

⇒ data flow diagrams

⇒ expert functionality

⇒ application interfaces

CCRS/SHERI

SHERI USERS

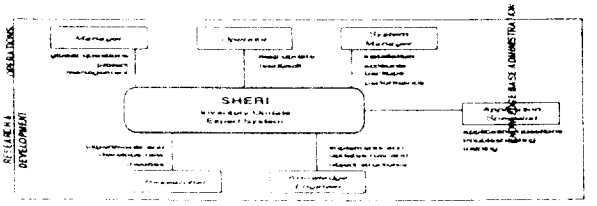

CCRS/SHERI

/...

SHERI STARTUP WINDOWS

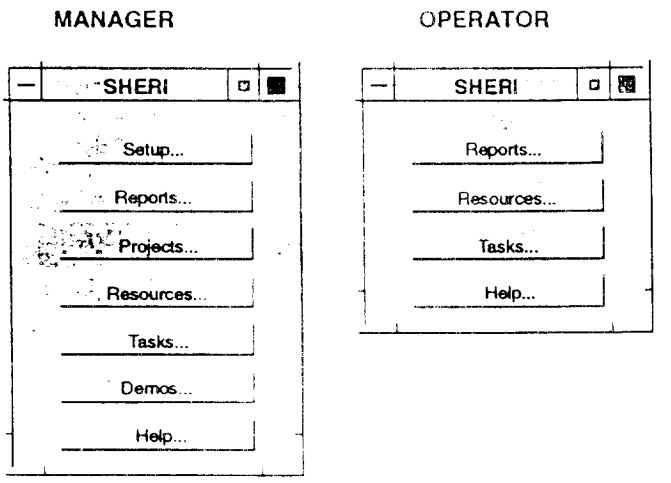

CCRS

SHERI PROJECTS WINDOW

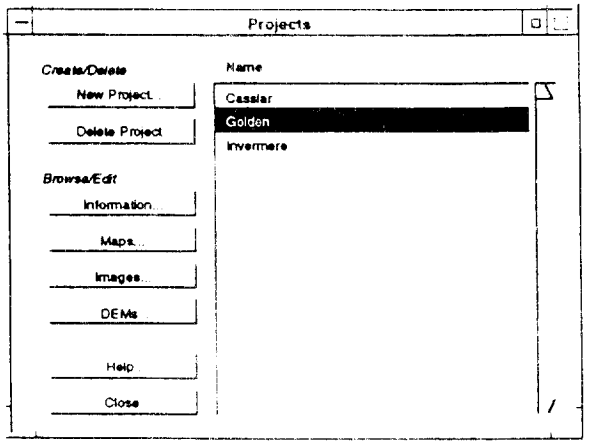

CCRS

/...

SHERI PROJECT MAP ADDITION

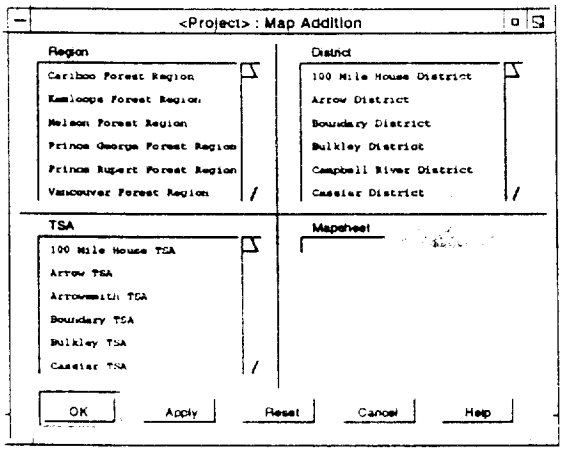

CCRS

SHERI PROJECT MAP ADDITION EXAMPLE

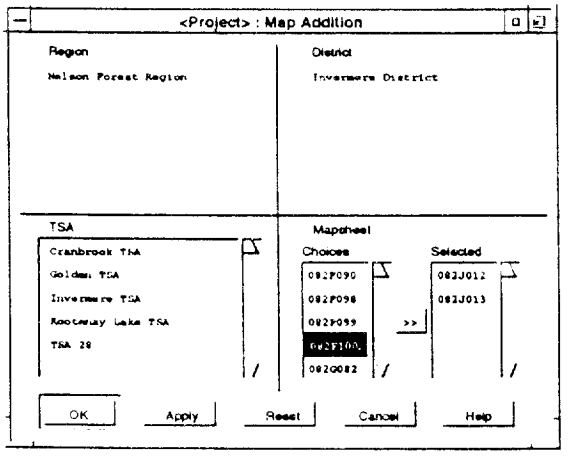

CCRS

/...

SHERI TASKS SELECTION EXAMPLE

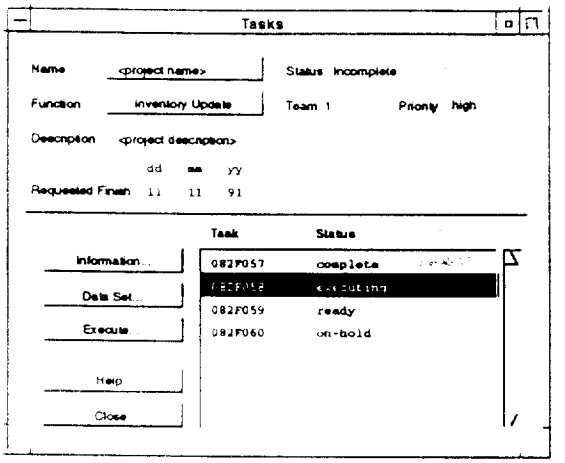

CCRS

PROJECT INFORMATION

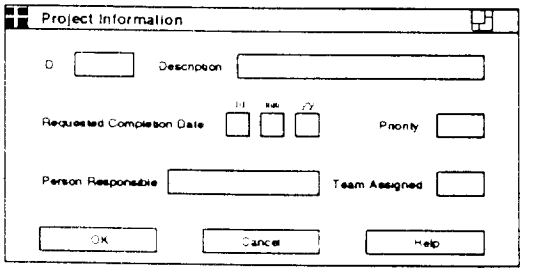

Project Information

⇒ define information associated with a project

CCRS

/...

PROJECT MAP SELECTION

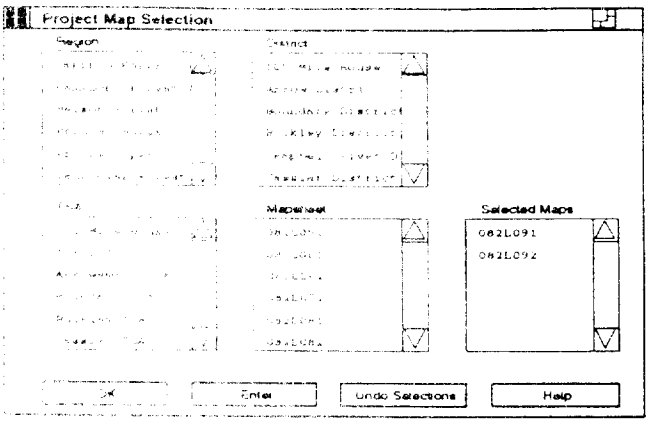

Project Map Selection

- select and list maps associated with a project

CCRS

PROJECT MANAGEMENT ACTIVATION SEQUENCES

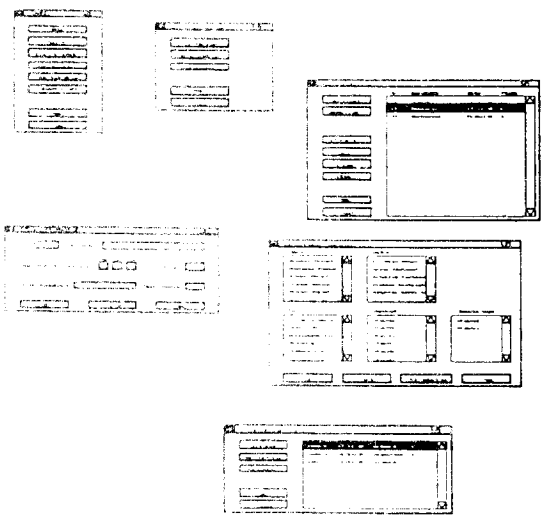

CCRS

/...

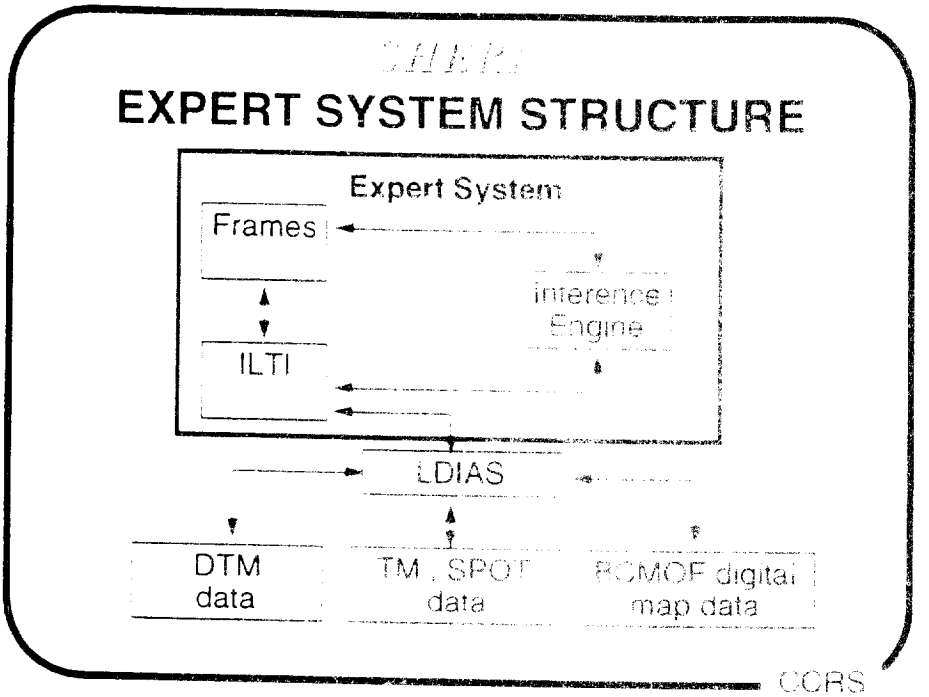
EXPERT SYSTEM STRUCTURE
Expert System
Frames
Inference Engine
ILTI
LDIAS
DTM data
TM , SPOT data
ROMOF digital map data
CCRS

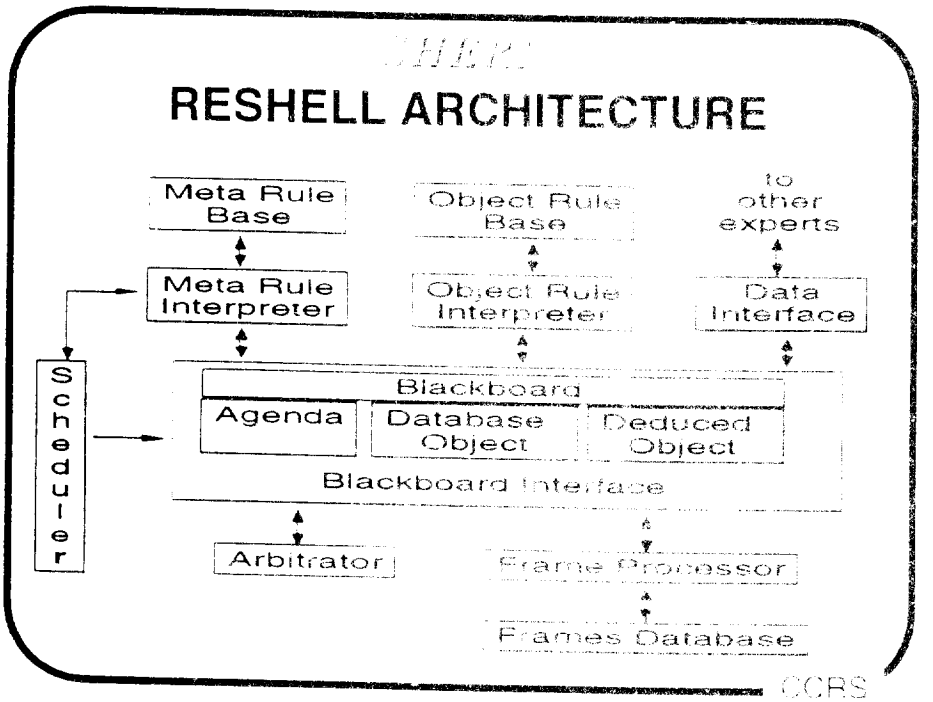
RESHELL ARCHITECTURE
Meta Rule Base
Object Rule Base
to other experts
Meta Rule Interpreter
Object Rule Interpreter
Data Interface
Scheduler
Blackboard
Agenda
Database Object
Deduced Object
Blackboard Interface
Arbitrator
Frame Processor
Frames Database
CCRS

/...

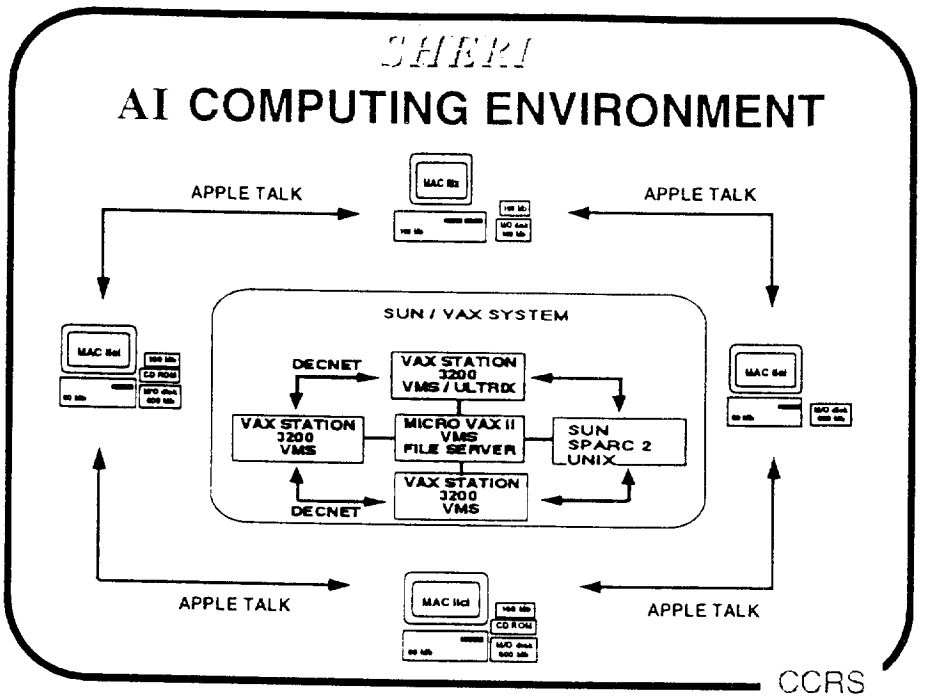
SHERI
AI COMPUTING ENVIRONMENT
APPLE TALK
APPLE TALK
SUN / VAX SYSTEM
DECNET
VAX STATION 3200 VMS / ULTRIX
VAX STATION 3200 VMS
MICRO VAX II VMS FILE SERVER
SUN SPARC 2 UNIX
VAX STATION 3200 VMS
DECNET
APPLE TALK
APPLE TALK
CCRS

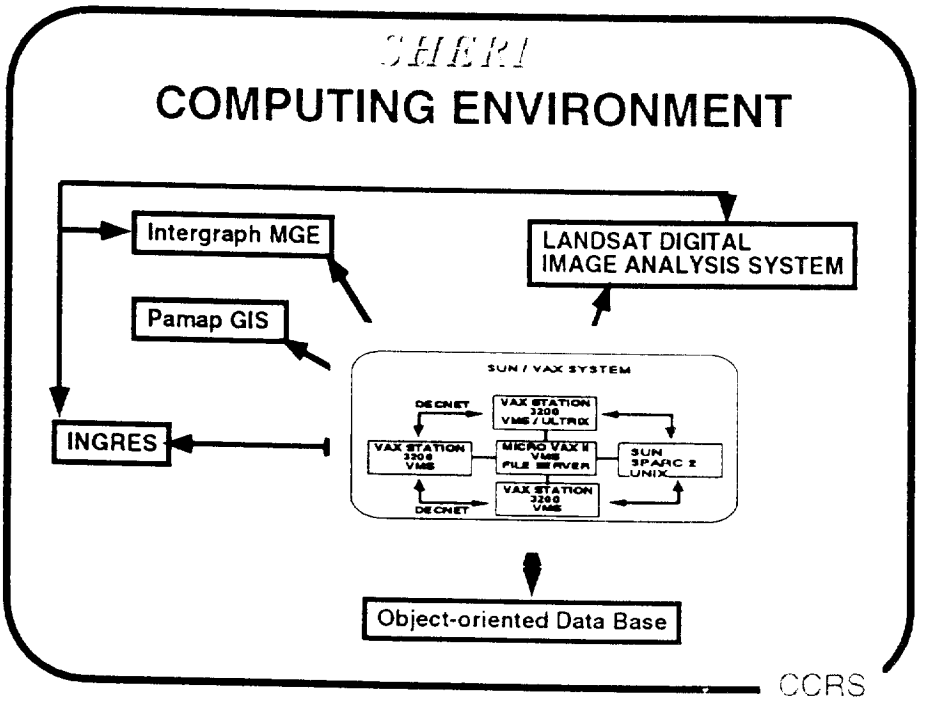
SHERI
COMPUTING ENVIRONMENT
Intergraph MGE
LANDSAT DIGITAL IMAGE ANALYSIS SYSTEM
Pamap GIS
INGRES
SUN / VAX SYSTEM
Object-oriented Data Base
CCRS

/...

HOW WILL SHERI BE TESTED?

THE INVENTORY BRANCH AND CCRS HAVE SELECTED TEST AREAS FOR UPDATING. INITIAL EXPERIMENTS ARE FOCUSED ON THREE TEST SITES NEAR INVERMERE, BRITISH COLUMBIA.

SHERI CAN BE INSTALLED AT BCMOF IN AUGUST, 1992. BCMOF CAN USE SHERI TO AID IN THEIR UPDATING AND INVENTORYING PROGRAMS. 5 AREAS WILL BE SELECTED FOR VALIDATION OF SHERI FUNCTIONALITY. KNOWLEDGE ACQUIRED WILL BE USED TO IMPROVE SHERI PERFORMANCE.

SHERI WILL BE TESTED AT CCRS FOR THESE SITES AND FOR OTHER REMOTE SENSING DATA.

BCMOF STAFF WILL BE TRAINED IN IMAGE ANALYSIS, EXPERT SYSTEM OPERATION, AND KNOWLEDGE BASE CREATION.

CCRS

WHAT WILL BE CREATED?

- ≈100 EXPERT SYSTEMS INCORPORATING KNOWLEDGE FROM SEVERAL DISCIPLINES.
- DISTRIBUTED PROCESSING AND CONTROL OF FOREST GIS UPDATING WITH REMOTE SENSING AND TOPOGRAPHIC INFORMATION.
- ADVICE ON FUTURE PRODUCTIVITY BY FOREST STAND IN MOUNTAINOUS TERRAIN.
- A MODERATE COST IMPLEMENTATION WHICH CAN EASILY BE AUGMENTED
- A COMMERCIALLY EXPLOITABLE CAPABILITY AT THE LEADING EDGE OF COMPUTER ENGINEERING.

CCRS

/...

Artificial Intelligence Research Projects

SHERI	*PIKES*
(System of Hierarchical Experts for Resources Inventories) (...until March 1993)	(Photo Interpretation Keys Expert System) (April 1991 -- March 1994)

SEIDAM

(System of Experts for Intelligent Data Management)

(January 1991 - March 1995)

CCRS

SHERI Status

- SHERI WILL BE TESTED IN SEPTEMBER, 1992 AT CCRS WITH BCMOF INVENTORY BRANCH PERSONNEL.
- THE EXPERT SYSTEMS SUPPORTING INVENTORY UPDATE AND REINVENTORY QUALITY CONTROL ARE FUNCTIONAL.
- SHERI WILL BE TESTED FROM SEPTEMBER, 1992 TO MARCH, 1993.
- SEIDAM WILL BUILD ON SHERI DEVELOPMENTS.

CCRS

/...

CONCLUSIONS

REMOTE SENSING DATA, INTEGRATED WITH GIS AND USER KNOWLEDGE IS AN EFFECTIVE TOOL FOR INVENTORY UPDATE.

THE USE OF SHERI WILL ALLOW THE GENERATION OF ACCURACY INFORMATION FOR LABELS AND POLYGON BOUNDARIES.

SHERI WILL DEMONSTRATE GIS AND GROWTH PREDICTION APPLICATIONS FOR TEST SITES IN THE KOOTENAYS.

SHERI WILL DEMONSTRATE HOW THE COMPLEX INTEGRATION OF SYSTEMS CAN BE SIMPLIFIED.

SIMPLIFICATION COMES ABOUT THROUGH THE FOLLOWING PROPERTIES:

- A 5X REDUCTION IN THE NUMBER OF PROMPTS.
- A CHANGE IN THE NATURE OF THE PROMPTS TO THE USERS' LANGUAGE.
- PAPERLESS ANALYSIS AND KNOWLEDGE-DRIVEN RESPONSES.
- MACHINE LEARNING BASED ON EXAMPLES (CASES)

CCRS

PHOTOINTERPRETATION KEYS EXPERT SYSTEM - PIKES

CCRS

/...

PIKES

- THE PHOTOINTERPRETATION KEYS EXPERT SYSTEM IS DESIGNED TO TRAIN PEOPLE HOW TO INTERPRET SATELLITE AND AIRCRAFT IMAGERY FOR FORESTRY.
- THE PIKES DEVELOPMENT WORK BEGAN IN 1991 WITH THE SELECTION OF THE CONTRACTORS: MACDONALD DETTWILER (PRIME), ALBERTA RESEARCH CENTRE, AND FERIHILL TECHNOLOGIES.
- PIKES WILL MAKE USE OF THE EXPERT SYSTEM RESHELL AND WILL USE TRAINING CASES AND PHOTO INTERPRETATION KEYS DEVELOPED BY EXPERTS.
- PIKES IS INTENDED TO ASSIST TRAINERS IN MORE EASILY TRAINING PEOPLE FOR PHOTOINTERPRETATION.
- THE PROJECT LEADER AT CCRS FOR PIKES IS KO B. FUNG.

CCRS

SYSTEM OF EXPERTS FOR INTELLIGENT DATA MANAGEMENT -SEIDAM

CCRS

/...

WHICH AGENCIES ARE INVOLVED IN SEIDAM?

ENERGY, MINES AND RESOURCES CANADA
- CANADA CENTRE FOR REMOTE SENSING

FORESTRY CANADA
- PACIFIC FORESTRY CENTRE

U.S. NATIONAL AERONAUTICS AND SPACE ADMINISTRATION
- APPLIED INFORMATION SYSTEMS RESEARCH PROGRAM

INDUSTRY, SCIENCE AND TECHNOLOGY CANADA
- STRATEGIC TECHNOLOGIES BRANCH

B.C. MINISTRY OF FORESTS
- INVENTORY BRANCH

B.C. MINISTRY OF ENVIRONMENT, LANDS AND PARKS
- SURVEYS AND RESOURCE MAPPING BRANCH

EEC JOINT RESEARCH CENTRE AT ISPRA, ITALY
- MICROWAVE SIGNATURES LABORATORY

CCRS

SEIDAM OBJECTIVE

TO CREATE A SYSTEM OF EXPERTS FOR INTELLIGENT DATA MANAGEMENT (SEIDAM) WHICH WILL INTEGRATE REMOTE SENSING DATA FROM SATELLITES AND AIRCRAFT WITH GEOGRAPHIC INFORMATION SYSTEMS AND MANAGE LARGE ARCHIVES OF REMOTELY SENSED DATA FOR DYNAMIC SELECTION OF DATA SOURCES AND SENSOR CHARACTERISTICS FOR QUERY-BASED RECOGNITION OF FOREST OBJECTS APPROPRIATE FOR ENVIRONMENTAL FOREST MONITORING.

CCRS

/...

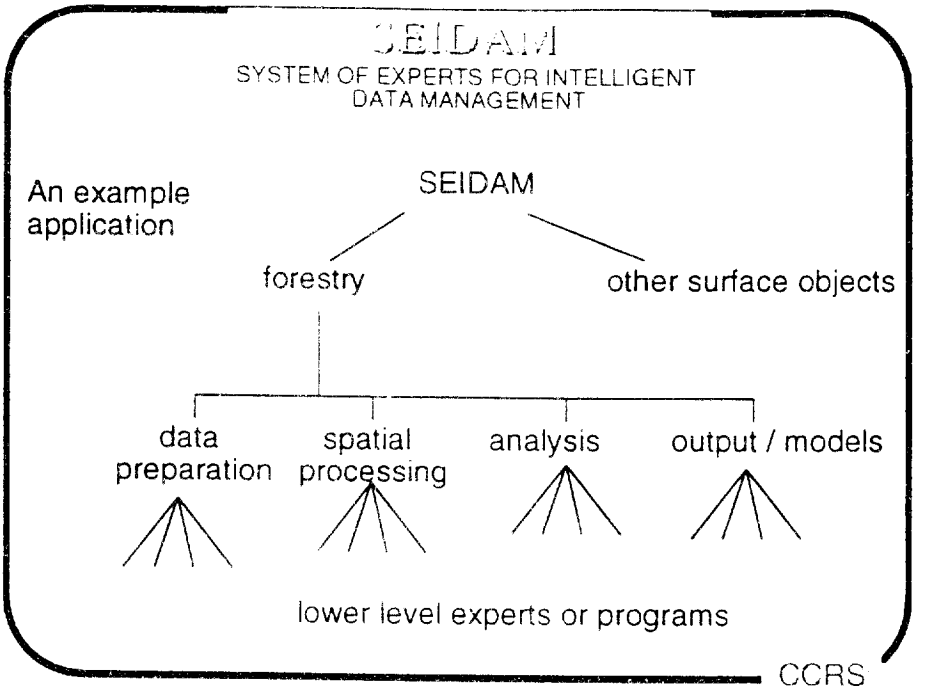
SEIDAM
SYSTEM OF EXPERTS FOR INTELLIGENT DATA MANAGEMENT
An example application
SEIDAM
forestry
other surface objects
data preparation
spatial processing
analysis
output / models
lower level experts or programs
CCRS

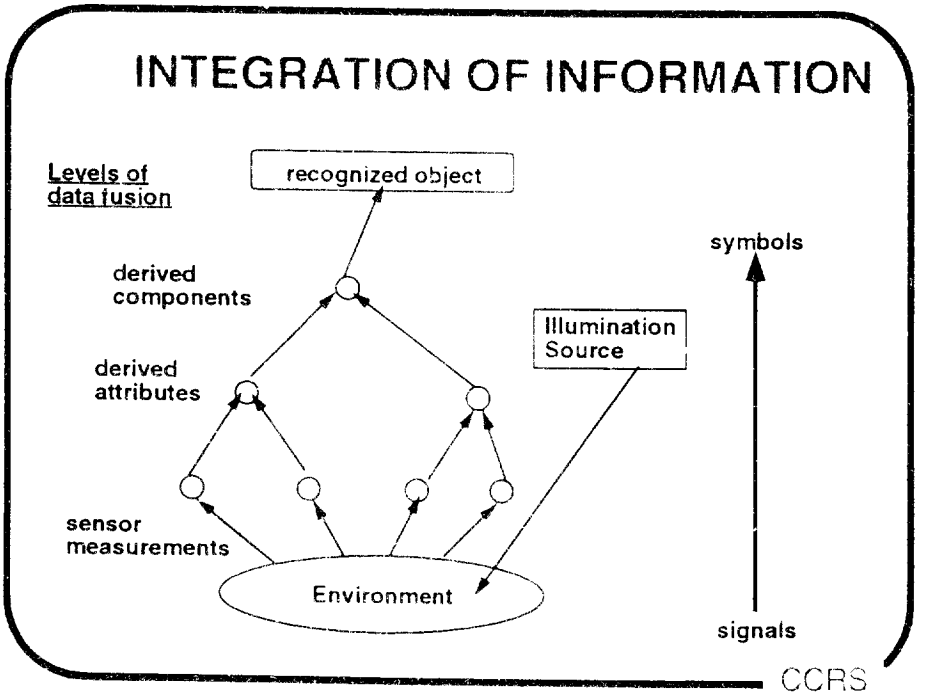
INTEGRATION OF INFORMATION
Levels of data fusion
recognized object
derived components
derived attributes
sensor measurements
Illumination Source
Environment
symbols
signals
CCRS

/...

WHY USE MULTIPLE DATA SOURCES?

- A SINGLE DATA SOURCE MAY NOT BE ABLE TO CAPTURE ALL THE SIGNIFICANT CHARACTERISTICS NEEDED TO IDENTIFY AN OBJECT.
- A SINGLE DATA SOURCE MAY BE SUBJECTED TO SYSTEMATIC ERRORS AND NOISE.
- MULTIPLE DATA SOURCES MAY PROVIDE COMPLEMENTARY INFORMATION.
- REDUNDANT INFORMATION FROM MORE THAN ONE DATA SOURCE INCREASES THE ACCURACY AND CERTAINTY OF OBJECT IDENTIFICATION.
- ONE IS MORE LIKELY TO HAVE DATA AVAILABLE AT THE DESIRED TIME.
- HISTORICAL GIS INFORMATION CAN GUIDE RECOGNITION PROCESS.

CCRS

PROBLEMS WITH MULTIPLE DATA SOURCES

- COSTS OF ACQUISITION
- COMPLEXITIES OF HANDLING MULTIPLE SENSORS:
  - VARIABLE SPECTRAL CHARACTERISTICS OF SENSORS.
  - VARIABLE SPATIAL RESOLUTIONS OF SENSORS.
    - HIGH RESOLUTION SENSOR MAY RESOLVE CLOSELY SPACED OBJECTS, THUS GIVING TOO MUCH DETAIL.
    - LOW RESOLUTION SENSOR MAY NOT RESOLVE OBJECTS OF INTEREST.
    - OBJECTS WILL VARY IN SHAPE AND TEXTURE FROM SENSOR TO SENSOR.
- DIFFERENT SENSORS MAY HAVE DIFFERING VIEWING GEOMETRIES, MAKING MATCHING AND REGISTRATION OF SPATIAL OBJECTS DIFFICULT.
- VARIABILITIES DUE TO DIFFERENT RESPONSES TO THE ATMOSPHERE.
- VARIATIONS DUE TO DIFFERING RECORDING CRITERIA, FORMATS AND STANDARDS.

CCRS

MISMATCHES BETWEEN GIS DATA AND REMOTE SENSING DATA

- SENSOR RESOLUTION MAY NOT BE SUFFICIENT TO RECORD SPATIAL FEATURES USED FOR POLYGON DELINEATION.
- GIS FEATURES MAY NOT BE VISIBLE IN IMAGES DUE TO NON-STATIONARITY OF OBJECTS (E.G. CROPS, WATER BOUNDARIES, BURNS, ETC.).
- GENERALIZATIONS USED FOR BASE MAP MAY CREATE SPATIAL DISPLACEMENTS WITH RESPECT TO IMAGE DATA.
- DIFFERENT GIS SOURCES MAY HAVE SPATIAL ERRORS BETWEEN THEIR RESPECTIVE BASE MAPS.
- IMAGE OBJECTS REFLECT SEASONAL VARIATIONS.

CCRS

SEIDAM Data Sources

Satellite:

LANDSAT 5 o
SPOT 3
ERS-1
JERS-1
NOAA/AVHRR
MOS-1A, B

Aircraft:

CCRS SAR (X, C - polarimetric)
CCRS MEIS (push broom scanner)
CCRS AMSS
NASA airborne SAR (X, L, P - polarimetric)
AVIRIS, TMS

Field Measurements:

GIS information
DTM
Ground calls
Ecosystem chemistry
Meteorological data

CCRS

/...

SEIDAM SUMMARY

- SEIDAM INTEGRATES DATA FROM MULTIPLE SATELLITES, AIRCRAFT, FIELD DATA, GEOGRAPHIC INFORMATION SYSTEMS, AND ENVIRONMENTAL AND FOREST MODELS IN ORDER TO RESPOND TO QUERIES ABOUT THE FORESTS.
- SEIDAM BUILDS ON THE SHERI TECHNOLOGY.
- SEIDAM WILL USE NEURAL NETWORKS FOR SPATIAL KNOWLEDGE ACQUISITION.
- SEIDAM IS AIMED AT THE DATA MANAGEMENT PROBLEMS FACING REMOTE SENSING OVER THE NEXT DECADE WHEN MORE THAN 60 SENSORS WILL BE GENERATING IMAGERY OVER THE GLOBE.
- SEIDAM PRESENTLY INCLUDES 50 EXPERT SYSTEMS. MACHINE LEARNING WILL BE USED TO EXPEDITE THE CREATION OF KNOWLEDGE AND NEW EXPERT SYSTEMS.

CCRS

RADIOMETRIC CORRECTIONS FOR QUANTITATIVE ANALYSIS OF MULTISPECTRAL, MULTITEMPORAL AND MULTISYSTEM SATELLITE DATA

G. Guyot

INRA Bioclimatologie

Montfavet France

/...

RADIOMETRIC CORRECTIONS FOR QUANTITATIVE ANALYSIS OF MULTISPECTRAL, MULTITEMPORAL AND MULTISYSTEM SATELLITE DATA

Gerard GUYOT and Xing-Fa GU
INRA, Bioclimatologie
B.P. 91, 84143 MONTFAVET Cedex (France)

ABSTRACT

The quantitative analysis of multispectral multitemporal and/or multisystem data must be based on radiometrically corrected satellite data converted into bidirectional reflectance factor at the ground level. In a first part, the different factors affecting the satellite data are analyzed : instrument modulation transfer function (MTF), absolute calibration of the sensors and non-coincidence of homologous spectral bands, atmospheric effects, topographic effects, target directional effects. In a second part the procedure which must be followed to obtain radiometrically corrected data is presented and the effects of disturbing factors on multitemporal, multiangular and mutisystem analysis are discussed.

1 - INTRODUCTION

The quantitative analysis of multispectral multitemporal and/or multisystem satellite data needs to use data which can be directly compared. The best way for obtaining comparable data is to transform the satellite digital counts into physical parameters such as the bidirectional reflectance factors at ground level, for example. But, this physical approach is only used by a few authors because it needs a strong physical background (Gu, 1991; Gu et al., 1991). Most of the thematic applications of satellite data are based on a statistical approach which give an easiest way for transforming the digital counts of image pixels into those of an other one (Cicone et Metzler, 1984; Colwell et Poulton, 1985; Crist et Cicone, 1984; Bildgen et al., 1989; Rover et al., 1987).

The radiometric data acquired by the satellite sensors are affected by a series of factors :

- proper characteristics of the sensors such as their modulation transfer function (MTF) affecting the spatial resolution;
- absolute calibration of the sensors and non-coincidence of homologous spectral bands the effects of which vary as a function of the shape of target spectra;
- Sun zenith angle and the Earth-Sun distance affecting the irradiance;
- atmospheric effects;
- topographic effects;
- Viewing geometry which effects depend on the non lambertian characteristics of the target and on atmospheric conditions;
- temporal effects depending on the evolution of the target characteristics.

/ . . .

At the present time the effects of these factors are well known. However, for a quantitative analysis of satellite data it is necessary to determine the relative weight of these factors in order to determine the corrections which can be neglected and which must be performed. For this reason the effects of the different disturbing factors will be analyzed in a first part and in a second part the relative weight of the corrections will be discussed for quantitative multitemporal, multiangular and multisystem image analysis.

2 - EFFECTS OF THE DIFFERENT FACTORS ON SATELLITE DATA

The discussion will be mainlybased on the analysis and intercomparison of SPOT-HRV and Landsat -TM sensors which have three homologous spectral bands (green, red, near-infrared).

2.1. Modulation transfer function (MTF)

The MTF of a satellite imaging sensor corresponds to the attenuation of the amplitude of input signal variation as a function of frequency. It is determined by the signal transfer characteristics of many different components (imaging optics, sensor, signal processing electronics),the atmosphere and more (Leroy, 1990). To simplify matter we will confine ourselves to the MTF of the instrument as a whole, which is the sum of the individual MTFs of each component. The instrument MTF is represented by a coefficient between 0 and 1 which depends on the frequency at which the signal varies (the smaller the coefficient, the higher the signal attenuation due to the instrument). The instrument MTF can be defined as the Fourier transform of the instrumental impulse response (Leroy, 1990). In order to reconstitute the signal received at the instrument entrance, one must therefore divides the Fourier transform of the output signal by the appropriate instrument MTF.

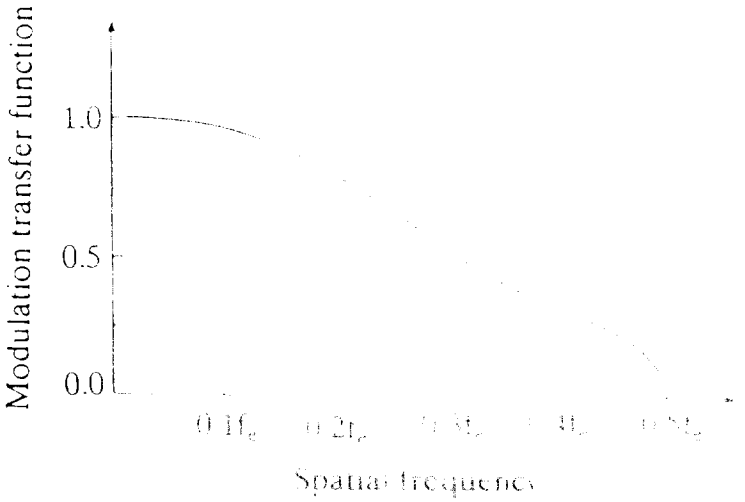

Figure 1 : Variation of MTF of Landsat-4 Thematic Mapper as a function of spatial frequency. (adapted from Schowengerdt et al., 1985)

To correct the image we need the MTF variation as a function of the spatial frequency. Since these data are not available for SPOT-HRV instrument we developed an approximate model by establishing a comparison with results obtained for the Thematic Mapper.

The image acquired by a satelliteborne imaging instrument is recorded by sampling the target area at sampling rates determined by the instrument design. In the case of SPOT HRV operating in the multispectral mode with nadir viewing, the rate is one sample every 20 m. For Landsat Thematic Mapper one sample is taken every 30 m. The MTF effect is greatest when adjacent pixels show maximum contrast. This corresponds to a spatial frequency of $f_e/2$ which is known as the Nyquist frequency. An ideal imaging instrument is one for which the MTF has a value of unity for all frequencies below the Nyquist frequency and zero for all those above.

For real instruments, the MTF corresponding to the Nyquist frequency is always less than unity. As the spatial frequency of landscape variations falls, the MTF tends steadily towards unity. This can be seen in figure 1 which shows the variation of the MTF of Landsat-4 Thematic Mapper as a function of Spatial frequency (Schowengerdt, et al., 1985).

Referring to figure 1, we note that the variation in MTF between 0.1 fe and 0.5 fe is practically linear. For frequency of less than 0.1 fe the value of MTF is unity. We thus chose to model the variation of the MTF of the SPOT-HRV instruments according to figure 2. The MTF corresponding to a given pair of horizontal and vertical spatial frequencies was determined by simple linear interpolation from the values given in Table 1.

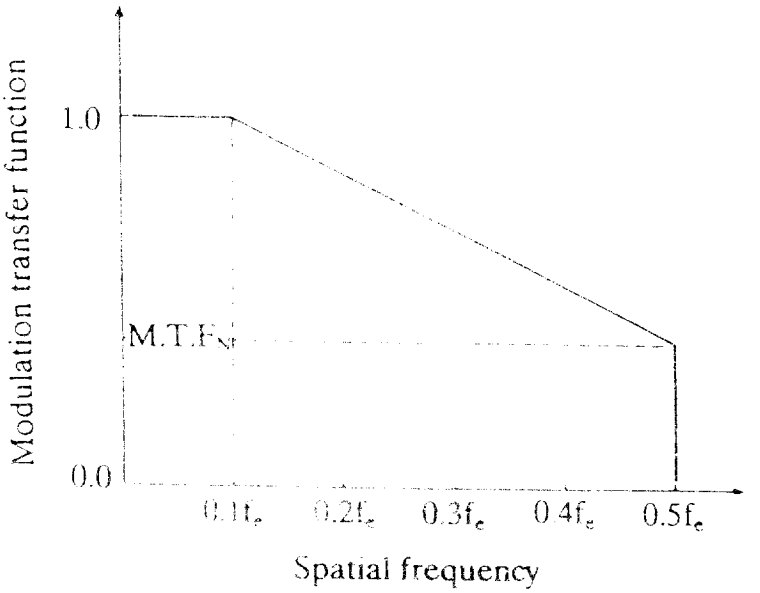

Figure 2 : Model for correction of MTF of SPOT-HRV imaging instruments (FTMn : MTF at the Nyquist frequency) (Guyot et al., 1990)

Table 1 : MTF values for SPOT 1 and 2 HRV instruments measured before launch at the Nyquist frequency.

Satellites	SPOT-1			SPOT-2		
Spectral bands	XS1	XS2	XS3	XS1	XS2	XS3
Horizontal MTF	0.41	0.38	0.36	0.42	0.42	0.41
Vertical MTF	0.48	0.41	0.28	0.49	0.46	0.38
Mean MTF	0.45	0.40	0.32	0.46	0.44	0.40

/...

To correct the image, we first determine the two-dimensional Fourier transform of the raw image. We then correct the image of the Fourier spectrum by dividing the real and imaginary values for each pair of horizontal and vertical frequencies by the corresponding MTF values. By applying the inverse transform to the image of the corrected spectrum, we obtain an image corrected for the instrument MTF. This method has been validated on SPOT data acquired on a test site (La Crau) in the south-east of France (Guyot et al., 1990; Gu, 1991, 1992).

Figure 3 shows the frequency of the corrections applied to the different pixels of an image. The correction is larger than 10% for more than the half of the pixels and it is greater than 50% for 13% of the pixels. This effect is observed because the correction applied to a given pixel depends on that pixel's immediate environment. MTF correction thus contributes to the improved interpretation of satellite imagery

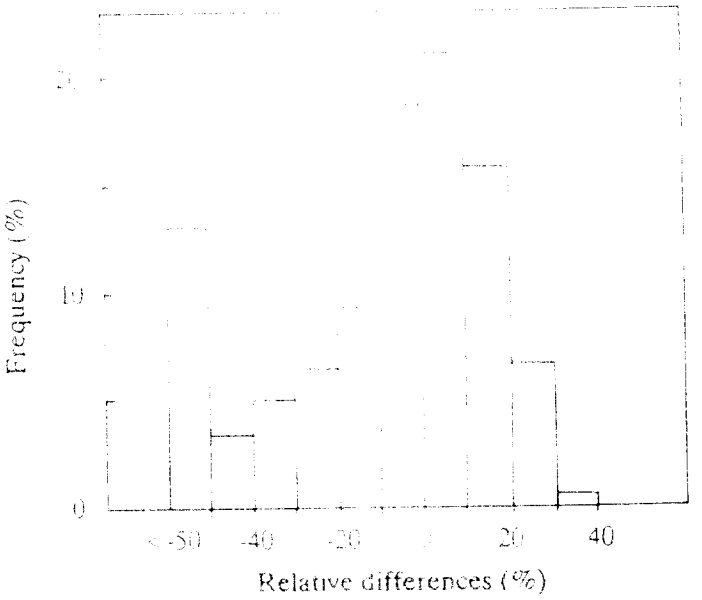

Figure 3 : Frequency histogram of corrections applied to the digital counts of the pixels of a SPOT-1 (HRV-1) image acquired on October 16, 1989 over La Crau (South-East France, KJ 49-262) (After Gu, 1992)

Contrary to methods involving the use of filters, which reduce the information content of the corrected imagery, the correction of MTF effects enables us to reconstitute the radiance counts corresponding to the different target objects while at the same time bringing out the boundaries between the different elements (fields, etc.) and the texture of each. It must be noted, however, that the reconstituted radiance counts (radiometric values) are those reaching the satellite-borne imaging instrument outside the Earth's atmosphere. The corresponding ground-level reflectances are determined by correcting first for instrument MTF effects then for atmospheric effects.

2.2. Absolute calibration and non-coincidence of homologous spectral bands

The comparison and the combination of multitemporal and multisystem satellite images requires also knowledge of the absolute calibration coefficients of the satellites. One of the most efficient methods used for the determination of these coefficients in the visible and near infrared domains is based on measurements performed at ground level on a test site (Slater et al., 1987; Santer et al., 1992; Gu et al., 1990, 1992). When these coefficients are known they can be used for the determination of the intercalibration coefficients of the sensors. The most accurate method

/...

consist in calibrating the different sensors the same day on the same test site (Gu et al., 1991). However, if these data are necessary they are not sufficient for interpreting multitemporal and multisystem satellite images. The measured radiances at the satellite level will depend on the shape of the reflectance spectra of the targets and on the relative spectral responsivity of the sensors.

As shown in figure 4, the relative spectral response of the sensors SPOT-1 HRV and Landsat-5 TM is different. The homologous spectral bands do not coincide and are centered on different wavelengths. The equivalent radiance $L(\lambda_1 - \lambda_2)$ measured in the spectral band comprised between the wavelengths λ_1 and λ_2, is defined by the following relationship :

$$L(\lambda_1 - \lambda_2) = \frac{\int_{\lambda_1}^{\lambda_2} L(\lambda) \cdot S(\lambda) \cdot d\lambda}{\int_{\lambda_1}^{\lambda_2} S(\lambda) \cdot d\lambda} \qquad (1)$$

with : $L(\lambda)$: target spectral radiance.

$S(\lambda)$: relative spectral sensitivity of the sensor.

As the radiance of a target viewed by a satellite sensor varies generally with the wavelength, the differences of the spectral sensitivities of the sensors in homologous bands induce differences in the measured equivalent radiances. These differences can be either positive or negative depending on the shape of the reflectance spectra. For example, the vegetation must have a larger radiance in TM-2 and 3 bands than in homologous SPOT XS1 and XS2 bands but, in the near-infrared the two sensors must give practically the same equivalent radiances (Figure 4).

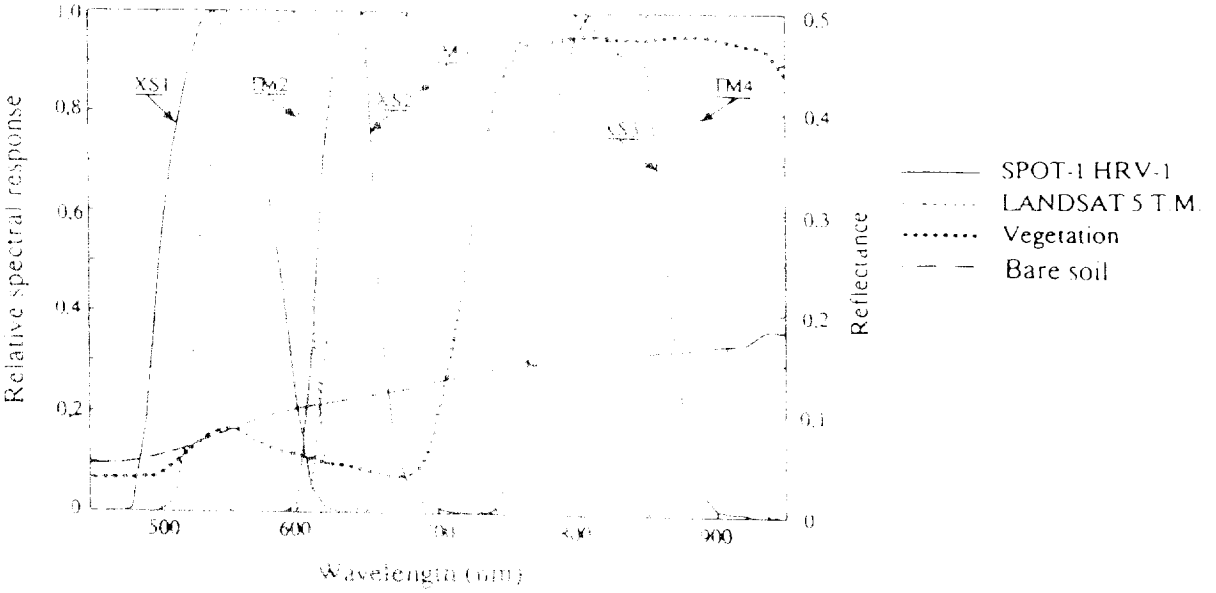

Figure 4 : Variation of the relative spectral response of the sensors SPOT-1 HRV and Landsat-5 TM compared to the reflectance spectra of a bare soil and of a dense plant canopy. (after Guyot and Gu, 1992)

/...

2.3. Atmospheric effects

As shown in figure 5 the signal reaching a satellite is largely affected by the atmosphere. At the ground level the irradiance has three components : the direct solar irradiance which is partly absorbed by atmospheric gases, the solar radiation diffused by the gas molecules and the aerosols and the radiation reflected by the surrounding of the target and partly backscattered by the atmosphere. Moreover the radiance measured at the satellite level has also three different components : the radiation coming directly from the target after its partial absorption by the atmosphere, the optical path radiance (depending on atmospheric diffusion) and the radiation reflected by the surrounding and diffused by the atmosphere.

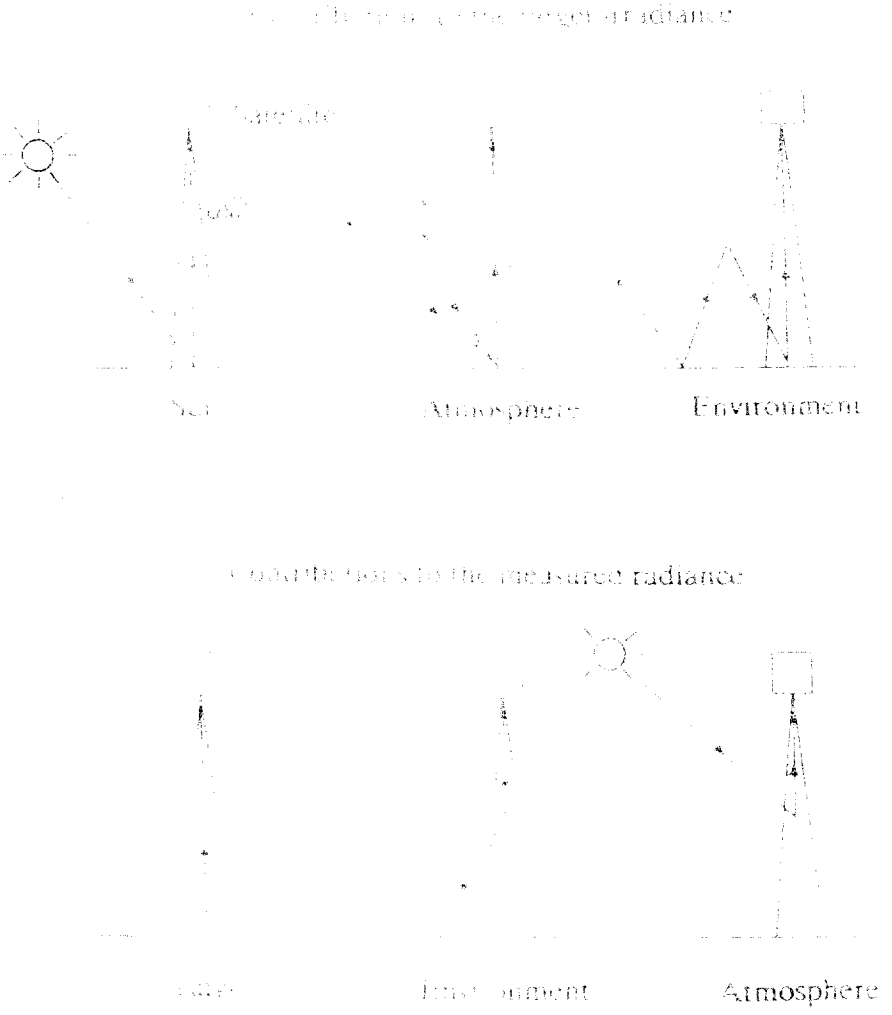

Figure 5 : Schematic representation of atmospheric effects on target radiance measured at satellite level. (After Guyot, 1988).

The apparent reflectance determined at satellite level R_{sat} can be schematically considered as equal to the sum of the contribution of the atmosphere and of the surrounding R_{as} and of the reflectance measured at ground level R_{grd} multiplied by the atmospheric transmittance for the double path $(t_a)^2$.

/ . . .

$$R_{sat} = (t_a)^2 R_{gnd} + R_{as} \quad (2)$$

If one consider a particular target, it is evident from equation (2) that the reflectance at the satellite level, will vary with atmospheric conditions. Equation (2) also shows that the same value of R_{sat} can correspond to different reflectances at the ground level, depending on the relative weights of atmospheric transmittance and optical path radiance. Moreover these effects vary with the considered spectral band : the shorter is the wavelength, the larger is the effect of atmospheric diffusion. These different effects are well known and different codes such as 5S (Tanré et al., 1990) are used operationally for the correction of atmospheric effects. Table 2 illustrates these atmospheric effects for two different targets viewed on the same SPOT image : a dry pebbly soil with a scarce vegetation (La Crau sèche) and irrigated meadows with dense vegetation (La Crau irriguée). One can see that the percent relative difference between the reflectances at satellite level and ground level is strongly dependant on the target reflectance and on the considered spectral band.

Table 2 : Atmospheric effects on the measured reflectance at satellite level over La Crau test site in the South-Est France. La Crau Sèche: dry pebbly soil with scarce vegetation, La Crau Irriguée : irrigated meadows with dense vegetation. (SPOT image acquired on September 30, 1989 with an horizontal visibility of 20 km)

Parameters	SPOT channels		
	Green (XS1)	Red (XS2)	Near-IR (XS3)
R_{as} (%)	[illegible]	6.4	5.9
$(t_a)^2$ (%) (double path)	58.3	64.4	68.2
La Crau Sèche			
R_{sat} (%)	[illegible]	18.6	23.8
R_{gnd} (%)	[illegible]	18.9	26.2
$100(R_{sat} - R_{gnd})/R_{gnd}$	+16.5	-1.7	-9.3
La Crau Irriguée			
R_{sat} (%)	12.0	11.1	31.5
R_{gnd} (%)	[illegible]	7.3	37.6
$100(R_{sat} - R_{gnd})/R_{gnd}$	+62.2	+52.1	-16.2

When the normalized difference NDVI is used for determining the standing green biomass or monitoring it evolution with the time, the atmospheric effects can induce some large distortions at the satellite level as shown in figure 6. If R_{Red} and R_{NIR} are the measured reflectances in red and near-infrared bands, NDVI is given by :

$$NDVI = (R_{NIR} - R_{Red}) / (R_{NIR} + R_{Red}) \quad (3)$$

The same value of NDVI can be obtained with the combinations of different values of R_{Red} and R_{NIR} at the ground level or at the satellite level. Figure 6 represents the variation of $NDVI_{gnd}$ at the ground level as a function of the red reflectance for different constant values of $NDVI_{sat}$ at the satellite level. As the red and near-infrared reflectances are differently affected by atmospheric conditions at the satellite level (Table 2), the calculation made for a clear

/...

atmosphere (20 km horizontal visibility) shows that the same value of $NDVI_{sat}$ corresponds to different values of $NDVI_{grd}$. Moreover $NDVI_{sat}$ is systematically smaller than $NDVI_{grd}$ and the difference between $NDVI_{sat}$ and $NDVI_{grd}$ increases when $NDVI_{grd}$ decreases. This remark shows that some very large errors can be introduced when the atmospheric effects are not taken into account.

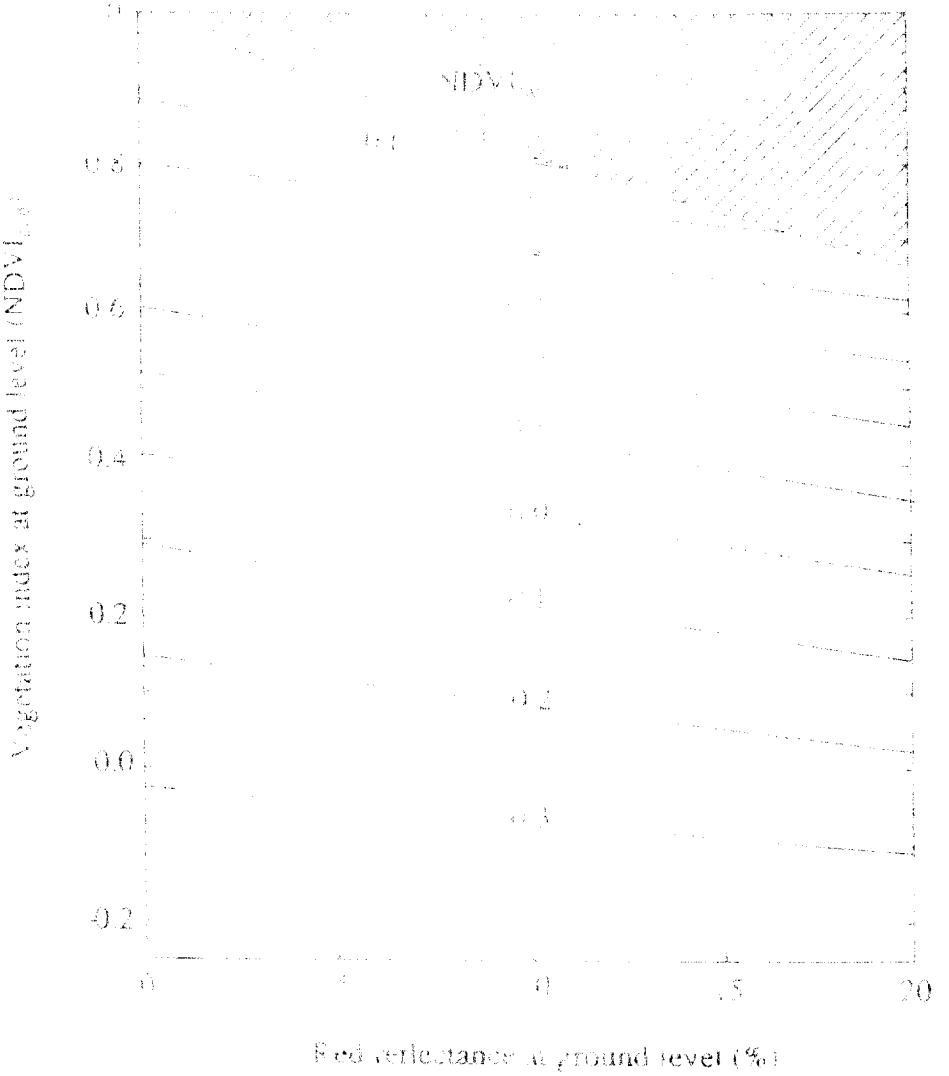

Figure 6 : Variation of $NDVI_{grd}$ at the ground level as a function of the red reflectance for different $NDVI_{sat}$ values determined at the satellite level (continuous lines). The calculation is based on SPOT data acquired over the South East France (04-15/87, 20 km horizontal visibility)

As the near-infrared band of NOAA AVHRR is quite wide (720-980 nm) comparatively to those of SPOT or Landsat TM (790-890 and 780-900 nm respectively) it includes some strong atmospheric absorption features due to O_2, CO_2 and H_2O. For this reason the data of NOAA-AVHRR have a larger temporal variability than SPOT or Landsat data. As one of the main use of NOAA-AVHRR is the global monitoring of the vegetation, it is absolutely necessary to correct the atmospheric effects before using its data. If the raw data are directly used some wrong interpretations can be drawn.

/...

2.4. Topographic effects

Three different effects are generally combined (Figure 7) :

- The orientation of the normal to the slope with respect to the Sun position affecting the direct and diffuse irradiance. In a mountainous area a pixel can be on the sunny or on the shady side where it just receives the diffuse irradiance (part AB of figure 7).

- The surrounding relief can mask the Sun for one part of the slope (part BC of figure 7) and can reduce the diffuse irradiance by masking one part of the solid angle under which the sky is viewed. In the masked part of the solid angle the slope receives the radiation diffused by the viewed slope which is generally less intense than the sky diffuse irradiance and has a different spectral composition.

- The increasing of the altitude reduces the atmospheric diffusion and absorption because the densest part of the atmosphere containing the heaviest aerosol load can be below the viewed area.

Moreover, comparatively to the same objects on a flat and horizontal surface, the directional properties of the reflectance are affected by the slope (Hugli and Frei, 1983)

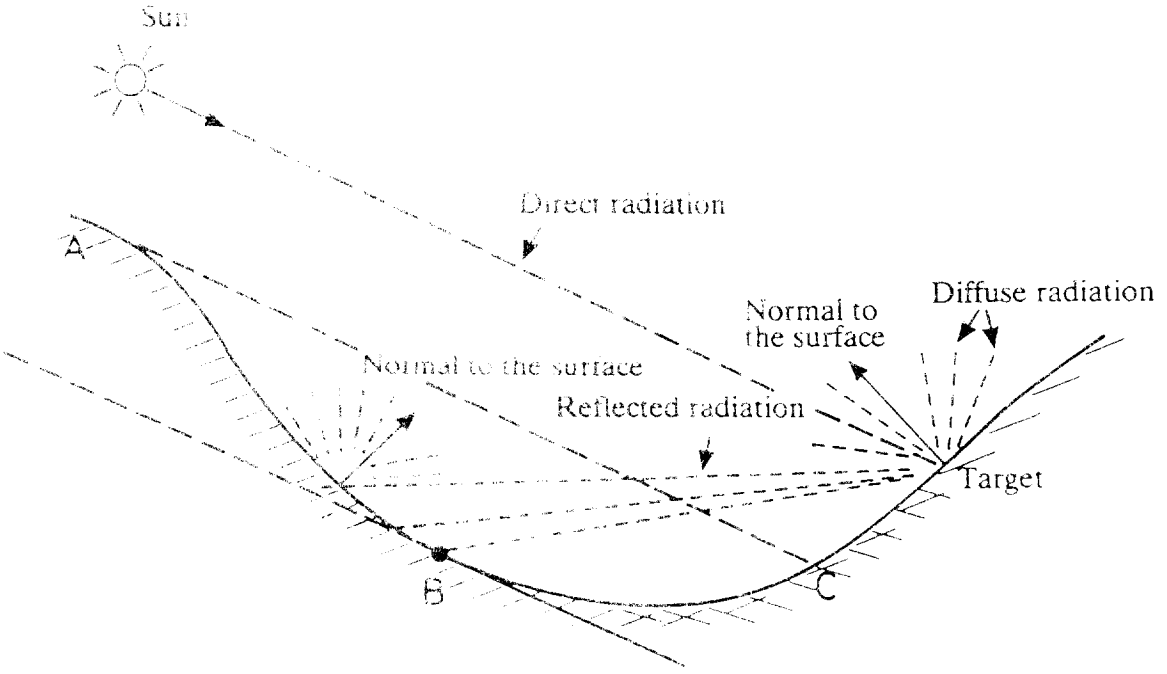

Figure 7 : Schematic representation of irradiance components in a mountainous area. (adapted from Proy, 1986)

To correct these effects it is necessary to use a digital terrain model enabling to determine the slopes, their orientations, the shadowing effects... The main difficulty consist in the determination of the diffuse irradiance from the sky and the environment and of its directional distribution. Different correction methods have been proposed by Kawata et al.(1988), Civco (1989), Le Men (1989), Ranson et al.(1986), Dave and Bernstein (1982), Proy (1986).

/...

2.5. Directional effects

As natural surfaces are not generally perfect lambertian diffusers, differences in viewing geometry affect the signal measured at the satellite level. Figure 8 shows an example corresponding to measurements performed on the test site selected for SPOT calibration (pebbly soil, sparsely covered by a low vegetation) in the South-East France (Gu et al., 1990; Guyot et al., 1990; Santer et al., 1992). One of the reasons for the selection of this test site was the limited angular variation of its bidirectional reflectance factor. However, Figure 8 shows that this angular variation cannot be neglected. When a plant canopy is considered, the angular variation of the bidirectional reflectance factor can be considerably large and it depends on the canopy geometry and on the spectral band considered (Guyot et al., 1980). The correction factor which must be applied for a off-nadir viewing is then dependant on the considered target.

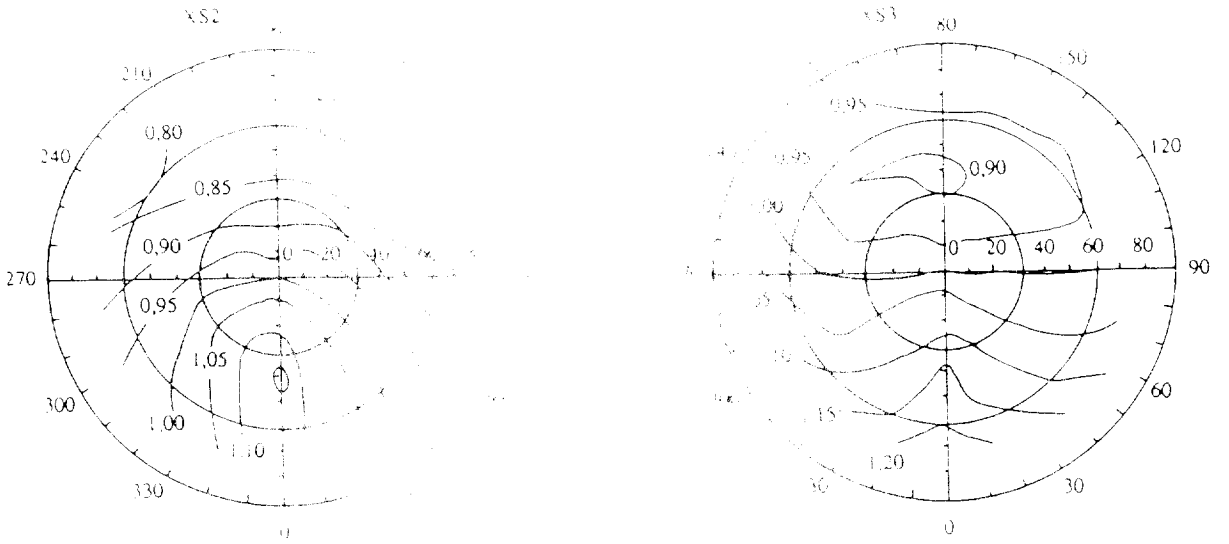

Figure 8 : Relative variation of the bidirectional reflectance factor of La Crau test site expressed as a function of nadir measurement. The concentric circles correspond to zenith view angles and the graduating of the external circle indicates the azimuth with respect to the Sun. Measurements performed with a SPOT simulation radiometer (July 27, 1988, 11h52 U.T.)

3 - IMPACT OF THE DIFFERENT EFFECTS ON IMAGE QUANTITATIVE ANALYSIS

As we have seen, the best way for obtaining comparable satellite data is to transform the satellite digital counts into reflectance at the ground level. This goal can be reached by the use of a step by step procedure. The first step consists in correcting the instrumental effects and more particularly the MTF in order to obtain digital counts proportional to the radiometric signal at the entrance of the satellite. These corrected digital counts are then transformed into radiances at the satellite level by using the calibration coefficients. The apparent reflectance of the pixels outside the atmosphere is then determined by dividing the apparent radiance by the equivalent solar

/...

irradiance at the satellite level. The solar irradiance on a plane perpendicular to the Sun direction and situated at the mean Earth-Sun distance is given in the characteristics of the different satellites. The equivalent solar irradiance is therefore calculated as a function of the Sun zenith angle and of the real Earth-Sun distance. When the apparent reflectance is obtained it is transformed into ground level reflectance by using an atmospheric transfer code. But this reflectance corresponds only to the real ground reflectance if the viewed area is flat and horizontal. If it is not the case the "ground level reflectance" corresponds to that of an imaginary horizontal flat surface. The real ground level reflectance is obtained after the introduction of topographic corrections. Moreover, if we want to compare data obtained by different satellites and/or under different view angles it is necessary to add corrections of spectral effects and of the viewing geometry.

This procedure is rather complex but it must be followed when accurate quantitative analyses of satellite data are necessary. For illustrating this conclusion three different cases will be successively analyzed in order to show the effects of the different factors.

3.1. Multitemporal image analysis

It is well known that the reflectance of natural surfaces vary with the time as a function of plant growth, soil moisture... Multitemporal satellite data can be used to monitor the evolution of the bidirectional reflectance factors of natural surfaces or to cover a larger area than that viewed on a single image. In the first case the phenomenon of interest is the evolution of the ground surface reflectance and in the second case this evolution will introduce errors which must be assessed and eventually corrected.

Table 3 : Reflectances (R) of different targets viewed by Landsat-5 TM on September 30 and their relative differences (Dif.) with the reflectances measured on October 16, 1989.

Targets	Spectral bands					
	TM2 (green)		TM3 (red)		TM4 (near-infrared)	
	R (%)	Dif. (%)	R (%)	Dif. (%)	R (%)	Dif. (%)
Crau sèche	15.7	-2.0	20.4	+0.5	25.5	5.1
Bare soil	14.4	0.0	16.4	+4.9	24.1	-8.3
Meadows	7.4	-6.8	6.4	0.0	37.4	4.3
Fruit trees	8.5	+3.5	9.9	+11.1	26.6	6.8
Forest 1	6.5	-15.3	7.4	8.1	19.6	3.6
Forest 2	5.7	-26.3	5.8	-18.0	18.0	1.1
Swamp	7.8	-10.2	8.0	-3.8	20.6	-2.4
Lake	15.0	10.0	15.8	-22.8	11.9	-60.5

In order to show that the temporal effects cannot be neglected even for a short time when the vegetation has a limited evolution, we have considered two successive Landsat TM images (30 September and 16 October 1989) corresponding to the same area in the South East France. At that time of the year (beginning of the autumn) the vegetation do not strongly evolves. However, as shown in Table 3 the relative differences between the ground level reflectances

/...

determined from satellite data, show some large relative differences depending on the considered targets

The Crau sèche corresponds to our the satellite calibration area. The two forests considered are Mediterranean forest with mainly evergreen trees and bushes. The very large differences observed for the lake are mainly due to the strong wind which was blowing on September 30.

The multitemporal measurements are also frequently performed with NOAA-AVHRR. When the sky is clear, this satellite can view a given area each day but under different inclinations of the view axis. This inclination of the view axis is accompanied by a variation of the length of the optical path within the atmosphere and a variation of the local time at which the measurements are performed. As these effects are just connected with a geometrical problem, it is relatively easy to correct them. However, this correction does not take into account the effect of the angular variability of the target bidirectional reflectance factor. Holben et al. (1986) have determined this effect for three cover types and have shown that this effect is partly reduced by the use of the normalized difference vegetation index (NDVI). But, as shown in figure 9 the NDVI variability remains quite large after the correction of the atmospheric effects. For correcting the target directional effects on NOAA-AVHRR data an empirical approach (Gutman, 1991) or a model (Roujean, 1991; Roujean et al., 1992) can be used. Figure 9 gives an example of results obtained after angular corrections performed with Roujean's model (1991). This example demonstrates the interest of such a correction for the interpretation of multitemporal data .

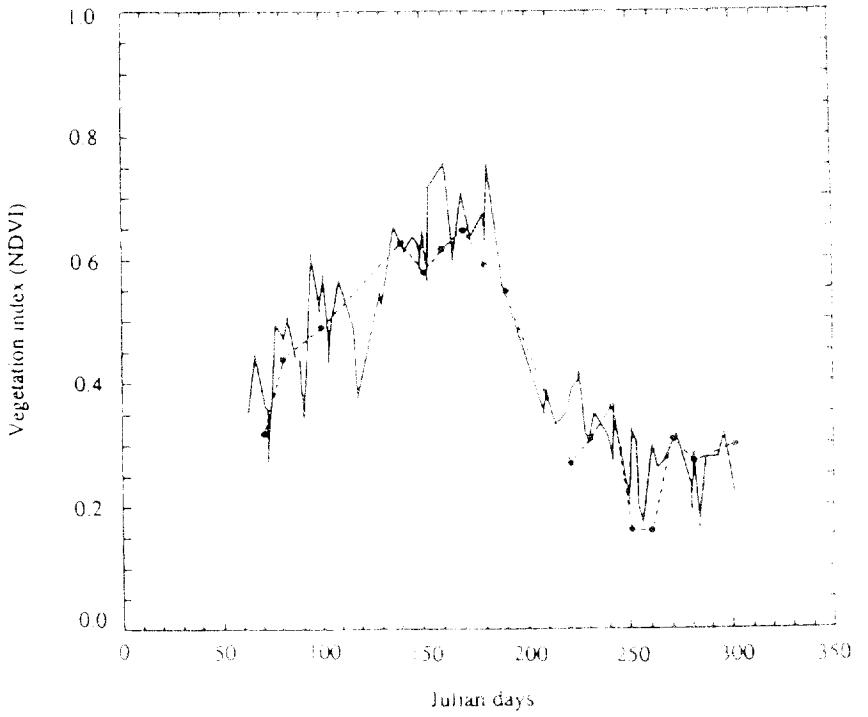

Figure 9 : Evolution of the normalized difference vegetation index (NDVI) along the year 1991 over La Beauce (Paris Basin). The continuous line corresponds to calculations performed on NOAA-AVHRR data (corresponding to series of 20 successive days) after the correction of atmospheric effects. The dashed line corresponds to the same data normalized by the Roujean's model.

/...

3.2. Multiangular image analysis

The angular variation of the bidirectional reflectance factor of natural surfaces can be used for obtaining some supplementary informations (variation fo plant canopy geometry...). These angular informations can be obtained from SPOT or NOAA-AVHRR data or from the combination of nadir viewing Landsat-TM and off-nadir viewing SPOT data acquired the same day.

If SPOT or NOAA-AVHRR data corresponding to different view angles are used, their com rison is only possible after the correction of the atmospheric effects. Moreover the time interval between the different images must be as short as possible in order to reduce the effects due to the variations of the optical characteristics of the target.

If nadir viewing Landsat-TM images are compared to off-nadir viewing SPOT images it is not only necessary to correct for the atmospheric effects but also for the non-coincidence of the spectral bands. Table 4 shows the effect of the non-coincidence of SPOT-HRV and Landsat-TM spectral bands for measurements performed the same day with nadir viewing. The observed differences vary as a function of the shape of the reflectance spectra of the different targets. This effect is amplified by the variation of the spectral composition of the equivalent solar irradiance in homologous spectral bands (convolution of the sensor spectral sensitivity with the solar spectrum).

Table 4 : Effect of the non coincidence of Landsat-TM and SPOT-HRV homologous spectral bands on the ground level reflectance of different targets. The data correspond to images acquired the same day (October 16, 1990) with nadir viewing.

Targets	SPOT HRV Reflectance (%)			Relative difference 100(HRV - TM)/HRV		
Spectral bands	Green	Red	Near-IR.	Green	Red	Near-IR.
Crau sèche	13.1	19.0	26.7	-18	-8	-0,4
Bare soil	13.8	16.6	24.5	-4	-3	-2
Meadows	7.7	7.5	37.8	+3	+15	-4
Fruit trees	8.5	12.0	28.0	-4	+8	-1
Forest 1	5.9	7.9	21.2	+7	+14	+5
Forest 2	5.3	6.0	19.0	+21	+22	+6
Swamp	7.5	8.6	20.2	+7	+10	+0,5
Lake	12.6	12.0	7.8	-7	-17	+40

3.3. Multisystem image analysis

The combination of multisystem images is done in order to reach different objectives : multitemporal, multiangular or multi-spatial resolution analyses. Besides the different effects which have been analyzed, the essential problem is that of the intercalibration of the sensors. The MTF effect plays also an important role when data corresponding to different spatial resolutions are compared. For example, if the analysis is performed at the level of NOAA-AVHRR pixels, the comparison with averaged SPOT or Landsat data is affected by AVHRR

/...

MTF (comparison of a single pixel with the average value of a large number of pixels eliminating the MTF effect).

In multisystem image analysis the observed differences are generally due to the combination of different effects. As they can have opposite actions their global effect can be smaller than the isolated effect of a given factor. As an example Table 5 shows the combined effects (spectral, temporal, directional) on SPOT and Landsat-TM data which can be compared with the data presented in Tables 3 and 4. As the reflectances are generally smaller in the visible than in the near-infrared, the observed relative differences are larger in the visible than in the near infrared.

Table 5 : Differences in the reflectance of different targets due to the combination of spectral, temporal and directional effects. The data used correspond to Landsat-TM and SPOT images of September 30 and October 16, 1989. On September 30 the inclination of the SPOT view axis was 10°. The SPOT image of October 16 (nadir viewing) is taken as a reference for expressing the differences.

Targets	Differences expressed in reflectance (%)			Relative differences (%)		
Spectral bands	Green	Red	Near-IR.	Green	Red	Near-IR.
Crau sèche	+2.1	+1.8	+0.6	+16	+9	+3
Bare soil	+1.2	+1.3	-1.1	+9	+8	+4
Meadows	-0.5	-1.9	+1.4	-7	-25	-4
Fruit trees	+0.4	-0.3	+1.5	+5	-3	+5
Forest 1	-1.1	-1.3	-0.9	-19	-16	-4
Forest 2	-2.0	-1.8	-1.6	-38	-30	-8
Swamp	-0.9	-1.0	-1.1	-12	-12	-5
Lake	-1.2	-4.0	-8.8	-10	-73	-113

4 - CONCLUSION

This short review shows that a large number of factors affect the comparison of multispectral multitemporal and/or multisystem satellite data. The effects of these factors can be quite large and it is absolutely necessary to correct for them when a quantitative analysis is performed.

Some corrections such as the MTF effect, the intercalibration of the sensors, the solar equivalent irradiance, the Sun elevation, the atmospheric effects... can be relatively easily performed. Some others such as the spectral , directional and temporal effects are more difficult to get under control. They will induce effects equivalent to a noise which will necessitate to introduce a threshold for the significance of the observed differences. this threshold will vary as a function of the characteristics of considered instruments and targets.

/...

REFERENCES

Bildgen P., Boulegue J., Gerovannis H., Gitg J. P., 1989; Essai d'utilisation simultanée des données Landsat MSS, TM et SPOT pour la comparaison des valeurs radiométriques des pixels. Bul. S.F.P.T. n° 115 : 11-13

Cicone R.C., Metzler M.D., 1984; comparison of Landsat MSS, Nimbus-7 CZCS, and NOAA-7 AVHRR features for land-use analysis. Remote Sens. Environ. 14 : 257-265.

Civco D.L., 1989; Topographic normalization of Landsat Thematic Mapper digital imagery. Photogram. Eng. Remote Sens., 46 : 643-647

Colwell R.N., Poulton C.E., 1985; SPOT simulation imagery for urban monitoring : A comparison with Landsat TM and MSS imagery an with high altitude color infrared photography. Photogramm. Eng. Remote Sens. 51(8) : 1093-1101.

Crist E.P., Cicone R.C., 1984; Comparisons of the dimensionality and features of simulated Landsat-4 MSS and TM data. Remote Sens. Environ. 14 : 235-246.

Dave J.V., Bernstein R., 1982; Effect of terrain orientation and solar position on satellite-level luminance observations. Remote Sens. Environ. 12 : 331-348.

Gu X.F., 1991; Etalonnage et intercomparaison des données satellitaires en utilisant le site test de la Crau (Appliqué aux images SPOT1-HRV, LANDSAT5-TM, NOAA11-AVHRR). Thèse de Doctorat, Méthodes Physiques en Télédétection, Université de Paris VII : 260 pp

Gu X.F., 1992; Analyse et correction des effets de la FTM sur les images SPOT-HRV. In XVII Congress of ISPRS, August 2-14, 1992, Washington, DC.

Gu X.F., Guyot G., Verbrugghe M., 1990; Analyse de la variabilité spatiale d'un site test - Exemple de la Crau (France). Photo-Interprétation 90-1, Fasc. 5: 39-52

Gu X.F., Guyot G., Verbrugghe M., 1992; Evaluation of measurement errors on ground surface reflectance for satellite calibration. International Journal of Remote Sensing (In press)

Gu X.F., Verbrugghe M., Guyot G., 1991; Inter-etalonnage de SPOT1-HRV, LANDSAT-TM et NOAA11-AVHRR dans les domaines du visible et du proche infrarouge. In Cinquième Coll. Int. Mesures Physiques et Signatures en Télédétection, 14-18 Jan. 1991, Courchevel (France) Ed. ESA Publ. Div. ESA SP-319: 45-48.

Gutman G., 1991; Vegetation indices from AVHRR : an update and future prospects. Remote Sens. Environ. 35 : 121-136.

Guyot G., 1989; Les signatures spectrales des surfaces naturelles. Collection Télédétection Satellitaire, Paradigme, Caen (France) : 178 pp.

Guyot G., Gu X.F., Clasure F., 1990; Correction de la FTM sur les images SPOT. Photo-Interprétation 1990-6 :17-28.

/ . . .

Guyot G., Gu X.F., 1992. Intercomparaison des images satellitaires multicapteurs. In XVII Congress of ISPRS, August 2-14, 1992, Washington, DC..

Guyot G., Gu X.F., Verbrugghe M., 1990; Caractérisation des propriétés optiques du site de la Crau. Rapport final Marché N° 833/CNES/87/4891/00, INRA Bioclimatologie Montfavet (France) : 79p.

Guyot G., Malet P., Baret F., 1980. Analyse des indicatrices de réflexion de l'orge et du blé, possibilités de la stéréoradiométrie. In Proceedings International Symposium ISP Hamburg, (Germany), International Archives of Photogrammetry, 22 : 372-381.

Holben B., Kimes D.S., Fraser R.S., 1986: Directional reflectance response in AVHRR red and near IR bands for three cover types and varying atmospheric conditions. Remote Sens. Environ. 17 : 37-53.

Hugli H., Frei W., 1983; Understanding anisotropic reflectance in mountainous terrain. Photogram? Eng. Remote Sens., 49 : 671-683.

Kawata Y., Ueno S., Kusaka T., 1988: Radiometric correction for atmospheric and topographic effects on the Landsat MSS images. Int. J. Remote Sens., 9 : 729-748.

Le Men H., 1989; Correction d'éclairement et calibration absolue des images SPOT; effets de la stéréoradiométrie. In C.R. Journées Télédétection, Images, Satellites et Milieux Terrestres en Régions Arides Tropicales, 14-17 Novembre 1988, Bondy (France) : 51-55.

Leroy M., 1990; Modèles des systèmes de mesure imageurs optiques. In Ecole d'Eté en Télédétection Spatiale : Aspects Physiques et Modélisation, Août 1988, Cepadues Ed. Toumlouse (France) : 311-363.

Proy C., 1986; Intégration du relief au traitement d'image de télédétection. Thèse de Docteur-Ingénieur de l'Institut National Polytechnique de Toulouse, 173pp.

Ranson K.J., Daughtry C.S.T., Biehl L.L., 1986; Sun angle, view angle, and background effects on spectral response of simulated balsam fir canopies. Photogram. Eng. Remote Sens., 52 : 649-658.

Roujean J.L., 1991; Modélisation des effets directionnels de la surface pour la normalisation de données satellitaires de télédétection. Thèse Doctorat Université Paul Sabatier, Toulouse.

Roujean J.L., Leroy M., Deschamps P.Y., Podaire A., 1992; Evidence of surface reflectance bidirectional effects from NOAA-AVHRR multitemporal data set. Int J. Remote Sens. 13 : 685-698.

Royer A., Charbonneau L., Brochu R., Murphy J.M., Teillet P.M., 1987; Radiometric comparaison of the LANDSAT-5 TM and MSS sensors. Int. J. Remote Sens., 8(4): 579-591.

Santer R., Gu X.F., Guyot G., Deuzé J., Devaux C., Vermote E., Verbrugghe M., 1992; SPOT Calibration on the test site "La Crau" (France).Remote Sens. Environ. (In press)

Schowengerdt R.A., Archwamety C., Wrigley R.C., 1985; Landsat Thematic-Mapper derived MTF. Photogramm. Eng. Remote Sens., 51 : 1395-1406.

/...

Slater P.N., Biggar S.F., Holm R.D., Jackson R.D., Mao Y., Moran M.S., Palmer J.M., Yuan B., 1987; Reflectance and radiance-based methods for the in-flight absolute calibration of multispectral sensors. Remote Sens. Environ., 22 : 11-37.

Tanré D., Deroo C., Duhaut P., Herman M., Morcrette J.J., Perbos J., Deschamps P.Y., 1990; Description of a computer code to simulate the satellite signal in the solar spectrum: The 5S code. Int. J. Remote Sens., 11(4): 659-668.

/...

MULTIVARIATE ANALYSIS TECHNIQUES

N.J. Mulder

ITC

Netherlands

/...

Invited paper

[illegible] Remote Sensing Data Analysis,
[illegible] Applications
[illegible] USA, 6-7 August 1992

[illegible] MULTIVARIATE ANALYSIS TECHNIQUES

[illegible] Bakker ITC,
[illegible] Informatics, RS-I
[illegible] Electrical Engineering
[illegible] The Netherlands

Abstract

Multivariate [illegible] have been applied in the context of statistical pattern [illegible] the purpose of feature extraction and data volume reduction [illegible] decennia now.
An overview is given [illegible] fundamentals of mva techniques with emphasis on assumptions and applicability. The fundamental relation is the frequency of coincidence of nominal, interval and ordinal (RS) data. It is shown that for most RS data the assumptions [illegible] about linearity and normal-ity of data are not valid. This [illegible] use of [illegible] causal models with residual uncertainty in model parameters. Multivariate [illegible] error methods are replacing classical mva techniques [illegible] minimum sum of squares.
Consequences of [illegible] for decision functions are discussed. Fashionable methods [illegible] neural networks, fuzzy sets and measures of belief adjustment [illegible]

Statistical Pattern Recognition and Multivariate Analysis.

In the late 60-ies and [illegible] multivariate analysis, especially principal components analysis was extensively used for spatial and spectral feature extraction.
In spatial feature [illegible] multiple dimensional data vectors were derived from fixed [illegible] windows varying in size from 3 x 3 elements to as large as 64 x 64 [illegible] elements.
Appendix A gives [illegible]

Theoretically, the [illegible] feature extraction is optimum in the minimum root mean squared sense [illegible] better than Fourier transforms, cosine transforms, Hadamard [illegible].
However, application of [illegible] intelligence, by looking at the discarded (residual) images, showed that [illegible] line and edge features were thrown away, while the obvious area [illegible] was kept. So something was wrong with the assumptions [illegible]

/...

Apparently, the assumption that [illegible]
to "information" is wrong.

Common sense showed that a re-definition [illegible] was in order.

Definition: Information is a relation between a question domain and its answer domain.

Q I a , I = {Q,A}.
The eye questions an image [illegible] and then looks for average values [illegible]

Image analysis starts with image segmentation [illegible] for four hypotheses:

H 0 homogeneous area
H 1 edge
H 2 line
H 3 noise

The features needed for testing these hypotheses [illegible] orthogonal Taylor expansion on [illegible] differential-operators:

$Diff^{-1}$ = average
$Diff^{0}$ = original
$Diff^{1}$ = gradient
$Diff^{2}$ = Hessian

With structure elements added [illegible]
The "new" definition of information [illegible] evidence.

Conclusion: for spatial feature extraction [illegible] components) analysis is inferior to [illegible] was shown to be superior to Fourier, Hadamard [illegible] are even superior to these methods.

Spectral Feature Extraction

Initially (1973/1974), when first MSS [illegible] were received [N.H.W. Donker and N.J. Mulder, 1976] applied PCA for data compression and even for colour coding, to the [illegible] image frame. Most of the time the data could be [illegible], but sometimes PC3 contained answers to questions related to [illegible] discrimination of plantations as against natural forest.
In an experiment for on-board data [illegible] N. Donker, 1979] documented that the [illegible] unstable, they would change with scanline!

Back to natural intelligence [illegible]

Q.1 - why are spectral data correlated?
A.1.1- because there are only few basic [illegible] at work possibly two, most of the time [illegible] a mixture of metal oxides.

/...

A.1.2- the reflection model:

$$band_i = Sun_i \times Cosine\ \theta_{Sun,normal} \times reflectance_i$$

has two common multiplicative factors for all spectral classes, Sun; and Cos θ!

Q.2 - are the data normally distributed?
A.2 - no! See the multiplicative reflection model; ellipses in reflectance space become ovals in reflection space.

Q.3 - is the assumption of orthogonal factors a realistic one?
A.3. - no, even in reflectance space, the process is that of spectral mixture in a mixture triangle of normalised band$_i$

$\{band_i / \Sigma\ Sun_i Cos\theta_i\}_r$ = weighted reflectance for band i

with corner points $\overrightarrow{veg}$, $\overrightarrow{soil}$, $\overrightarrow{water}$. [the triangle is oblong]

Conclusion: for spectral feature extraction, the assumptions, implicitly made about orthogonality of factors, linearity (additive) and stability, are not valid when applied to multispectral data.

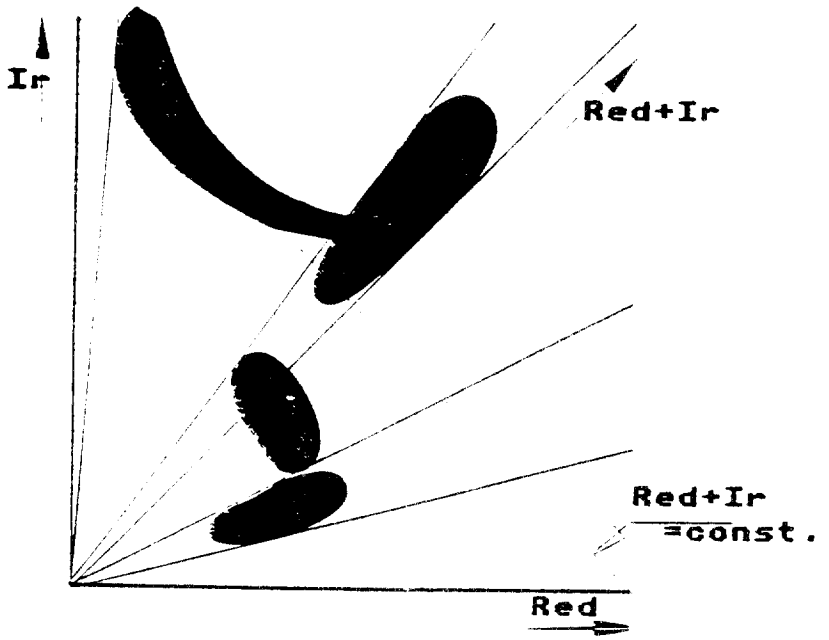

Fig. 1 Non-linear, non-orthogonal effects in spectral data.

/...

Consequences: statistical factor analysis has now (since 1976 at ITC) been replaced by an analysis of physical factors as represented by the reflectance model. Mapping the data reflectance triangle $\vec{V}'$, $\vec{S}'$, $\vec{W}'$ onto the colour triangle R', G', B' and mapping data intensity to display intensity.

$$b_i \rightarrow b_i' = b_i / \Sigma b_i \quad [\vec{V}', \vec{S}', \vec{W}'] \rightarrow [\text{Colour}_i'] \quad \text{(reflectance)}$$

$$\Sigma b_i \rightarrow \Sigma \text{Colour}_i \quad \text{(photons)}$$

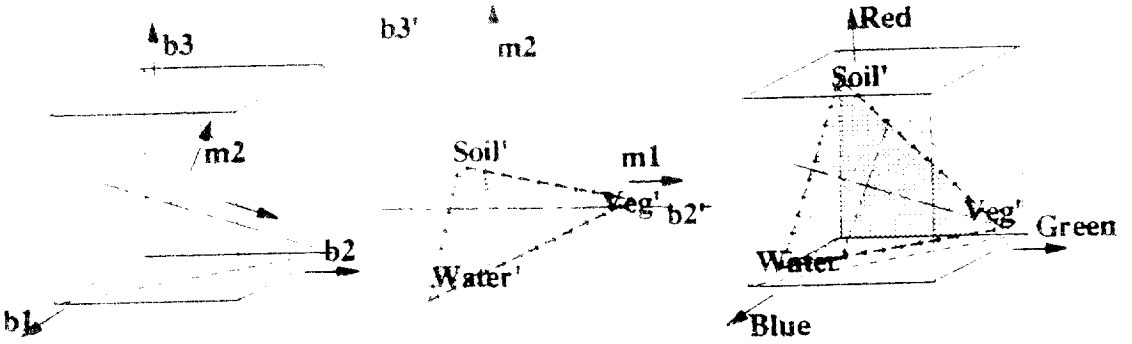

Data Cube (b1,b2,b3) | Data triangle on m1,m2 or on b1',b2',b3'. bi' = bi/sum_i(bi) | Colour cube on R,G,B. Colour triangle on m1,m2 or on R'B'G'.

Fig.2 Model based spectral image analysis.

Statistical classification: frequency of coincidence, minimum cost of error.

$$\left.\begin{matrix} \text{class} \\ f1 \\ f2 \end{matrix}\right\} \text{(map)} \rightarrow \text{Freq (class, f1, f2)}$$

If a representative sample has been taken of class; ←-- GIS, features f1, f2 then, given (f1, f2), the hypothesis of object ←-- class j can be evaluated: (f1,f2)--→ Freq(class)

If the benefit of truth is 1$, and the cost of falsehood is (-)1$, then minimum cost = max. truth = max. likelihood.

Else a high cost for some class' ≠ class is equivalent to multiply the number of representatives for that class by the relative cost factor
--→ minimum cost ≠ maximum truth --→ weighted maximum likelihood.

/...

Danger!commercial packages assume normal distributions for Frequency(Class, f1, f2)! As argued under PCa, this is a false assumption.
→ Use a non-parametric classifier such as K-NN for minimum sensitivity to wrong assumptions.

Fuzzy sets, belief adjustment, certainty factors.
Ref. [Mulder,N.J. and H. Middelkoop, 1990]
The maximum belief decision rule is not the maximum truth rule
The maximum belief decision rule is not the minimum cost rule!
Fuzzy logic is redundant as the mechanism of on/off regulators and sensors is well understood and documented. Statistics of time spent in the on or off state are used to calculate likelihoods and cost of error functions.

Neural networks are unnecessarily complicated means of finding decision boundaries in feature space. In a typical case, the training time for a neural network was 3000 x training K-NN and the performance was 5% less. Comparisons in literature of statistical pattern recognition vs. neural nets are based on the (mis)use of parametric maximum likelihood classifiers.
Ref. [N.J. Mulder and L.J. Spreeuwers, 1991]

References

[N.H.W. Donker and N.J. Mulder] "Analysis of MSS Digital Imagery with the aid of Principal Component Transform", presented at 13th Congress of ISP, Comm.VII, Helsinki 1976; ITC, Enschede, the Netherlands
[N.J. Mulder and N. Donker] "An Evaluation of Spectral- and Intensity- Data Compression Methods", ESA contract no. 3601/78/NL/HP(SC) (1979); ITC, Enschede, the Netherlands

[N.J. Mulder and L.J. Spreeuwers] "Neural Networks applied to the Classification of Remotely Sensed Data", in IGARSS'91 Remote Sensing: Global Monitoring for Earth Management, Vol.4, pp. 2211-2215, Proceedings of 1991 Intern. Geoscience and Remote Sensing Symposium, Helsinki Univ. of Technology, Espoo, Finland - June 3-6, 1991

/...

Appendix A

Spatial and Spectral principal components transformation in an "object oriented" style.
In the initial application of pct to RS data [Mulder & Donker, 1976], we tended to copy the relevant statistical programmes and put them in (Fortran) code. For most students and staff, this did not make it easier to understand a black box of tricks. Especially the spatial pct needed quite some amount of explaining.
On the software side the direct translation of formulae to code led to redundant code, as each "new" formula needed a new chunk of code. Also the generated code was not efficient in terms of keeping important variables in registers.

A solution to the above problems is based on a style of programming where the final goal is defined first. Reaching the goal we look for existing simple operations which transform whole images in the pct, requiring few variables, which can stay in registers.

Goal for spatial principal components transformation:
From one image, produce e.g. four new images for which the co-variance matrix is orthogonal. These principal component images should be ordered on co-variance (eigen value of the co-variance of an "original" set of four images).

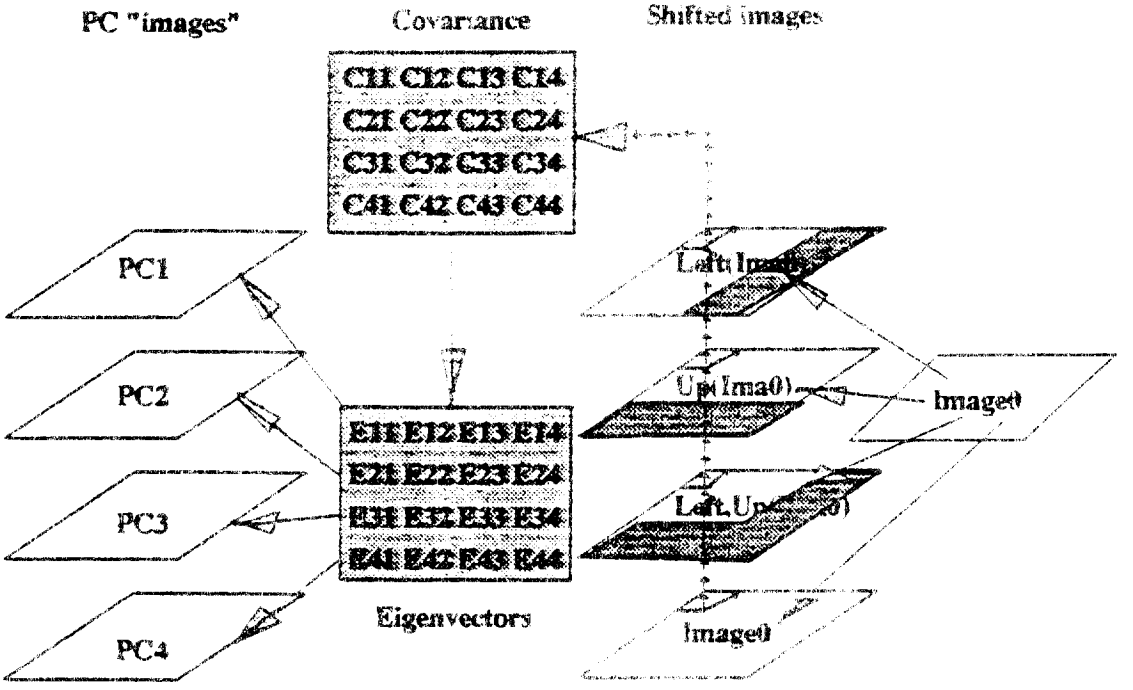

goal state

Fig. 2 Goal directed problem specification in a spatial pct

/...

In order to reach the end goal, a sub goal must be reached with four images and their co-variance matrix.

These four images should represent the spatial relations between an element in the original image and e.g. its three next neighbours, for all elements of Im 0.

Instead of calculating a 4 x 4 co-variance matrix from a set of sub-images

{(Im(x,y),Im(x+1,y),Im(x,y+1),Im(x+1,y+1))} we calculate the co-variance matrix from a set of images with four components $\{\overrightarrow{Im}(x,y)\}$

where $Im_1(x,y) = Im_0(x,y)$, $Im_2(x,y) = Im_0(x+1,y)$, $Im_3(x,y) = Im_0(x,y+1)$

$Im_4(x,y) = Im_0(x+1,y+1)$.:

This is equivalent to the following operations:

```
Im1=copy(Im 0),shift (0)
Im2=copy(Im 0),shift (left)
Im3=copy(Im 0),shift (up)
Im4=copy(Im 0),shift(up,left)
```

Both copy and shift operations are put in a single machine instruction repeated over all "pixels" of the intersect set of Im 1, Im 2, Im 3, Im 4 and hence the operation is very fast.
Refining the goal state descriptions we need to calculate co-variances of the goal set pc 1...4, which can only be done after pc transform which requires the co-variance matric of the set of image "sample" vectors in Im 1..4 of figure 1b.

To calculate a co-variance matrix, a statistical handbook would provide a formula like:

$$C(i,j) = \Sigma_k (x_{i_k} - \mu_i)(x_{j_k} - \mu_j) \; / \; (K - 1).$$

For the complete C matrix, we need loops for k, i and j, while an average vector $\vec{\mu}$ must have been precalculated requiring another loop. Direct coding of the statistical formula gives messy software.
In theoretical physics, however, we know that the shape of a cloud (cluster) of stars or other matter can be characterised by moments:

$$M^p_{i,j} = \sum_{k=1}^{k} x^r_{i_k} x^s_{j_k} \cdot f_{i,j} \quad \text{with } p = r + s$$

and for all members of the set of observation $f_{i,j} = 1$ else $f_{i,j} = 0$:

$$M^0 = \Sigma_k \, x^0_{i_k} \, x^0_{j_k} \qquad M^1_i = \Sigma_k \, x^1_{i_k} \, x^0_{j_k}$$

/...

$$M^1_j = \Sigma_k \, x^0_{i_k} . \, x^1_{j_k} \qquad M^2_{(i,j)} = \Sigma_k \, x_{i_k} \, x_{j_k}$$

The summation is done over all objects in the set with cardinal number k.

The relation between moments and statistics is:

$$M^0 \longleftrightarrow k \qquad M^1 i \longleftrightarrow \mu,i \times k \qquad M^1 j \longleftrightarrow \mu,j \times k$$

$$M^2(i,j) \longleftrightarrow C(i,j) \times k + \mu,i \times \mu,j$$

or

$$C(i,j) = \frac{M^2(i,j)}{k} - \frac{M^1 i}{k} \cdot \frac{M^1 j}{k}$$

$$C(i,j) = \frac{M^2(i,j)}{M^0} - \frac{M^1 i}{M^0} \cdot \frac{M^1 j}{M^0}$$

Normalizing C(i,j) to k - 1 instead of k does not make sense as, for a single point, all central moments must be 0 instead of 0/0!

Substitution of the moments in the covariance formula produces the covariance matrix from which the appropriate algorithm from a subroutine library like "Numerical Recipes" will produce an eigen vector matrix and corresponding eigen values.

The PC transform proper is a matrix transformation per vector of four image elements

$$\begin{bmatrix} Im1 \\ Im2 \\ Im3 \\ Im4 \end{bmatrix} \rightarrow \begin{bmatrix} PCT \end{bmatrix} \rightarrow \begin{bmatrix} PC1 \\ PC2 \\ PC3 \\ PC4 \end{bmatrix}$$

This image transformation can be "objectionized" by

```
Clear image # PC i
For input j = 1 to 4
    multiply-add (PC(i,j) x im(j), imagePC(i))
next input j
```

/...

IMAGE SCANNERS AND INTERACTIVE WORKSTATIONS FOR SEMI-AUTOMATIC MAPPING WITH EMPHASIS ON LOW-COST SOLUTIONS

T. T. Sarjakoski

Finnish Geodetic Institute

Helsinki, Finland

/...

COMPRESSION OF DIGITAL COLOR IMAGES BY THE JPEG

Lasse Harmo and Tapani Sarjakoski

Finnish Geodetic Institute
Ilmalankatu 1 A
SF-00240 Helsinki
Finland
E-mail: lasse.harmo@fgi.fi

ABSTRACT

Image compression is not only desirable it is also a necessity for the utilization of large digital images, e.g. digitized aerial color images. The JPEG standard proposal offers an alternative for carrying out the image compression task. The JPEG method itself and its suitability for photogrammetric work are studied, with special attention being paid to the geometric degradation of digital images in image compression. In our experience JPEG image compression seems to be a good choice for color image compression. It gives a compression ratio of about 1:10 without considerable degradation in the visual or geometric quality of the image.

KEY WORDS: Image compression, standardization, geometric degradation

1. INTRODUCTION

Compression of digital images is desirable because of the large volume of data in the images. It is especially useful in applications where many large images have to be archieved in a limited storage space or where digital images are transmitted over limited channels.

The basic idea in image compression is to remove redundancy from the image data. This is usually done by mapping the image to a set of coefficients. The resulting set is then quantized to a number of possible values which are coded by an appropriate encoding method. Nowadays, the most popular methods for removing redundancy are based on the discrete cosine transform (DCT), differential pulse code modulation (DPCM), vector quantization (VQ) and on the use of Laplacian pyramids.

The image compression standard proposed by the JPEG group offers a viable way of accomplishing the image compression task. This paper gives an overview of the JPEG compression method, which is still quite new to the photogrammetric community. Because the digital images used in the photogrammetric work tend to be very large, it is not reasonable to compress the whole image in a single compression step. A scheme for doing this is in smaller parts is proposed. The geometric effect of JPEG image compression on full-color images is empirically studied. We wanted to test our assumption that JPEG image compression does not affect the image geometry if small compression ratios are used. We also wanted to know what happens when the amount of compression becomes large.

2. IMAGE COMPRESSION BY THE JPEG

The following overview of the JPEG is based on an article by Wallace (1991), although other references also exist (C-Cube Microsystems, 1990; Storm Technology, 1990).

2.1 Background

The standard for image data compression discussed in this paper was proposed by the Joint Photographic Experts Group (JPEG), an ISO/CCITT working group, whose aim is to develop an international standard for continuous-tone still picture compression (ISO working group: JTC1/SC2/WG10 in collaboration with CCITT SGVIII).

The JPEG traces its origins to videotex related project in the early 1980s. Its goal has, however, become more general as the number of applications needing a compression standard has grown. In the compression method selection process - conducted by the JPEG group - three compression algorithms out of 12 were chosen for a closer look in the 1987. Finally in early 1988 a discrete cosine transform (DCT)-based compression was chosen for standard development. In 1988 and 1990 the DCT-based method was further defined, tested and documented. After that the standard proposal started on its way through a normal ISO standardization process: from a Committee Draft (CD) to a Draft International Standard (DIS) and from there to an International Standard (IS).

A paper to be presented at the XVII ISPRS Congress, 2-14 August 1992, Washington, D.C. Will be printed on the proceedings, Archives of ISPRS, Commission III, Volume

/...

The final ISO standard for image compression according to the JPEG will eventually be divided into two parts. Part 1 will specify the requirements and guidelines for the JPEG image compression, and Part 2 will contain the compliance tests taken. Although the JPEG standard proposal is already widely used in many applications, it will still be some time before the International Standard (IS) for the JPEG image compression is approved.

2.2 Baseline Sequential Encoding

The goal of the JPEG is to develop an image compression standard for compressing still-frame, continuous-tone images. The standard should cover as wide a range of applications as is feasible for a single standard. To satisfy the demand for versatile utilization the proposed JPEG standard is divided into four different modes: sequential encoding, progressive encoding, lossless encoding and hierarchical encoding. One or more distinct codecs (encoder/decoder -pairs) is specified for each of these modes.

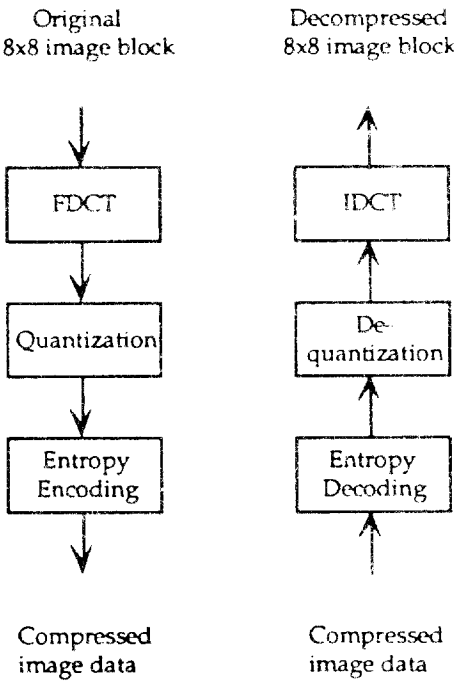

Figure 1. Baseline JPEG compression scheme.

Although the JPEG provides a variety of possibilities for encoding, it also gives a "basic" compression scheme - Baseline sequential coding - for straightforward use. In the following we shall concentrate on this Baseline method. This restriction is justified because Baseline encoding is sophisticated enough for many applications; it already explains the idea behind most of the JPEG modes and because totally lossless methods cannot provide sufficient data reduction when a huge amount of data is considered.

The Baseline coding method of the JPEG contains three sequential steps: Forward DCT (FDCT), quantization and entropy encoding (Fig. 1). The processing scheme is applied to a stream of 8x8 pixel blocks in grey scale images. The use of small image blocks takes into account the fact that the correlation between adjacent pixels is usually high in images of natural scenes. Decompression is achieved by following the processing steps in the opposite direction: entropy decoding, dequantization and Inverse DCT (IDCT).

2.2.1 **FDCT** For this step, the image is divided into 8x8 pixel blocks, each one of which is transformed by two-dimensional DCT, producing 64 output coefficients (set of basis-signal amplitudes). The transformed coefficient matrix is ordered so that the mean value of the coefficients (DC) is placed in the upper left corner of the grid; the remaining 63 coefficients (AC) are ordered so that low-frequency coefficients are closer to the DC value than the coefficients for high-frequencies.

2.2.2 **Quantization** After the FDCT, each cell in the 64 element coefficient matrix is quantized to a corresponding value in the predetermined quantization table. This is done to reduce the number of different coefficient values and to increase the number of zero value coefficients. Quantization is applied by dividing each DCT coefficient by the quantization step size and rounding the result of this division to the nearest integer. The quantized DC coefficient is encoded as the difference from the DC term of the previous block. All of the quantized coefficients (DC+ACs) are then ordered into a "zig-zag" sequence (Fig. 2). This makes entropy encoding more efficient because the nonzero low-frequency coefficients are placed before the high-frequency ones.

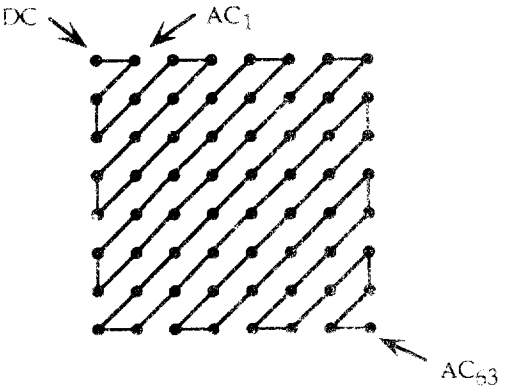

Figure 2. Zig-zag sequence.

2.2.3 **Entropy Encoding** The final step in the JPEG's DCT -based compression is entropy encoding, in which the quantized coefficients are losslessly encoded to a more compact form. Although the JPEG proposal specifies two entropy encoding methods (Huffman and arithmetic coding), the Baseline compression uses Huffman coding only.

/...

2.2.4 Color Image Compression The Baseline sequential coding is for 8-bit images but it can be applied to color images as well. The color image compression can be done by compressing multiple channels one by one or by an approach in which the 8x8 blocks from each channel are compressed interleaved. Although the Baseline method compresses color images presented by any color model, it is best for images that are in color spaces such as YUV (Y for luminance, UV for chrominance) in which the color components are independent. Because the chrominance values need not to be considered as frequently as luminance values, the spatial resolution of the U and V components can be decreased. Subsampling of the chrominance channels reveals the advantage of using color spaces such as YUV in compression and explains why color images can be compressed with a better ratio than grey scale images.

3. COMPRESSION OF LARGE DIGITAL IMAGES

In general, when large digital images are considered, it is not reasonable to compress the whole image in a single compression step. An approach in which the original image is divided into tiles 'large enough' to be used as compression units is useful in applications in which only some of the image is required immediately. A catalogue indicating where each variable size block begins in the file is needed for quick access of image parts (Fig. 3).

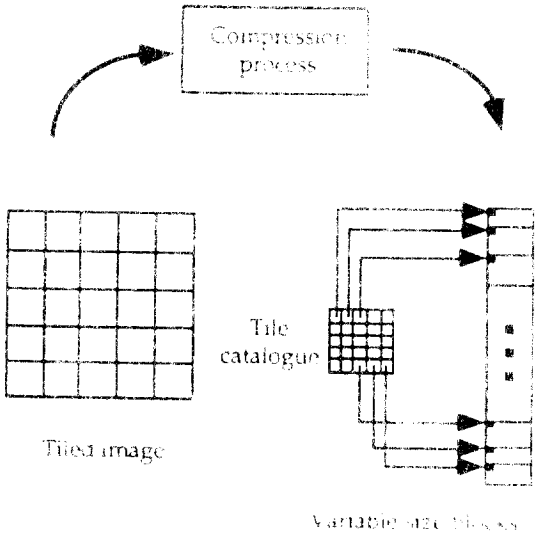

Figure 3. Piecewise compression of a large digital image.

In this piecewise compression scheme only the such parts of the image that are really needed are decompressed. The time required for decompressing a few tiles is moderate compared with that for decompressing the whole image. Large images are usually also rather cumbersome to handle, and thus slow virtual memory swaps are necessary. Because the compression algorithms used for compression of large digital images are usually lossy, it is obvious that compression should not be done in intermediate steps.

4. GEOMETRIC DEGRADATION OF DIGITAL IMAGES IN THE COMPRESSION PROCESS

Geometric degradation of digital images in the compression process is especially interesting in photogrammetry because there the geometric quality of the images is important. The geometric quality of an image can be degraded in a compression process in two ways: 1) by degrading the radiometric quality of an image after compression such that measured targets are blurred or ambiguous and therefore pointing becomes inaccurate or impossible and 2) by shifting objects in line or column (or both) direction. Both of these degradations can be global or local by nature.

Geometric degradation depends to a considerable extent on the compression method used but it also depends on the contents of the compressed images and the amount of compression. It is clear that if the compression method is a lossless one then there is no danger of geometric degradation. On the other hand, all lossy methods are a possible source of geometric degradation of type one. Some of these methods might affect shifts as well - this applies particularly to methods where global knowledge is used for compression. Because compression methods usually have difficulties on spatial objects with large intensity variations in their neighborhood, it is reasonable to expect geometric degradation at these targets.

A research of (Akey & Mitchell, 1988) is an example of a study where geometric degradation of the compression process is examined. In their work they studied the geometric effect of a discrete cosine transform-based image compression. It was found that the DCT-based compression moved the measured cross targets as much as 3.5 pixels when the compression ratio was about 1:16 on 8-bit images. As assumed, the error decreased when the compression decreased.

5. GEOMETRIC EFFECT OF THE JPEG

We studied empirically the geometric effect of the JPEG image compression on full color images. We wanted to test our assumption that JPEG image compression does not affect to the image geometry if small compression ratios are used. We also wanted to know what happens when the amount of compression becomes large.

5.1 Test Arrangements

The test image was an aerial color photograph digitalized by the Sharp JX-600 desktop scanner in full-color mode and with a resolution of 600 dpi. This scanned image (Original) was compressed according to the Baseline JPEG image compression scheme, using the Storm Technology's PicturePress™ software with a Micron Xceed™ ICDP-II Picture Accelerator. The image was compressed into three different levels (Excellent, High and Fair) with compression ratios of about 1:7,

The visual quality of the image Excellent was very good. The image High was also quite good in the visual examination although some compression effects were seen. The visual quality of the image Fair was poor - the size of the compression blocks (8x8 pixels) was clearly visible, and all the edges were heavily smoothed. Despite this degradation in visual quality, we used the image Fair in the test as an example of a case in which the compression has become too large.

For the test 50 homogeneous linear features were chosen from the center area of the images. The features selected were larger than the compression blocks and were situated on areas where geometric degradation wass likely to occur (edges with large intensity variations). They were homogeneous in the sense that all were about 70 pixels long and represented the edges of roofs.

This test set was repeatedly measured on all test images using manual pointing - 20 times with the uncompressed image and 10 times with the compressed images. The linear features were pointed with visual interpolation. In this, sub-pixel pointing was achieved by zooming the viewed image area so that every pixel on the image was doubled before pointing.

The root-mean-square errors (rmse) for perpendicular differences between the endpoints of linear features were calculated. These root-mean-square errors were combined to represent the pointing precision of the linear features on each image.

To test the accuracy of the JPEG image compression, we kept a set of average features from the Original data as a reference when the rmse for perpendicular differences in the compressed test sets were calculated. The set of average features was formed by calculating averages from the endpoint coordinates of the linear features measured.

A set of average features was determined for each test set. Features from these sets were directly compared with the set of average features from the Original set. Again, root-mean-square errors for perpendicular differences between the endpoints were calculated.

5.2 Pointing Precision of Linear Features on Test Images

The pointing precision of the linear features on test images was calculated according to the test arrangements. Features with a perpendicular difference greater than 3 times the root-mean-square error of the corresponding data set were kept as gross errors and were rejected. The pointing precisions of the linear features on test images are presented in Table 1.

Compressed test sets were compared with the Original set one by one. The hypothesis H_0 in our case is written as

$$H_0: \delta^2_{Original} = \delta^2_{Compressed} \quad (1)$$

Table 1. Pointing precision of linear features on test images presented by maximum error (max v_y) and root-mean-square error (rmse). These values are expressed in pixels. Degrees of freedom for different test sets are also presented (υ).

Test sets (compression ratio)	max v_y	rmse	υ
Original	0.90	± 0.28	1842
Excellent (1:7)	0.84	± 0.27	886
High (1:15)	0.88	± 0.26	878
Fair (1:66)	1.15	± 0.39	864

and H_1 is

$$H_1: \delta^2_{Original} \neq \delta^2_{Compressed} \quad (2)$$

The F-test was used to test the statistical significance of the hypothesis above. The ratio between the sample variances was used as a test parameter

$$z_F = \frac{s^2_{Original}}{s^2_{Compressed}} \quad (3)$$

The hypothesis H_0 is rejected with the risk α if

$$z_F \geq F_{1-\alpha/2}(\upsilon_{Original}, \upsilon_{Compressed}) \quad (4)$$

or

$$z_F \leq \frac{1}{F_{1-\alpha/2}(\upsilon_{Compressed}, \upsilon_{Original})} \quad (5)$$

where $\upsilon_{Original}$, $\upsilon_{Compressed}$ are the degrees of freedom and F represents the F-distribution. The significance levels on which the appropriate null hypothesis H_0 can be rejected are presented in Table 2.

Table 2. The test set Original and other test sets are compared by using the F-distribution. The significance level on which the appropriate null hypothesis H_0 can be rejected is shown in percent. The test is based on the values presented in Table 1.

Excellent (1:7)	High (1:15)	Fair (1:66)
80.2 %	99.7 %	99.9 %

The pointing precision on the set Excellent does not differ from that on the set Original. These test sets are also considered equally distributed according to the F-test. But in the set High there is a difference between the compressed set and the set Original. However, the

finding that the set High is even more precise than the set Original is somewhat surprising. One explanation is that the staircase effect on the test images is smoothed through image compression, and so the pointing is easier to repeat. The pointing precision in the set Fair is clearly poorer than the precision in the set Original. According to the F-test, the sets Fair and Original almost surely originated from a different data generation process. The compression used in this case is simply too large - the pointing of linear features is no longer unambiguous.

5.3 Pointing Accuracy of Linear Features on Test Images

The set of average features from the Original image were used as a reference when the rms errors for perpendicular differences were determined. The results from these calculations are presented in Table 3. The set of average features from the compressed images was also directly compared to the Original set of average features. Results from these comparisons are shown in the Table 4.

Table 3. The errors for perpendicular distances calculated by using the set of average features from the Original data. Maximum errors (max v_y) and root-mean-square errors (rmse) are presented. Values are expressed in pixels. Degrees of freedom for different test sets are also presented (υ).

Test sets (compression ratio)	max v_y	rmse	υ
Excellent (1:7)	1.00	± 0.30	886
High (1:15)	1.40	± 0.31	878
Fair (1:66)	3.32	± 0.65	864

Comparison of the results in the tables shows that the set Excellent is very close to the set Original. The set High is also quite close to Original. However, the values in Tables 3 and 4 indicate that there may be errors of a systematic nature in some features of High. In Fair the number of large errors has grown so much that the difference from Original is obvious.

After the test we checked the features that caused the largest residuals in the set Fair. The linear features having the four (4) largest misplacements in a perpendicular direction were caused by the fact that the image compression ratio was too large for those objects. The original edge had either disappeared totally or been smoothed so badly that the pointing was more like guesswork. In two of the cases the disappeared edge had a similar kind of linear feature in the close neighborhood. This coincidence caused a systematic error in the pointing.

Table 4. The difference between the set of average features from the test set Original and the set of average features from the compressed test sets. Maximum error (max v_y) and root-mean-square errors (rmse) are presented. Values are expressed in pixels. Degrees of freedom for different test sets are also presented (υ).

Test sets (compression ratio)	max v_y	rmse	υ
Excellent (1:7)	0.27	± 0.12	99
High (1:15)	0.73	± 0.18	99
Fair (1:66)	2.76	± 0.50	99

6. CONCLUSIONS

We have empirically studied the geometric effect of JPEG image compression on full-color images. The visual quality of the image Excellent (compression ratio 1:7) was very good, and no remarkable degradation in the geometric quality of this image was found in the test. The visual quality of the image High (1:15) had slightly deteriorated when compared with the Original one. A small geometric degradation effect in the case High was found in the test - some of the linear features were misplaced. In summary, Baseline JPEG image compression does not have a geometric effect on the image geometry when compression ratios of about 1:10 are used. Some geometric degradation effect may occur with higher compression rates.

Our examination was based on the use of visual pointing instead of numerical feature extraction methods. We believe that the results are applicable when digital images are used for visual, interactive mensuration in workstations. The use of JPEG image compression might have varying effects to different kinds of numerical feature extraction methods. This gives a topic for further research.

REFERENCES

Akey, M. L., Mitchell, O. R., 1984. Detection and Sub-Pixel Location of Objects in Digitized Aerial Imagery. A paper presented in the Seventh International Conference on Pattern Recognition, Montreal, 1984.

C-Cube Microsystems, 1990. C-Cube Microsystems Workshop v 1.0.

Storm Technology, 1990. PicturePress User's Manual v 1.0

Wallace, G., 1991. The JPEG Still Picture Compression Standard. Communications of the ACM, 34(4): 30-44.

/...

REQUIREMENTS OF A STEREO WORKSTATION FOR GIS ENVIRONMENT

Tuomo Sarjakoski and Jussi Lammi

Finnish Geodetic Institute
Ilmarinkatu 1 A
SF-00240 Helsinki
Finland

Commission II

ABSTRACT

Integration of digital stereo images into GIS databases offers new possibilities for the end-users. This paper studies the requirements of a stereo workstation needed in this utilization. The basic requirements of a stereo workstation are the capability for stereoscopic viewing and possibility to do precise 3D measurements. Especially in the GIS environment the demand to display and edit vector formatted 3D data as conveniently as possible becomes important. Implementation of a stereo workstation allows a variety of solutions both in hardware and in functional sense. Nowadays stereo displays are off-the-self products and they can be added to the existing graphic workstations. General guidelines for a stereo workstation design are given and implementation of an experimental stereo workstation is discussed.

KEYWORDS: Stereo workstation, GIS, Digital imagery, User interface

1. INTRODUCTION - STEREO IMAGERY IN GIS ENVIRONMENT

Figure 1 illustrates the principle how digital stereo imagery should be used in GIS environment. Digital imagery is stored as a part of a GIS database, to be used in combination with 3D data. Workstations with stereoscopic viewing systems are used for interactive interpretation and mensuration purposes. A production phase in which the analog images are digitized and geometry is determined is a prerequisite for storing the images in a GIS database.

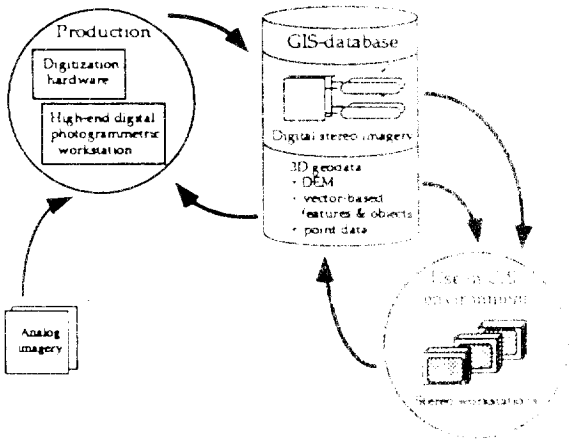

Figure 1. Production and use of digital stereo imagery in GIS environment.

This scenario is a part of the general trend of hybrid GIS approaches in which raster-formatted image data and vector-formatted feature data are used jointly (see e.g. Fritsch, 1988). Relating this to the use of digitized aerial photographs, it is often stated that digital orthophotos will become the most important mode of use. Urban environment, however, is demanding regarding the production and use of digital orthophotos. Urban environment is human-made. It contains a lot of objects that are clearly three-dimensional. Vertical faces are rather a rule than an exception. They cause many shades to appear on aerial photographs. It is thus a demanding task to produce an orthophoto which is positionally accurate for all the details (Bähr &Wiesel 1991). A complex or complete DEM (digital elevation model) or even a complete 3D DTM (digital terrain model) would be required. Digital orthophoto imagery always lacks of 3D information, which puts it in contrast with digital stereo imagery.

To summarize, stereo imagery based on digitized color photographs seems to be very suitable to be incorporated in urban GIS databases for the following reasons:

- Digital orthophoto is not always feasible because it does not contain 3D information.
- Production of digital stereo imagery does not require digital elevation model. In this aspect, digital orthophotos are much more demanding because a "complete" 3D elevation model is necessary.
- Color information is important for visual

A paper to be presented at the XVII ISPRS Congress, 2-14.8.1992, Washington, D.C. Will be printed on the International Archives of Photogrammetry and Remote

/...

interpretation purposes, especially when digitized material is used on occasional basis by non-professional image interpreters. From economical point this is also feasible as the marginal costs of color photography, compared to black-and-white, are rather low today.

Stereo workstation is a prerequisite for utilizing digital stereo imageries in interactive manner. The technology for stereo workstation is available and several photogrammetric stereo workstations have been designed and implemented (see e.g. the review by Dowman, 1991).

The objective of this paper is to study requirements of a stereo workstation when it is targeted to be a tool for an end-user of digital stereo imagery in GIS environment. In this respect we want to further promote the "*democratization* of photogrammetry" (Leberl, 1991) We try to define general design principles and we also summarize ideas presented earlier by us (Sarjakoski, 1990; Sarjakoski & Lammi, 1991; Lammi, 1992).

2. ENVIRONMENTAL SETUP FOR WORKSTATION DESIGN

Personal-computer based text processing have radically changed our attitude towards the production of "typewriter-quality" text and publishing: typing was considered as a profession and the technicalities of making printing originals were often considered as an obstacle for making printed publications. Today we hardly have any typist in an office, rather, there is a "multi-job" secretary who might help in finishing of the machine-readable documents made by the experts in various fields. The desktop publishing software has made the conventional typing fully obsolete in many areas and reduced the costs significantly.

We claim that easy-to-use stereo workstations integrated with geographical information systems will have impacts comparable to the described changes above. Interpretation and mensuration of stereo photographs will be made by non-professional "operators" - to a great extent. Photogrammetric data collection will not be regarded as a mapping project but rather just-on-time (JOT) principle will be followed in data collection.

The attitude towards stereo workstations will be in future very much the same as it is towards office automation today. Environmental setup will be such that

- Each user has his own workstation (read: a man machine interface to a computing device consisting at least of a graphics display, a keyboard and a mouse)
- The price of the workstation is so low that it is economically appropriate to supply each user with his own workstation, even if he does not use it continuously.
- All the necessary pieces of software is accessed thorough this interface.
- Many pieces of the software are integrated to be part of larger information systems.
- All the software follow a uniform interface design principle or standard (Motif, Windows, Apple windows, SunView etc.).
- The systems must be so easy-to-use that the necessary training time is not more than one hour - one day, assuming the user already has a basic understanding of the application domain.

Stereo workstation must now be a functional extension of this single, multipurpose workstation. The necessary hardware extensions should be minimal.

3. FEASIBLE HARDWARE SOLUTIONS

The analysis of the requirements of a stereo workstation in GIS environment should be started from the analysis of functional requirements. To lay out a foundation for this work, the feasible hardware configurations of sterero workstations are here reviewed in the light of current and near-future technology.

3.1 Stereoscopic display systems

Practically, there are three realistic alternatives for stereoscopic display system - one of them is based on the optical split of the screen while the other two approaches use the polarization technique. Difference between the polarization methods is in the type of used polarization and in the technique of realization. Stereoscopic viewing in these polarization based approaches is done either by using passive glasses and circular polarization or active glasses and linear polarization. Both of these methods enable free viewing of the stereomodel while optical split is always tied on the used mirror system.

3.1.1 Optical split of the screen A familiar example of the optical split is a mirror stereoscope - stationary analog images are viewed through oculars and the mirror system of the instrument forces left eye to see the left image and right eye to see the right one. The idea is exactly the same with this type of stereoscopic display system only the images are changed to the digital ones. Both images of the stereopair are shown all the time on the screen (or screens) and they are viewed through a mirror stereoscope in front of the display.

3.1.2 Polarization approach with passive glasses In the polarization approach with passive glasses the images of the stereopair are alternately shown on the display. A screen-sized liquid crystal modulator - synchronized to alternation with the graphics hardware - provides different polarization for left and right eye images. Special polarizing glasses worn by the operator decode the polarized images correspondingly to the left and right eye. This kind of a stereoscopic display system is realized and manufactured by

/...

Tektronix. Images are handled in interlaced mode, i.e., the other image is displayed on the odd and the other one on the even lines of the display. This, of course, decreases the quality of the stereomodel.

3.1.3 Polarization approach with active glasses The technique in this approach is very much the same as it was in the approach with passive glasses. Again a time multiplexed stereopair is shown on the display but this time the shutter is mounted into a pair of active glasses. The active system contains two linear polarizers for both eyes. Between them is a liquid-crystal cell which can rotate light by 90° so that light meant to the right eye only is blocked from the left eye. Realization of this approach is done by StereoGraphics Corporation with CrystalEyes system. The liquid crystal cells are synchronized to the refresh rate of the monitor via a wireless infrared link.

3.1.4 Use of stereoscopic display systems In Table 1 we have listed the effect of different stereoscopic display systems on various design aspects. Note that when display systems are discussed in general there is also other things to be considered, these include e.g. optimal size of the screen (physical dimensions), dot-size and available colors (full-color, grey-scale).

There are a lot of applications where stereoscopic display systems are not necessary. Even some of the tasks that benefit from the use of stereoscopy can also be done without it. There also exist people who cannot see stereoscopically. In all these cases the chosen stereoscopic display system should not disturb other work. We believe that stereo workstations based on multiple screens are preferable in this sense. They give the best support for the multipurpose principle of the workstation: all existing software may be used without modifications, even simultaneously with the "stereo software" (or even stereoscopic viewing) under the window system.

3.2 Three-dimensional control

Three-dimensional control over 3D object data is required from the stereo workstation. Ergonomy and suitability of the three-dimensional control device greatly affects to the usability of the stereo workstation. The control device itself can be a single device or a combination of two or more devices, possible choices are e.g. keyboards, mice, trackballs, joysticks, footwheels, lightpens, touchscreens, digitization pads, digitizing gages, datagloves. Typically each of these device produce increments in some device-dependent coordinate system - how the increments are interpreted depends on the used software.

Although a variety of different possibilities are available for three-dimensional control, already a very modest configuration is adequate. These "basic" configurations include e.g. a mouse or digitization tablet with buttons for height control (as e.g. in the DVP, Nolette et al., 1992).

3.3 Capacity of future workstations

It has been forecasted in a paper by Frank et al. (1991) that in the late 90s we may see the following specifications for a personal GIS workstation:

- a CPU with 500 MIPS,
- 500 Megabytes of main memory,
- 5 Gigabytes of storage space on hard disks an additional 50 Gigabytes on optical disk,
- a workstation screen with 2000 by 2000 pixels and
- a communication device with 100 Megabytes per second transfer rate.

Moreover, they expect that a workstation with these capabilities will cost about the same as today's personal computer with moderate capabilities.

Table 1. The effect of different stereoscopic display systems on various design aspects

	Polarization with passive glasses (Tektronix)	Polarization with active glasses (CrystalEyes)	Optical split of the screen
Free stereoscopic viewing	yes	yes	no
Enable multiple viewers in stereoscopic mode	yes	yes	no
Image resolution in stereoscopic mode	1/2	1/2	full
Multiple screens mandatory	no	no	no (yes)
Multiple screens in simultaneous use	possible	not possible, due to flickering	possible
Support for multiple, simultaneous programs	yes, but realistic only if multiple screens	no, because mono windows cannot be used with stereo	yes, with multiple screens

/...

The progress in computer technology today is so fast that the forecast above can be considered to be realistic. It also indicates that stereo workstations should be based on a personal-computer principle, i.e. the CPU is dedicated for the tasks of a single user. It guarantees flexibility and an immediate access time even if the whole system is loaded.

4. FUNCTIONALITY

The basic functional principle of a stereo workstation is simple (almost naive): we have to be able to edit 3D object data that is projected on images. The 3D object data is related to the physical, three-dimensional reality. This does not mean that 3D object data is all the time consistent with the physical reality, depending on the consistency the following types of 3D object data can be found:

- Old data. This was relevant in the past but now the reality has changed.
- Current data. This is consistent with the reality.
- Data of planned situation. This type of data describes the physical reality in the future.

We need only three different tools to achieve the required functionality, those tools are create object, delete object and modify object. As a matter of fact, even the modification tool is unnecessary because all objects can be modified by first deleting them and then creating again in a modified form. However, this approach is not very intuitive and it is also wrong if the identity of the object instance is wanted to be preserved.

The actual editing of 3D object data can be done in many ways depending on how the object parameters are given and who is in charge for editing. In this context we divide editing modes into four groups: stereoscopic editing, image-wise editing, editing with automatic height control and automatic editing. Stereoscopic editing is done when stereoscopic vision is used for editing of 3D object data. Editing becomes image-wise when two or more images are used independently for editing. Editing with automatic height control is an example of semi-automatic approach - user selects the targets to be correlated and the correlation process gets the match from one or more images. Automatic editing is in case when 3D objects are edited without manual intervention.

5. IMPORTANT TECHNICAL ISSUES

5.1 Viewing tools and windowing

Because the technique used in stereo workstations is different from the one used in analytical plotters, some differences will also arise in use. In analytical plotters we have easily used the technique of fixed measuring marks, moving images but in the stereo workstations the paradigm of fixed view, moving graphics is the one in prevail. The approach of fixed view, moving graphics is not only more economic to realize than the approach of fixed measuring point, moving images but in the case of free stereoscopic viewing it is also more ergonomic and more intuitive. Stereo workstations also contain a lot of possibilities embedded. A good example is the superimposition of graphics which is an expensive accessory in analytical plotters but which is always available in each window of the stereo workstation.

Although the actual work is done on a fixed view, a new fixed area has to be accessed within a reasonable time. However, there is no real-time requirement on the change of the viewing area. Typically the change of the viewing area could be done e.g. by pointing the area of interest from an overview image or by using the scroll bars (or side rulers) in the windows. In some cases it could be wise to allow automatic change of the fixed view on edges of the fixed viewing area - when edges are confronted, change is automatically done. In case the update of images is realized very fast, the illusion of moving images might be given. Note that all these methods are supposed to be served as alternatives for the user - they do not exclude each other.

It is almost self-evident that stereo workstations have to be designed on the principle of multiply windows. This approach is already familiar from many applications, such as text processing, graphics or drawing programs and 3D CAD programs.

In the approach of multiply windows, there seems to be a need for at least following windows: overview, mono, stereo and zoom window. Any of these can be hidden until needed. The overview window contains an image from the whole working area in low resolution, it enables quick change of the viewing area and makes the general location easier. Images in mono windows are used for all work that does not require stereoscopic viewing. Beside orthophotos, also the left and right image of the stereopair are shown in mono windows for image-wise editing. Images of the stereopair are show on the stereo window in such an relation as the used stereoscopic display system requires. Usually the position of the stereo window is strictly tied on the dimensions of the monitor and can not be moved from this position. To enable a closer look of images, a special zoom windows have to be provided. In our opinion, this is a better approach than the direct use of mono or stereo windows for zoomed images because good control of the neighborhood of the zoomed area is never lost. When 3D objects are edited the results of the editing should be projected to all windows containing the object in hand.

5.2 Tools for manipulating graphical objects

To give an idea of how to change the conventional ways of measuring to more flexible ones, we shortly describe the manipulation of graphical objects in stereo workstations. A variety of commercial design/drawing software have achieved such a functional maturity in object data manipulation that they should, in some extent, be taken as a model while designing tools for stereo workstations. Some of the principles used in these software seem to be even so good and commonly accepted that it is hard to suggest any better alternative for

/...

interactive work in stereo workstations. When these techniques are taken into use in mapping applications, collection and maintenance of object data becomes as easy as the use of common drawing programs. Good examples of advanced design/drawing software are e.g. Intergraph's Microstation, Deneba's Canvas or Adobe's Illustrator.

Interactive drawing programs, based on the use of object graphics, work with a very simple principle. Although there exists a variety of different object types (e.g. point, line, polygon, closed polygon, rectangle or solid), the way of editing is very much the same in each case. A set of tools or functions are provided for the user in a menubar or similar. Depending on the type of the function, a tool can either be used directly as such (create object) or it may require that user has activated an object or group of objects into which the tool is applied (delete object, modify object). In the latter case object activation is done e.g. by pointing a graphical object with cursor.

In the case of stereo workstations some automation is possible in tools. Beside completely automatic tools, some semi-automation can easily be realized (controlled data collection). The most obvious is a tool for automatic height determination when an object is located manually in one of the images. Because the actual work is done in GIS related applications, a sufficient amount of topology related tools have to be either embedded or available in tools (e.g. snap to an neighbor object). In all cases, even with the most advanced object manipulation tools, the editing principles adopted from the design/drawing software are valid.

5.3 Graphics superimposition

The graphical display of object data on the image is called superimposition of data. When stereoscopic viewing is concerned we can correspondingly speak of stereoscopic superimposition. Generally the overlay of graphics is done with fully covering wireframe techniques. It is likely that superimposition of wireframes only is not optimal for visual perception and when purely covering colors are used, vision of the image parts under the graphics is blocked. An alternative for pure superimposition is the use of such a transparent overlay that enable vision of image through graphics.

Transparent graphical layer for an image can be achieved by transforming the image into another color space than RGB and doing the overlay of graphics in this new color space. The applied color space transformation have to be such that it separates the luminance and chrominance values of the image. Selected objects are then drawn into the chrominance channels keeping the luminance unchanged. The inverse transformation applied to this image gives the superimposed result. If this type of transparent overlays are used it becomes necessary to manipulate the pixel values of digital images directly. This requirement makes it clear that only copies of original images are used and these used copies never saved over the originals.

The IHS color space is one possibility to do transparent overlays. The components of this color coordinate system - intensity, hue and saturation - are easy to perceive because of the similarity to human vision. Actually there are quite many color spaces (e.g. HLS, HSB and HSV) that have same or similar concepts but they normally differ from the IHS model by the used coordinate system (Foley et al., 1990: 590-595). In all cases the intensity (luminance, brightness, value) is kept unchanged, while the values in hue and saturation are changed for transparent superimposition. Beside these color spaces, it could be interesting to test properties of some direct transformations from RGB space to another Cartesian 3D color space. These color spaces include the YUV- and YIQ -color models (Foley et al., 1990: 589-590).

The use of transparent graphical superimposition does not mean that wireframes may not be used at all. On the contrary, both of these techniques are used so that the best possible result is achieved. It seems quite reasonable that even the transparent objects are enclosed by wireframe graphics. Proper antialiasing techniques have to be used for quality superimposition of edges.

5.4 Sub-pixel accuracy

It is well known that objects can be measured from digital images with sub-pixel accuracy. However, many of the used numerical techniques are devoted for automatic interpretation and measuring of targets (tie points, control points) that are not interesting in the sense of interactive GIS applications. The methods we discuss here are merely devoted for sub-pixel superimposition of graphical objects.

Sub-pixel accuracy can be achieved by performing real-time resampling of images on some interval less than a pixel. Use of this technique expects that a fixed measuring mark is used instead of moving graphics. In realizations with moving graphics a method for sub-pixel pointing is e.g. the use of a set of convolved cursors where "the system automatically selects the cursor that best represents the sub-pixel position at any moment" (Helava, 1991).

One of the most straightforward method to achieve the sub-pixel accuracy in interactive work is the idea of visual interpolation. When the graphical objects are superimposed on the image the position of any object will be observed by a human by integrating the object visually into its surroundings. The best possible fit of these objects can be achieved by editing necessary objects so that the neighborhood supports the fit visually. The sub-pixel pointing can be embedded in the graphics routines: graphical objects to be edited are forced to move in smaller steps than one pixel. This moving in sub-pixel steps is easy to realize inside the drawing routines of graphical objects. Similar kind of idea is used if antialiasing techniques are used for moving in sub-pixel steps. This antialiasing approach is, however, a somewhat questionable because background under the graphics is already fuzzy.

/...

Although the problem of sub-pixel accuracy is interesting, its real importance should not be overemphasized. In our opinion an accuracy of about 0.5 - 0.25 pixel is the level that is supposed to be got from the stereo workstation.

5.5 Integration to other applications

In this article a stereo workstation is regarded as an interface to a Geo database. It is also assumed that it is used simultaneously with other applications like task specific planning software. This necessities fluent flow of data between the system components. Figure 2 illustrates the situation. For the purpose of integration it is important that the communication between the systems is realized by using standardized communication protocol. How this should be realized is left open in this study. Some kind of spatial query language or GeoSQL is needed, however.

Regarding the communication between the Geo database management system and the stereo workstation software, the need for image representation standards must be emphasized. We feel strongly that the digital imagery must be stored by using image compression methods like JPEG. In addition, a standardized method is needed for retrieving compressed images in tiled form. Representation of the parameter information (like the orientation of an image) requires standardization as well (see Sarjakoski & Lammi, 1991 and Lammi & Sarjakoski, 1992).

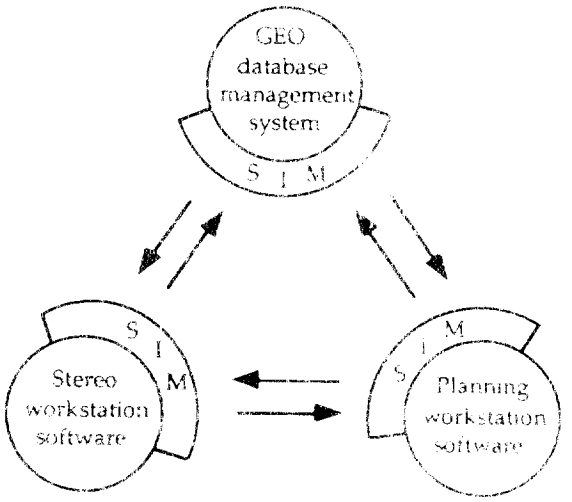

SIM = Standard Interface Module

Figure 2. The flow of data between the system components.

6. DESIGN ISSUES FOR USER INTERFACES

Introduction of menu and mouse driven window systems for graphics workstations has been the most important innovation for easy-to-use user interfaces. Gradually all workstation vendors have accepted their use. However, the use of nice looking windows does not guarantee user-friendliness.

Design of good user interfaces for computing systems is a relatively new field for systematic scientific study. Its goal must be in understanding how to facilitate efficient human-computer interaction - the term efficient covers a broad spectrum of ergonomic, psychological, cognitive and other aspects.

Frank et al. (1992) have identified user interfaces to be one of the most important items for GIS research in the near future. In this section we want stress the need for systematic use of some methodologies in the design of user interface(s) for a stereo workstation. Two specific issues - user models and metaphors - are studied more closely.

6.1 User models

User model refers to a systematical implementation of the important features describing the user. The main interest in the user model research is in systems which can adapt themselves to different users at run time. The most important function of user models is to predict user's actions and preferences and change its functionality accordingly, for instance in database search. Rich(1983) has devised three dimensions for describing user models:

1) one model of single canonical user versus a collection of models for individual users,

2) models describing explicitly by the system designer or by the users themselves versus models inferred by the system on the basis of user's behavior,

3) models of fairly long-term user characteristics such as areas of interest or expertise versus models of relatively short-term user characteristics such as the problem the user is currently trying to solve.

Brajnik et al. (1990) list three advantages of using user models: the economy of interaction, user acceptability and effectiveness and efficiency of the use of the target system.

6.2 Metaphors

A metaphor is a "figure of speech in which a word or phrase denoting one kind of object or action is used in place of another to suggest a likeness or analogy between them" (Websters Third New International Dictionary). Recently metaphors have been referred a lot in studies related to the user interfaces. The desktop metaphor first popularized in Apple Macintosh uses concepts and terms like "document", "folder", and "put into a trashcan" instead of more conventional computer terms "file", "directory" and "delete a file". The power of the use of metaphors is based on the idea that novice users of the computer can use it as a helpful tool without need to study the computer terminology. Its functionality will be understood through analogy.

/...

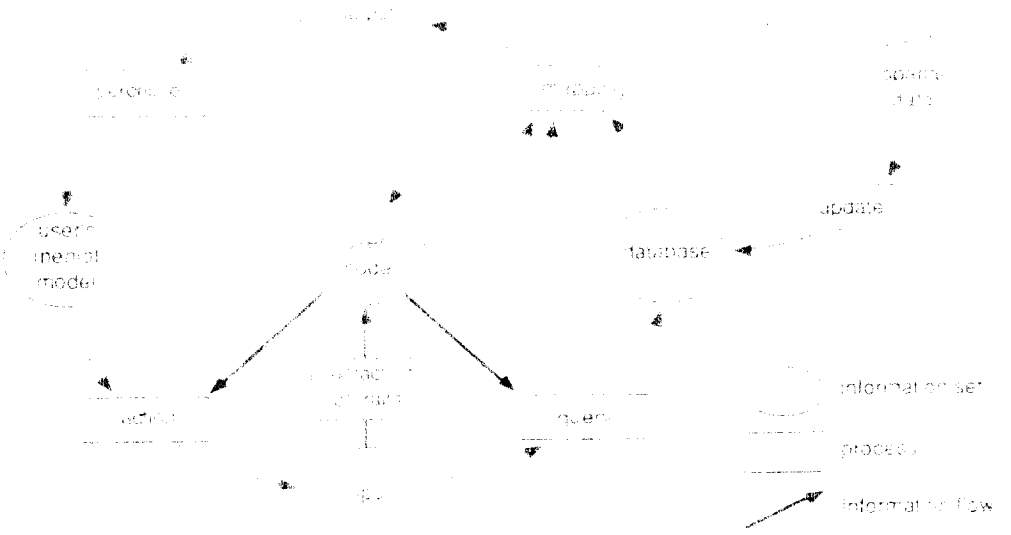

Figure 3. The position of a user model in GIS communication systems (Lindholm & Sarjakoski, 1992)

6.3 User models and metaphors for stereo workstations

The hypothesis of this work is that a stereo workstation in GIS environment is used by broad users of geographical data for various purposes. The user models must incorporate the most important characteristics of the tasks. These include at least

application areas
- town planning
- landscape architecture
- building design
- road design
- utility planning
- traffic analysis
- forestry applications
- map revision = update of geo-database

professions and educations
- architect
- civil engineer (construction, roads, traffic...)
- forestry expert
- surveyor

The user models will affect on many functional aspects
- language
- terminology
- functionality of the system
- availability of various tools
- graphical interface and menu layout
- extensions with application specific tools

Figure 3 illustrates the position of a user model in a communication system. Although it comprises also query systems, the same principle applies for stereo workstations at least partly.

Our believe is that with today's knowledge and technology it would be over-ambitious to apply user modelling so that the model would be inferred during the session. It is rather suggested that a tailored interface is made for each user. This will make it possible to use all the useful application and user specific metaphors and peculiarities facilitating efficient and ergonomic use. This kind of approach makes it necessary that the workstation software is clearly modularized so that it consist of 1) a kernel software and 2) tools for the tailoring of the user interface. The tools, on the other hand, are a combination of some kind of macro language and an easy-to-use interface editor. Apple Macintosh HyperCard and its successors are a good example of appropriate tools. Who is then responsible for the tailoring process? Our believe is that often an "interface specialist" is needed for making the tailoring work. It is also likely that experienced users are willing to make some tailoring by themselves - as experienced users of text processing systems write their own macros.

A tailored user interface may also be regarded as a knowledge-based layer on the top of the system (Sarjakoski, 1988) in which the knowledge base contains the user model.

7. OUR EXPERIENCES

Our implementation of a stereo workstation at the Finnish Geodetic Institute (an Apple Macintosh IIfx microcomputer has been chosen. It has a Motorola 32-bit microprocessor 68030 that runs with 40 MHz. RAM is extended to 32 MB. Three button mouse, Logitech MouseMan is used as a three-dimensional control device. The internal hard disk has the capacity of 160 MB. External hard disk (1 GB) is added to enable quick access for large image data often used, this disk is

/...

connected by using a SCSI link. An optomagnetic diskunit with cartridges of 600 MB is used to store the digital imagery. Compression/decompression is done by the Storm Technology's PictureFress software with Micron Xceed ICDP-II Picture Accelerator.

The display system consists of two monitors, one is used as a monomonitor (RasterOps/Sony 19" with RasterOps 24L 1024*768 24-bit full-color graphics card) while the other one is used in stereomode (Tektronix SGS625/ Sony 19" stereoscopic display system, with Radius PrecisionColor 24X 1152*882 24-bit full-color graphics card). The used stereoscopic display system is based on polarization technique with passive glasses.

Images used in our stereo workstation were digitized by the Sharp JX-600 scanner in full-color mode and resolution of 600 dpi. Stereopairs were formed in a preprocessing phase where images of the stereopair were rectified to a common rectification plane so that the requirements of the normal case of stereo-photogrammetry are fulfilled. The same principle has also been used in other stereo workstation implementations as in Azizi (1991).

The stereo workstation at the Finnish Geodetic Institute is based on the fixed view, moving graphics -paradigm. It is designed to have several windows for a single stereomodel. One of these windows is totally reserved for stereoscopic viewing and it is placed alone on the stereoscopic display monitor.

Because used digital images are quite large they are handled in parts, i.e., displayed windows contain only a small part of the original image. When some other part is wanted to be displayed it has to be read from the mass storage. The selection of the viewed area is done by pointing the area of interest on the overview image. This overview image is a lower resolution version of the original (left) image.

The selected working area is displayed on the mono window (one for each image). These mono windows may be used whenever stereoscopic viewing is not needed. A pair of special zoom windows is provided for a closer look of images. These zoom images give also a possibility to do more accurate visual interpolation while editing. Image for stereoscopic viewing is produced from the prerectified mono images either by duplicating columns or leaving every other line from the images away. These images are shown on the stereomonitor left over the right.

Windows containing the displayed image data can be moved inside the monitors. This does not apply to the stereo window because it is strictly tied on the dimensions of the stereomonitor. Several images can be opened simultaneously inside the restriction of the RAM space (32 MB).

An ordinary three button mouse is considered as a 3D input device. All the steps produced by moving the mouse are handled as increments in the model space. Third dimension is achieved by reading the center and right mouse button presses as height increments. Model space coordinates of the 3D point are changed to the ground coordinates and this point is projected to the left and right image.

8. SUMMARY AND CONCLUSIONS

In this work we have regarded a stereo workstation as an end-user tool or system for the utilization of stereo imagery and other data stored in GIS database. The idea of multipurpose workstation is emphasized. A stereo workstation is a functional extension of an ordinary graphics workstation. The necessary hardware extensions should be minimal. The cost of the workstation have to be so low that each user can have a workstation dedicated solely for him.

The workstation software should be designed to support interactive work as well as possible. The principles of many CAD and drawing programs should be followed. The fixed view - moving graphics is used in them exclusively. We argue that for the stereo workstation software it is not only the most economical but also the most ergonomic solution. Special attention should also be paid to sub-pixel accuracy and visually pleasant superimposition of graphics.

The issues of user interface design become important as the workstation is targeted for end-users outsize the mapping field because "for GIS users, the user interface *is* the system" (Frank et al., 1991). Sound methods should be developed for user interface design. We have proposed that the methods of user modelling should be studied and finally applied. Application and profession oriented metaphors could be used to make the system easy to adopt. Each user should be supplied with his/her own interface.

Strict modularity should be applied on all levels of the system. Geo-database management system must be a well defined entity or sub-system with a standardized interface for communication with the stereo workstation software and other related applications like a software for some planning purpose. The same or similar interface must be for immediate communication between the stereo workstation software and other application software. The stereo workstation software itself should be layered so that it consists of a kernel software and tools for complete tailoring of the user interface.

REFERENCES

Azizi, A., 1991. Implementation of a digital stereo-photogrammetric system based on the use of pre-rectified images. The Photogrammetric Journal of Finland, 12(2): 7-19.

Brajnik, G., Guida, G., Tasso, C., 1990. User modelling in expert man-machine interfaces: a case study in intelligent information retrieval. IEEE Transactions on Systems, Man and Cybernetics, 20(1):166-185.

Bähr, H.-P., Wiesel, J., 1991. Cost-benefit analysis of digital orthophoto technology. In. Ebner et a., pp.59-73.

/...

Dowman, I., 1991. Design of digital photogrammetric workstations. In: Ebner et al., pp. 28-38.

Ebner, H., Fritsch, D., Heipke, C. (editors), 1991. Digital Photogrammetric Systems. Wichmann, Karlruhe. 344 pages.

Foley, J.D., van Dam, A., Feiner, S.K., Hughes, J.F., 1990. Computer Graphics, Principles and Practice. 2nd edition. Addison-Wesley Publishing Company. pp. 589-595.

Frank, A.U., Egenhofer, M.J., Kuhn, W., 1991. A perspective of GIS technology in the nineties. Photogrammetric Engineering and Remote Sensing, 57(11): 1431-1436.

Fritsch, D., Schilcher, M., Yang, H., 1988. Object oriented management of raster data in geographic information systems. In: Int. Arch. Photogramm. Remote Sensing, Kyoto-Japan, Vol. 27, Part B4, pp. 538-546.

Helava, U., 1991. State of the art in digital photogrammetric workstations. The Photogrammetric Journal of Finland, 12(2): 65-76.

Lammi, I., 1992. Design and Implementation of a Stereo Workstation for Photogrammetric Work in GIS Environment. M.Sc. thesis. Helsinki University of Technology. 71 pages.

Lammi, J., Sarjakoski, T., 1992. Compression of digital color images by the JPEG. A paper to be presented at the XVII ISPRS Congress, 2-14.8.1992, Washington, D.C., USA. 5 pages.

Leberl, F., 1991. The Promise of Softcopy Photogrammetry. In: Ebner et al., pp. 3-14.

Lindholm, M., Sarjakoski, T., 1992. User models and information theory in the design of a query interface for GIS. A paper to be presented at the International Conference: GIS from Space to Territory, Theories and Methods of Spatio-Temporal Reasoning, 21-23.9.1992, Pisa, Italy. 18 pages.

Nolette, C., Gagnon, P.-A., Agnard, J.P., 1991. The DVI Design, operation, and performance. Photogrammetric Engineering and Remote Sensing, 58(1): 65-70.

Rich, E., 1983. Users are individuals: individualizing user models. Internationa Journal of Man-Machine Studies, 18(3):199-214.

Sarjakoski, T., 1988. Artificial intelligence in photogrammetry. Photogrammetria, 43(5/6): 245-270.

Sarjakoski, T., Lammi, J., 1991. Stereo workstations and digital imagery in urban GIS environment. In: Ebner et al., pp. 274-288.

Sarjakoski, T., 1990. Digital stereo imagery - a mass product in the future? In: Int. Arch. of Photogramm. Remote Sensing, Tsukuba-Japan, Vol. 28, Part 4, pp. 211-220.

/...

SUITABILITY OF THE SHARP JX-600 DESKTOP SCANNER FOR THE DIGITIZATION OF AERIAL COLOR PHOTOGRAPHS

Tapani Sarjakoski
Finnish Geodetic Institute
Ilmalankatu 1 A
SF-00240 Helsinki
Finland

Commission II

ABSTRACT

Digitization of aerial photographs is one of the bottlenecks in the current transition phase in the introduction of fully digital photogrammetric systems. Owing to their low cost, desktop scanners offer an interesting alternative. This paper examines as a case study the suitability of the Sharp JX-600 desktop scanner for the digitization of aerial color photographs. The structure of the scanner is reviewed. A method for calibrating the scanner geometrically is given and the calibration results are presented. The image quality of the scanned images is analyzed. Finally, a method is introduced for calibrating the scanner individually for each scanned image.

KEYWORDS: Image scanner, Digital color images, Calibration, Geometry

1. INTRODUCTION

We are currently going over from analog/analytical photogrammetric methods to fully digital/analytical methods. Computer technology is now mature enough to handle large digital imageries related to aerial photographs. There are available powerful personal computers or workstations that are well suited for interactive work with large digital imageries when furnished with appropriate photogrammetric/mapping/GIS software. Mass-storage devices, such as conventional magnetic disks, opto-magnetic disk-drives and DAT tape-drives, offer adequate storage capacity for aerial images, especially if the medium resolution (50µm - 30µm pixel size) is used.

However, the transition phase is not going as smoothly as it might owing to certain bottlenecks; one of these is digitization of aerial photographs by scanning. High-precision scanners suitable for photogrammetric work certainly exist, but their price is so high that they are beyond the pocket of many potential users of digital photogrammetric methods.

Owing to their low cost, desktop scanners offer an interesting alternative for digitization. They have been designed mainly for use in color publishing tasks. A typical desktop scanner has a scanning area of A4 or A3 size and a spatial resolution of up to 600 dpi. Spectral resolution typically varies from 8-bit grayscale to 24-bit RGB color.

This paper evaluates the suitability of the Sharp JX-600 desktop scanner for the digitization of aerial color photographs. Some other scanners have similar specifications and thus the methods and recommendations discussed here may also have more general applicability. The emphasis is on the geometric aspects of the scanner. It is in our interest to establish if the inherent "weaknesses" of the scanner could be taken into account so that scanned images could be used for photogrammetric purposes. A calibration procedure and a subsequent digital rectification process for the scanned images are seen as a way of producing distortion-free output images.

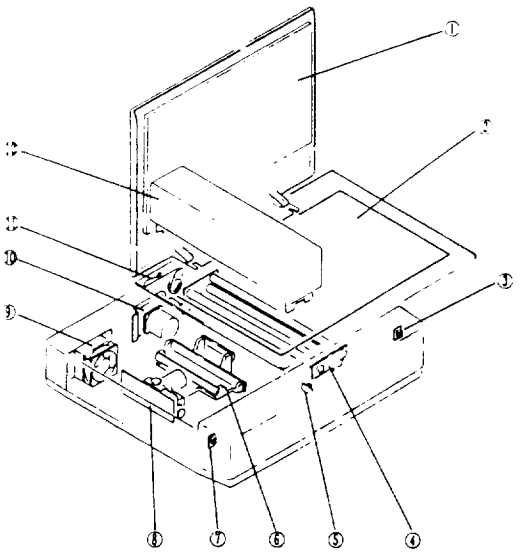

Fig. 7-1

① OR (Original) cover unit
② Table glass
③ WB (White balance) sensor
④ Fluorescent lamp unit
⑤ Lamp unit sensor
⑥ Optical system unit
⑦ Left sensor
⑧ CCD board (in the optical system unit)
⑨ Fan
⑩ Drive unit
⑪ Table drive wire
⑫ Lamp unit

Figure 1. The general structure of Sharp JX-600[1].

[1]Figures 1, 2, and 3 have been quoted from Sharp JX-600 Service Manual, with the permission of Sharp Electronics (Europe) GMBH.

2. OPTO-MECHANICAL STRUCTURE OF THE SHARP JX-600 DESKTOP SCANNER

2.1 General Description

The Sharp JX-600 is a so-called flatbed scanner. The original document is held in a moving glass-plate table. The whole image is digitized by a line sequential scanning in which the table - driven by a stepping motor - is moved (Figure 1). The intensity values within a line are recorded by a MN3666 CCD linear image sensor, which has 7500 photoelectronic conversion elements of 6 µm arranged in a straight line in a 9 µm pitch. Light is transmitted from the table to the CCD sensor with an optical system consisting of a lens and three mirrors (Figure 2). The reduction factor is 4.7 so that the 9 µm pitch equals 42.3 µm on the plate. The largest image size is 10200 x 7032 elements with 600 dpi resolution. Color images are scanned in one pass, and colors are separated with a flashing three-color fluorescent lamp unit. A separate lamp unit is placed above the table for scanning transparent originals.

2.2 The Geometrical Quality of Images

Two aspects of the geometrical quality of digital output images deserve special attention: 1) permanent geometrical distortions and 2) repeatability in the geometrical sense. Given the characteristics of the SHARP JX-600 scanner, what kind of geometrical quality can we expect? The following characteristics of the opto-mechanical structure of the scanner are important:

- CCD-sensor. This construction uses a single linear CCD array. Taking this into account and also the type of device (solid-state), the geometrical quality of a single scanned line is not likely to be deteriorated.
- Optical System. The optical system can be divided into two parts: 1) the body of the scanner and 2) the moving table.

The body of the scanner consists of the CCD sensor, a reduction lens and three mirrors, all mounted in a rather robust frame. The position of the lens and the CCD array can be adjusted with alignment screws. It can be assumed that the system is stable. The most suspectable element of the system is the reduction lens, its geometrical distortions will directly affect the geometry of the output image. Moreover, radial distortion would affect the main-scan direction, and tangential distortion would cause the image to be bent or curved in the same direction. Such effects are even likely because of the rather simple lens used. Any bends in the mirrors would cause similar effects. Improper angular alignment of the optical system with respect to the body and the table of the scanner would result non-orthogonality to the output image.

The glass plate - part of the moving table - will affect the geometry of the image. However, the thickness of the glass plate is not likely to vary so much that it would cause problems (See also 2.2.3, Flatness of the Table).

2.2.1 Guides of the Table. The moving table has an asymmetric guide system. On the drive- (rear) side there is a double-U guide with ball bearings that controls the table vertically and horizontally. On the opposite side (front) of the table there is no horizontal guidance; the vertical guidance is realized so that the glass plate of the table lies directly on a hard-plastic coated track. This solution does not prevent the table from being lifted from the track if any force is applied in this direction. Thus the following image geometry-related features are typical for this construction:

- Any bends in the two double-U guides would cause corresponding regular deformations in the image.
- Any slackness in the bearings of the double-U guides would cause irregular deformations in the image.
- Any lift in the front side of the table will affect the image, owing to the "free guidance" of the front side.
- The asymmetry of the guide-system and the "free guidance" of the front side may be favorable, as tensions in the drive system will be avoided.

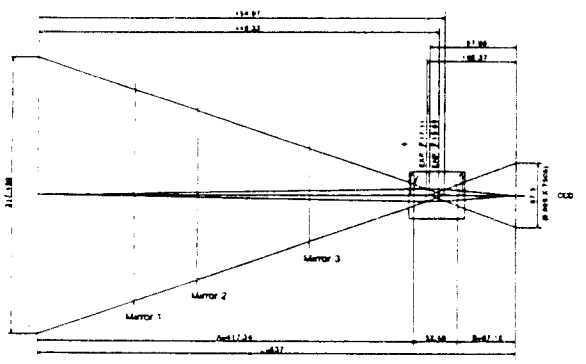

Figure 2. The optical system of Sharp JX-600

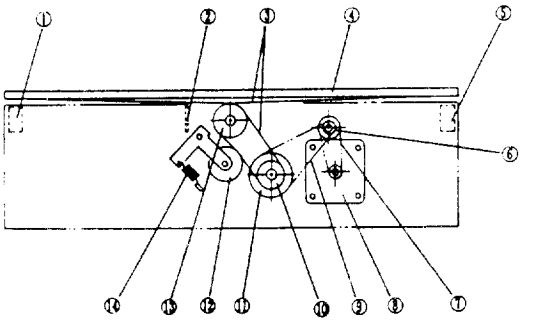

Fig. 7-3

① WB sensor
② Lamp unit sensor
③ Table drive wire
④ Table glass
⑤ Left sensor
⑥ Reduction pulley
⑦ Belt 1
⑧ Pulse motor (About 0.02116mm/step)
⑨ Belt 2
⑩ Drive pulley
⑪ Idle pulley
⑫ Tension pulley
⑬ Wire pulley
⑭ Tension spring

Figure 3. The drive system of Sharp JX-600.

/...

Note that any vertical translocation of the table or the original image will yield a translation in the main-scan direction. This effect is especially strong at the edges of the scanning area, where the direction of the optical beams is such that a 100 µm vertical shift corresponds to a shift of 35 µm in the main-scan direction.

2.2.2 **Drive System of the Table.** The drive system moves the table in the sub-scanning direction. The system is driven by a pulse motor, which drives the idle pulley via two belts. The idle pulley drives the wire around the drive pulley and moves the table back and forth (Figure 3). With respect to the geometry of the output image, there are some inherent weaknesses in the drive system. Any eccentricities in the pulleys will cause periodic errors in the sub-scan direction. Irregularities in the strength of the belts and the wire would probably cause similar effects. Such errors presumably remain stable from scan to scan within a short period of time. However, if any of the belts or wires slide on the pulleys, the zero point of the corresponding periodic error is moved, and the probably regular pattern of systematic errors in the sub-scan direction would be different.

2.2.3 **Flatness of the Table.** If there are some irregular deformations in the flatness of the glass plate on the table, the corresponding errors would show up in the main-scan direction. Because of the direction of the optical beams, this effect would be at its minimum near the central axis of the table and at its maximum near the edges.

2.2.4 **Flatness of the Document.** By the lack of flatness of the document means the tightness of the document to be scanned against the table. If the flatness is not sufficient, the effect would be exactly the same as with the lacking flatness of the table. The flatness is guaranteed rather well when a paper original is scanned because the cover unit presses the original firmly against the glass. When diapositives are scanned, a plastic scattering plate is placed on the top of the diapositive. This plate is very light and does not assure sufficient pressure to keep the diapositive flat.

2.2.5 **Color Separation.** Color images are scanned in one pass, and the colors are separated with a three-color fluorescent lamp unit. This approach seems to be very robust in that it guarantees the correct geometric registration between the three-color elements.

3. CALIBRATION

3.1 Error Model

Based on the reasoning above and some experimental calibration attempts, a functional error model comprising the following two polynomial-type parts was defined:

$$dy = a_1 y + a_2 y^2 \qquad (1)$$

$$dx = b_0 x + b_1 y + b_2 y^2 + c_1 f_1 + \dots + c_n f_n \qquad (2)$$

y = pixel coordinate in the main-scan direction (column, direction of the CCD sensor)

x = pixel coordinate in the sub-scan direction (line, movement of the table)

dy, dx = respective geometric transformations

a_1 = scale error in the main-scan direction

a_2 = error in the main-scan direction, due to the 2nd order radial distortion of the lens

b_0 = scale error in the sub-scan direction

b_1 = non-orthogonality of the image

b_2 = error in the sub-scan direction, due to the 2nd order radial distortion of the lens

f_i = local errors in the sub-scan direction (this model approximates the local errors, which are assumed to be constant within a certain interval of 200 lines, depending on the selected n)

c_i = coefficients for the local errors ($f_i = 1$ if y is between $i-1$ and i, otherwise $f_i = 0$)

The general principle in the calibration was that the shape and size of any geometric feature of the original image should be restored in the digitized image. The polynomials (1) and (2) describe the deformations that may occur between the two images. The model includes first- and second order terms for the errors caused by the optical system. The periodic errors in the sub-scan direction are modeled simply by assuming the error to be constant within a certain interval. More sophisticated models, such as cubic splines or piecewise linear interpolations, could be applied. This was not considered necessary in this context.

3.2 Calibration Scans

The accuracy of the error model was examined with a photogrammetric precision grid or gitter. The gitter has a grid of lines in an area of 240 x 240 mm^2. The interval between the lines being precisely 5 mm, except for the 2 outermost lines for which the interval is 4 mm (Figure 4). The grid lines are engraved on a glass (about 10 mm) glass plate.

The gitter was scanned in four different positions so that the scanning area was covered rather completely. Each time the gitter was in a slightly tilted position (Figure 4). This assures that the whole area is covered with observations (see below). The image size was 10200 x 7032 pixels in each of the four scans. All four scans were completed within about 2 hours.

3.3 Determination of Line Deformations by Digital Methods

The next step in the calibration procedure was to determine the line deformations. This step was repeated for each of the four images separately. In this context line deformation means the displacement of the gitter lines with respect to their correct or ideal position. All the grid lines were divided into 46 sections 4.3 mm long, the line crossings being outside the sections. The displacement in perpendicular direction with respect to the line was determined for each section. These displacements were determined keeping an ideal grid, rectangular in correct scale, as a reference. The position of this reference was defined approximately by pointing four corner points of the grid and adjusting the grid to them in a least-squares sense (see

/ . . .

The objective of this phase was to determine the perpendicular displacements in sub-pixel accuracy. The displacement values were determined using digital image processing methods. With the approximate position of the ideal grid as a starting point, a 4.4 mm x 0.8 mm rectangle was defined around each line section. This rectangle was further divided into 68 bins (Figure 5). The pixels having the lowest gray-level values were located within each bin, and the average of their displacement values was used as a displacement value for the bin. Finally, the displacement value for the whole section was computed as the average of the bin displacement values.

The procedure described above was developed by trial and error. It proved to be rather robust with respect to the distribution or histogram of the graylevel values. As will be seen below, it certainly produces displacement values in sub-pixel accuracy. This is due partly to the method of multiple averaging but partly to the tilted position of the grids, which causes an aliasing effect on the lines. Some earlier experiments indicated clearly that accuracy will be degraded if the tilt is very small (less than 20 mm over the whole 230 mm edge).

3.4 Estimation of the Error Model

The parameters of the error model were estimated by least squares adjustment in which the displacement values were treated as observations. All four images were treated simultaneously using the following the adjustment model:

$$DX_{ij} = A_j - C_j Y_{ij} + \cos(a_j)\, dx(x_{ij}, y_{ij}) - \sin(a_j)\, dy(x_{ij}, y_{ij}) \quad (3)$$

$$DY_{ij} = B_j + C_j X_{ij} + \cos(a_j)\, dy(x_{ij}, y_{ij}) + \sin(a_j)\, dx(x_{ij}, y_{ij}) \quad (4)$$

j	=	index for each image
i	=	index for each line section or observation
X_{ij}, Y_{ij}	=	grid coordinates of the center point of line section (the axes of the XY-coordinate system coincide with the grid lines)
DX_{ij}	=	the displacement value for Y-axis directed line sections
DY_{ij}	=	the displacement value for X-axis directed line sections
A_j, B_j, C_j	=	the three parameters for free shift and rotation of the grid in each of the images (j)
x_{ij}, y_{ij}	=	image coordinates of the center point of a line section (ij)
$dx(x_{ij}, y_{ij})$	=	the total effect (in the sub-scan direction) of the error model for a line section (ij)
$dy(x_{ij}, y_{ij})$	=	the total effect (in the main-scan direction) of the error model for a line section (ij)
a_j	=	tilt angle of the grid in each of the images (j).

The parameters for free shift and rotation of the grid in each image are necessary because the position and rotation of the grid is known only approximately within each image. As the tilt angle is rather small, the values of cos(aj) and sin(aj) are close to 1 and 0, respectively. Therefore the errors in main- and sub-scan direction will mainly affect DY and DX, respectively. The adjustment model is based on the assumption that errors are repeatable, .i.e, there is no significance difference in the systematic errors between any two scans. The validity of this assumption is studied below.

The parameters of the adjustment model were solved by the least-squares adjustment using the displacement values of the line sections as observations or sample points.

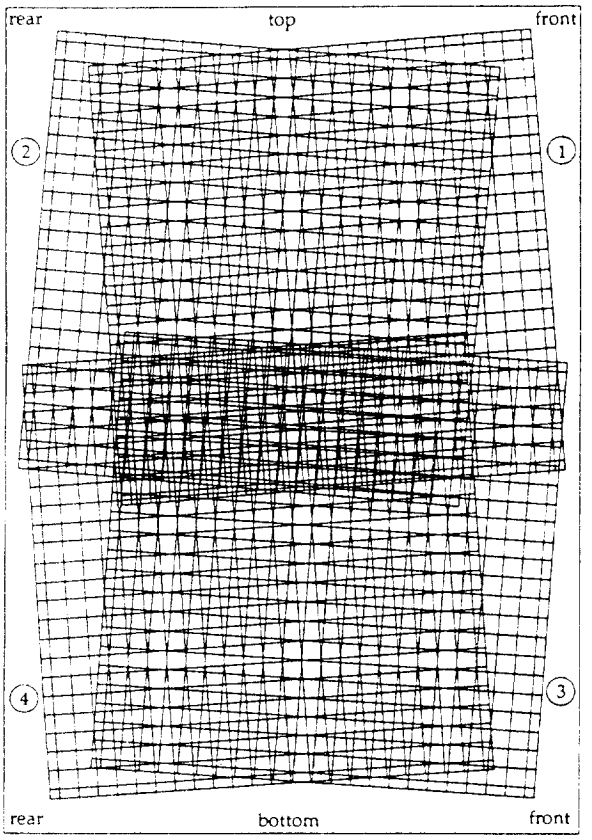

Figure 4. The grid pattern and the four set-ups of the precision gitter used in calibration.

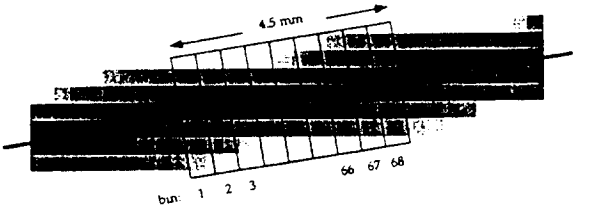

Figure 5. A graphical illustration of the method used to compute the displacement of a line section. The displacement value is computed as the average of the value of each bin. For each bin the displacement value is obtained as the average of the perpendicular distances of the centers of the "darkest" pixels, using the ideal position of the line (dark line) as a reference.

/...

3.5 Summary of the Calibration Results

The main results of the calibration are given in Tables 1-3 and Figures 6-12.

Preliminary adjustments showed that the polynomial terms a_1, a_2, b_1, b_2, b_3 get significant values in conjunction with any data set and that they must always be included in the error model. The terms of the 2nd-order radial and tangential distortion of the optics get very significant values (Table 2). The effect of higher-order polynomials was also studied but it was soon clear that they did not reduce the residual mean square error (r.m.s.e.) computed from the residuals of the displacement values.

Figures 6 and 7 show clearly that there is a periodic error in the direction of the drive system ('sub-scan direction'). Figure 7 indicates that this phenomenon remains from scan to scan. Image 1 differs from the other images in having a large number of gross errors. Its radiometric image quality is probably not fully stabilized, because the scanner was not tuned-up for long enough.

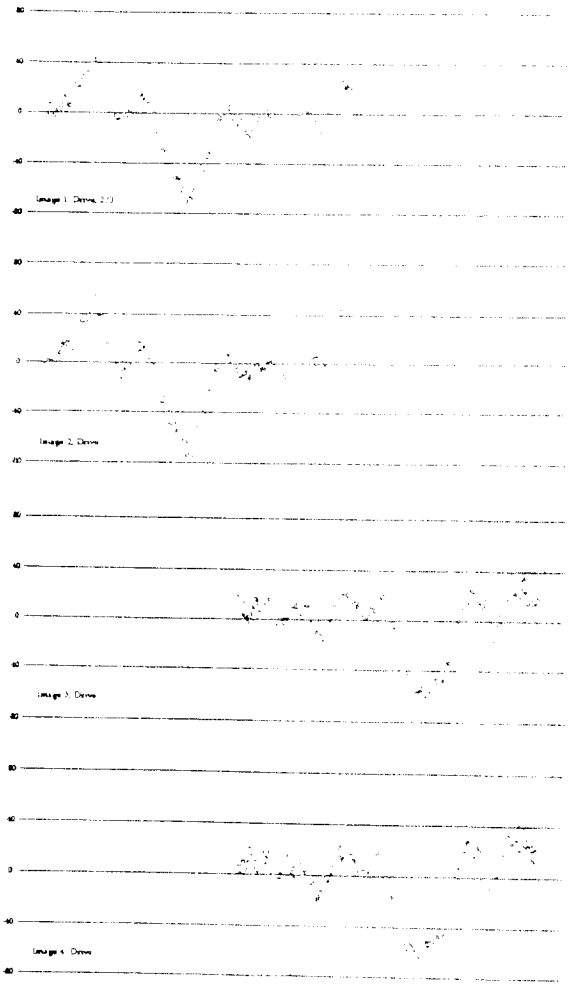

Figure 6. Systematic errors in the drive (sub-scan) direction. The residuals based on the basic model are plotted image-wise using a sub-scan projection.

Table 1. Statistics of the adjustment with the final error model. The area is restricted to a window of 10" (6000 lines x 6000 lines). Local corrections in the drive-direction are made with the bin interpolation, bin size = 50 lines. Gross errors (residual ≥ 30 µm) have been removed.

	Residual-mean-square-errors, µm			Final number of observations		Number of gross errors	
Image	Optics	Drive	Both	Optics	Drive	Optics	Drive
1	9.5	9.8	9.7	754	704	0	57
2	7.2	6.1	6.7	753	760	0	1
3	6.8	5.0	7.2	779	780	0	0
4	9.2	6.8	8.3	776	767	0	12
Total:	8.7	7.1	7.9				

Table 2. Effect of the polynomial parameters of the error model at the extreme points of the scanning area (10200 x 7032 pixels). The center point of the scanning area is assigned to be the origin. Consequently, all the parameters get zero-values in the center of the scanning area and maximums of the absolute values in the corners (where abs(x) = 5100 and abs(y) = 3516). The values refer to the same error model as in Table 1.

Parameter	Coefficient	Effect of the parameter (dx, dy) at the corners of the scanning area, µm
Main-scan direction (Optics)		
a_1	y	-26
a_2	y^2	144
Sub-scan direction (Drive)		
b_1	x	-96
b_2	y	-96
b_3	y^2	120

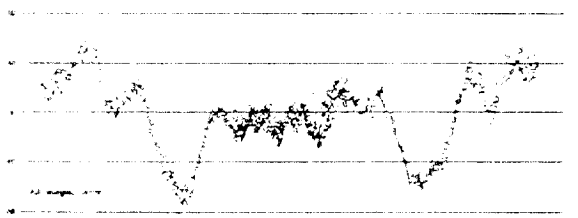

Figure 7. Systematic errors in the drive (sub-scan) direction. The residuals based on the basic model are plotted for all the images using a sub-scan projection.

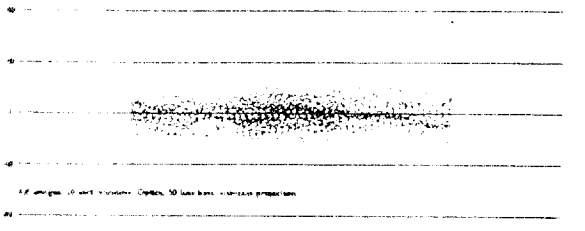

Figure 8. Systematic errors in the drive (sub-scan) direction. The residuals based on the basic model and local corrections with bin-interpolation (bin size: 50 lines) are plotted for all the images simultaneously in a window area of 10" using a sub-scan projection. All the gross errors (residual ≥ 30 µm) have been removed.

/...

Figures 9, 10 and 11 display the errors in the direction of the optics (main-scan direction). It is seen that there are some systematic errors, particularly in Image 3, that the polynomial error model is unable to adopt. The deformation is caused by the tendency of the glass plate to be lifted 0.1 - 0.4mm at one end of the scan (bottom), thus immediately causing this kind of deformation. The ultimate reason is that the opposite end of the table "hangs in the air" without vertical support.

Figures 8 and 12 show the residuals based on the "final" adjustment, in which a window of 10" in the center of the scanning area is used. The local effects of the periodic errors have been compensated by using bins of 50 lines. Observations with residuals of $\geq 30\mu m$ have been removed as gross errors. Figure 12 shows that a main-axis dependent systematic error still remains in the optics.

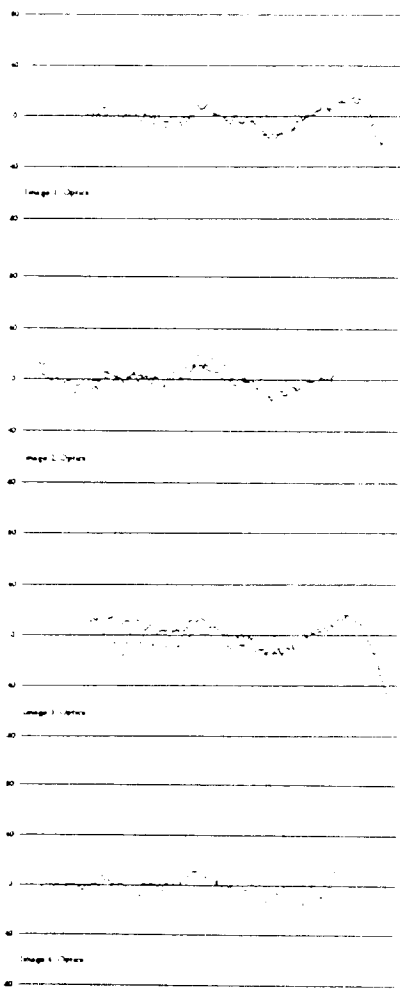

Figure 9. Systematic errors in the optics (main-scan) direction. The residuals based on the basic model are plotted image-wise using a main-scan projection.

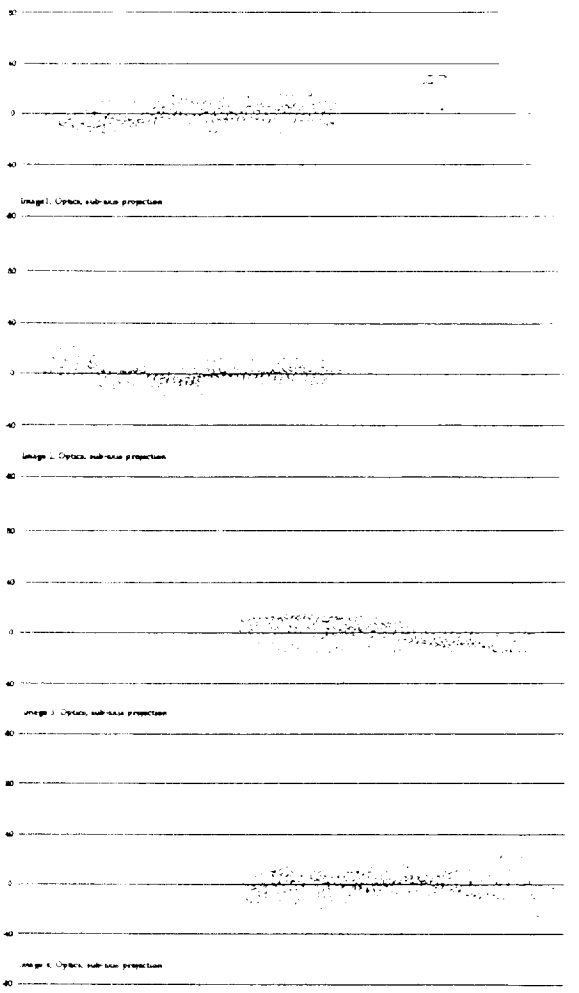

Figure 10. Systematic errors in the optics (main-scan) direction. The residuals based on the basic model are plotted image-wise using a sub-scan projection.

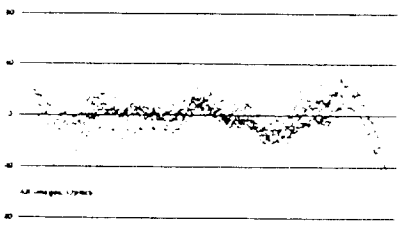

Figure 11. Systematic errors in the optics (main-scan) direction. The residuals based on the basic model are plotted for all the images simultaneously in a window area of 10" using a main-scan projection.

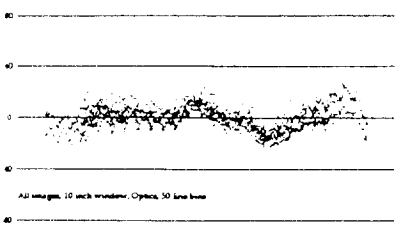

Figure 12. Systematic errors in the optics (main-scan) direction. The residuals based on the basic model are plotted for all the images simultaneously in a window area of 10" using a sub-scan projection.

/...

Table 1 summarizes the statistics of this final adjustment. The r.m.s.e. value computed from all the observations is 7.9 μm, which is about 1/5 of the pixel size. There are no big variations in the r.m.s.e. values of the optics and drive system, although the values are slightly better for the drive system. This may be because the model did not take into account all the systematic errors of the optics.

3.6 Conclusions of the Calibration

The calibration procedure described above has convinced us that our original assumptions of the geometrical characteristics of the SHARP JX-600 scanner are to a great extent valid. The tests have shown that

- The use of photogrammetric grids and digital image processing methods is capable of producing observations with sub-pixel accuracy. The tests reported in this work show that the accuracy is on the order at least 1/5 of the pixel size of 42.3 μm. Additional tests have shown that even an accuracy of 1/10 of the pixel size can be achieved.

- The geometric deformations of the scanned imaged are very much as expected: the drive system causes a periodic systematic error in the sub-scan direction and the optical system causes strong systematic errors in main- and sub-scan directions, due to the 2nd order radial and tangential distortions. There is also a smaller periodic error in the main-scan direction that was not considered in our error model. In this respect the error model could be expanded.

- The stability or repeatability of the scanning results is rather good in terms of image geometry, at least within a short interval. The edges of the scanning area are problematic, owing to the table's insufficient guidance system. This should be improved to provide better vertical support to the front of the table.

- The magnitude of the geometric deformations is so great that they must be taken into account when the scanned images are used for photogrammetric purposes.

- With proper treatment of the systematic errors, the geometry of the scanned images can be controlled to give an accuracy level of at least 1/5 of the pixel size (r.m.s.e. value). This level satisfies the photogrammetric requirements very well.

- Only the center part of the scan area should be used for scanning aerial photographs 9" x 9" in size. Control of the geometrical distortions is best in the center area of the scanner.

4. PROPOSAL FOR CONTINUOUS CALIBRATION

The calibration procedure described above relies on the use of photogrammetric precision gitters which are scanned separately for calibration purposes. This approach is acceptable for periodic calibration. In every-day use the geometric quality of the scanned images should be monitored continuously. This can be done by scanning a geometrically precise test pattern or grid together with each image.

For calibration purposes it would be advantageous to have a grid completely covering the actual 9" x 9" scanning area. This is not feasible in practice as the grid pattern would be rather annoying on the scanned images. A grid surrounding the image frame would be more practicable as the frame could then be scanned with the image. The grid frame could be permanently engraved on the glass plate of the table. For scanning transparencies such as aerial photograph diapositives, a special scattering plate could be made of glass, having the grid frame engraved. This plate would also improve the flatness of the diapositive.

A calibration procedure similar to that described above should be made for each image separately. The horizontal parts (top and bottom) of the frame could be used to control the geometry in the main-scan direction, and the vertical parts (front and rear) in the sub-scan direction. Note that calibration would be fully automatic and thus no manual observation work is needed. The continuous calibration may also be regarded as a quality control and monitoring phase to confirm that the values of the parameters in the error model have not changed. If obvious changes are seen, their reason be pinpointed and the appropriate action taken.

5. IMAGE SHARPNESS

Image sharpness was studied briefly by scanning a non-transparent, black-and-white test chart. The chart was scanned in color-mode at three locations with respect to the main-scan direction: front, center, and rear. Figure 13 shows the results. In the center (b) 11 or 12.5 linepairs/mm are visible, in the rear (c) 9 or 10 and in the front (a) 8 or 9.

This test, although brief, confirms our general observation that image sharpness is best in the center of the scanning area, and that the front part of the image is somewhat less sharp than the rear. This asymmerty might be due to the optical system being out-of-focus. However, this could be corrected by proper adjustment. The slight unsharpness that remains at the edges is typical of optics-based imaging systems.

Some experiments were carried out to compare color and gray-scale scanning modes. The results for the color mode were at least as good as those for the gray-scale mode. In some cases, image resolution (linepairs/mm) in the sub-scan direction was slightly better in the color-mode.

/...

EXTRACTION OF QUANTITATIVE INFORMATION FROM REMOTE SENSING DATA AND INTEGRATION INTO GIS

E. Baltsavias

Federal Institute of Technology

Zurich, Switzerland

/...

METRIC INFORMATION EXTRACTION FROM SPOT IMAGES AND THE ROLE OF POLYNOMIAL MAPPING FUNCTIONS

Emmanuel P. Baltsavias, Dirk Stallmann

Institute of Geodesy and Photogrammetry
Swiss Federal Institute of Technology
ETH-Hoenggerberg, CH-8093 Zurich, Switzerland
Tel.: +41-1-3773042, Fax: +41-1-3720438, e-mail: manos@p.igp.ethz.ch

Commission IV

ABSTRACT

This paper handles the aspect of metric information extraction from SPOT images and focuses mainly on sensor modelling and the geometric accuracy potential of polynomial mapping functions, and secondly on the use of these functions for automated derivation of DTMs and generation of digital orthophotos.

The sensor modelling is based on V. Kratky's strict geometrical model. First, an accuracy analysis is provided based on points of varying definition quality covering the whole image format and having a height range of 1700 m. Different computation versions and an accuracy comparison is presented. Kratky also provides polynomial mapping functions to transform from image to image, object to image, and image to object space. The mapping functions are much faster, easier to implement, and almost equally accurate as compared to strict transformations. The accuracy of these functions will be assessed. This is crucial, since these polynomial functions are subsequently used for automatic DTM and orthophoto generation.

The automatic DTM generation is based on a modified version of the Multiphoto Geometrically Constrained Matching (MPGC). The polynomial functions for the image to image transformation are used to define geometric constraints in image space. Thus, the search space is reduced along almost straight epipolar lines and the success rate and reliability of matching increase. The deviation of the epipolar lines from straight lines will be analysed for different image positions, heights and height approximations. The generation of digital orthophotos is fully automated and is based on polynomial functions modelling the object to image transformation. Aspects regarding speed and accuracy will be analysed.

KEY WORDS: remote sensing, SPOT, geometrical accuracy, constrained matching, DEM, orthophoto

1. INTRODUCTION

SPOT data is extensively used because of its geometric resolution and secured availability, and the stereo capability of the sensor. This data can supply substantial topographic and thematic information to GIS. Today, problems exist firstly in the extraction of the appropriate information from satellite images, especially in an automated manner, and secondly in the integration of this information into GIS. The geometric accuracy of SPOT has been extensively investigated during the last years. Different models of varying complexity, rigour and accuracy have been developed (*Kratky, 1989a; Westin, 1990; Konecny et al., 1987; Toutin, 1985, Gugan, 1987*) up to SPOT block adjustment (*Veillet, 1990*). Various tests have proven that the geometric accuracy potential of SPOT is below 10 m in both planimetry and height. However, strict transformations from image to image, object to image, and image to object space are computationally very intensive and pose problems on the implementation of real-time positioning in analytical photogrammetric instruments. *Kratky, 1989b*, proposed the use of polynomial mapping functions (PMFs) that are much faster and almost equally accurate (maximum error less than 1 m in object and 1 µm in image space) as compared to the strict transformations. The aim of this paper is to test the geometric accuracy of PMFs and check their usefulness for automated DTM and orthophoto generation. Since the PMFs are derived using the results of the strict SPOT model, their accuracy depends on the accuracy of the latter. Thus, investigations on the accuracy of Kratky's strict model and ways to improve it will also be presented.

2. KRATKY'S SPOT MODEL

Kratky's model processes single and stereo panchromatic level 1A and 1B SPOT images. It is an extended bundle formulation considering in a rigorous way all physical aspects of satellite orbiting and of earth imaging, together with geometric conditions of the time-dependent intersection of corresponding imaging rays in the model space. The ephemeris data (position and attitude) are not necessary but they may be used optionally. Orbital perturbations are taken into account by allowing the SPOT orbital segment to be shifted with respect to its expected nominal position. The total number of unknowns per image is 14 - 6 elements of exterior orientation, linear and quadratic rates of change for the rotation angles, a change Δf for the camera constant, and a quadratic distortion in x (corresponding to a shift of the principal point along the CCD sensor). The quadratic

/...

rates may be dropped (linear model). Six weighted constraints keep the orbital positions of the two sensors within statistical limits from the expected nominal orbits or the ephemeris data. Twelve absolute constraints are enforced in order to keep projection centres moving strictly along appropriate elliptical orbital segments. Thus, linear and quadratic rates of change in X, Y, Z, which are eventually used as given values, are calculated. The minimum number of full control points is 4 for the linear model of attitude changes and 6 for the quadratic.

3. TEST DATA

A stereo SPOT panchromatic level 1A model over W. Switzerland was acquired (Figure 1). The inclination of the sensor's optical axis was 23.4° R and 19.2° L respectively, leading to a B/H ratio of ca. 0.8. The acquisition dates were 20.7.1988 and 27.8.1988 with significant radiometric differences between the two images, particularly in agricultural areas. The elevation range was 350 - 3000 m. The following preprocessing was applied to the original digital images:

- reduction of periodic and chess pattern noise
- Wallis filtering for contrast enhancement
- Wallis filtering for edge enhancement (optional)

136 points of good to very poor definition covering the whole image format and with a height range of 350 - 2100 m were used as control and check points. They were measured with an accuracy of approx. 5 m in 1:25,000 topographic maps. Their pixel coordinates were measured in one image manually, and in the second (a) manually, and (b) with least squares template matching using the first image as reference. The following versions were computed with Kratky's model:

(a) linear versus quadratic rates of change for the rotation angles

(b) 6, 10, and 30 control points

(c) pixel coordinates of second image determined manually versus through matching

The results (without exclusion of any point) are listed in Table 1.

The linear and quadratic models give similar results. This was the case in previous investigations too. The quadratic model gives slightly better results in Y, but worse results in Z with 6 control points. There is a big improvement in Z from 6 to 10 control points but no improvement from 10 to 30 points. There is an large improvement in Z when the pixel coordinates in the second image are measured by matching. For the 10 control point version, the manual measurements lead to a by 85% worse RMS in Z as compared to the matching measurements! Version linear, 10 control points, matching measurements was selected for the further work.

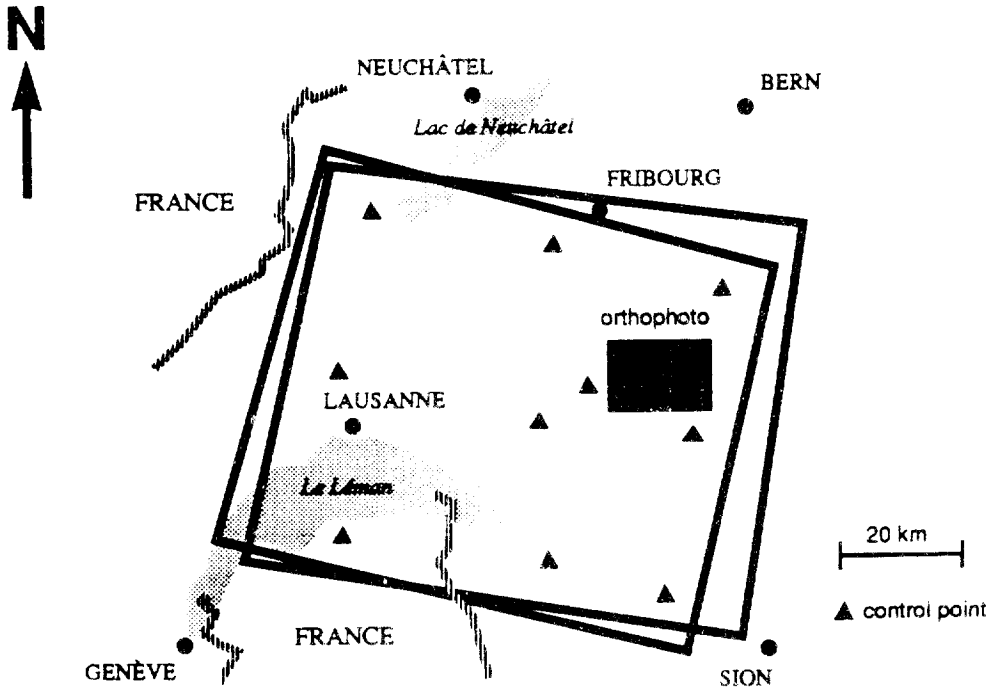

Figure 1 SPOT stereo model with 10 control points. The test region for orthophoto generation (map sheet 1225) is also marked.

/...

Table 1 Precision and accuracy measures for Kratky's SPOT model using different versions

Version*		s_0†	RMS of control points [m]			Number of check points	RMS of check points [m]		
			X	Y	Z		X	Y	Z
L6	man‡	6.1	2.7	2.1	3.6	130	8.6	10.0	14.0
Q6		8.8	2.3	0.5	4.0	130	8.7	9.7	16.0
L10		5.4	2.3	3.0	3.7	126	8.8	9.1	11.5
Q10		5.1	2.5	2.1	3.3	126	8.8	8.9	11.8
L30		6.0	4.2	3.6	4.2	106	8.5	9.1	11.4
Q30		6.0	4.2	3.4	4.3	106	8.5	9.1	11.3
L6	match**	5.6	1.4	2.9	1.0	130	8.9	10.9	12.0
Q6		3.8	1.0	0.2	1.4	130	8.9	10.3	14.1
L10		5.2	2.0	3.3	3.5	126	9.0	10.3	6.3
Q10		4.1	1.7	1.8	3.1	126	9.1	9.9	6.4
L30		6.0	4.0	4.2	4.7	106	9.3	9.3	7.0
Q30		5.7	3.8	3.9	4.3	106	9.5	9.3	7.0

*L, Q ..... linear and quadratic model respectively
†s_0 ..... a posteriori standard deviation of unit weight
‡man ..... pixel coordinates in second image measured manually
**match..... .....pixel coordinates in second image measured by least squares matching

4. FAST POLYNOMIAL MAPPING FUNCTIONS

After the strict SPOT model is estimated the PMFs are derived by the following approach (Figure 2). A 5 x 5 regular grid is defined in the left image. By using the results of the rigorous solution and three heights (the minimum and maximum of the scene, and their average), map coordinates for 75 object points are computed. These are projected in the right image again using the rigorous solution. By using the known coordinates in all three spaces, the coefficients of polynomial functions to map from image to image, image to object, and object to image space (in both directions, i.e. 6 polynomials altogether) are computed by least squares adjustment. Thereby, the object space is reduced to two dimensions by extracting the elevation, i.e. Z is an independent parameter connecting all three spaces. One polynomial is computed for each coordinate to be determined, and for the mappings involving the object space separate polynomials are determined for left and right image. The degree of the transformation, the number and the form of needed terms were determined experimentally. The degree of the polynomials is 3 - 4 with 11 - 16 terms. Kratky provides for each mapping two sets of polynomials, a basic and an extended. The extended has two more terms involving mainly powers of y or Y. It should be used if the quadratic model was used in the rigorous solution. If the linear model was used, then the basic polynomials suffice. A similar, although less accurate, approach with five, instead of three, heights is also used by the algorithm of the company TRIFID which is integrated in the Intergraph Digital Photogrammetric Station 6287 for SPOT modelling and digital orthophoto generation.

In our tests the PMFs (basic model) were determined after the previously mentioned rigorous solution with the linear model, 10 control points and the matching measurements. The pixel and object coordinates of the 136 points were determined by the PMFs and compared to their known values. The differences did not exceed 1 m in object and 1 µm in image space, thus verifying Kratky's results. The accuracy of PMFs was also tested by another method. By using the image to image PMFs and three out of the four pixel coordinates (x', y', x'', y'') of each point, the heights can be determined and compared to the known values. This was done for the triplets (x', y', x''), (x'', y'', x'), (x', y, y''), (x'', y'', y'). The last two cases gave RMS errors of ca. 135 m, which is not surprising since the image base is approximately in the x direction. The first two cases gave the same RMS of 6.2 m which is identical to the results of the rigorous solution.

Having established that the PMFs are fast and accurate enough the next step was their integration in image matching for DTM generation.

5. MODIFIED MPGC USING PMFs FOR AUTOMATIC DTM GENERATION

Automatic DTM generation from SPOT images has been extensively pursued and is particularly attractive for poorly mapped countries. Many algorithms have been developed but none exploits geometric information from the SPOT sensor to guide and support the matching. A

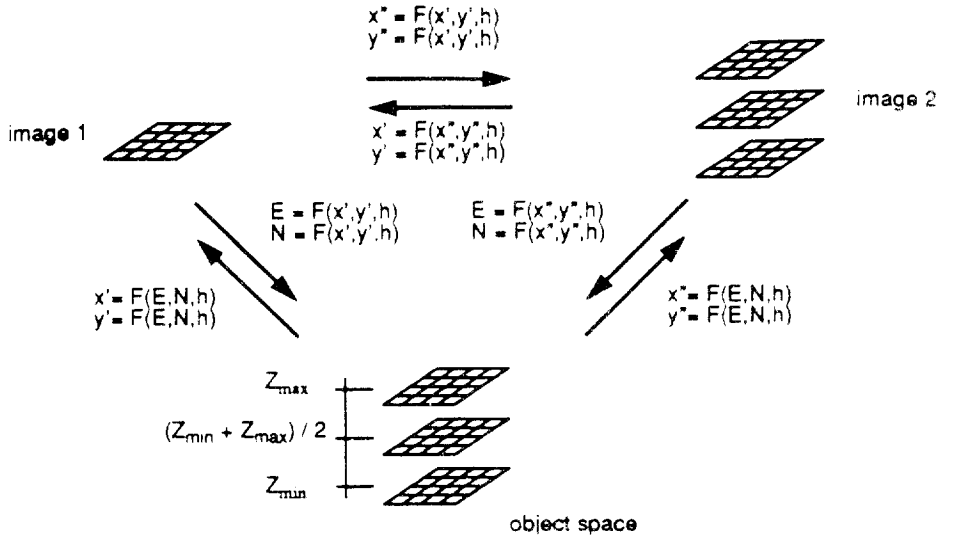

Figure 2 Derivation of fast polynomial mapping functions

reason for that is the fact that the SPOT sensor is linear and thus the perspective relations are valid only within an image line. It was often stated that the epipolar geometry does not exist for SPOT images and that resampling to epipolar images requires a DTM. However, strictly speaking the epipolar geometry does not even exist for frame cameras (which is why most bundle adjustment programs use additional parameters). So, the aim of our investigations was to check to what extent by using Kratky's PMFs an epipolar geometry could be established.

To check that, the following approach was used. A height error ΔZ (two versions; ΔZ = 50 m and 100 m) was added and subtracted to the known heights of the 136 points. For each point, these two erroneous heights and the image to image PMFs were used to transform the pixel coordinates of the left image in two points in the right image. They defined a straight line which passed through the known correct pixel coordinates of the point. The question that had to be answered was whether by arbitrarily changing the height, the projection by using PMFs of the left point in the right image would fall on this straight line, i.e. whether this straight line was the epipolar line (Figure 3). Thus, the known height was sequentially incremented by 25 m in positive and negative direction (leading to object points like P_n in Figure 3), and the projection of the left point in the right image and its distance from the straight line were computed. This distance is a measure of deviation from straight epipolar lines. The results for all 136 points are listed in Table 2. The results are identical for both versions of ΔZ, and for positive and negative increments. As it can be seen from the table a deviation of 0.25 pixels is reached only with a height error of over 7 km! Since such errors are impossible, even more for matching which requires good approximations in order to be successful, straight epipolar lines can be assumed.

Table 2 Deviations from a straight epipolar line for different height errors

Threshold of distance to the straight line [pixel]	Mean Z error to reach the threshold [km]	Standard deviation of Z error to reach threshold [km]
0.25	7.44	0.15
0.5	10.53	0.21
1	14.90	0.30
2	21.08	0.42

The above knowledge was used to modify the Multiphoto Geometrically Constrained Matching (*Baltsavias, 1992*) for automatic DTM generation. The points to be matched were selected in one of the two images (reference image). For each point, by using a height approximation and an error ΔZ as above, the epipolar line in the other image was determined. If only approximations for the pixel coordinates exist, then a height approximation can be derived by the image to image PMFs from the pixel coordinates of the point in the reference image and the x pixel coordinate in the other image. Weighted geometric constraints force the matching to search for a corresponding point only along the epipolar line. This reduction of the search space from 2-D to 1-D increases the success rate and reliability of the matching results.

Additionally, less iterations are required and the DTM production time is decreased. More details on this matching approach and extended tests are published in *Baltsavias* and *Stallmann, 1992*.

6. DIGITAL ORTHOPHOTO GENERATION

The object to image PMFs were used to transform a DTM into SPOT images for orthophoto generation. The PMFs, while being very accurate, offer tremendous advantages regarding speed, a crucial factor for orthophoto production. The speed can be further increased by suitable factorisation. As an example let's consider the basic object to image polynomial

$$F(E, N, h) = \mathbf{a}^T \mathbf{p} \tag{1}$$

with

$$\mathbf{a}^T = (1 \;\; h \;\; E \;\; N \;\; hE \;\; hN \;\; E^2 \;\; EN \;\; N^2 \;\; hE^2 \;\; E^3 \;\; E^2N \;\; h^2EN \;\; hE)' \tag{2}$$

$$\mathbf{p}^T = (p_1 \;\; p_2 \;\; \cdots \;\; p_{14}) \tag{3}$$

involving 30 multiplications and 13 additions. By a suitable factorisation its form changes to

$$\begin{aligned} & p_1 + h(p_2 + Ep_5 + Np_6) \\ & + E(p_3 + E(p_7 + hp_{10} + Ep_{11} + Np_{12})) \\ & + N(p_4 + Np_9 + E(p_8 + h(hp_{13} + Np_{14}))) \end{aligned} \tag{4}$$

involving 14 multiplications and 13 additions. Even larger computational savings can be achieved by using incremental updating of the results of the previous pixel within the column (or row). Updating in column direction is faster than row updating as there are less terms involving N than E. The first pixel of each column can be updated from the results of the first or last pixel of the previous column. The implementation of this approach involves 5 multiplications and 8 additions, and for the first pixel of the columns 7 multiplications and 14 additions. The respective number for the extended PMFs is 5 multiplications and 9 additions, and 8 multiplications and 16 additions. A speed increase of factor 3 in comparison to equation (4) has been achieved. An orthophoto of a whole SPOT scene, using bilinear interpolation, needs only 15 min. on a Sparcstation 2. This is faster than other much more expensive digital orthophoto systems that utilise special hardware (the PRI^{2}SM workstation of I^{2}S for example needs 20 min.).

The accuracy of the orthophotos produced by the PMFs is very good. In *Baltsavias et al., 1991* accuracies (RMS) of 5 m - 6 m are reported. Hammon, Jensen, Wallen and Assoc., a California based company that has integrated our software within ARC/INFO, made tests with 8 SPOT scenes having big height ranges (up to 60 m - 4200 m).

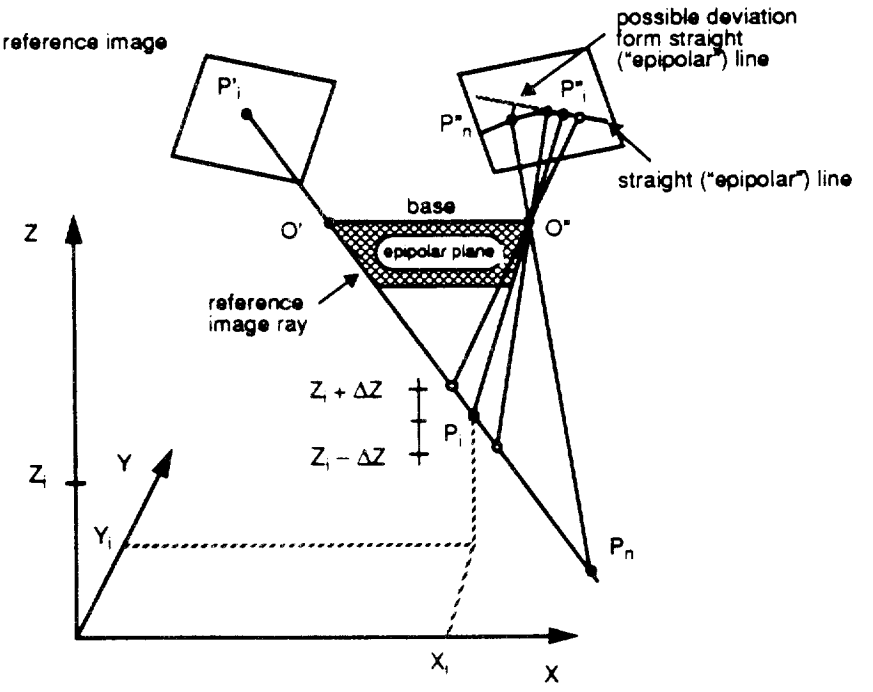

Figure 3 Approximation of epipolar geometry for SPOT images

/...

For the orthophoto production the USGS 30 m DTM was used. The accuracy (RMS) was within 40 ft, and for some scenes less than 30 ft, against the USGS 7.5 min. topographic map.

Digital orthophotos were also produced with the above mentioned SPOT data in W. Switzerland (Figure 4). The 25 m Swiss DTM of the 1:25,000 map sheet 1225 (see Figure 1) having an RMS accuracy of 4.1 m and covering an area of 17.5 x 12 km was used for the orthophoto generation. The height range was 680 m - 2150 m. Orthophotos were produced using both images of the stereo pair and four different versions. In all orthophotos the orthophoto pixel spacing was 8.333 m and the interpolation bilinear. The implementation of the PMFs was either by the incremental approach (fast version) or by using equation (4) (slow version).

Version 1: DTM densification by factor 3, projection using basic PMFs (from linear model), fast

Version 2: DTM projection with basic PMFs (linear model), threefold densification of anchor points, fast

Version 3: like version 1 but slow

Version 4: like version 3 but using extended PMFs from quadratic model

A version like version 3 but with extended PMFs from the linear model gave the same results as version 3. A version like version 4 but with anchor point densification instead DTM densification gave the same results as version 4.

The accuracy of the orthophotos were tested in two ways. The first test was a relative (inner) accuracy test comparing the orthophotos of the same version from the two SPOT images. Corresponding points should ideally have the same pixel coordinates. By using template matching the actual parallaxes (i.e. planimetric map coordinate differences) were detected. Version 1 showed increasing parallaxes of up to many pixels (mainly in x) while moving from left to the right part of the orthophoto. Version 2 showed a similar behaviour but less pronounced. Versions 3 and 4 showed a very good (subpixel) closure between left and right orthophoto, whereby version 4 was slightly superior in y. The reason for this behaviour lies in rounding errors that in the case of the incremental approach are accumulating. Since the processing starts from the top left corner and proceeds columnwise, it is clear that the errors for versions 1 and 2 increase in the right part of the orthophoto. This increase is enhanced by the fact that the heights are larger in the right part of the image. Version 2 gives better results than version 1 (and it is also faster) because less DTM points (by a factor 9) are transformed with the PMFs and thus less errors are accumulated. The errors are larger in x than in y because the PMF coefficients in x are larger than in y. To reduce these errors (a) double precision variables should be used (which was the case in the current implementation; however, the heights and the X, Y coordinates of the DTM origin are 4-byte real variables), and (b) the first pixel of each column should be computed by using equation (4). Thus, errors can accumulate only within one column. By computing strictly (i.e. by equation (4)) the pixel coordinates of not the first but the middle line of the orthophoto, the accumulation of errors within one column can be reduced to half its length. If these precautions are not met and the optimal accuracy is sought for, then the slow version should be used. In this case it is irrelevant whether DTM or anchor point densification is used, but the latter should be preferred as it is faster.

The second test checked the absolute accuracy and used 8 out of the 136 points that were imaged in these orthophotos. Their known pixel coordinates were transferred from one of the SPOT images in the orthophotos through template matching. Thus, planimetric map coordinates were derived, the heights were bilinearly interpolated from the DTM, and these values were compared to the known values. The accuracy measures are listed in Table 3.

Table 3 Accuracy measures (differences) for different options of orthophoto generation

SPOT image*	version	absolute maximum		average		absolute average		RMS	
		X	Y	X	Y	X	Y	X	Y
left	1	21.9	15.0	7.9	6.4	8.5	7.6	11.1	8.9
right	1	32.8	17.1	-13.1	5.2	14.3	7.2	17.9	8.6
left	2	7.5	14.6	1.4	7.3	3.5	7.9	4.5	9.4
right	2	18.2	15.0	-6.8	3.7	8.2	6.5	10.1	7.5
left	3	9.7	14.6	-1.9	7.7	3.8	8.0	4.8	9.8
right	3	12.8	14.0	-3.7	2.7	5.6	6.2	6.8	7.0
left	4	10.6	14.1	-3.0	7.2	4.4	7.6	5.5	9.2
right	4	15.0	14.2	-4.8	4.5	6.0	7.2	7.8	7.8

*Orthophoto from left or right SPOT image

/...

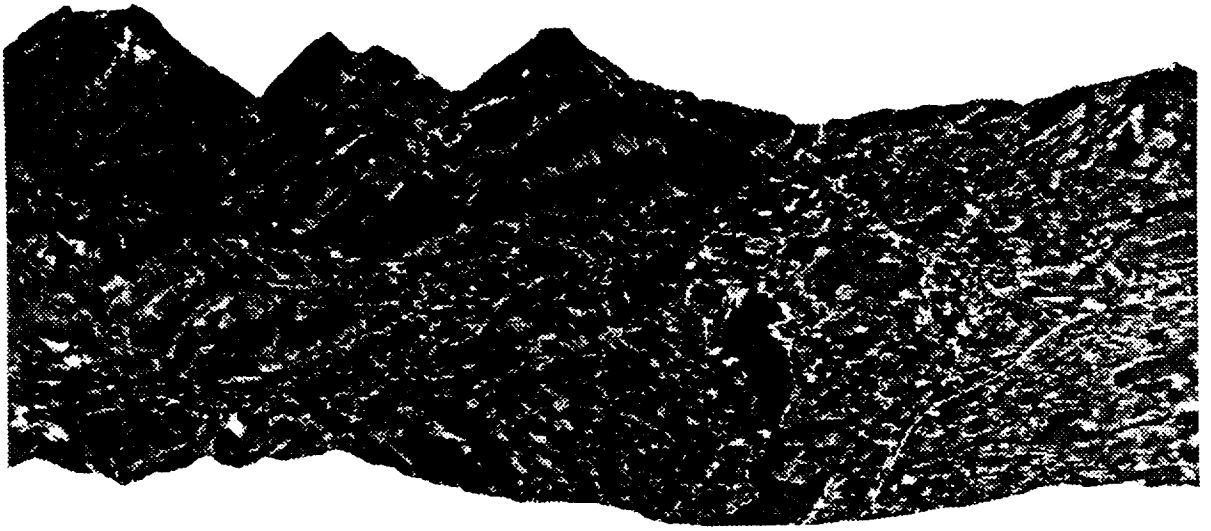

Figure 4 Orthophoto of map sheet 1225 draped over the DTM (1.5x increased heights), seen from north under 60° zenith angle

7. CONCLUSIONS

It has been shown that with Kratky's strict photogrammetric model for SPOT images an accuracy of 9 - 10 m in planimetry and 6 m in elevation can be achieved. Remarkable is the improvement of the elevation accuracy though point transfer by least squares matching.

The PMFs are faster, equally accurate and easier to implement than the strict transformations. Consequently they are suitable for use in image matching and digital orthophoto generation.

A very good approximation of the epipolar line can be derived from the PMFs. The application of the SPOT geometry reduce the search space to 1-D thus increasing the success, reliability and speed of the image matching.

A orthophoto of one SPOT scene can be produced in only 15 min. to a subpixel accuracy (< 10 m). Attention should be paid to the accumulation of rounding errors when incremental updating is used.

8. ACKNOWLEDGEMENTS

The authors express their gratitude to the Bundesamt für Landestopographie, Bern, Switzerland for providing the SPOT images and DTM data.

9. REFERENCES

Baltsavias, E. P., 1992. Multiphoto Geometrically Constrained Matching. Ph. D. Dissertation, Mitteilungen Nr. 49, Institute of Geodesy and Photogrammetry, ETH Zurich, 221 p.

Baltsavias, E. P., Gruen, A., Meister, M., 1991. DOW - A system for generation of digital orthophotos from aerial and SPOT images. In: Proc. of 12th Asian Conference on Remote Sensing, 30 October - 5 November, Singapore, Vol. II, H-1-1-1 - H-1-1-7.

Baltsavias, E. P., Stallmann, D., 1992. Advancement in matching of SPOT images by integration of sensor geometry and treatment of radiometric differences. In: Proc. of 17th ISPRS Congress, Commission IV, 2 - 14 August, Washington D. C., USA.

Gugan, D. J., 1987. Practical aspects of topographic mapping from SPOT imagery. Photogrammetric Record, 12(69):349-355.

Konecny, G., Lohmann, P., Engel, H., Kruck, E., 1987. Evaluation of SPOT imagery on analytical photogrammetric instruments. PERS, Vol. 53, No. 9, pp. 1223 - 1230.

Kratky, V., 1989a. Rigorous photogrammetric processing of SPOT images at CCM Canada. ISPRS Journal of Photogrammetry and Remote Sensing, Vol. 44, pp. 53 - 71.

Kratky, V., 1989b. On-line aspects of stereophotogrammetric processing of SPOT images. PERS, Vol. 55, No. 3, pp. 311 - 316.

Toutin, Th., 1985. Analyse mathématique des possibilités cartographiques du système SPOT. Doctoral thesis, Ecole Nationale des Sciences Géographiques, Paris.

Veillet, I., 1990. Block adjustment of SPOT images for large area topographic mapping. In: Int. Archives of Photogrammetry and Remote Sensing, Vol. 28, Part 3/2, pp. 926 - 935.

Westin, T., 1990. Precision rectification of SPOT imagery. PERS, Vol. 56, No. 2, pp. 247 - 253.

/ . . .

ADVANCEMENT IN MATCHING OF SPOT IMAGES BY INTEGRATION OF SENSOR GEOMETRY AND TREATMENT OF RADIOMETRIC DIFFERENCES

Emmanuel P. Baltsavias, Dirk Stallmann

Institute of Geodesy and Photogrammetry
Swiss Federal Institute of Technology
ETH-Hoenggerberg, CH-8093 Zurich, Switzerland
Tel. +41-1-3772439, Fax +41-1-3721085, e-mail: manos@p.igp.ethz.ch

ISPRS SYMPOSIUM IV

ABSTRACT

This paper presents a matching algorithm for automatic DTM generation from SPOT images that provides dense, accurate and reliable results and attacks the problem of radiometric differences between the images. The proposed algorithm is based on a modified version of the Multiphoto Geometrically Constrained Matching (MPGC). It is the first algorithm that explicitly uses the SPOT geometry in matching, restricting thus the search space in one dimension, and simultaneously providing pixel and object coordinates. This leads to an increase in reliability, and to reduction and easier detection of blunders. The sensor modelling is based on Kratky's polynomial mapping functions to transform between the image spaces of stereopairs. With their help epipolar lines that are practically straight can be determined and the search is constrained along these lines. The polynomial functions can also provide approximate values, which are further refined by the use of an image pyramid.

Radiometric differences are strongly reduced by performing matching not in the grey level but in gradient magnitude images. Thus, practically only the information in stripes along the edges is used for matching. Edges that exist in only one image can be detected by subtracting quasi registered images in the upper levels of an image pyramid and by consistency checks. The points to be matched are selected by an interest operator in preprocessed gradient images. Gross errors can be detected by statistical analysis of criteria that are provided by the algorithm.

The results of an extensive test using a stereo SPOT model over Switzerland will be reported. Different cases of radiometric differences, and matching with different options and the qualitative comparison of the results based on forty thousand check points will be presented.

KEY WORDS: SPOT, automatic DEM generation, image matching, geometric constraints, radiometric differences, accuracy analysis

1. INTRODUCTION

The motivation behind this research was the aim to improve matching of SPOT images by integration of the sensor geometry and the treatment of radiometric differences. As far as the authors know, none of the published matching methods explicitly exploits the SPOT geometry to restrict the search space. Since SPOT does not have a perspective geometry in flight direction, accurate epipolar images can not be generated without the use of a DTM and thus the existing matching algorithms perform a 2-D search. The authors investigated Kratky's polynomial mapping functions (PMFs) (*Kratky, 1989a*) which transform from image to image, image to object and object to image space. For the computation of the coefficients of the PMFs the results of a rigorous bundle adjustment are used. The PMFs are much faster and almost equally accurate as the rigorous transformations. When the row of an imaged point is projected by using the PMFs onto the other image of a stereo pair (epipolar line) [illegible] approximation a straight line. If a straight line is defined by the projection of a small ray segment which is centred at the correct point position in object space, then the deviation of the epipolar line from the straight line would be 0.25 pixel for a height error of more than 7 km. More details on the characteristics of the PMFs can be found in *Baltsavias and Stallmann, 1992*.

Attempts to circumvent the problem of radiometric differences have concentrated on using images acquired within a short time interval. However, this is difficult to achieve and does not solve the problem. The along-track stereo will strongly reduce these problems but can not eliminate them due to different perspective views, clouds and occlusions. Fusion and matching of multitemporal and multisensor data, as in change detection applications, will retain their importance even in the era of along-track stereo. Thus, the authors decided to attack this problem, which has been up to now treated only to a limited extent. The idea is to use gradient magnitude images, thus eliminating radiometric differences in areas of low

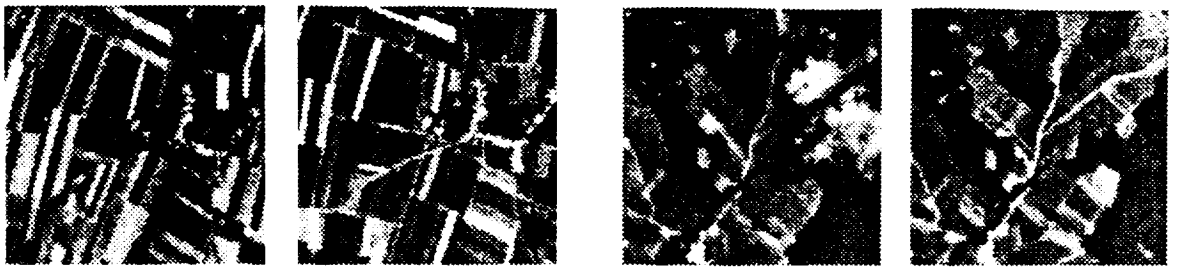

Figure 1 Radiometric differences due to agricultural activities (left pair) and due to clouds and shadows (right pair).

texture. Preliminary investigations have shown that the majority of the edges remain stable. However, different edges exist due to clouds, shadows, different perspective views, new edges within fields due to agricultural activities, human intervention, water level, snow coverage, changes in the tree canopies etc. (Figure 1). A method should be developed to try to detect the different edges through consistency checks.

2. TEST DATA

A stereo SPOT panchromatic level 1A model over W. Switzerland was acquired. The inclination of the sensor's optical axis was 23.4° R and 19.2° L respectively, leading to a B/H ratio of ca. 0.8. The acquisition dates were 20.7.1988 and 27.8.1988 with significant radiometric differences between the two images, particularly in agricultural areas. Figure 1 shows some typical image parts with large radiometric differences. The elevation range was 350 - 3000 m. The following preprocessing was applied to the original digital images:

- reduction of periodic and chess pattern noise
- Wallis filtering for contrast enhancement

136 control and check points were used with Kratky's rigorous SPOT model (*Kratky, 1989b*). 10 for the points were used as control points with a linear model of the attitude rates of change. The pixel coordinates were measured in one image manually and transferred to the second one by template matching. The RMS of the check points was 9 - 10 m in planimetry and 6 m in height.

3. MODIFIED MPGC

MPGC is described in detail in *Baltsavias, 1991*. It combines least squares matching (involving an affine geometric transformation and two radiometric corrections) and geometric constraints formulated either in image or object space. The constraints lead to a 1-D search space along a line, thus to an increase of success rate, accuracy and reliability, and permit a simultaneous determination of pixel and object coordinates. Any number of images (more than two) can be used simultaneously. The measurement points are selected along edges that are nearly perpendicular to the geometric constraints line. The approximations are derived by means of an image pyramid. The achieved accuracy is in the subpixel range. The algorithm provides criteria for the detection of observation errors and blunders, and adaptation of the matching parameters to the image and scene content.

In the case of matching of SPOT images the geometric constraints were formulated as follows. First, given a measurement point in one of the images (template image) a height approximation is needed. If the existing approximations refer to the pixel coordinates, then the height is computed by using the pixel coordinates in the reference image, the x pixel coordinate in the second image and the image to image PMFs. This height Z is altered by a height error ΔZ. Using the heights $Z + \Delta Z$, $Z - \Delta Z$, the pixel coordinates in the template image are projected by the image to image PMFs in the second image where they define the geometric constraints (epipolar) line. The centre of the patch of the second image which is used for matching is forced to move along this line by means of a weighted observation equation of the form

$$v_c = (x + \Delta x)\cos\beta + (y + \Delta y)\sin\beta - p \qquad (1)$$

where (x, y) the approximate pixel coordinates of the corresponding point in the second image and $(\Delta x, \Delta y)$ the unknown x-shift and y-shift.

Equation (1) is equivalent to the distance of a point $(x + \Delta x, y + \Delta y)$ (the patch centre of the second image) from a straight line. The epipolar line is expressed by the normal equation of a straight line, where p is the distance of the line from the origin and β is the angle between the perpendicular to the line and the x-axis.

If the patch of the second image does not lie on this line, then it jumps onto the line right in the first iteration. With our data, the epipolar lines are approximately horizontal, i.e. any error in the y-direction will be eliminated right in the first iteration. An example is shown in Figure 2. Since the epipolar lines are horizontal, the measurement points must be selected along edges that are nearly vertical in order to ensure determinability and high accuracy. Some advantages of the geometric constraints will now be presented. SPOT images include due their small scale a high degree of texture, i.e. edges. Measurement points lying along nearly straight edges can not be safely determined with other matching techniques, but with our approach they can as they lie at the intersection of two

/...

nearly perpendicular lines. Figure 3 illustrates such an example. Another usual problematic case is that of multiple solutions. With geometric constraints side minima can only result if they fall along the epipolar line. Figure 4 shows an example with and without geometric constraints.

An extension of our approach, which has not been implemented yet, is the application of such constraints for the 4 corners of the patch of the template image. This patch represents a part of the object surface which can be modelled by different surfaces (e.g. horizontal plane, inclined plane, 2nd degree surface). Depending on the type of the surface, the heights of the 4 corner points can be defined analytically. For example, if an inclined plane is selected, the heights at the 4 corner points are a function of the height at the patch centre and the two

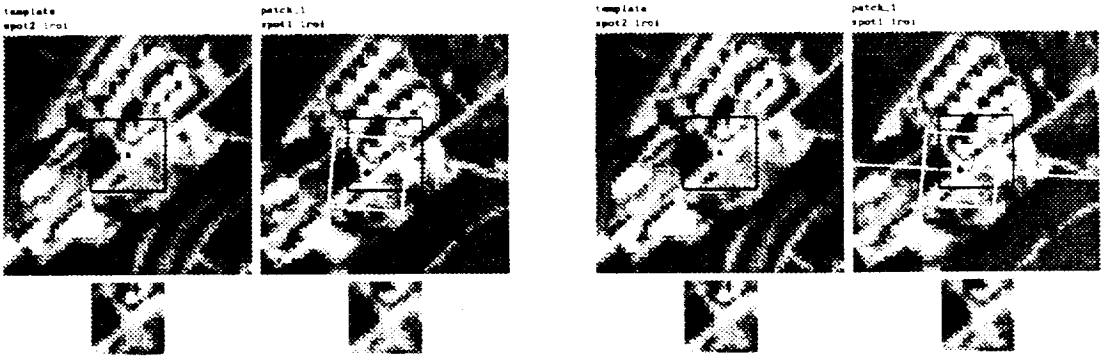

Figure 2 Matching without (left) and with (right) constraints. 10 iterations without and 5 iterations with constraints were needed. The "epipolar line" is the white line in the right image. The black frame is the initial position and the white frame with the black centre cross the final position.

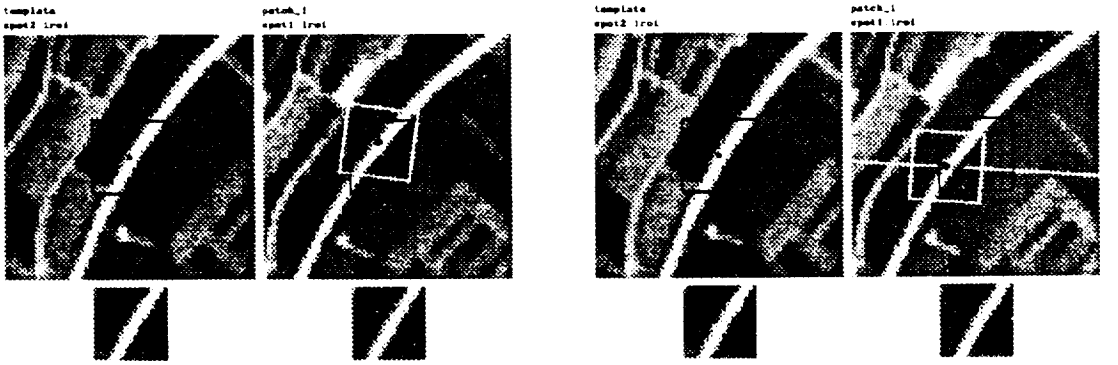

Figure 3 Matching along edges without (left) and with (right) constraints.

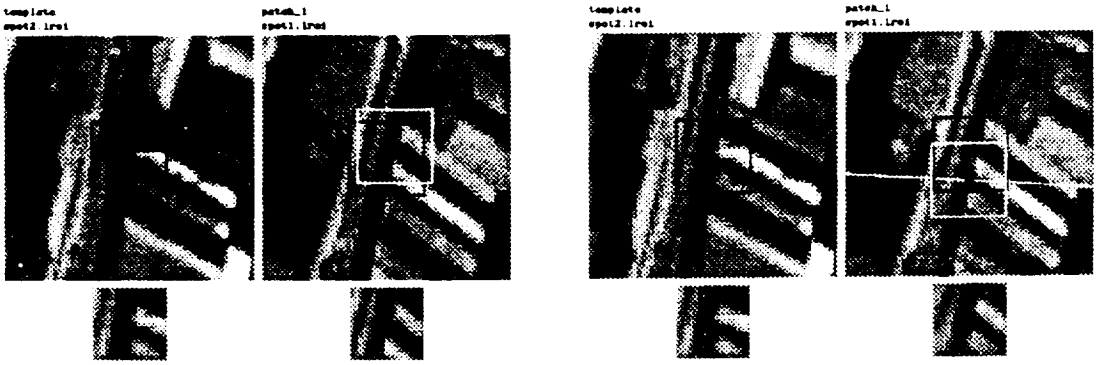

Figure 4 Multiple solution matching without (left) and with (right) constraints.

/...

inclination angles of the plane. Thus, geometric constraints can be formulated by using the known pixel coordinates of all corner points, their heights (which are a function of the height at the patch centre and the plane parameters) and the PMFs (note that their coefficients are the same for all points). The unknowns to be solved for are the plane parameters and the height at the patch centre. This approach is an indirect object-based matching approach. It has the advantage that permits the determination of the local surface parameters (and not just the height at the patch centre), and that it constrains the 4 corners, i.e. restricts the affine geometric transformation. Using an inclined plane model, which is implicitly implied by the affine transformation of the current approach, the new approach also results in computational advantages as the number of unknowns reduces from 6 to 3. However, the problem to be solved is the a priori determination of a suitable surface model.

4. DATA PREPROCESSING AND SELECTION OF MEASUREMENT POINTS

First, the gradient magnitude images are computed. To reduce weak edges due to noise, which is very noticeable in SPOT images, all gradients with a magnitude less than a threshold T can be set equal to T. The threshold is selected as a function of the mean and the standard deviation of the gradient magnitude image (in this case T = mean - standard deviation). The same function should be used for both images to ensure equal treatment. The threshold should not be too high otherwise (a) useful texture is deleted, and (b) the edges are broken and significant differences between the two images occur due to different edge strength. This approach eliminates noise but also low texture which is however not very likely to lead to accurate matching results. An example is shown in Figure 5.

As already mentioned, the measurement points are selected along edges nearly perpendicular to the epipolar lines. In order not to reduce the number of the selected points too much (and thus their density, which influences the DTM accuracy), points along edges with an angle of $\pm 45^{\circ}$ with the perpendicular to the epipolar line should also be selected. To avoid clustering of good points a thin-out window for non-maxima suppression can be defined. To avoid selecting points lying at small and faint noisy edges the points are selected in the first level of the image pyramid. Our approach is to match the same number of points in all pyramid levels. Thus, a selected point must have the aforementioned properties in all pyramid levels. Generally, the approach to be followed is to detect good points in all levels of the image pyramid of the template image and keep the points that appear in all pyramid levels. However, these SPOT images had a lot of texture and this was expressed in all pyramid levels. By going up in the image pyramid, the relative number of selected points was actually increasing.

To avoid selecting points at regions of radiometric differences, especially the ones with a large area extent (like clouds), the following approach can be used. Using the PMFs and an average height of the scene (derived either from a priori knowledge or from the average height of the control points used in the rigorous SPOT model), or a polynomial transformation derived from the pixel coordinates of the control points, the search image is registered with the template image. If the registration were perfect, a simple subtraction of the two images would give us the different edges. Since the registration is not perfect, an image pyramid is created so that at the highest level the misregistration error is within pixel range. Then through subtraction, the different edges are detected by binarising the difference image with an absolute threshold. This binary image can eventually be dilated in order to avoid selecting points whose patch would partially fall inside areas with radiometric differences. These disturbance areas are projected in all pyramid levels and convolved with the selected points in order to clean the selected points. An example is shown in Figure 6.

5. DERIVATION OF APPROXIMATIONS

In this test the approximations were either given manually or derived from a given DTM. The proposed general approach is the following. After the PMFs are computed an average height is used in order to determine the position of the selected points in the search image. To check the quality of these approximations the 136 points

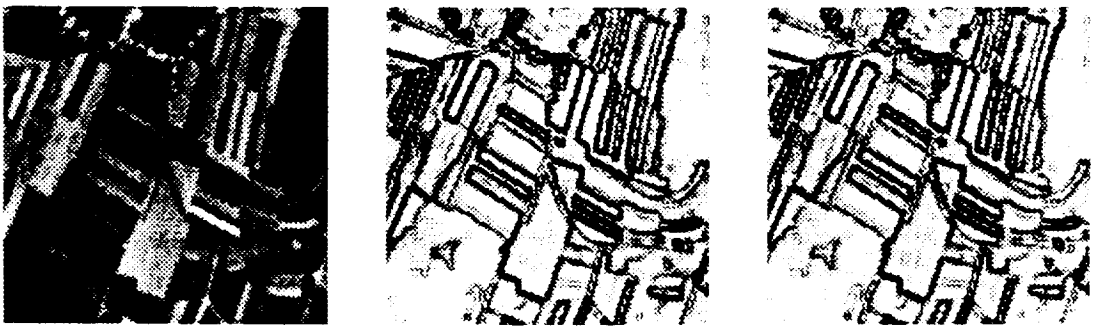

Figure 5 Grey level image (left), gradient magnitude image (middle), thresholded gradient magnitude image (right)

/...

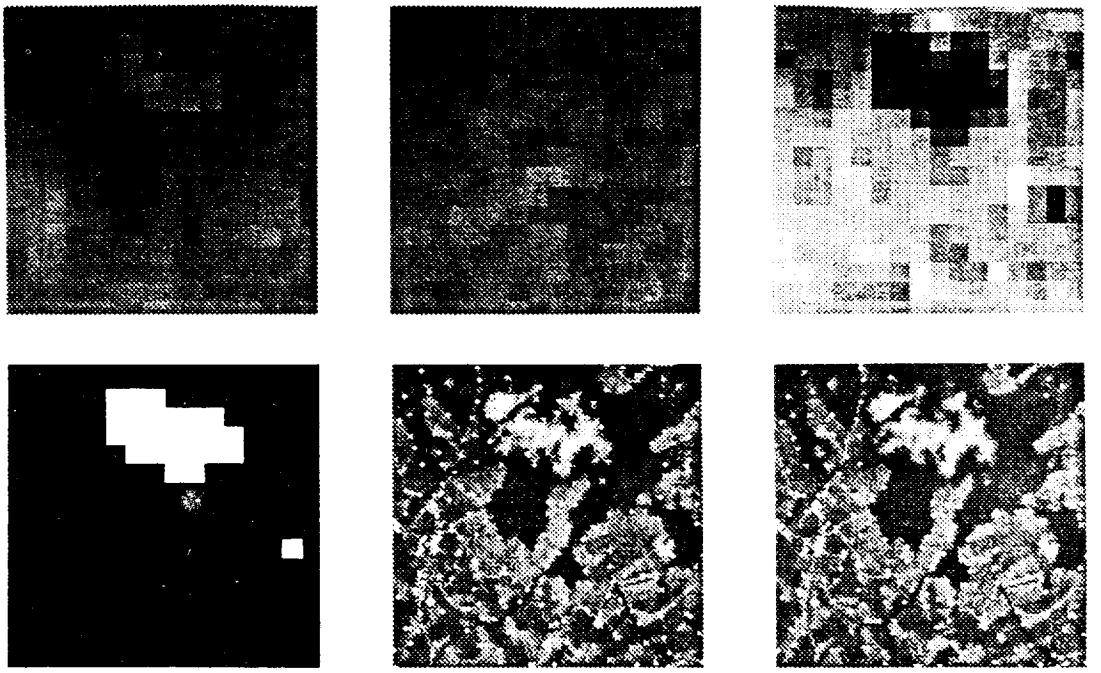

Figure 6 Top row: left (left) and right (middle) SPOT image at 4th pyramid level and normalized difference image (right). Bottom row: binarized difference image (left), image with selected points (middle), image with cleaned selected points (right)

were projected onto the search image by using an average height of 1000 m, and these pixel coordinates were compared to the known ones. The RMS differences were 32 pixels in x and 2 pixels in y, with the maximum error being 72 and 5 pixels respectively. Thus, a refinement of these approximations by an image pyramid approach is necessary. An alternative approach would be to actually transform and resample the search image by using the PMFs and the average height. In this case, the disadvantages are (i) the computational costs for the transformation and the resampling, and (ii) the degradation of the data. The advantages include: (i) matching can be performed using only shifts, thus resulting in computational gains which in case of many points exceed the loses, (ii) detection of radiometric differences can be applied as proposed above, and (iii) since the y-parallax of the co-registered images is very small, the images can be viewed stereoscopically (which anyway is required in digital photogrammetric workstations).

6. ACCURACY TESTS

The accuracy of the matching algorithm was tested by using the 25 m DTM of Switzerland which is generated by the Bundesamt für Landestopographie. The DTMs of the 1:25,000 map sheets 1224 and 1225 were acquired. Each DTM has 701 x 481 nodes in E-W and N-S direction respectively. The DTMs are produced by bicubic interpolation in x and y direction, whereby the known heights are supplied by digitised contours, lake contours and spot heights. The accuracy of these DTMs was checked by bicubic interpolation of the heights of ca. 1000 spot heights and comparison to their known values which have an accuracy of 1 - 2 m. The 1224 DTM was derived from ca. 107,000 height values and has an accuracy (RMS) of 1.9 m. The height range is 900 m but the terrain is generally smoothly changing. The 1225 DTM was derived from 252,000 height values, has an accuracy of 4.1 m and a height range of 1500 m. Although it is not the most extreme case that can be encountered in Switzerland, the terrain is in most parts steep. Forests cover ca. 20% of map sheet 1224 and 35 - 40% of map sheet 1225. In the latter there are also lakes covering ca. 4% of the area. Some clouds were present. The radiometric differences were larger in map sheet 1224 which included agricultural areas.

The aim of this test was to check the accuracy potential of the algorithm. Thus, good approximations derived from the given DTMs were used. The measurement points and their approximations were derived as follows. First, an orthophoto for each DTM using one of the SPOT gradient magnitude images was generated. The points were selected in the first pyramid level of the orthophoto by using a thin-out window of 3 pixels (27183 and 26064 points in the map sheets 1224 and 1225 respectively) and were projected into the original orthophoto images. After exclusion of the points at the areas of radiometric differences through subtraction with the orthophotos from the second SPOT image, 20,180 and 22,592 points remained. The X, Y coordinates of these points were readily available (since the images were orthophotos) and the height was bilinearly interpolated from the given

/...

DTMs. Using the object to image PMFs, pixel coordinates were derived and matching could be performed.

For matching the following 5 different versions were run:

Version 1: patch size 17 x 17, no geometric constraints, conformal transformation

Version 2: patch size 17 x 17, constraints, conformal transformation

Version 3: patch size 17 x 17, constraints, shifts only

Version 4: patch size 17 x 17, constraints, conformal transformation, grey level image

Version 5: patch size 9 x 9, constraints, shifts only

All versions used gradient magnitude images with the exemption of version 4 that used grey level images. The choice of these versions was based on preliminary investigations that were performed with some of the worst out of the 136 points. The aim was to compare constraints vs. no constraints, grey level vs. gradient magnitude images, conformal vs. shift transformation, and shifts with different patch sizes. The case of affine transformation was excluded a priori because in many cases it is not stable since the selected points lie at edges and thus two scales and one shear are often not determinable.

Some points were unsuccessfully matched either because they were transformed outside the search window or because they needed more than 20 iterations. Table 1 shows these results.

Table 1 Matching versions

Version	1224		1225	
	Successfully matched points	Iterations per point	Successfully matched points	Iterations per point
1	94.4%	5.6	97.1%	5.2
2	97.7%	4.1	98.5%	4.2
3	99.2%	3.4	99.2%	3.8
4	94.4%	4.9	97.2%	4.3
5	98.4%	3.6	98.9%	3.6

These results were analysed for automatic detection of blunders. The criteria that have been used for quality analysis are: standard deviation of unit weight from the least square matching, correlation coefficient between the template and the patch, number of iterations, x-shift (i.e change from the approximate values), standard deviation of x-shift, y-shift, standard deviation of y-shift, and the size of the 4 shaping parameters (two scales, two shears). With the conformal transformation only two shaping parameters were used (one scale, one shear). After matching, the median (M) and the standard deviation of the mean absolute difference from the median (s(MAD)) were computed for each criterion. The median and the s(MAD) were used instead of the average and the standard deviation because they are robust against blunders. The threshold for the rejection of one criterion was defined as M ± N * s(MAD). N was selected to be 3 for all criteria with the exemption of the number of iterations, the two shifts and the two scales which should be left to vary more (N = 4). A point was rejected (i) when one of its criterion did not fulfil the aforementioned threshold (relative threshold derived from the image statistics), or (ii) one of its criteria did not fulfil a very loosely set threshold, e.g. for the correlation coefficient 0.2 (absolute threshold, valid for all images). The same N and absolute thresholds were used for all versions. Table 2 gives information on the amount of rejected points.

Table 2 Points rejected by automatic blunder detection

Version	1224		1225	
	Percentage over successful points	Remaining good points	Percentage over successful points	Remaining good points
1	16.1%	15987	15.7%	18504
2	11.4%	17485	12.7%	19417
3	9.2%	18173	9.0%	20391
4	18.1%	15606	17.2%	18183
5	10.8%	17714	8.7%	20394

As it can be seen from Table 1 and Table 2, the amount of successfully matched points decreases and the percentage of detected blunders increases when (i) no geometric constraints are used (version 1), and (ii) grey level images are used (version 4). From the remaining versions, the ones using shifts result in more successful points because they are more stable (robust) than the one using the conformal transformation. The conformal transformation includes a scale which is not always well-determinable. Constrained matching needs less iterations per point than unconstraint version, especially when only shifts are used. The differences between the two shift versions are minimal although their patch size differs considerably. The above results are valid and similar for both map sheets in spite of the different terrain form and land usage.

For the accuracy analysis two comparisons were made:

- The matched points are bilinearly interpolated in the reference DTM grid and the differences between the interpolated heights and the heights as estimated by matching are computed (Table 3).
- And a new DTM was derived from the matched points and compared to the reference DTM (Table 5).

/...

Table 3 Differences of estimated heights (cleaned data) to heights bilinearly interpolated in the reference DTM

Version	1224		1225	
	absolute max.	RMSE	absolute max.	RMSE
1	31.7	7.2	42.9	8.9
2	33.8	8.4	44.8	9.4
3	38.7	9.5	47.6	11.2
4	40.9	9.6	48.0	10.0
5	41.7	10.2	52.7	10.7

Table 4 Differences of estimated heights (raw data) to heights bilinearly interpolated in the reference DTM

Version	1224		1225	
	absolute max.	RMSE	absolute max.	RMSE
1	203.3	11.5	158.8	12.6
2	175.1	12.6	157.5	13.3
3	251.2	14.0	236.8	15.9
4	198.8	19.5	224.1	17.1
5	248.7	19.0	298.3	18.3

Table 5 Differences between new and reference DTM

Version	1224		1225	
	absolute max.	RMS	absolute max.	RMS
1	94.3	8.9	271.5	19.9
2	93.6	9.5	235.6	18.6
3	94.7	10.4	191.6	18.5
4	107.8	10.9	233.0	19.3
5	98.6	10.4	52.7	17.0

Table 3 represents the accuracy of our matching approach. The accuracy is in the subpixel level! The figures of Table 5 are worse due to interpolation errors (330,000 points were interpolated from 16,000 - 20,000 points). Still the results for map sheet 1224 are close or less than 10 m. The results for map sheet 1225 are worse due to the mountainous terrain, many forests and the lake. With denser measurement points they should be close to the results of map sheet 1224 as Table 3 also indicates.

Version 1 (without constraints) is surprisingly good. The reason is that the approximations were very good. Additionally the points were chosen along nearly vertical edges. Thus, the precision in x-direction is good and errors in y (gliding along the edge) influence minimally the estimated heights due to the horizontal base. Additionally, the results of version 1 are based on fewer points due to many detected blunders (Table 2). This reduced density, however, influence the accuracy as it can be seen for map sheet 1225 (Table 5). The advantages of the use of the constraints will become more apparent in a realistic case when the approximate values are poorer.

Version 4 is worse than the similar version with gradient magnitude images (version 2). The difference is not so big again due to good approximations and many reduced points for version 4. The shift versions (3 and 5) perform quite well. Version 5 gives the best results of Table 5 for map sheet 1225 due to the small patch size which models better the irregular terrain surface, and the large number of correct points which reduces the interpolation errors.

The improvement of the results due to blunder detection is remarkable. Table 4 shows the same results as Table 3 but for the raw data (including blunders). The results are as the average 37% worse than those of Table 3.

For visualisation the absolute differences d between the two DTMs which are higher than the threshold value t are combined with the orthophoto and marked as white areas (Figure 7 and Figure 8). The new DTM was derived from the points of version 2 and the threshold is defined by:

$$t = \bar{d} + RMS(d) \qquad (2)$$

with $\bar{d}$ mean of absolute differences.

Differences higher than the threshold can be found especially in three types of areas (Figure 7 and Figure 8 at a, b and c):

(a) At the mountain-ridges and cliffs. At these regions there are surface discontinuities and forests. Additionally interpolation errors occur because the density of the selected points was low at these regions and thus the terrain surface could not be modelled correctly (see Figure 9 with the triangles used for DTM interpolation).

(b) At forest areas, because the matched points are on the tree tops and the reference DTM refers to the earth surface.

(c) On the lake surface. The selected points lied on either sides of the lake, and at certain places much higher than the lake surface. Thus, the large triangle that were used for the DTM interpolation (Figure 9) were lying much higher than the lake surface.

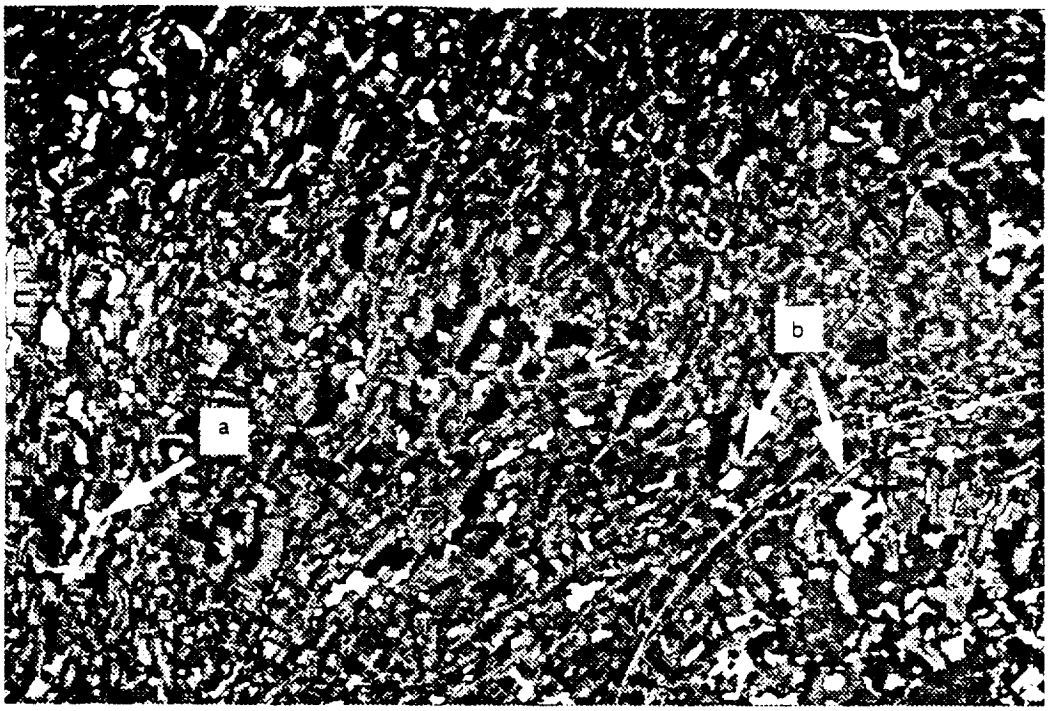

Figure 7 Orthophoto of map sheet 1224 with overlay of DTM differences > 17 m (white areas)

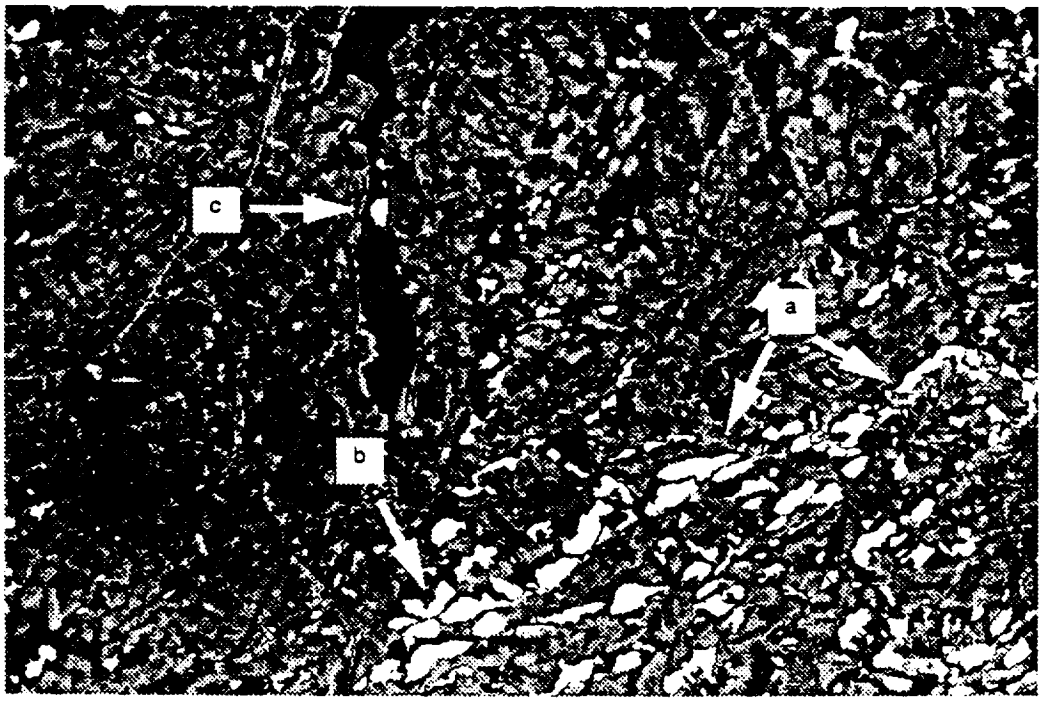

Figure 8 Orthophoto of map sheet 1225 with overlay of DTM differences > 30 m (white areas)

/...

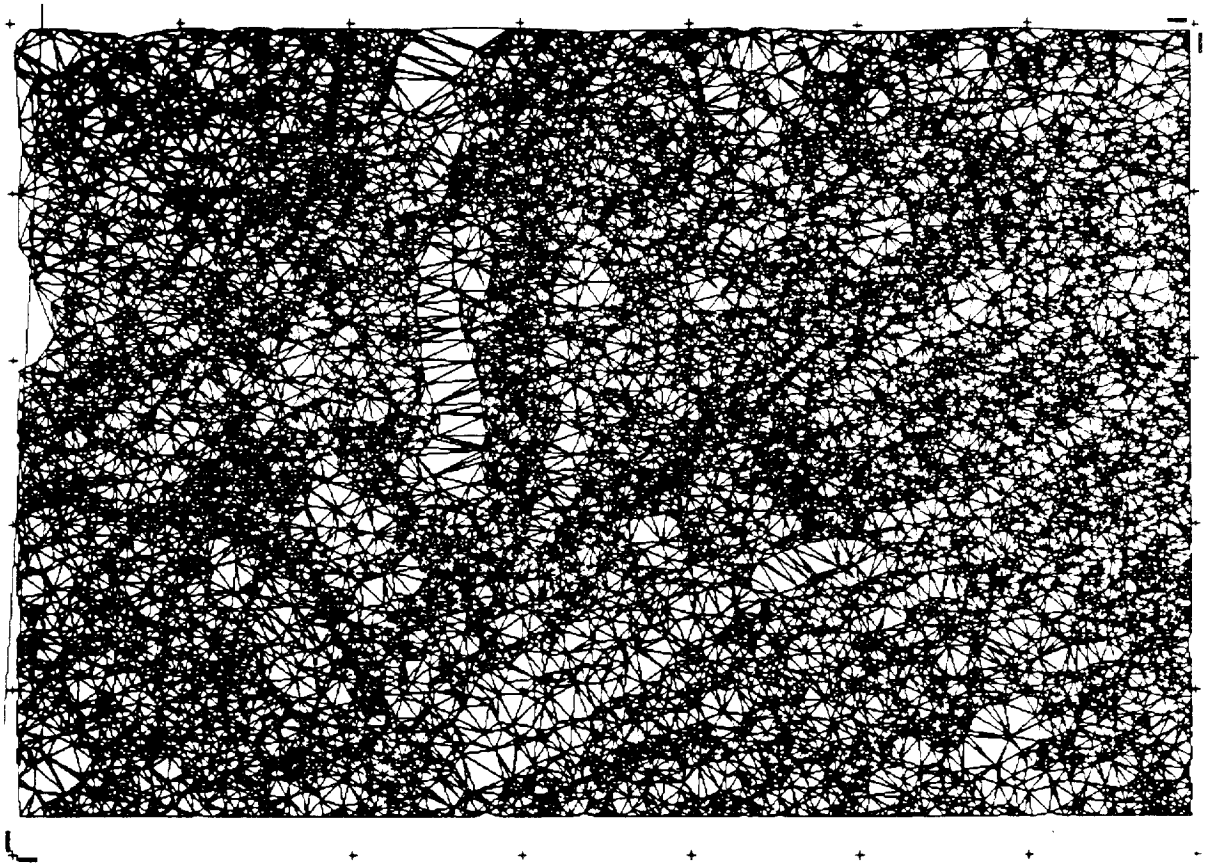

Figure 9 Triangulation mesh for DTM interpolation of map sheet 1225

7. CONCLUSIONS

A matching algorithm for SPOT images was presented that uses the SPOT geometry to impose constraints that reduce the search space from 2-D to 1-D. The algorithm severely reduces the problems caused by radiometric differences can simultaneously use any number of images (more than two) and determines in on step pixel and object coordinates. The use of gradient images magnitude instead of grey level images improves the results. A conformal transformation is suggested. However, the use of only shifts also leads to good results, slightly inferior to those of the conformal transformation.

Problematic cases like multiple solutions and occlusions are reduced and the computation times decreases due to the 1-D search. An intelligent blunder detection scheme is proposed that uses criteria derived solely from the statistics of the results.

The accuracy of the matching is excellent (RMS less than 10 m for 36,000 check points). The accuracy of the interpolated DTM depends clearly on the density of measurement points and for sufficient density it can also be in the 10 m range.

8. ACKNOWLEDGEMENTS

The authors express their gratitude to the Bundesamt für Landestopographie, Bern, Switzerland for providing the SPOT images and DTM data and appreciate their cooperation in the accuracy analysis of the results.

9. REFERENCES

Baltsavias, E. P., 1992. Multiphoto Geometrically Constrained Matching. Ph. D. Dissertation, Mitteilungen Nr. 49, Institute of Geodesy and Photogrammetry, ETH Zurich, 221 p.

Baltsavias, E. P., Stallmann, D., 1992. Metric information extraction from SPOT images and the role of polynomial mapping functions. In: Proc. of 17th ISPRS Congress, Commission IV, 2 - 14 August, Washington D. C., USA.

Kratky, V., 1989a. On-line aspects of stereophotogrammetric processing of SPOT images. PERS, Vol. 55, No. 3, pp. 311 - 316.

Kratky, V., 1989b. Rigorous photogrammetric processing of SPOT images at CCM Canada. ISPRS Journal of Photogrammetry and Remote Sensing, Vol. 44, pp. 53 - 71.

/...

DOW - A SYSTEM FOR GENERATION OF DIGITAL ORTHOPHOTOS FROM AERIAL AND SPOT IMAGES

E. P. Baltsavias, A. Gruen, M. Meister
Institute of Geodesy and Photogrammetry
ETH - Hoenggerberg, CH - 8093, Zurich, Switzerland

ABSTRACT

In this paper the concept of a digital orthophoto workstation (DOW) is introduced. The aim and potential applications as well as the software and hardware requirements for such a workstation are outlined. The implementation of this concept at the Institute of Geodesy and Photogrammetry, ETH Zurich, is presented. This development is realised by using Sun general purpose computers without special hardware. The modular structure of the software, a friendly graphics-supported user-interface and appropriate input/output devices are important aspects of the system. Emphasis is placed on flexibility, throughput, accuracy, ease-of-use and low cost.
Examples using SPOT panchromatic and aerial images are given. This data has been used for accuracy studies using a strict SPOT geometrical model, generation of digital orthophotos with overlayed vector information, 3D visualisation (production of synthetic images and image sequences) and radiometric adjustment of mosaics. Aspects concerning speed of production and accuracy of the orthophotos will also be addressed.
The importance of digital orthophotography for updating or creating of GIS databases and the advantages of integration of such raster data in GIS will be demonstrated by an example of integration into ARC/INFO.

INTRODUCTION

Orthophotos and orthophotomaps are becoming increasingly popular products. They are easy to produce and they constitute an inexpensive substitute and addition to topographic maps, especially when the latter are not easy to produce or update. Orthophotomaps include a wealth in pictorial information and essential vectorial information in implicit or explicit form as well. The production of orthophotos has been boosted by the recent advancement of digital techniques. They offer an enormous flexibility and a high throughput at low cost, without the image quality degradation of the analogue techniques (losses of accuracy and resolution, difficult mosaicking, especially for colour images). Although digital orthophotos can be produced faster and cheaper than analogue orthophotos, their main advantage is that they lead to new possibilities and applications. The most important of them is the integration of digital orthophotos in GIS. The orthophoto can be used as one data plane in GIS. Different perspective views, visualisation processes and simulations can be easily produced and merged with other attribute, vector and raster data, thus becoming a valuable tool for planning and environmental monitoring. Furthermore, digital orthophotos pave the way for automated image analysis and digital mapping.
Today there exist more than thirty systems for digital orthophoto generation, many of them commercially available. A brief compilation of these systems is given in *Baltsavias et al., 1991*. Many systems make use of special hardware. Thus, their cost is inflated, the hardware is often not programmable in a high level languague, and the available software can not be easily, if at all, modified or extended. Other systems have not sufficient processing power, memory and disk capacity. The software and hardware modules are often not complete. These are some basic restrictions which led us to the development of a flexible, powerful and expandable Digital Orthophoto Workstation (DOW).

/...

CONCEPT OF A DIGITAL ORTHOPHOTO WORKSTATION

Our DOW concept is based on the following principles:

- *commercial hardware and software standards*
  - UNIX operating system
  - Programming in C and C++
  - Access to third party boards (e.g. VMEbus, SBus)
  - XWindows, PHIGS
  - NFS
- *powerful, flexible, general purpose computers without special hardware*
  - workstation based distributed computing
  - networking and sharing of the resources
  - easy upgrading and extension
  - wide platform of additional third party software and hardware
  - support of I/O devices especially for image acquisition and hard- and softcopy output ; availability of device drivers
  - programmability in a transportable, high level languague
  - powerful programming tools
  - multi-tasking and multi-user capabilities
  - fast and high resolution display system
  - powerful window system
  - high processing speed
  - sufficient and upgradable main memory and disk capacity
  - fast I/O and bus transfer rates
  - reasonable price
- *modular and flexible software development*
  - easy modification and expansion of existing software
  - common data formats
  - user-friendly graphics based interface
  - hybrid system, i.e. support of manual, semi-automatic and automatic processing

Based on the above principles we have decided to use as the system platform Sun workstations. The only additional hardware are boards for image acquisition. The functions of a DOW in a full configuration may be described by the following modules:

1) *Input.* Image acquisition (scanning, digitisation) with CCD frame cameras or scanners. Geometric and radiometric calibration of CCD sensors. Import from data bases.
2) *Image handling and display.* Pan, scroll, zoom, geometric transformations. Mono and stereo display of images.
3) *Image processing.* Noise reduction, edge- and contrast enhancement, data reduction and preselection, algebraic and logical operations, thresholding and binary operations.
4) *Image analysis and mensuration.* Manual measurement of pixel coordinates and grey values, 2D and 3D feature determination by different matching algorithms (semi-automatic or automatic), feature extraction, line following, various segmentation procedures, etc.
5) *Orientation, calibration and point positioning.* Software for sensors having a perspective or linear array geometry (model orientation, resection, intersection, monoplotting).
6) *DTM generation.* Interpolation algorithms, derivation of regular grids, contour lines, profiles, etc.
7) *DTM editing.* Verification, blunder detection, clipping, etc.
8) *Orthophoto generation.* Differential rectification (simultaneous and sequential solutions). Orthophotos of images with perspective or linear array (SPOT etc.) geometry.
9) *Orthophoto editing.* Mosaicking, aesthetic corrections, editing of individual pixels and image regions.
10) *Quality control.* Manual check and editing of orthophotos and hybrid products in

/...

mono and/or stereo display mode.

11) *Interactive vector graphics*. Generation and overlaying of symbols, annotation, contours, map grids and legend, polygon and line overlaying, colour assignment, polygon filling.

12) *Raster to vector and vector to raster conversions*.

13) *Visualisation*. 3D wireframe models, shading, integration of raster and vector (graphics overlay, maps) information, draping of orthophotos, other images and digitised maps over 3D wireframe models (texture mapping), colour editing, combination of multichannel images, animation.

14) *Output*. Soft- and hardcopies. Plotting routines for graphics. High quality film output. Export to data bases.

15) *Graphics and window based user-interface*.

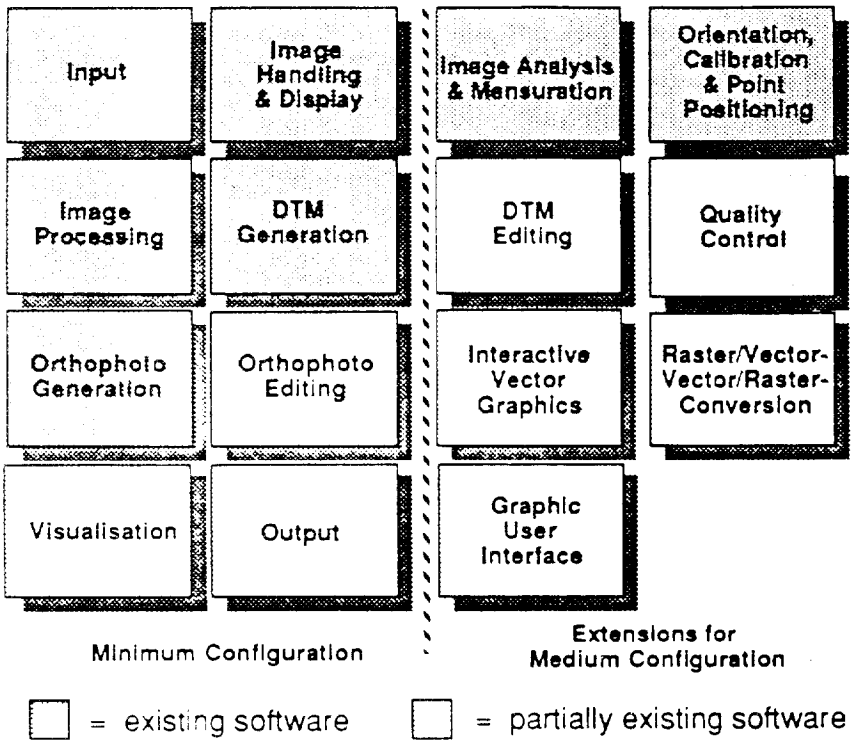

Figure 1. DOW functions of a minimum and medium configuration

Depending on the available resources and requirements a DOW with a minimum, medium or full configuration can be set up. A minimum configuration may require modules 1), 2), 3), 6), 8), 9), 13), 14). A medium configuration would additionally require modules 4), 5), 7), 10), 11), 12), 15) and probably an interface to GIS/LIS data bases (see Figure 1). A fully configured system would include various high quality I/O devices, complete image processing and remote sensing packages, and would be closely linked to a GIS.

REALISATION OF A DIGITAL ORTHOPHOTO WORKSTATION

A digital orthophoto workstation has been realised at the Institute of Geodesy and Photogrammetry, ETH Zurich, along the concept previously outlined. The DOW is integrated in the more general concept of a Digital Photogrammetric Station (DIPS) (*Gruen and Beyer, 1991*). Thus, the DOW shares the hardware and software of the DIPS and forms a subset of the latter. DIPS is based on Sun servers and workstations which are connected via Ethernet and share the resources using NFS. The Sun network is linked to VAX, IBM PC and Apple computers for data exchange. Two analytical plotters equipped with CCD cameras and an external Optronics 5040 Scanner/Laser Plotter can be used for

/...

scanning of films and hardcopies, the latter being also used as an output device. Information on the characteristics of the DIPS and some of its component workstations are given in *Baltsavias et al., 1991*.
For a comfortable DOW a workstation with the following characteristics is necessary: sufficient main memory, high computing performance, high bus bandwidth for transfer of data between memory, frame buffer and disk, sufficient disk capacity with high data transfer rate, powerful graphics accelerator and optionally a 32-bit resolution display. With the current state-of-the-art and the expected developments the bottleneck seems to be the bus bandwidth. Among the Sun workstations, a Sparcstation 2 (and even more the expected new Sparcstation 3) conforms best to these requirements and at a modest price (the list price of a base system is $25,000). A standard Sparcstation 2 comes with an 8-bit display, however true colour and multiple overlays are supported using the 3D graphic GS and GT options.
The modules of the currently existing software, with the exception of minor new developments, are described in detail in *Baltsavias et al., 1991*. The functions of DOW for which software exists are shown in Figure 1. Almost all the software (with the exception of the HIPS image processing package and TOUCHUP, a public domain raster editor) has been developed within our group. Most parts are written in C with some individual programs being in Fortran-77. The programs provide for a user-friendly interface with windows, pull-down menues, sliders, interactive settings etc. based on the SunView window system. All in-house developed software conforms to the same image format standards.

EXAMPLES

In the following, we will concentrate on the processing of SPOT images, but also give an example of aerial photo processing. The geometric processing of SPOT images is based on the model of *Kratky (1989a, 1989b)* and related software developed by him. He uses a strict mathematical model for processing of single or stereo images of Level 1A. The model permits either a linear or a quadratic variation of the rotation angles. Practical tests have shown that the two models give very similar results. Kratky provides fast polynomial mapping functions, which are computed after an initial adjustment with the strict model, to transform from image to image, image to object and object to image space. These transformations, whose parameters are computed by least squares adjustment, are much faster than a strict transformation and their accuracy difference to the latter is less than 1 m in object or 1 μm in image space. For orthophoto generation the polynomial transformation from object to image space is needed. Two sets of polynomial parameters are available: the basic model with 14 parameters and the extended one with 16 parameters. Kratky also provides a module that compares the coordinates of the control and check points from the strict adjustment to those obtained by the polynomial transformation, thus permitting an accuracy evaluation of the latter.

Model	Number of control points	Number of check points	RMS con (m) X	RMS con (m) Y	RMS che (1) (m) X	RMS che (1) (m) Y	RMS che (2) (m) X	RMS che (2) (m) Y
L	9	17 + 4	3.7	4.4	4.2	6.6	12.8	15.4
Q	9	17 + 4	3.5	4.0	4.4	6.6	12.4	13.5

L ... linear model
Q ... quadratic model
RMS con ... Root Mean Square Error for control points
RMS che (1), che (2) ... Root Mean Square Error for well- and poorly-defined check points

Table 1. Accuracy test for a SPOT single image (scene 53-255, Central Switzerland)

An accuracy test was performed for the image from which the orthophoto was to be produced. Its results are given in Table 1. All measurements were performed by students. The points were manually measured in the images and in a 1:25,000 scale

/...

topographic map. They were primarily road crossings, although some less well-defined points like corners of forest boundaries were also included. The linear and the quadratic models give similar results. The results are listed for two groups of well- and poorly-defined points with 17 and 4 check points respectively. The accuracy difference between the two groups is obvious, confirming the strong dependence of achieved accuracy on the quality of point definition

Figure 2. Shaded relief of the DTM used for the SPOT orthophoto production.
DTM data and image: © Bundesamt fuer Landestopographie, Bern, Switzerland

Figure 3. Digital orthophoto with overlayed contours and map grid tick marks
DTM data: © Bundesamt fuer Landestopographie, Bern, Switzerland

The orthophoto, covering a 17.5 by 12 km^2 portion of the SPOT image, was produced

/...

using i) an extended polynomial transformation based on the quadratic model (version 1) and ii) a basic polynomial transformation based on the linear model (version 2). The a posteriori standard deviation of unit weight from the adjustment to compute the transformation parameters was in x and y: 0.1 µm, 0.0 µm (version 1) and 0.3 µm, 0.1 µm (version 2). A comparison of the coordinates as computed by the strict model and the polynomial transformations showed a maximum difference of 1 m in object and 1 µm in image space, thus confirming Kratky's values. The DTM data, derived from digitised topographic map contours, had a 25 m grid spacing and was not free of errors (see the terrace effects in the representation of DTM as an image, using shading, in Figure 2). The orthophotos had a pixel spacing of 8.33 m. A part of the orthophoto (version 1) with overlayed contours of 150 m interval and tick marks at 2 km intervals is shown in Figure 3. The orthophoto was draped over the DTM and images of the texture-mapped terrain were produced, as the one shown in Figure 4 (at the centre the mountain Pilatus, west of the city of Lucerne)

Figure 4. Texture-mapped terrain in parallel projection (part of an animation sequence)

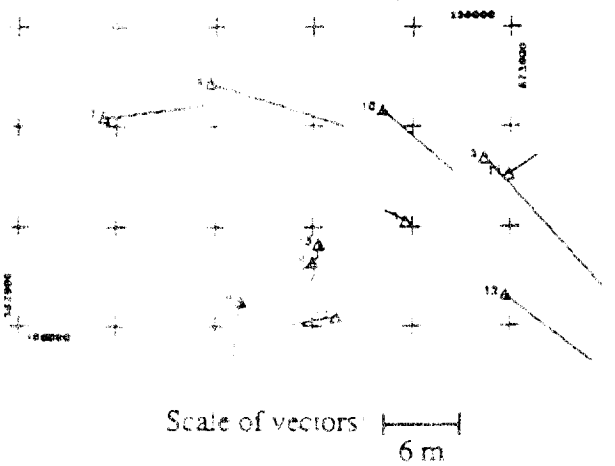

Figure 5. Planimetric differences between map and orthophoto

The planimetric accuracy of the two orthophotos was tested by using 11 check points measured in one orthophoto manually, in the second one by least squares matching and in a 1:25,000 scale map. A plot of the residuals for version 1 (those of version 2 were very similar) is shown in Figure 5. The achieved planimetric accuracy (RMS) was 6 m in Easting and 5 m in Northing, thus fulfilling the requirements for mapping at scales 1:25,000 and smaller. A comparison of these results to the check point RMS of the strict model adjustment shows that there was no loss of accuracy by using the appproximate polynomial transformation solution.

a)

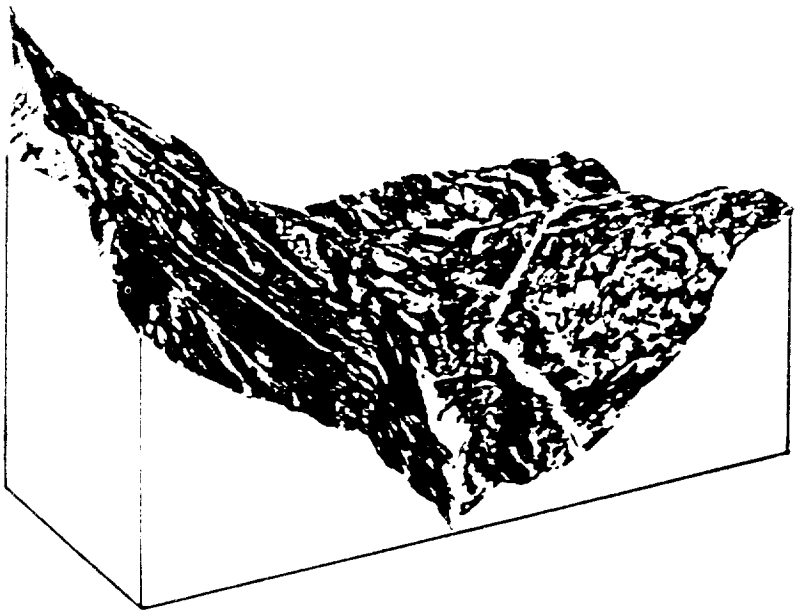

b)

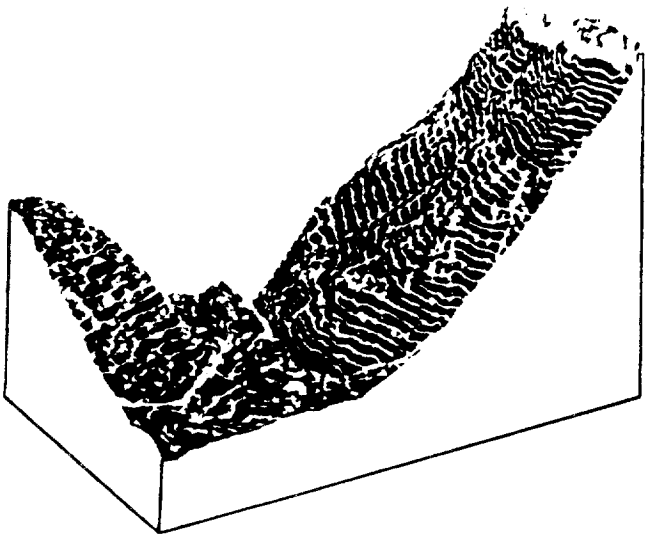

Figure 6. a) Texture-mapped terrain in parallel projection,
b) like a) but another view with overlayed contours

/...

The second example refers to aerial images of the Simplon region in southern Switzerland. The original DTM had a 25 m grid spacing. The image data was digitised with a 50 µm square pixel size (corresponding to 0.8 m ground resolution) on an Optronics 5040 from 1:16,000 scale images. Figure 6a) shows the texture-mapped terrain in parallel projection. In Figure 6b) another view is shown overlayed with contours having an interval of 20 m.

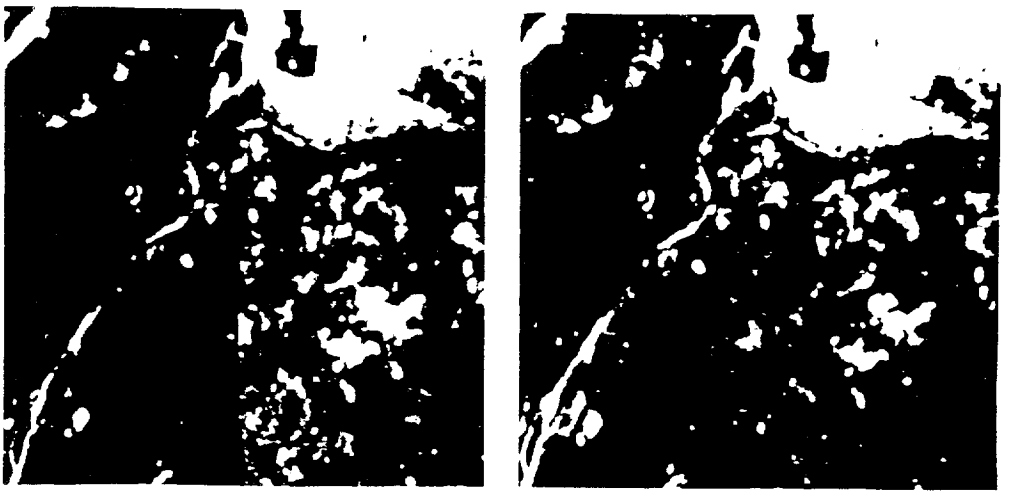

a) b)

Figure 7. Mosaic of 2 by 2 images: a) original, b) after radiometric adjustment

Figure 7 shows the radiometric adjustment of four overlapping image frames for mosaicking. The images were acquired by scanning aerial images with CCD cameras on a Prime-Wild S9 analytical plotter. Due to the low dynamic range of the CCDs, the gain and offset had to be adjusted for each image separately in order to avoid saturation, leading thus to considerable radiometric differences.

GIS INTEGRATION

First results of the integration of the orthophoto software into ARC/INFO Rev. 6.0 are presented in *Wang et al., 1991*. The improvements of Rev. 6.0 made the integration of orthophotos very easy. For example, the Image Integrator now provides more choices for integration of raster and vector data within ARC/INFO. Orthophotos can be easily integrated (since they are already spatially referenced to map coordinates) and managed in an image catalogue. Attribute selection operations can be used to identify a subset of images from the catalogue that are to be displayed as a backdrop to a graphic session. Since the orthophoto is geometrically corrected, map update procedures (digitising, editing etc.) with ARCEDIT can be performed on-screen without the need for registration and rubber sheeting of vector data. The production of cartographic quality orthophotomaps can be accomplished with ARCPLOT. A combination with the TIN surface modelling program and GRID, a raster GIS modelling and geoprocessing package, permits a better analysis and visualisation. The tools within ARC/INFO are functionally integrated at all times. One result of this is the ability to operate on a whole network of multi-media information types with different data structures. For example, a spatial query can be done through a display of a coverage (a digital analogon of a single map sheet or layer) overlayed on an orthophoto. The query can extract data from a tabular DBMS such as ORACLE to list attributes. One of the attributes could be a key to a stored image, CAD drawing or document image (all these can be indexed to geographic features on a map using the DBMS). This image or drawing is then automatically extracted and displayed in another window. This fully integrated concept with access to multi-media data is fundamental for future GIS environments.

/...

PROCESSING SPEED

A comparison of the computing performance for various operations on two Sun Sparcstations is given in Table 2. All operations include I/O of data, whereby the data had to be transferred from disk through Ethernet. For the image to image registration, an affine transformation and a bilinear interpolation have been used. A comparison between different types of grey level interpolation is shown in Table 3. Finally, the computational advantages of a densification of the anchor points over a transformation of all points from object to pixel space becomes obvious from Table 4.

	Sparc. 1 (1)	Sparc. 2 (2)	Relation (1) / (2)
Wallis filter (contrast enhancement)	43.7	20.5	2.1
Image to image registration	39.6	16.9	2.3
Aerial orthophoto generation (10fold AP densification)			
bilinear interpolation	53.0	22.6	2.3
bicubic interpolation	148.2	64.4	2.3
SPOT orthophoto generation (10fold AP densification)			
extended model, bilinear interpolation	-	25.8	
SPOT polynomial transformation from object to image			
extended model, no AP densification	-	10.5	
Radiometric correction of mosaic	16.4	7.7	2.1
3D parallel view of wireframe model	302.0	134.0	2.3
3D parallel view of orthophoto	164.0	69.8	2.3

Units = sec/1 Mbyte of data (e.g. frames of 1000 x 1000 pixels at 8 bit)
AP ... anchor point

Table 2. Computing performance for various operations at different Sun Sparcstations

	Nearest neighbour (1)	Bilinear (2)	Bicubic (3) *
sec/Mb	11.2	17.2	64.1
Ratio: (1) to (3) / (1)	1.0	1.5	5.7

† Includes checking of all pixels whether they are inside the limits of the digital image
* Includes stretching of grey values to range [0 , 255]

Table 3. Time comparison for different types of grey level interpolation † (Sparcstation 2)

	AP 20 (1)	AP 10 (2)	AP 5 (3)	AP 1 (4)
sec/Mb	3.0	3.4	4.5	9.5
Ratio: (1) to (4) / (1)	1.0	1.1	1.5	3.2

† Includes object to image space transformation and affine transformation from image to pixel space of all anchor points (for SPOT, direct transformation from object to pixel space), densification of anchor point pixel coordinates by bilinear interpolation (with checking of all pixels whether they are inside the digital image and whether the heights are valid)
AP n -> x , y densification factor of anchor points is n
AP 1 -> all object points are strictly transformed into the pixel space

Table 4. Time comparison for different anchor point densifications † (Sparcstation 2)

/...

CONCLUSIONS

It has been shown that a new generation computer workstation, without additional hardware for speed-up of computing times, may well serve as a dedicated digital orthophoto workstation. The advantages of this concept are obvious: ease of use, flexibility in software maintenance, extension and new development, openness to third party products, compatibility to external groups, full growth potential in parallel with the computer advancement, and low costs. These are reasons for us to continue with the further development of our system towards a fully operational and completely configured unit.

If restrictions in display depth are not a problem, then an inexpensive low end workstation (here: a Sun Sparcstation 2) shows a remarkable computational performance and offers an excellent solution to the DOW system problem. In order to give an indication of the computational performance of a Sparcstation 2 based system, we can extrapolate the computing time of Table 2 for orthophoto generation. The computation of an orthophoto, derived from a full aerial photo (230 x 230 mm^2) with 50 µm pixel size, would take about 8 minutes. This is much faster than analogue orthophoto production and is tolerable for off-line production for all practical purposes. A 36 Mbyte orthophoto of a full SPOT panchromatic scene can be produced in about 15 min.

Of course, computational speed must not be the only performance criterium. Nevertheless, it is still a crucial factor and serves as an argument for system manufacturers to add expensive hardware. But, considering the advancements in computing power of the latest RISC CPUs, which can be expected to be integrated in workstations over the next two years, we anticipate that computing time, as offered by low end workstations, will no longer be an issue. This clearly paves the way for inexpensive DOWs and similar systems performing other digital photogrammetric functions.

Furthermore, digital orthophotos can be very accurate. A test using SPOT images showed that even under non-ideal conditions the planimetric accuracy was approximately 5m and thus can fulfil the requirements for mapping at scales 1:25,000 and smaller. The integration of digital orthophotos in GIS and the combination with vector and other raster data is straightforward and opens new, exciting possibilities for a very broad spectrum of users that can now perform their tasks in-house, on time and with low cost.

ACKNOWLEDGEMENTS

The authors would like to express their gratitude to the Bundesamt fuer Landestopographie, Bern, Switzerland for providing the DTM data for the SPOT image and the shaded relief representation of the DTM, B. Ruedin for software support and L. Hurni (Institute of Cartography, ETH Zurich) for scanning image data on the Optronics 5040.

REFERENCES

Baltsavias E. P., Gruen A., Meister M., 1991: A Digital Orthophoto Workstation. Proceedings of ASPRS Annual Convention, March 25 - 29, Baltimore, Vol. 5, pp. 150 - 160.

Gruen A., Beyer H. A., 1991: DIPS II - Turning a Standard Computer Workstation into a Digital Photogrammetric Workstation. ZPF - Zeitschrift fuer Photogrammetrie und Fernerkundung, No. 1, pp. 2 - 10.

Kratky V., 1989a: Rigorous Photogrammetric Processing of SPOT Images at CCM Canada. ISPRS Journal of Photogrammetry and Remote Sensing, Vol. 44, pp. 53 - 71.

Kratky V., 1989b: On-Line Aspects of Stereophotogrammetric Processing of SPOT Images. Photogrammetric Engineering and Remote Sensing, Vol. 55, No. 3, pp. 311 - 316.

Wang S., Shanks R., Katibah E. F., 1991: Integrating Low-Cost Digital Orthophotography with ARC/INFO Rev. 6.0. Presented paper at the 11th Annual ESRI User Conference, May 20-24, Palm Springs, California.

/...

INTEGRATIONS OF SEA SURFACE TEMPERATURE DATA SETS USING MOS-1 SATELLITE DATA FOR VALIDATION AND MONITORING

S. Takeuchi

Remote Sensing Technology Center

Tokyo, Japan

/...

INTEGRATION OF SEA SURFACE TEMPERATURE DATA SETS USING MOS-1 SATELLITE DATA - FOR VALIDATION AND MONITORING -

Shoji Takeuchi, Yasunori Nakayama and Tsuyoshi Tomita
Remote Sensing Technology Center of Japan
7-15-17, Roppongi, Minato-ku, Tokyo 106, Japan

ABSTRACT:

Sea Surface Temperature(SST) data sets have now occupied one of the important elements of global and regional environmental data sets. A systematic integration of SST data set using MOS-1 data has been conducted as one of the activities for ISY in Japan. According to the importance of the physical background for SST retrieval as well as the practical utilization of the data set, two kinds of data sets were developed for validation of SST retrieval by satellite data and for monitoring of the change of SST distribution around Japan Islands.

The data set for the validation was developed by creating sub-images in which the image centers always correspond to the locations of the four ocean data buoys fixed at the oceanic areas around Japan by Japan Meteorological Agency. According to continuous measurement of SST by the buoys, the precise comparison of satellite data with sea truth of SST are expected to be achieved. More than one hundred data taken in different dates were accumulated during three years and they were evaluated in order to derive the optimal equation for SST retrieval by VTIR data.

Another type of SST data set was developed for regional monitoring of SST distribution around Japan Islands. The data set was created by superimposing multi-date VTIR data in order to eliminate cloud cover, and was generated monthly for monitoring the change of SST distribution, especially the yearly change of Kuroshio Current from 1989 to 1992. The result of the validation described above was applied to the regional SST data set, which enabled to achieve the monitoring of the precise regional SST by MOS-1 satellite.

KEY WORDS:
SST Data Set, SST Retrieval by Satellite Data, SST Validation, SST Monitoring, Cloud Elimination, Cloud Discrimination.

1. INTRODUCTION

As one of the activities for International Space Year(ISY) in Japan, a project for the systematic studies on Sea Surface Temperature(SST) retrieval using MOS-1 satellite data has been carried out under the supervision by SST Working Group and the sponsorship by National Space Development Agency of Japan(NASDA), the leading agency for SST as one of the earth science project of ISY.

SST has now become one of the major applications of satellite data in oceanography and also the SST data set now occupies one of the important element of global or regional environmental data sets. For the SST data set the physical process for SST retrieval is quite important as well as its practical use because SST may be used for a scientific purpose as one of the basic physical parameter for earth environment. Especially the validation for the accuracy of SST retrieval is indispensable to secure the reliability of the data set.

A typical study for this kind of validation has been conducted for NOAA/AVHRR long time by NOAA/NESDIS (Ref.1) and MCSST(Multi Channel SST) algorithm is now used widely for SST retrieval by AVHRR data according to the result of the validation. For oceanic areas around Japan, several studies for the validation using NOAA/AVHRR (Ref.2 and 3) have been conducted. By considering the importance and the universality of this kind of validation for the SST data set, an integrated data set by MOS-1 data combined with sea truth of SST was developed for the purpose to achieve the same kind of validation for SST retrieval from MOS-1 data.

Another type of data set using VTIR was developed in order to achieve the regional monitoring of the change of SST conditions around Japan Islands. This data set was created by superimposing of multi-date VTIR data during about one week. The superimposition of multi-date data was effective for the elimination of cloud cover and for the observation of SST conditions in whole oceanic areas around Japan. The result of the validation described above was used by applying the optimal split-window equation to this regional VTIR data set, which gave the evidence to obtain precise SST distributions in cloud-free areas from this regional data set.

Presented for the 17th ISPRS Congress UN/ISPRS Workshop on Remote Sensing Data Analysis Methods and Applications, Washington,D.C.,U.S.A. 6-7 August 1992.

/...

2. MOS-1 MULTI-SENSOR DATA SET FOR VALIDATION

2.1 Configuration of the Data Set

The major sensor of MOS-1 for SST observation is VTIR(Visible and Thermal Infrared Radiometer). However, another type of sensors (MSR, Microwave Scanning Radiometer and MESSR, Multispectral Electronic Self Scanning Radiometer) are also on board, and there may be some possibilities to improve the accuracy of SST estimation by combining of these sensors with VTIR. Therefore, an integrated data set for the validation was developed by the combination of these multi-sensors and also combined with sea truth data of SST by several ocean data buoys located around Japan Islands. According to a preliminary evaluation of this data set, the possibility of improvement of the accuracy by the combination of VTIR with MSR was expected to be obtained as well as the limit of the accuracy of SST estimation and the optimal equation for SST estimation by VTIR.

The general configuration of the data set is shown in **Fig.1**. The data set was developed by creating sub-images in which the image centers always correspond to the locations of the four ocean data buoys fixed at the different oceanic areas around Japan (**Fig.2**). The MESSR data, which can be used for the study of the discrimination of cloud cover by VTIR, was created in the manner that they were overlaid onto a part of VTIR data because of their narrow coverage. NOAA/AVHRR data set was also created in the same configuration as VTIR in order to be used for the comparison of the accuracy of SST estimation by AVHRR with that by VTIR.

According to the continuous observation of SST by the ocean data buoys, the precise comparisons are expected to be achieved between the satellite data and the sea truth of SST by the buoys. Although the oceanic areas for the comparison are limited to the areas where the buoys are fixed, the sufficient variation of the conditions for SST observation can be obtained by accumulating many satellite data taken in different dates. The data set was accumulated during three years (from 1988 to 1990), and total more than one hundred cloud-free VTIR scenes were obtained, while about one third of VTIR scenes were obtained for MSR scenes because MSR coverage was limited to near-nadir of VTIR coverage.

The summary of the characteristics of the sensors used for the data set is shown in **Table.1** and the data processing flow for generation of the data set is shown in **Fig.3**.

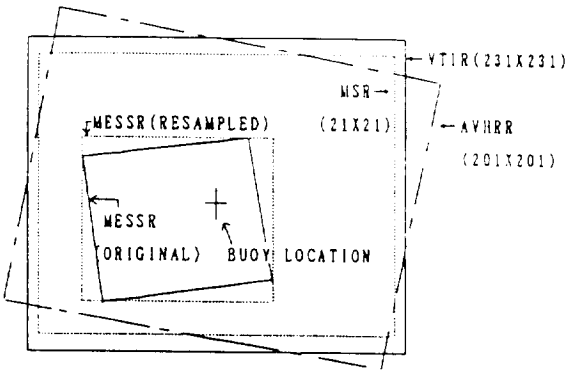

Fig. 1 General aspect of multi-sensor data set for validation of SST retrieval.

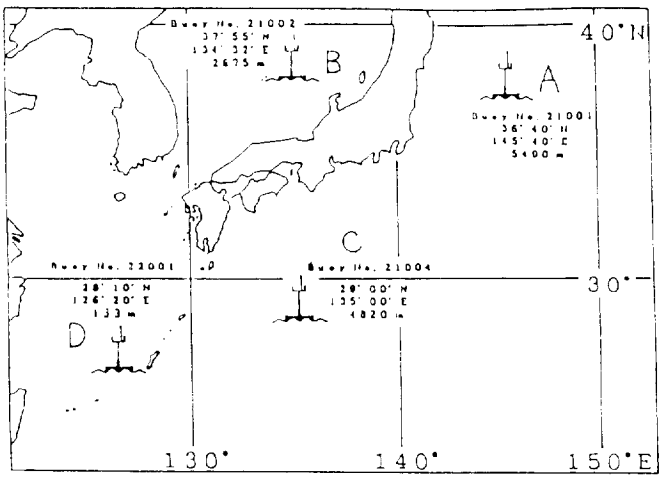

Fig. 2 Location of the four ocean data buoys by Japan Meteorological Agency.

Table. 1 Wavelength characteristics and ground resolutions of the sensors used for the data set creation.

Sensors	MOS-1/VTIR	MOS-1/MSR	MOS-1/MESSR	NOAA-11/AVHRR
Bands	Wavelength	Wavelength	Wavelength	Wavelength
Band-1	0.5 - 0.7 μm	23.8±0.2 GHz(10msec*)	0.51 - 0.59 μm	0.58 - 0.68 μm
Band-2	6.0 - 7.0 μm	23.8±0.2 GHz(47msec*)	0.61 - 0.69 μm	0.725- 1.10 μm
Band-3	10.5 - 11.5 μm	31.4±0.25GHz(10msec*)	0.72 - 0.80 μm	3.55 - 3.93 μm
Band-4	11.5 - 12.5 μm	31.4±0.25GHz(47msec*)	0.80 - 1.10 μm	10.30 - 11.30 μm
Band-5	Sat. Zenith A. **			11.50 - 12.50 μm
Band-6				Sat. Zenith A. **
Ground Resolutions	Band-1 0.9Km Band-2～4 2.7Km	Band-1 & 2 32Km Band-3 & 4 23Km	Band-1～4 50m	Band-1～5 1.1Km

* Integration Time.

** Satellite zenith angle data are added after the data set creation.

/...

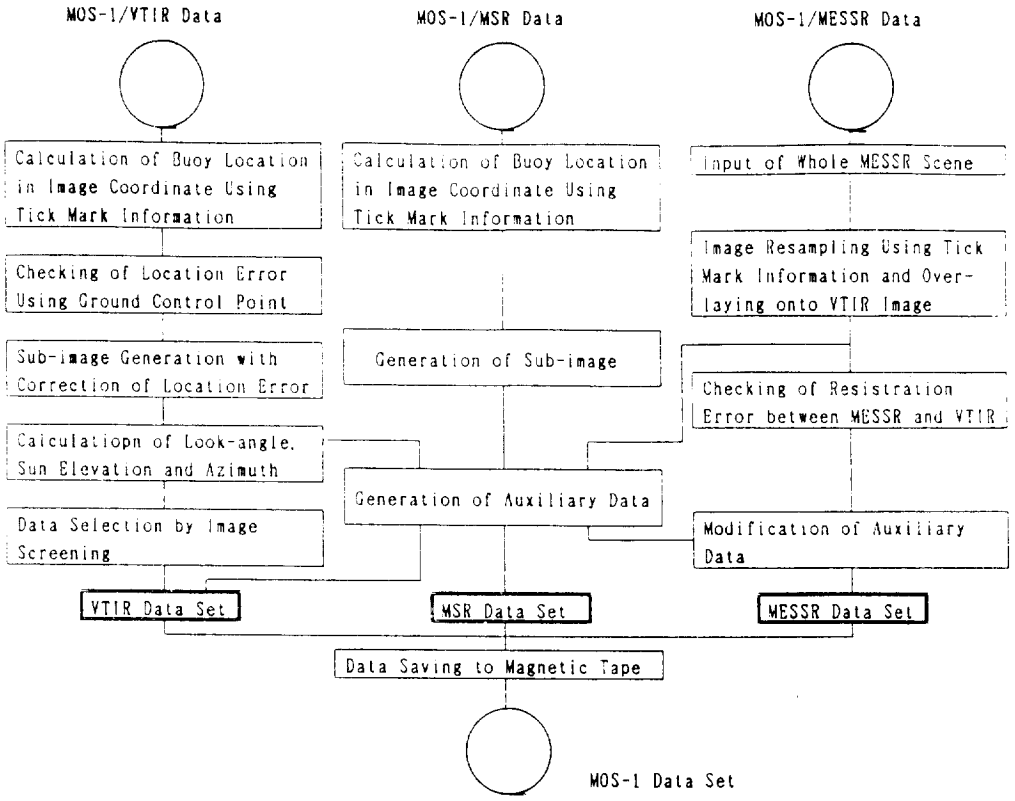

Fig. 3 Data proccesing flow for generation of MOS-1 multi sensor data set for validation.

2.2 Preliminary Validation by the Data Set

The general form of the equations for SST estimation by satellite data is represented by the linear combination of multiple thermal-infrared channels. A typical example of this kind of equation is MCSST for AVHRR (for day time) represented as follows;

$$SST = a1T11 + a2(T11-T12) + a3(T11-T12)(\sec\theta - 1) + a4 \quad (2.1)$$

where a1,a2,a3 and a4 are coefficients, T11 and T12 are brightness temperature for 11-μm and 12-μm channels of AVHRR respectively, and θ is the satellite zenith angle.

The coefficients in Eq.(2.1) can be derived directly by the regressive analysis using the brightness temperature of the satellite data and the sea truth of SST when the satellite passes. A sufficient data set for covering the wide variation of SST observation conditions (date, season, temperature-range, etc.) is necessary in order to get the universal equation to be applied widely.

The regressive analysis using the following equation was applied to MOS-1/VTIR data set, which is basically the same as Eq.(2.1) except that the 6-μm channel of VTIR was added as one of the variables;

$$SST = a1T3 + a2(T3-T4) + a3(T3-T4)(\sec\theta - 1) + a4T2 + a5 \quad (2.2)$$

where T3, T4 and T2 are the brightness temperature(°C) of VTIR channel-3(11-μm), channel-4(12-μm) and channel-2(6-μm) respectively.

The same regressive analysis using the combined data set of VTIR with MSR was also tested with the following equations;

$$SST = a1T3 + a2(T3-T4) + a3MTi + a4 \quad (2.3)$$

where MTi(i=1,4) means the brightness temperature of MSR channel-1 to channel-4.

The result of the regessive analysis with Eq.(2.2) is shown in **Table.2.** This result suggests that there is no significant contribution of the satellite zenith angle and 6-μm channel for the accuracy of SST estimation, while the difference of the brightness tempetarure between 11-μm and 12-μm brings the primary improvement for SST estimation(see also **Fig.4**). Also, the equation obtained by the regression is considered to be the optimal equation for SST retreival using VTIR because the equations obtained by the conventional studies give relatively lower accuracy for the same data set (see the lower part of Table.2).

/...

Table. 2 Results of regressive analysis for MOS-1/VTIR data set.

Equations for SST Estimation	Error(°C)		Coefficients*4				
	SD*3	BIAS*3	a_1	a_2	a_3	a_4	a_5
a. Regression by T_3 only	1.626	0.0	1.2682	—	—	—	-1.8770
b. Regression by T_3&(T_3-T_4)	1.088	0.0	1.3602	2.1882	—	—	-1.7136
c. Regression by T_3&(T_3-T_4)&secθ *2	1.084	0.0	1.0652	2.0483	0.9252	—	-1.6991
d. Regression by T_3&(T_3-T_4)&T_2	1.091	0.0	1.0692	2.1362	—	-0.0209	-2.3304
e. Equation by Takeuchi&Kanou[4]	1.363	-0.37	1.0	1.395	—	—	0.363
f. Equation by Takayama&Maeda[5]	1.125	-0.003	1.0	2.815	—	—	-1.657
g. Equation by Matsumoto&Tsuchiya[6]	1.219	-0.12	1.045	1.441	—	—	-0.297

*1 Total number of data used is 101 *2 Actual variable form is (T_3-T_4)(secθ-1).
*3 SD and BIAS means standard deviation and bias of error respectively.
*4 a_1～a_5 correspond the same coefficients in Eq.(2.2) respectively.

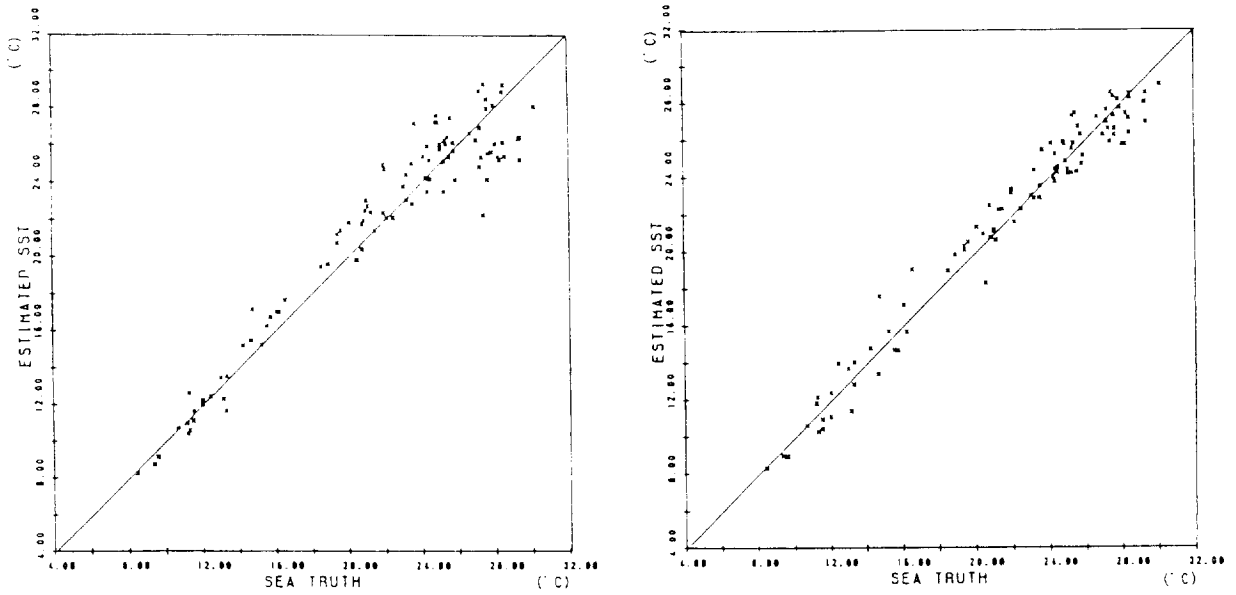

Case-a in Table. 2
(Regression using T_3 only. SD*=1.626)

Case-b in Table. 2
(Regression using T_3&T_3-T_4. SD*=1.088)

Fig. 4 Examples of scattering diagram between sea truth and estimated SST.
* SD means standard deviation of error.

Table.3 shows the result of the regression using Eq.(2.3) and this result suggests that the combination of MSR with VTIR can bring some improvement of accuracy (about 0.3 °C) compared with that by VTIR only. There is some difficulty to apply the combination of MSR with VTIR for practical use of MOS-1 data, because the MSR coverage is limited to only 300 Km width by one satellite pass. However, the result of Table.3 is very important to suggest the effectiveness of multi-sensor utilization and also the future development of the sensor system for SST observation.

Actualy the result of the regression may be much affected by the difference of the data set. Therefore, the VTIR data set was divided into two sets, phase-1 and phase-2, according to the order of data set accumulation, and the cross evaluation for the accuracy using this pair data set was tested. The result is shown in **Table.4** and this result suggests that there is no significant difference among the accuracies by the different combinations of the equation and data set. Therefore the equation obtained from the phase-1 or phase-2 data set is also acceptable for practical use although the equation by the total data set(phase-1+phase-2) is preferable to be used. This result also seems to indicate the reasonbleness of the data set for the purpose of the validation.

/...

Table. 3 Results of regressive analysis for VTIR/MSR combined data set.

Equations for SST Estimation	Error(°C) SD*2	Coefficients *3			
		a_1	a_2	a_3	a_4
a. Regression by T_3&(T_3-T_4) only	1.192	1.1760	1.5645	——	-3.0030
b. Regression by T_3&(T_3-T_4) & MT_1	0.917	0.9587	1.0498	0.0925	10.8499
c. Regression by T_3&(T_3-T_4) & MT_2	0.915	0.9597	1.0748	0.0913	10.6728
d. Regression by T_3&(T_3-T_4) & MT_3	0.897	1.0092	1.2254	0.1814	22.2708
e. Regression by T_3&(T_3-T_4) & MT_4	0.901	1.0094	1.2343	0.1817	22.2797

*1 Total number of data used is 30.

*2 SD means standard deviation of error.

*3 a_1～a_4 correspond the same coefficients in Eq.(2.3) respectively.

Table. 4 Results of cross evaluation using two different VTIR data sets.
(The equation used for the evaluation is the same as that for case-b in Table.2.)

Equations Applied for SST Estimation	Data Set Applied for Evaluation(Number of Data)	Error(°C) SD*1	Error(°C) BIAS*1	Coefficients*2 a_1	Coefficients*2 a_2	Coefficients*2 a_5
a. Equation by Phase-1 Data Set	Phase-2 Data Set (59)	1.069	0.072	1.0630	2.0185	-1.4067
b. Equation by Phase-2 Data Set	Phase-1 Data Set (42)	1.111	0.033	1.0336	2.3410	-1.4640
c. Equation by Phase-1 Data Set	Phase-1+Phase-2 (101)	1.096	0.073	1.0630	2.0185	-1.4067
d. Equation by Phase-2 Data Set	Phase-1+Phase-2 (101)	1.093	0.015	1.0336	2.3410	-1.4640
e. Equation by Phase-1+Phase-2	Phase-1+Phase-2 (101)	1.088	0.0	1.0602	2.1882	-1.7136

*1 SD and BIAS means standard deviation and bias of error respectively.

*2 a_1～a_5 correspond the same coefficients in Eq.(2.2) respectively.

3. REGIONAL SST DATA SET BY VTIR DATA

3.1 Method for Data Set Creation

The primary merit for SST observation by a satellite is of course to achieve the monitoring of SST conditions in wide areas, global or regional basis. As MOS-1 does not equip on-board data storage unfortunately, only a regional product for SST is possible to be achieved.

The most significant interference for the regional data set creation is the existence of cloud cover. As far as the thermal infrared region is used for observation, the only solution for this problem is to superimpose multi-date data to eliminate the cloud cover. The superimposition of multi-date data also may bring a demerit to make SST patterns fuzzy, especially in the oceanic areas where the SST patterns are being changed rapidly. Therefore, the duration for data superimposition should be limited to at most several days, which seems to give the reasonable SST patterns and also acceptable cloud coverage rate for monitoring of the regional SST conditions. The elimination of cloud cover can be actually achieved by selecting the highest temperature pixel among the pixel data at the same location from the multi-date data.

The cloud discrimination is also an important process to discriminate the cloud-cover from the cloud-free areas because precise SST values are given only in the cloud-free areas. However, the conventional cloud discrimination technique applied to NOAA/AVHRR data can be hardly applied to VTIR data due to the lack of near-infrared channel and also due to their high level sensor noise. In addition, the cloud discrimination sometimes results mis-discrimination of cloud-free areas where a large spatial SST difference exists by a front that may inform the existence of an important and interesting oceanic phenomenon. Therefore only simple technique in which the cloud is discriminated using the threshold in visible and thermal-infrared channels was applied to the regional VTIR data set. So, actually a human interpretation using the spatial pattern of SST should be used for a practical cloud discrimination.

The total data processing flow for createing the regional SST data set by VTIR is shown in Fig. 5.

/...

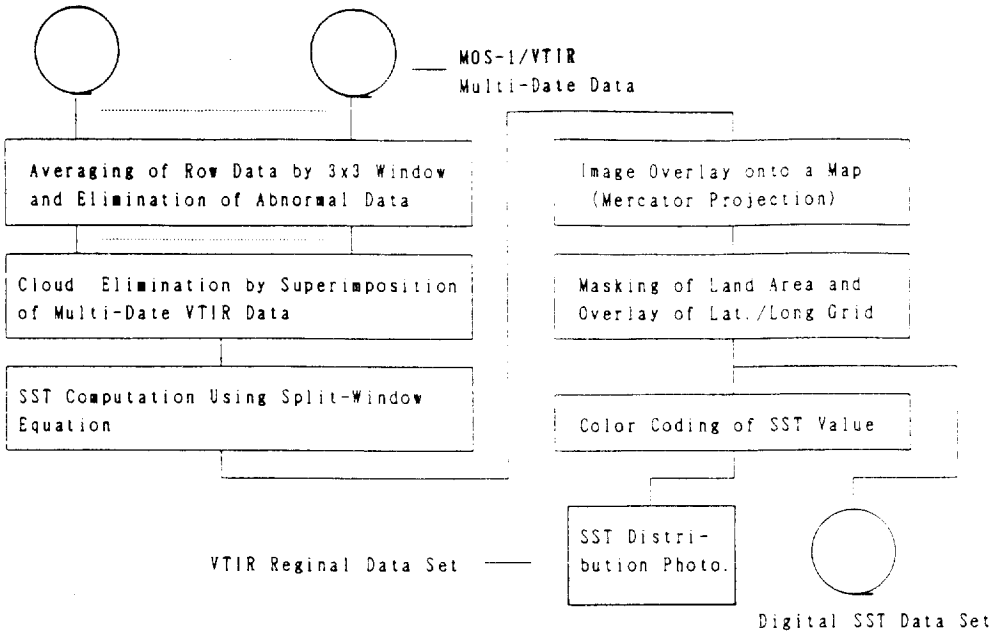

Fig. 5 Data processing flow for VTIR regional SST data set.

3.2 Result of Regional Data Set Integration

The primary aim for integration of the regional SST data set around Japan Island is to monitor the yearly change of Kuroshio Current, one of a big scale of warm current in the world. The change of the Kuroshio brings out a significant influence on marine environment along the coast of the Pacific Ocean and on fishing industries. The cycle of the change has been two or three years and at the beginning of the data set integration (Spring in 1990), the Kuroshio meandered at the coastal region of the Pacific Ocean, that is one of the typical flow pattern of the Kuroshio. The starting time of the data set was June in 1989, when the Kuroshio flew straight. Thus the monitoring of the changing patterns of the variation cycle of the Kuroshio Current can be expected by the continuous integration of the regional data set during about three years (1989 - 1992).

Each data set was created monthly by superimposing multi-date VTIR data during about one week. Both of MOS-1 and MOS-1b satellite were used as VTIR data source to compensate relatively narrow VTIR coverage (about 1,500 Km width) compared with that of AVHRR. For SST computation from the superimposed VTIR data, the equation by the phase-1 validation data set described in Table.4 was actually used because the regional data set creation has been carried out parallel with the integration of the validation data set. The use of multi-date data was very effective to eliminate the significant amount of cloud cover and to monitor the whole flow of the Kuroshio (see **Plate.1**).

4.DISCUSSION

The foregoing procedure seems to be a typical procedure for integrating SST data sets using a certain new satellite sensor. However, many problems are still remained to be solved for the practical utilization of the SST data set.

4.1 Approach for Validation

An alternative approach may be considered to achieve the validation of the accuracy for SST retrieval, for example, the usage of the SST observation data by ships as the sea truth. Actually this approach has some difficulties for achieving the exact synchronization of the sea truth with a satellite pass, because it requires a wide range and a lot of simultaneous observations by ships. The preliminary test using the same approach resulted relatively lower accuracy compared with the result of Table.2 for VTIR, which was considered to be due to the mis-synchronization of the sea truth.

The demerit of the approach of this project is that it requires quite long time to achieve the integration of the sufficient data set to be used for the validation. In the case of MOS-1/VTIR about three years accumulation was necessary because of the relatively low success rate (probably less than 30 %) for obtaining cloud-free VTIR scenes at the exact locations of the ocean data buoys. One of the solution for this problem may be the parallel validations using the different coverages of the different ground stations, which may be expected to increase the success rate for cloud-free satellite data.

/...

4.2 Cloud Discrimination

The problem of cloud cover is considered to the most essential for the practical use of the SST data set. Especially the discrimination of cloud cover and cloud-free is still the difficult process to be achieved. The preliminary test using the MESSR and VTIR data set described in 2.1 was conducted for evaluation of the performance of VTIR channels for cloud discrimination, however, no effective parameters were found except the visible channel of VTIR (see **Table.5**). This result suggests the difficulty for the practical application because the visible channel tends to be much affected by the atmospheric condition and also sun elevation (i.e. sun-glitter).

Also the cloud discrimination brings another problem that too tight condition for cloud-free results the loss of the important and interesting SST patterns because the spatially steep changes of SST patterns are sometimes identified as cloud by a conventional cloud discrimination technique. Therefore, at present, a practical approach is 'not' to apply the tight method of cloud discrimination to the data set to keep the necessary information of SST patterns and to leave the exact cloud discrimination to a human interpretation.

4.3 Monitoring of Ocean Current by SST

The primay aim of the reginal data set described above was the monitoring of the Kuroshio Current. This approach has some limitations for monitoring of an ocean current because SST can only represent the ocean phenomena at the sea surface. Especially in the summer season the sea surface forms a high temperature stable layer due to high air temperature, and the flow pattern by a ocean current can hardly be observed by SST. Acutually, the effective period for monitoring of the flow of the Kuroshio Current is restricted from the end of October to the beginning of June.

Another restriction for monitoring is the weather condition in the winter season (especially in January and February) around Japan Islands, by which the mayor ocean areas of the Kuroshio Current is generally covered by cloud.

These restrictions are inevitable as far as the thermal-infrared information is used for observation. One solution may be the use of the synthetic aperture radar (SAR) image for monitoring. A preliminary study using EERS-1/SAR and NOAA/AVHRR images indicates a possibility for monitoring of the flow of the Kuroshio by SAR image.

4.4 Combination of Multi-Sensors

Some of the problems for the creation of SST data set can be resolved by the combination of multi-sensors. An example was shown in 2.2, which enabled to improve the accuracy limitation of SST retrieval by VTIR using the combination of MSR with VTIR. The utilization of SAR images described in 4.3 also can be one of the effective utilization of multi-sensors.

As to the combination of VTIR with AVHRR, it is rather difficult to find the general merit because almost of the sensor characteristics (wavelength, coverage, and frequency of observation etc.) of VTIR can be replaced by AVHRR. However, this combination can be applied to monitor the ocean phenomena changing very rapidly using the time difference of the satellite pass between MOS-1 and NOAA. An typical example is shown in **Plate.2**, in which the movement in the growth of a large scale of eddy can be monitored by the AVHRR and VTIR time sequential images.

Table. 5 Correlations between VTIR channel parameters and the cloud coverage rate by the MESSR image sumerimposed onto the VTIR image obtained from the regressive analysis using MESSR and VTIR combined data set.

< VTIR channel parameters >

A_1、A_2、A_3、A_4: Average values of Band-1, 2, 3 and 4 with 3x3 window

S_1、S_2、S_3、S_4: Standard deviations of Band-1, 2, 3, and 4 with 3x3 window

	VTIR channel parameters							
Correlation by single regression	A_1	A_2	A_3	A_4	S_1	S_2	S_3	S_4
	0.676	0.184	0.288	0.478	0.656	0.034	0.339	0.206
Correlation by multiple regression	$A_1+A_3+A_4$		$S_1+S_3+S_4$		A_1+S_1	A_3+S_3	A_3+A_4	S_3+S_4
	0.718		0.662		0.709	0.432	0.501	0.374

/...

5. CONCLUSION

As one of the ISY activities in Japan, the SST data sets were integrated with MOS-1 data for the purpose of the validation of SST retrieval and the monitoring of the regional SST around Japan Islands. These data sets are expected to contribute to promote the studies on the retrieval of physical parameters on earth environment from MOS-1 data as well as the practical utilization of MOS-1 data.

Since many problems are remained to be solved for truly practical usage of the data set, further studies should be continued on cloud discrimination and multi-sensor combination, especially the combination of microwave and radar images. Therefore, the integration of the similar kind of data set described in this report will become more important and should be extended in the future.

ACKNOWLEDGMENT

The authors thank to National Space Development Agency of Japan for the sponsorship of this project and to the cooperative members of the SST Working Group as well as the chairman, Dr. Teramoto for their advises and corporations. We also thank to Japan Meteorological Agency for offering the ocean buoy data indispensable for the validation.

REFERENCES

1)McClain et al (1985): Comparative Performance of AVHRR-based Multi-channel Sea Surface Temperature, J. of Geophysical Research, 90, 11587-116901.

2)Sakaida and Kawamura (1991): Estimation of Sea Surface Temperatures around Japan Using the Advanced Very High Resolution Radiometer on NOAA-11 (Impress to J. of the Oceanographical Society of Japan).

3)Yokoyama and Tanba (1991): Estimation of sea surface temperature via AVHRR of NOAA-9 - Comparison with fixed buoy data, International J. of Remote Sensing, 12, pp.2513-2528.

4)Takeuchi and Kanou et al (1988): Atmospheric Correction of MOS-1/VTIR Data Using Split-Window (Japanese), Proceedings of the 8th Japanese Conference on Remote Sensing.

5)Takayama and Maeda (1989): Sea Surface Temperature Observation by VTIR (Japanese), J. of the Remote Sensing Society of Japan, Vol.9, No.1, 43-51.

6)Matsumoto and Tsuchiya (1990): Sea Surface Temperature and Precipitable Water Estimation Using MOS-1/VTIR Data (Japanese), J. of the Remote Sensing Society of Japan, Vol.10,No.1 19-28.

/...

DEFORESTATION ASSESSMENT USING SATELLITE IMAGERY AND GIS TECHNIQUES

D. Alves

National Institute for Space Research

Sao Jose de Campos, Brazil

/...

DEFORESTATION ASSESSMENT USING SATELLITE IMAGERY

and

GIS TECHNIQUES

Diógenes S. Alves
National Institute for Space Research
Image Processing Division
C.P. 515 - CEP 12201 - S. José dos Campos - SP
e-mail: dalves@dpi.inpe.br

ABSTRACT

Satellite imagery makes possible the assessment of deforestation in large areas such as the Brazilian Amazon on an yearly basis. Integration of remotely sensed data with different types of spatial data is crucial for the assessment of the different impacts of deforestation. GIS techniques provide a flexible framework for the integration of this data. Some of the problems related to the creation of this kind of GIS are presented.

BACKGROUND

The extent and the rate of deforestation in the tropics has become an interesting subject because of the growing concern about the impact of forest clearing on biodiversity and emission of green-house gases. Several estimates of deforestation were produced for Brazilian Legal Amazonia, most of them based on satellite imagery, a unique source of data due to the difficulties of access and the dimensions of the region.

The availability of Landsat Multispectral Scanner (MSS) and Thematic Mapper (TM) imagery at the National Institute for Space Research (INPE) made it possible to perform comprehensive surveys of deforestation in the Amazon. In 1980, results of the first wall-to-wall assessment of deforestation based on MSS data were published by INPE and former Brazilian Institute for Forest Development (IBDF) (Tardin et al, 1980). Starting in 1988, INPE has been developing a series of studies using Landsat TM imagery, which allowed to estimate Legal Amazonia rate of deforestation over the last decade (INPE, 1992; Watson et al, 1992).

The use of MSS and TM imagery for the assessment of deforestation has allowed to measure both the extent and the rate of deforestation for comparatively short time intervals, in some cases, on an yearly basis. Particularly, TM 30-meter resolution and the geometric quality of its images has proved to be appropriate for that purpose. Also, Landsat imagery has been daily recorded at INPE since 1973 what gives complete yearly coverages of the whole area. It could be noted that data from other orbital sensors has been used in some studies. However, available data are either insufficient to produce yearly coverages of the entire region, as in the case of the Satellite Pour l'Observation de la Terre (SPOT), or do not have an adequate resolution for the measurement of relatively small areas deforested each year, like 1.1-km NOAA Advanced Very High Resolution Radiometer (AVHRR).

/...

Starting in 1990, INPE refined its methodology and decided to create a geographic information system - the *Amazonia* Information System (Alves et al, 1992) - to keep the results of its surveys in a georeferenced data base. The adoption of GIS techniques simplifies the integration of deforestation maps with other kinds of maps and spatial data helping in the assessment of the different impacts of deforestation.

GIS STRUCTURE

The *Amazonia* system groups maps of deforestation, vegetation types, administrative boundaries and other data (Alves et al, 1992). The maps of deforestation were produced by INPE while some other data were acquired in digital form from other agencies or just digitized from existing maps.

The production of the maps of deforestation basically involves the analysis of TM imagery and is described in this document. It comprises the following steps:

1. Image selection

Legal Amazonia is covered by 229 Landsat TM scenes. For each year of study, the entire image dataset is analyzed for selection of the best images (basically, images with no or minimal cloud cover)

2. Image analysis

Visual interpretation of each image is performed. The extent of deforestation is mapped for the first year of the series and increments of the total deforested area are drawn for all other years. All work is done with 1:250.000 scale products.

Automatic classification for the identification of the areas of interest is not used for 2 major reasons: because computer power to process the entire amount of imagery is not available and also because the margin of error of the available classifiers is usually greater than the average annual increase of the deforested area.

3. GIS data acquisition

Image overlays produced by the interpretation process are geo-referenced with the help of control points and digitized into the SGI system (de Souza et al, 1990), which is the basis for *Amazonia*.

INTEGRATING REMOTE SENSING DATA INTO A GIS

The main reason to build the *Amazonia* system is that it provides a group of techniques to combine data extracted from satellite imagery (mostly deforested areas) with different types of maps and find relationships among data, e.g. deforestation occurring for each type of vegetation or each administrative unit.

The integration of data from different sources requires the use of adequate techniques to make data in different projections, scales and even classification systems compatible or comparable. This can usually be done by *Amazonia/SGI* programs and functions for projection transformation and data reclassification.

Projection transformation and data reclassification are standard procedures for geographic information systems that in some sense only change the form of the data for further analysis or map production.

Combining two or more data from different sources is a more complex task and one of the most serious challenges is the overlay of maps with features that have different forms in different maps (e.g. rivers) and features that do not have well defined boundaries (e.g. the separation of two different vegetations types).

Several problems could be noted, among which we'll refer to the following:

1. Combining imagery with "topographic" maps:

Administrative boundaries, roads, drainage and some other information are extracted from existing "topographic" 1:250,000 scale maps. However, combining data from these kind of map with features extracted from satellite imagery (e.g. deforested areas) has been the origin of several problems:

a. Some map features, such as rivers, may change over time, particularly if available maps are relatively old. Consequently the same features appear differently in the images and the maps.

b. There is no complete coverage of topographic 1:250,000 scale maps for Brazilian Amazonia. Several areas are covered by maps with poor geometric quality that difficults georeferencing.

2. Combining imagery with "thematic" maps

Class boundaries in many thematic maps are just "reference lines" and not precise limits as is often the case of the transition between two different vegetation classes. This fact difficults the assessment of the relationship between data from the imagery and the classes from thematic maps.

In addition, in the case of Amazonia, most thematic maps are produced at a more reduced than 1:250,000 scale, such as RADAM project data at the 1:1,000,000 scale, requiring the conversion of projection and scale for data integration and an analysis of the error induced by the use of different scales.

REFERENCES

Alves, D.S., L.G. Meira Filho, J.C.L. d'Alge, E.K. Mello, J. S. de Medeiros, J.R. dos Santos, J.D. de Oliveira, J.C. Moreira, A.T. Tardin, 1992 "The Amazonia Information System". XVII ISPRS Congress, Washington, D.C., August 1992

de Souza, R.C.M., Alves, D.S., Camara Neto, G., 1990 "Development of Geographic Information and Image Processing Systems at INPE" (original in Portuguese), Proceedings, Brazilian Symposium on Geoprocessing, S. Paulo, May 1990

Instituto Nacional de Pesquisas Espaciais (INPE) "Deforestation in Brazilian Amazonia". S. José dos Campos, May 1992, 4 p

Tardin, A.T. et all, 1980 "Projeto Desmatamento", Report, INPE-1649-RPE/103, January 1980

Watson, R.T., L.G. Meira Filho, E. Sanzuela, A. Janetos, "Greenhouse Gases: Sources and Sinks", A1 - Climate Change, Pre-publication Copy, 1992
